AD-A269 026

QUANTUM OPTOELECTRONICS

POSTCONFERENCE EDITION

DTIC
ELECTE
SEP 0 1 1993
S E D

**1993 TECHNICAL DIGEST
SERIES VOLUME 8**

**MARCH 17–19, 1993
PALM SPRINGS,
CALIFORNIA**

REPORT DOCUMENTATION PAGE

Public reporting burden for this collection of information is estimated to average 1 hour per response, including the time for reviewing instructions, searching existing data sources, gathering and maintaining the data needed, and completing and reviewing the collection of information. Send comments regarding this burden estimate or any other aspect of this collection of information, including suggestions for reducing this burden, to Washington Headquarters Services, Directorate for Information Operations and Reports, 1215 Jefferson Davis Highway, Suite 1204, Arlington, VA 22202-4302, and to the Office of Management and Budget, Paperwork Reduction Project (0704-0188), Washington, DC 20503.

1. AGENCY USE ONLY *(Leave blank)*	2. REPORT DATE	3. REPORT TYPE AND DATES COVERED
		Final Report 15 Feb 93 – 14 Jan 94

4. TITLE AND SUBTITLE

Quantum Optoelectronics

Organization of the 1993 Photonics Science topical Meetings

5. FUNDING NUMBERS

F49620-93-1-0181

6. AUTHOR(S)

Dr Jarus W Quinn

7. PERFORMING ORGANIZATION NAME(S) AND ADDRESS(ES)

Optical Society of America
2010 Massachusetts Avenue NW
Washington DC 20036

8. PERFORMING ORGANIZATION REPORT NUMBER

AFOSR-TR· 93 0638

9. SPONSORING/MONITORING AGENCY NAME(S) AND ADDRESS(ES)

AFOSR/NE
110 Duncan Avenue Suite B115
Bolling AFB DC 20332-0001

10. SPONSORING/MONITORING AGENCY REPORT NUMBER

2301/DS

11. SUPPLEMENTARY NOTES

12a. DISTRIBUTION/AVAILABILITY STATEMENT

UNLIMITED

12b. DISTRIBUTION CODE

13. ABSTRACT *(Maximum 200 words)*

The following symposium was held

Advanced Solid State Lasers
Compact Blue-Green Lasers
Integrated Photonics Research
Nonlinear Guide-Wave Optics
Optical Amplifiers & Their Applications
Optical Design for Photonics
Photonics in Switching
Quantum Optoelectronics
Shortwavelength: Physics With Intense Laser Pulses
Soft X-Ray Protection Lithography
Ultrafast Electronics & Optoelectronics
Optical Computing
Spatial Light Modulators

93-20315

14. SUBJECT TERMS

93 8 31 035

16. PRICE CODE

17. SECURITY CLASSIFICATION OF REPORT	18. SECURITY CLASSIFICATION OF THIS PAGE	19. SECURITY CLASSIFICATION OF ABSTRACT	20. LIMITATION OF ABSTRACT
UNCLASS	UNCLASS	UNCLASS	UL

Quantum Optoelectronics

Summaries of papers presented at the Quantum Optoelectronics Topical Meeting

March 17–19, 1993
Palm Springs, California

1993 Technical Digest Series
Volume 8

POSTCONFERENCE EDITION

DTIC QUALITY INSPECTED 1

Sponsored by
Optical Society of America

Technical Cosponsor
IEEE/Lasers and Electro-Optics Society

Optical Society of America
2010 Massachusetts Avenue, NW
Washington, DC 20036–1023

CONTENTS

OLEANDER ROOM

8:30 am–10:00 am
QWA, MICROCAVITY AND VERTICAL EMITTERS
Constance J. Chang-Hasnain, *Stanford University, Presider*

8:30 am (Invited)
QWA1 Combined quantum effects for electron- and photon-systems in semiconductor microcavities, M. Yamanishi, Y. Lee, *Hiroshima Univ., Japan.* We demonstrate experimental results on alteration of spontaneous emission and discuss a novel scheme for the generation of photon-number-squeezed state. **(p. 2)**

9:00 am
QWA2 Controlled atomic-like spontaneous emission from implanted erbium in a Si/SiO$_2$ Microcavity, A. M. Vredenberg, N. E. J. Hunt, E. F. Schubert, D. C. Jacobson, J. M. Poate, G. J. Zydzik, *AT&T Bell Laboratories.* We propose a model system for studying microcavity effects on spontaneous emission. Erbium-doped transparent Si/SiO$_2$ microcavities show emission intensity enhancement, peak narrowing, and lifetime changes. **(p. 4)**

9:15 am
QWA3 Quantum microcavities and quantum well excitons: an optimum system for strong optical coupling, Y. Arakawa, A. Ishikawa, M. Nishioka, C. Weisbuch, *Univ. Tokyo, Japan.* The strong light-matter coupling occurring between quantum well excitons imbedded in planar monolithic DBR-Fabry-Perot cavities and fundamental-mode photons is demonstrated. **(p. 6)**

9:30 am
QWA4 Threshold dependence on cavity length and mirror reflectivity in Fabry-Perot microcavity semiconductor lasers with high-contrast mirrors, D. L. Huffaker, D. G. Deppe, C. J. Pinzone, T. J. Rogers, B. G. Streetman, R. D. Dupuis, *The Univ. Texas at Austin.* Data are presented showing that short-cavity lasers are found to have significantly lower thresholds in comparison to long-cavity lasers, for otherwise nearly identical structures. **(p. 8)**

9:45 am
QWA5 Asymmetric gain in a vertical-cavity surface-emitting laser, F. Brown de Colstoun, C. W. Lowry, G. Khitrova, H. M. Gibbs, A. E. Paul, S. W. Koch, *Univ. Arizona;* T. M. Brennan, B. E. Hammons, *Sandia National Laboratories.* Light injected into a surface-emitting laser operating near threshold causes localized asymmetric gain modifications. The shift of the new peak is proportional to the injected power and reaches 36.2 GHz. **(p. 10)**

10:00 am–10:30 am COFFEE BREAK

OLEANDER ROOM

10:30 am–12:00 pm
QWB, MODULATORS: 1
David A. B. Miller, *AT&T Bell Laboratories, Presider*

10:30 am
QWB1 Interleaved-contact electroabsorption modulator using doping-selective electrodes with 25°C to 95°C operating range, K. W. Goossen, J. E. Cunningham, W. Y. Jan, D. A. B. Miller, *AT&T Bell Laboratories.* We demonstrate a MQW modulator with multiple stacked *p-i*(MQW)-*n-i*(MQW)-*p-* regions, such that each *i* region is electrically driven in parallel, allowing large Stark shifts at low voltages. For a 0-6-volt swing we achieve >22% reflectivity change from 25°C to 95°C. **(p. 14)**

10:45 am
QWB2 Functionally all-optical bistable *p-i-p-i-n* device with asymmetric GaAs/AlAs coupled QW absorption layers and an AlAs resistive layer, Yasunori Tokuda, Yuji Abe, Noriaki Tsukada, *Mitsubishi Electric Corporation, Japan.* A functionally all-optical bistable operation, based on the inner self-electro-optic effect, was achieved for a *p-i-p-i-n* device with asymmetric coupled QW absorption layers. **(p. 16)**

11:00 am
QWB3 Visible wavelength LEDs and reflection modulators with AlGaAs/AlAs QWs, B. Pezeshki, J. A. Kash, *IBM T. J. Watson Research Center;* Daxin Liu, S. M. Lord, J. S. Harris, Jr., *Stanford Univ.* Using the direct gap transition in indirect gap AlGaAs/AlAs QWs, we fabricate room temperature LEDs and Fabry-Perot reflection modulators operating at about 615 nm. **(p. 18)**

11:15 am
QWB4 Responsivity and excitonic electroabsorption in proton implanted GaAs/AlGaAs MQW modulators, T. K. Woodward, B. Tell, W. H. Knox, J. B. Stark, M. T. Asom, *AT&T Bell Laboratories.* Proton-implanted AlGaAs/GaAs MQW modulators exhibit suppressed responsivity, and increased saturation intensity, while continuing to exhibit excitonic electroabsorption. **(p. 20)**

11:30 am
QWB5 Nonlinear optical properties in infrared region in quantum well—an application of intersubband transitions, J. B. Khurgin, Shaozhong Li, *Johns Hopkins Univ.* Nonlinear optical properties of quantum wells, based on the intersubband transitions, have been examined theoretically. It is found that large susceptibility ($\chi^{(2)}$ and $\chi^{(3)}$) can be achieved. The comparison with interband transitions is also made. The implications for the design of nonlinear infrared optical devices are discussed. **(p. 22)**

11:45 am
QWB6 Intersubband transitions in high indium content InGaAs/AlGaAs QWs grown on GaAs with a graded InGaAs buffer, H. C. Chui, S. M. Lord, M. M. Fejer, J. S. Harris, Jr., *Stanford Univ.* We report observation of intersubband transitions in In(y)Ga(1-y)As (y = 0.3., 0.5)/AlGaAs QWs. The 1-2 intersubband transition energies of 311 meV and 351 meV are among the largest reported. **(p. 24)**

12:00 pm–1:30 pm LUNCH BREAK

OLEANDER ROOM

1:30 pm–3:00 pm
QWC, FUNDAMENTAL PROCESSES
Yoshihisa Yamamoto, *NTT, Presider*

1:30 pm (Invited)
QWC1 Quiet electrons, noisy photons: quantum statistical effects in waveguide transport, M. Büttiker, *Univ. Basel, Switzerland.* Quantum statistical effects of time-dependent electron-current and photon-intensity fluctuations at the contacts of few-channel, phase-coherent, multiprobe conductors and waveguides are analyzed. **(p. 28)**

2:00 pm
QWC2 Squeezing with input state of large-phase uncertainty, I. Lyubomirsky, M. Shirasaki, H. A. Haus, *Massachusetts Institute of Technology.* Squeezing in a nonlinear Mach-Zehnder interferometer is analyzed for a number state input. The same degree of squeezing is obtained with a number state as with a coherent state input. **(p. 30)**

2:15 pm   (Invited)
QWC3   Quantum nondemolition measurement of photon number using a mesoscopic electron interferometer, Akira Shimizu, *Univ. Tokyo, Japan.* A quantum nondemolition photodetector using an electron interferometer composed of double quantum wires is discussed in addition to possible uses of other mesoscopic interferometers. **(p. 32)**

2:45 pm
QWC4   Semiconductor laser with dispersive loss: quantum noises and amplitude squeezing, R. F. Nabiev, *E. L. Ginzton Lab., Stanford Univ.* The quantum mechanical treatment of the amplitude and phase noise characteristics of internal and output light of semiconductor laser with dispersive loss element inside the resonator is presented. **(p. 34)**

3:00 pm–3:30 pm   COFFEE BREAK

OLEANDER ROOM

3:30 pm–5:00 pm
QWD, QUANTUM WELL LASERS
H. Temkin, *Colorado State University, Presider*

3:30 pm   (Invited)
QWD1   Multiquantum barrier (MQB): is it a good spice for semiconductor laser performances?, K. Iga, *Tokyo Institute of Technology, Japan.* The multiquantum barrier (MQB) is a semiconductor superlattice which can reflect electrons by interference. In this paper we review the recent progress of MQB-loaded semiconductor lasers and tunneling diodes. **(p. 38)**

4:00 pm
QWD2   Optimum strained MQW structure in 680-nm AlGaInP laser diodes for low threshold and high power, T. Tanaka, S. Kawanaka, H. Yanagisawa, S. Yano, S. Minagawa, *Hitachi Ltd., Japan.* Reliable high-power operation of strained MQW AlGaInP LDs is achieved at wavelengths around 680 nm by using thin QWs with large compressive strain. This suppresses the increase in threshold current and the red-shift of oscillation wavelength. **(p. 42)**

4:15 pm
QWD3   Narrow linewidth long wavelength phase-locked laser array with mode controlling grating filter, Jie Dong, Shigehisa Arai, Tetsu Ikeda, *Tokyo Institute of Technology, Japan.* Narrow linewidth of 203 kHz in a narrow beam divergence (FWHM = 4.7°) GaInAsP/InP 1.5 μm wavelength phase-locked laser array with a mode controlling grating filter (GFA) has been achieved. **(p. 44)**

4:30 pm
QWD4   Highly nondegenerate (>1 THz) four-wave mixing in MQW laser structures, M. C. Tatham, G. Sherlock, C. P. Seltzer, *BT Laboratories, UK.* Highly nondegenerate four-wave mixing is used to investigate ultrafast carrier dynamic processes in strained and unstrained QW lasers, and their contribution to nonlinear gain. **(p. 46)**

4:45 pm
QWD5   Optical properties of tensile and compressively strained (GaIn)P-(AlGaIn)P MQWs, Martin D. Dawson, Geoffrey Duggan, *Sharp Laboratories of Europe, Ltd., UK.* (GaIn)P-(AlGaIn)P bulk and quantum well heterostructures, with (GaIn)P layers under both tensile and compressive strain on a GaAs substrate, have been studied by low temperature photoluminescence and photoluminescence excitation spectroscopy. **(p. 48)**

OLEANDER ROOM

5:15 pm
QPdP, POSTDEADLINE PAPERS
Larry A. Coldren, *Univ. of California Santa Barbara, Presider*

GRAND BALLROOM EAST

8:30 am–10:00 am
QThA, MICROCAVITY AND VERTICAL EMITTERS: 2
Kenichi Iga, *Tokyo Institute of Technology, Japan*

8:30 am   (Invited)
QThA1   Microcavity VCSELs, J. L. Jewell. *Photonics Research Inc.;* A. Scherer, B. Van der Gaag, L. M. Schiavone, J. P. Harbison, L. T. Florez, *Bellcore.* Experiments lasing thresholds in sub-half-micron diameter microcavity VCSELs imply very low losses and validate the feasibility of ultralow threshold lasers. **(p. 52)**

9:00 am
QThA2   Threshold reduction of 1.3-μm GaInAsP/InP surface-emitting laser by a maskless circular planar buried heterostructure (PBH) regrowth, T. Baba, K. Suzuki, Y. Yogo, K. Iga, F. Koyama, *Tokyo Institute of Technology, Japan.* A newly introduced maskless PBH regrowth has improved the hetero-interface of buried tiny circular active region of GaInAsP/InP surface-emitting laser. The threshold current of 1.3-μm range BH-type device was reduced to 2.2 mA at 77 K under cw condition. **(p. 54)**

9:15 am   (Invited)
QThA3   Pixels consisting of a single vertical-cavity laser-thyristor and a double vertical-cavity phototransistor, Hideo Kosaka, Ichiro Ogura, Hideaki Saito, Mitsunori Sugimoto, Kaori Kurihara, Takahiro Numai, Kenichi Kasahara, *NEC Corp., Japan.* Bi-directionally cascadable optical pixels comprising low-threshold (1 mA) high-efficiency (0.25 W/A) surface-emitting laser-thyristors and wide-bandwidth (50 Å) high-photocurrent-gain (230 A/W) double vertical-cavity phototransistors are described. **(p. 56)**

9:45 am
QThA4   Intensity modulation bandwidth limitations of vertical-cavity surface-emitting laser diodes, M. G. Peters, M. L. Majewski, L. A. Coldren, *UC–Santa Barbara.* A small-signal equivalent circuit model has been developed for vertical-cavity surface-emitting lasers enabling quantitative analysis of intensity modulation bandwidth limitations due to extrinsic and intrinsic components. **(p. 60)**

10:00 am–10:30 am   COFFEE BREAK

GRAND BALLROOM EAST

10:30 am–12:15 pm
QThB, MODULATORS: 2
E. E. Mendez, *IBM T. J. Watson Research Center, Presider*

10:30 am
QThB1   Analog differential self-linearized QW self-electro-optic effect modulator, E. A. De Souza, L. Carraresi, G. D. Boyd, D. A. B. Miller, *AT&T Bell Laboratories.* This device gives a difference in two optical output powers linearly proportional to electrical or optical drive, allowing bipolar processing in novel image processing arrays. **(p. 64)**

10:45 am
QThB2   AlGaAs/InGaAs/GaAs MQW voltage tunable Bragg reflector with interdigitated contacts, O. Blum, X. Wu, K. Gulden, T. K. Gustafson, *UC–Berkeley;* J. E. Zucker, *AT&T Bell Laboratories.* We report the first tunable QW Bragg reflector with interdigitated contacts. This modulation scheme produces >12% change in reflectivity for only + 1 volt applied. **(p. 66)**

11:00 am
QThB3 Large, low-voltage absorption changes and absorption bistability in novel, three-step asymmetric QWs, J. A. Trezza, M. C. Larson, S. M. Lord, J. S. Harris, Jr., *Stanford Univ.* We developed novel QW structures which use changes in overlap integrals to exhibit very large negative and positive differential absorption changes and absorptive bistability. **(p. 68)**

11:15 am
QThB4 High-contrast, all-optical GaAlInAs//AlInAs MQW reflection modulator at 1.3 μm, M. F. Krol, R. K. Boncek, *USAF Rome Laboratory;* T. Ohtsuki, G. Khitrova, B. P. McGinnis, H. M. Gibbs, N. Peyghambarian, *Univ. Arizona.* A high-contrast, all-optical GaAlInAs asymmetric reflection modulator at 1.3 μm has been demonstrated. An on/off contrast ratio exceeding 1000:1 has been achieved. The operating speed was measured and found to approach 1 GHz. **(p. 70)**

11:30 am
QThB5 Mixing of electronic states and control of optical transitions in asymmetric triple QW structures, N. Sawaki, S. Fukuta, H. Goto, *Nagoya Univ., Japan;* T. Suzuki, H. Ito, K. Hara, *Nippondenso Co., Ltd., Japan.* The resonance or the anti-crossing of electronic states enhances the variation of optical absorption and luminescence spectrum in GaAs/AlGaAs coupled triple QWs under electric fields. **(p. 72)**

11:45 am
QThB6 Saturation and carrier sweepout in electro-absorptive GaAs/GaAsAlAs MQW diodes, D. J. Goodwill, J. S. Massa, G. S. Buller, S. J. Fancey, *Heriot-Watt Univ., UK;* A. Wachlowski, *Alcatel Austria Elin Research Centre, Austria.* Saturation in the responsivity spectra of GaAs/GaAlAS MQW photodiodes at high intensity (40 kW/cm²) has been correlated with *carrier* sweepout times measured by time-resolved photoluminescence. **(p. 74)**

12:00 pm
QThB7 High contrast reflection electro-absorption modulator with zero phase change, J. A. Trezza, B. Pezeshki, M. C. Larson, S. M. Lord, J. S. Harris, Jr., *Stanford Univ.* We develop the theory for creating zero-chirp vertical-cavity modulators. A zero phase shift device which modulates reflectivity from 96% to 4% is presented. **(p. 76)**

12:15 pm–1:30 pm LUNCH BREAK

GRAND BALLROOM EAST

1:30 pm–3:00 pm
QThC, EXCITON AND CARRIER DYNAMICS: 1
Wayne H. Knox, *AT&T Bell Laboratories, Presider*

1:30 pm (Invited)
QThC1 Coherent exciton effects in quantum wells, E. O. Gobel, *Philipps-Univ. Marburg, Germany.* Coherent exciton dynamics and interaction in various quantum wells and superlattices is studied by means of femtosecond four-wave mixing spectroscopy. **(p. 81)**

2:00 pm
QThC2 Time-resolved optical orientation used to examine Coulomb screening and phase space filling in quantum well excitonic saturation, M. J. Snelling, P. T. Perozzo, R. Bambha, A. Miller, *Univ. Central Florida;* D. C. Hutchings, *Univ. Glasgow, UK.* Picosecond excite-probe measurements show that phase space filling and Coulomb screening contribute almost equally to excitonic saturation and give an electron spin relaxation time of 50 ps. **(p. 82)**

2:15 pm
QThC3 Quantum mechanical oscillations of the electron capture time in quantum wells, B. Deveaud, D. Morris, A. Regreny, *France Telecom, France;* M. Barros, P. Becker, *AT&T Bell Laboratories.* Resonances in electron capture are observed using femtosecond pump probe and luminescence for 60-Å well when one well level is 36 meV below the barrier. **(p. 84)**

2:30 pm (Invited)
QThC4 AC–Stark shift of the Fermi edge singularity in modulation-doped quantum wells, I. Brener, W. H. Knox, J. E. Cunningham, *AT&T Bell Laboratories;* D. S. Chemla, *UC–Berkeley.* We present the first observation to our knowledge of the AC–Stark shift of the Fermi-edge singularity in modulation-doped quantum wells and discuss the new phenomena observed in this regime. **(p. 86)**

3:00 pm–3:30 pm COFFEE BREAK

GRAND BALLROOM EAST

3:30 pm–4:45 pm
QThD, EXCITON AND CARRIER DYNAMICS: 2
Benoit Deveaud, *CNET, France*

3:30 pm (Invited)
QThD1 Femtosecond dynamics of room-temperature excitons in II–VI MQWs, Anthony M. Johnson, Philippe C. Becker, Donghan Lee, Miriam R. X. de Barros, Robert D. Feldman, Alan G. Prosser, Richard F. Austin, Robert E. Behringer, *AT&T Bell Laboratories.* Femtosecond pump–probe experiments yield the first direct measurement of the relative bleaching strength of room-temperature excitonic absorption by "cool" free e-h pairs and "cold" excitons. **(p. 90)**

4:00 pm
QThD2 Femtosecond dynamics of exciton gain in (Zn,Cd)Se/ZnSe quantum wells, M. Hagerott, J. Ding, A. V. Nurmikko, *Brown Univ.;* Y. Gan, D. Grillo, J. Han, H. Li, R. L. Gunshor, *Purdue Univ.* Femtosecond spectroscopy has been applied to characterize exciton energy relaxation and formation of gain in the ZnCdSe/ZnSSe quantum well at T = 77K and beyond. By both pump–probe spectroscopy and degenerate four-wave mixing, we show how a strongly inhomogeneous n = 1 HH exciton resonance permits rapid energy relaxation and the formation of population inversion in the quasi-2D exciton system, before the onset to an electron-hole plasma. **(p. 92)**

4:15 pm
QThD3 Femtosecond studies of ultrafast large-angle polarization rotation in GaAs/Al$_x$Ga$_{1-x}$As MQWs under uniaxial stress, M. Wraback, H. Shen, J. Pamulapati, M. Dutta, P. Newman, *U.S. Army Research Laboratory;* Y. Lu, *Rutgers Univ.* The pump–probe technique was used to measure the dynamic probe polarization rotation resulting from the bleaching of anisotropic exciton absorption in uniaxially stressed MQWs. **(p. 98)**

4:30 pm
QThD4 Fast optical switching and amplification in a MQW vertical microcavity, R. Raj, J. L. Oudar, M. Bensoussan, *France Telecom, France.* We demonstrate external beam amplification by stimulated emission in an optically excited vertical microcavity. A gain of 8 dB over a 2-THz spectral band with a switch-off <20 ps is obtained before the occurrence of laser emission. **(p. 100)**

6:00 pm–7:30 pm CONFERENCE RECEPTION (Quantum Optoelectronics)

7:30 pm INFORMAL DISCUSSION

FRIDAY, MARCH 19, 1993

GRAND BALLROOM EAST

8:30 am–10:00 am
QFA, WIRES AND DOTS
C. Weisbuch, *Thomson CSF-LC.*, France, Presider

8:30 am   (Invited)
QFA1   Characterization studies and luminescence of quantum wires and dots, Jean-Yves Marzin, *CNET, France.* Abstract not available at press time. **(p. 107)**

9:00 am
QFA2   Effects of size fluctuation on the optical properties of very narrow InGaAs/InP QW wires, S. Nojima, M. Notomi, M. Nakao, T. Tamamura, *NTT Opto-electronics Laboratories, Japan.* Quantum-wire size fluctuation is directly evaluated for the first time using atomic force microscopy; its effects on the photoluminescence spectrum and polarization anisotropy are discussed. **(p. 108)**

9:15 am
QFA3   Fabrication of GaAs quantum wires (∼10 nm) by MOCVD selective growth, S. Tsukamoto, Y. Nagamune, M. Nishioka, Y. Arkawa, *Univ. Tokyo, Japan.* We fabricated GaAs triangular shaped quantum wires with ∼10 nm lateral width by MOCVD selective growth technique, showing both photoluminescence spectra and high-resolution scanning electron micrographs. **(p. 110)**

9:30 am   (Invited)
QFA4   GaInAs/InP long-wavelength quantum wires and boxes: fabrication technology and lasers, Shigehisa Arai, *Tokyo Institute of Technology, Japan.* Improvements in the regrowth process of a low-pressure OMVPE and the usage of p-type InP substrate have enabled a room temperature cw operation of GaInAs/InP quantum-wire laser. Approaches to high-performance lasers consisting of low-dimensional quantum well structures are presented. **(p. 112)**

10:00 am–10:30 am   COFFEE BREAK

GRAND BALLROOM EAST

10:30 am–11:45 am
QFB, OPTICS AND TRANSPORT IN REDUCED DIMENSIONALITY
Manfred Pilkuhn, *Universitat Stuttgart, Germany*

10:30 am   (Invited)
QFB1   Pros and cons of reduced energy relaxation at low dimensions for optoelectronics devices, H. Benisty, *Univ. Paris 6, France.* Reduced electron relaxation in quantum boxes and unperfect quantum wires explains their degraded optical properties but should improve dramatically the performances of intersubband infrared devices. **(p. 116)**

11:00 am
QFB2   Thermal and coherent carrier escape from QWs in an electric field, A. M. Fox, R. G. Ispasoiu, *Univ Oxford, UK;* C. T. Foxon, *Univ. Nottingham, UK.* We identify coherent tunneling and thermal carrier escape mechanisms in electrically biassed GaAS/Ga$_{0.67}$Al$_{0.33}$As QWs by the temperature dependence of the photocurrent I–V curves. **(p. 118)**

FRIDAY, MARCH 18, 1993—*Continued*

11:15 am
QFB3   Temperature dependence of electron and hole emission rates from a single QW with asymmetric barriers, R. P. Bambha, M. J. Snelling, P. Li-Kam-Wa, A. Miller, *Univ. Central Florida;* J. A. Cavailles, D. A. B. Miller, J. E. Cunningham, *AT&T Bell Laboratories.* Laser excite-probe measurements are used to determine thermionic emission rates as a function of temperature and electric field in a *p-i-n* doped waveguide. **(p. 120)**

11:30 am
QFB4   Optical nonlinearities associated with piezo-electric field screening in [111] strained-layer InGaAs/GaAs QWs, Arthur L. Smirl, D. S. McCallum, A. N. Cartwright, Thomas F. Boggess, *Univ. Iowa;* T. S. Moise, L. J. Guido, R. C. Barker, *Yale Univ.,* B. S. Wherrett, *Heriot-Watt Univ., UK.* We show that measurements of nonlinearity enhancements in strained [111] MQWs are due to screening by long-lived carriers, not in-well screening. **(p. 122)**

Microcavity and Vertical Emitters 1

QWA 8:30am–10:00am
Oleander Room

Constance J. Chang-Hasnain, *Presider*
Stanford University

Combined Quantum Effects for Electron- and Photon-Systems in Semiconductor Microcavities

Masamichi Yamanishi and Yong Lee

Department of Physical Electronics, Faculty of Engineering, Hiroshima University, 1-4-1 Kagamiyama, Higashihiroshima 724 JAPAN

Phone No.   +81-824-22-8425
Fax No.   +81-824-22-7195

One of most important conclusions in cavity-quantum-electrodynamics is that spontaneous emission of an atom can be controlled by squeezing zero-point fluctuations of the photon fields surrounding the atom in both spatial and frequency domains[1]. As for quantum optoelectronic device application, in addition to quantum control of photon system, it is of great important to dynamically control electron system as well in order to alter spontaneous emissions. This can be easily realized in semiconductor systems by a combined use of distributed Bragg reflectors (DBRs) and the quantum confined Stark effect (QCSE) for control of photon and electron systems, respectively. The main purpose of this talk is to demonstrate our experimental results on physical phenomena originating from quantum control of electron- and photon-systems[2,3], and its implications for device-applications[4] involving the possibility of a novel scheme for the generation of photon-number squeezed state[5].

We invesgated two kinds of microstructures with and without well-designed quantum microcavities, named quantum microcavity (QMC) and weak microcavity (WMC), respectively. The QMC-device was designed in such a way that a GaAs single quantum well (QW) was located at an antinode position of the standing wave of the zero-point fluctuations in a half-wavelength ($\lambda_r/2$) cavity. The WMC-device, in which the replacement of the p-doped DBR layer by the bulk p-doped $Al_{0.2} Ga_{0.8}As$ layer leads to free-space emissions, was made as a reference to the QMC-device. When the emission wavelength of the QW was tuned to the resonant wavelength of the cavity: λ_r due to QCSE, the PL intensity detected along the normal direction to the cavity surface was strongly enhanced to be about 40 fold as high as that of the WMC-device. This clearly indicates that the coupling efficiency (β) of the spontaneous emission into the resonant mode of the cavity can be easily and dynamically controlled by applied voltages (electric fields).

A particular interest lies in controllable beam steering of the spontaneous emission through the tuning of emission wavelength caused by QCSE. When the emission wavelength: λ_p was shorter than the cavity resonant wavelength: λ_r, i.e., $\Delta\lambda < 0$, the conical beam pattern was observed. When $\Delta\lambda > 0$, the radiations were, on the other hand, focused around the axis normal to the device surface. Such alterations of the beam patterns as well as emission intensity result from whether or not the emission wavelength fulfills the resonant condition for the cavity.

Our data have demonstrated the possibility of β-switching by *dc*-voltages

applied to microcavities involving QW-active layers. When the voltage applied to the *p-i-n* diode is pulsively switched in such a way that the emission wavelength is tuned to the resonant wavelength λ_r, the light output intensity was observed to quickly follow the voltage pulse[6]. The response time of the output intensity was obtained to be substantially shorter than the recombination lifetime of carriers, ~10nsec., confirmed by a standard pulse-excitation technique, in the QWs located in the QMC device. When the amplitude of the voltage pulse is further increased to switch the emission wavelength toward shorter one than the resonant wavelength, we found very short double pulses in the output intensity.[6]

Furthermore, we discuss a novel scheme for the generation of photon-number squeezed state on the basis of population-dependent spontaneous emission lifetime in the microcavities[5] in addition to the suppression of pump-fluctuation. In the proposed scheme, the population dependence of the electron lifetime results from a resultant effect of field screening due to the populated electron in the biased QWs and of detuning-dependent lifetime in the microcavities. In fact, the population dependent lifetime, $\tau_{sp}(N_c)$ with a negative N_c-derivative theoretically demonstrates to give rise to anticorrelation between subsequent emission events, resulting in a remarkable expansion of frequency range for the suppression of photon-number fluctuation noise beyond the inverse of the lifetime, $1/\tau_{sp}$. According to our estimation, one may expect an increase in the cut-off frequency for the noise suppression, ~ $50 \times (1/\tau_{sp})$.

References

[1] See, for example, P.Goy,J.M.Raimond, M.Gross and S.Haroche, Phys. Rev. Lett. **50** (1983) 1903 for an atomic system. Yamamoto,S.Machida, K.Igeta and G.Bjork, Coherence,Amplification, and Quantum Effects in Semiconductor Lasers, Ed. Y. Yamamoto (Wiley, New York,1991) pp.561-615 for a semiconductor system.

[2] N.Ochi, T. Shiotani, M.Yamanishi, Y.Honda and I.Suemune, Appl. Phys. Lett. **58** (1991) 2735.

[3] Y. Honda, Y. Lee, M. Yamanishi, N. Ochi, T. Shiotani and I. Suemune, Surf. Sci., **267** (1992), 612.

[4] M.Yamanishi, Y.Yamamoto and T.Shiotani, IEEE. Photonics Tech. Lett. 3 (1991) 888. ; G. Bjork and Y. Yamamoto, IEEE J. Quantum Electronics QE-**27** (1991) 2386.

[5] M. Yamanishi and Y. Lee, unpublished.

[6] T. Shiotani, K. Tanaka,Y. Lee and Y. Yamanishi, unpublished.

Controlled Atomic-like Spontaneous Emission from Implanted Erbium in a Si/SiO2 Microcavity

A.M. Vredenberg, N.E.J. Hunt, E.F. Schubert, D.C. Jacobson, J.M. Poate, and G.J. Zydzik,
AT&T Bell Laboratories, 600 Mountain Ave., Murray Hill, NJ 07974, Ph. (908) 582 2020

Since the advent of vertical cavity surface-emitting lasers, a renewed interest has also emerged for the *spontaneous* emission from Fabry-Pérot microcavities. Changes in spontaneous emission characteristics in a 1D microcavity were predicted long ago,[1] but have been demonstrated only recently in the optical domain for solid-state, *e.g.* semiconductor, structures where changes in spectral purity, lifetime, and emission intensity were observed.[2] However, the interpretation of these effects is somewhat obscure, because these structures are highly absorbing and often involve band-to-band, rather than atomic, transitions. In the present study, we use optically transparent Si/SiO2 cavities, consisting of two coplanar Si/SiO2 distributed Bragg reflectors (DBR) around a ($\lambda/2$) SiO2 active region, which was doped with ~0.2 at.% Er^{3+} ions through MeV ion implantation. The Er^{3+} ions in SiO2 exhibit a sharp, atomic-like, intra-4f transition around λ_{em}=1.54 μm, which is effectively shielded by the outerlying filled $5s^2$ and $5p^6$ shells. Recently, we reported on the considerable enhancement of the spontaneous emission intensity out of such an Er-doped microcavity.[3] In this paper, we present a more detailed study of the modified spontaneous emission, including fluorescence decay measurements to study the effect of the cavity on the spontaneous emission rate.

The layout of the vertical microcavity is shown in Fig. 1, along with a typical Er doping profile. After implantation, radiation-induced defects were removed by a 900 °C anneal (1 h). The calculated bottom and top mirror reflectivities are 99.8% and 98.5%, respectively. Photoluminescence (PL) measurements were performed on a cavity with a resonance wavelength (λ_{res}) of 1.55 μm, as probed by reflectivity measurements. The incident excitation power density was too low for lasing to occur. Figure 2 compares PL spectra taken along the optical axis from a cavity and from a structure from which the top mirror was removed through selective wet chemical etching. The 'no-cavity' spectrum exhibits a double peak structure, with a maximum at 1535 nm and with tails extending toward shorter and longer wavelengths. These features are typical for Er-doped silica. The PL spectrum from the cavity is markedly different: (1) the peak intensity is enhanced by nearly 60, (2) the luminescence peaks at λ_{res}, and (3) the width of the luminescence line is reduced to one third. All of these effects result from the alteration of spontaneous emission by the microcavity.
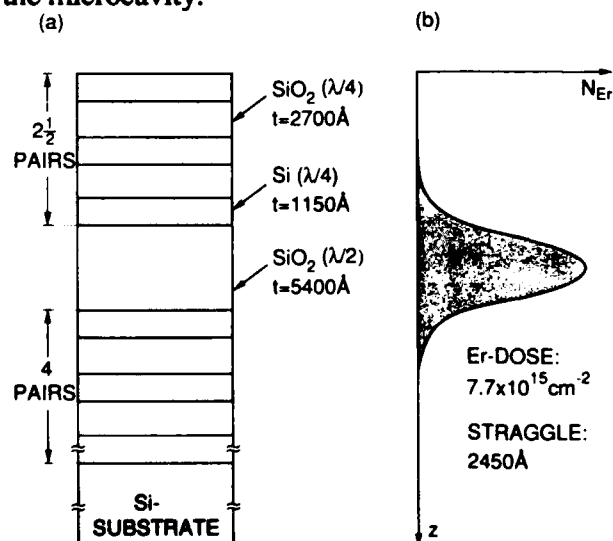

Fig. 1 (a) Schematic illustration of the Si/SiO2 resonant cavity structure and (b) the Er profile after 3.55 MeV implantation.
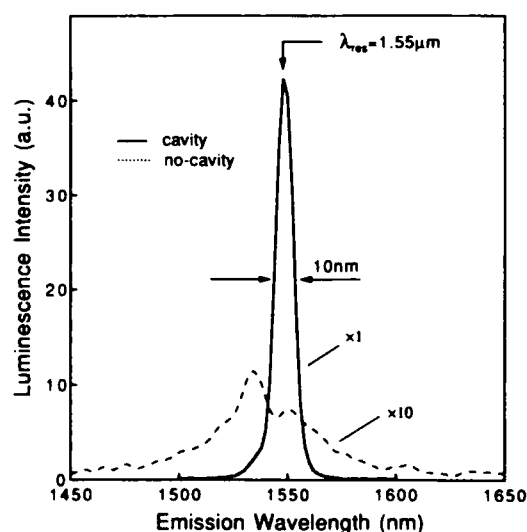
Fig. 2 PL of implanted Er in a 1.55 μm cavity, and in a structure without the top reflector.
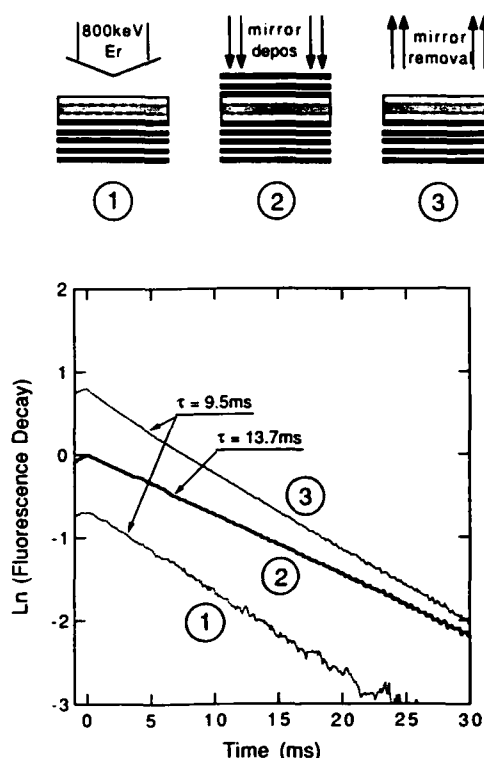
Fig. 3 Luminescence decay measurements after pulsed excitation of an Er-implanted structure before top mirror deposition, in a completed cavity at 1.44 µm, and after removal of the top mirror. The curves are normalized to their peak intensity and offset for clarity.

For emission in a narrow solid angle around the optical axis through the top reflector, the emission rate enhancement factor, F, for excited ions in the resonance antinode position is given by:[4]

$$F = 2\left(\frac{1+\sqrt{R_{bot}R_{top}}}{1-\sqrt{R_{bot}R_{top}}}\right)\left(\frac{1-R_{top}}{1-\frac{1}{2}(R_{top}+R_{bot})}\right) \quad (1)$$

For our structure this yields $F = 830$, *i.e.* some 14 times larger than the measured one. This discrepancy results from: (1) reduced mirror reflectivities, due to thickness variations in the DBR layers, (2) a finite emission collection angle, resulting in spectral broadening for the PL from the cavity, (3) the presence of the bottom DBR in the no-cavity structure, and (4) the spread in the Er distribution. Combined, these contributions are estimated to decrease F (compared to a structure without top mirror) by a factor of ~14, in agreement with the observed discrepancy. The change in spectral purity indicates that the near-normal emission is determined by the resonance width of the cavity, rather than host-dependent spectral broadening mechanisms.

The cavity is also expected to change the (total) emission rate of the excited Er^{3+} ions: for an 'on-resonance' cavity (with $\lambda_{res} \geq \lambda_{em}$) the emission rate should increase, characterized by a shorter excited state lifetime, and vice versa for an 'off-resonance' cavity (with $\lambda_{res} < \lambda_{em}$).[1] To demonstrate this, first a structure without top mirror was implanted with 800 keV Er, and annealed at 900 °C for one hour. Time-resolved luminescence after pulsed excitation of this sample (curve 1 in Fig. 3) showed single-exponential decay, characterized by a lifetime of 9.5 ms, typical for a radiative transition of Er^{3+} in SiO_2. Deposition of the top DBR then resulted in a 1.44 µm cavity and the luminescence decay of this structure (curve 2) had a lifetime of 13.7 ms. Thus, the cavity is 'off-resonance' and the lifetime has indeed increased. Finally, in order to verify if the enhanced lifetime was a true cavity effect, the top mirror was removed through selective wet etching. The luminescence out of this structure decayed with a lifetime of 9.5 ms (curve 3), comparable to the (similar) situation before the deposition of the top mirror. We note that changes in radiative lifetime can be easily obscured in semiconductor structures by photon recycling effects. Such photon recycling effects have a very small probability in our transparent Si/SiO_2 structure.

In summary, altered spontaneous emission from Er^{3+} in transparent ($\lambda/2$) microcavities was observed. This includes, for a resonant cavity, an intensity enhancement of nearly two orders of magnitude, emission wavelengths dictated by λ_{res}, and an increase of spectral purity. Suppressed emission was observed for an off-resonance cavity, where a lifetime enhancement of ~40% occurred. These results can be directly interpreted as microcavity effects on the spontaneous emission characteristics. Indeed, the Er-doped transparent Si/SiO_2 cavity appears to be the ideal system for studying microcavity effects.

REFERENCES

1 E.M. Purcell, Phys. Rev. 69, 681 (1946).
2 H. Yokoyama, Science 256, 66 (1992).
3 E.F. Schubert, A.M. Vredenberg, N.E.J. Hunt, Y.-H. Wong, P.C. Becker, J.M. Poate, D.C. Jacobson, L.C. Feldman, and G.J. Zydzik, Appl. Phys. Lett. 61, 1381 (1992).
4 X.-P. Feng, Optics Comm. 83, 162 (1991).

QUANTUM MICROCAVITIES AND QUANTUM WELL EXCITONS : AN OPTIMUM SYSTEM FOR STRONG OPTICAL COUPLING

Y. Arakawa[a], A. Ishikawa[a], M. Nishioka[a], C. Weisbuch[a][b]

(a) Institute for Industrial Science, University of Tokyo, 7-22-1 Roppongi, Minato-ku, Tokyo 106, Japan
(b) Laboratoire Central de Recherches, Thomson-CSF, 91404 Orsay cedex, France

Several approaches are being attempted to obtain narrow spectral lines and/or controlled spontaneous emission on localized (impurity ions) or delocalized crystal excitations (free electron-hole pairs, excitons). A first way is to quantize electron motion, in an increasing manner in 1, 2 or 3 dimensions, in structures called quantum well,s wires or dots structures. While the approach to quantum wires and dots is being pursued since about 10 years, it did not yield so far any convincing improvement of the optical and optoelectronics properties of solids, in the same way as quantum wells did when compared to "traditional" bulk materials. Another, more recent approach is to remark that broad emission lines and isotropic emission (in the broad sense) are obtained because there is a 3D continuum of photon states available which allow transitions at any direction and energy at which a suitable electronic excitation of the crystal is present. One of the approaches to restrict the available photonic states is that of the photonic bandgap materials, in which the material (more precisely its optical constants) is modulated in all three directions in order to open energy gaps in the propagation equation of optical waves, identically to the energy gap opening of electron states in solids due to the periodic ion potential. A second way is to bury the light-emitting material in an optical cavity, such that optical modes are separated by more than the emission linewidth. In such a case emission will only occur into one optical mode, with a linewidth detemined by the mode linewidth, and all energy-unmatched crystal excitations will reach this single desexcitation mode through energy and momentum relaxation, as far as non-radiative recombination is negligible.

Many of the advantages of the quantum microcavity systems have already been evidenced, most often on 1D planar Fabry-Perot (FP) microcavity structures, which can easily be fabricated thanks to the modern layer deposition techniques such as the epitaxy of semiconductor materials. Luminescence line narrowing, spontaneous emission increase or decrease, emission directionality, electric field control, tendency towards thresholdless laser action, etc... were among these important properties.

We present in this communication a study of the optical coupling strength between the quantized optical mode of a planar microcavity and excitons in quantum wells located at the center of the λ-long cavity. This strength is measured from the reflectivity and transmission of all-semiconductor cavities directly grown by MOCVD, consisting in quantum wells imbedded between two DBR quarter-wave stack mirrors. We have then a very interesting physical situation, that of coupled oscillators : photons are well-known to be describable in terms of quantum oscillator modes (this is the very field of quantum electrodynamics QED). One of such modes - the resonant one - is singled out in a cavity ; excitons are excitations of semiconductor crystal with a well defined energy, and can also be described as harmonic oscillators from the point of view of their optical response. These two oscillators, one optical and the other "mechanical", are coupled through the usual light-matter interaction. Semiconductor cavities actually provide a very versatile implementation of such coupled oscillators : as the growth speed is non-uniform, samples are wedge-shaped, and the FP frequency continously shifts over the sample. One can therefore study the resonance behaviour of the coupling between excitons and photons by measuring the optical response of different points on the sample ; the strength of the exciton-photon coupling can also be changed from

sample to sample by the choice of the number of QW's in the cavity.

It is well-known that, independantly of their physical nature, capacitively (i.e. dispersion)coupled oscillators exhibit a two-mode splitting at resonance : under such conditions, energy is periodically switched back and forth between the two oscillators, at a rate given by the coupling strength Ω. This is the usual Rabi oscillation of atomic systems under a strong electromagnetic field. The optical response of the coupled system then yields two frequencies, separated by Ω. Figures 1 and 2 display the reflectivities of several points on a microcavity and the peak positions around the resonance respectively.

This experiment has significance both for fundamental physics and device applications. Fundamentally, it demontrates the strength of the exciton-photon coupling in the microcavity, recently evidenced up to room temperature. Device-wise, these experiments show at once that : (i) a few QW's can control the optical response of high-Q microcavities : (ii) under resonant conditions, a coupled-mode phenomenon develops.

It should be remarked that several devices have structures very similar to the ones reported here : Vertical-Cavity Surface Emitting Lasers (VCEL's), Fabry-Perot electro-optic modulators, Non-Linear optical etalons. They all take advantage in some respect of the device improvement brought along by resonant cavity modes . They however so far never relied on the QED effects reported here, i.e. the resonant interaction of a single photon mode with excitons. What is expected from such effects is much better devices such as an exciton laser, or electro-optic or non-linear devices with just a few QW's, instead of the usual ≈ 100 QW's. It then means that the figure of merit is largely increased due to the diminished active volume. Also, coupled-modes should prove very sensitive to any external perturbation, be it an electric field or a saturation optical beam.
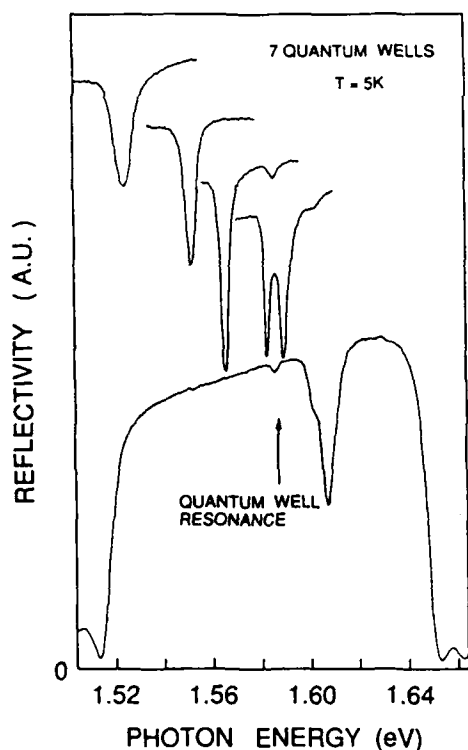

Fig.1 : QW microcavity reflectivity curves for various detuning conditions between cavity and QW exciton frequencies, obtained by choosing various points on the wafer. Note the line narrowing approaching and at resonance, the resonance mode splitting, and the indication of a light-hole exciton mode splitting around 1.605eV.
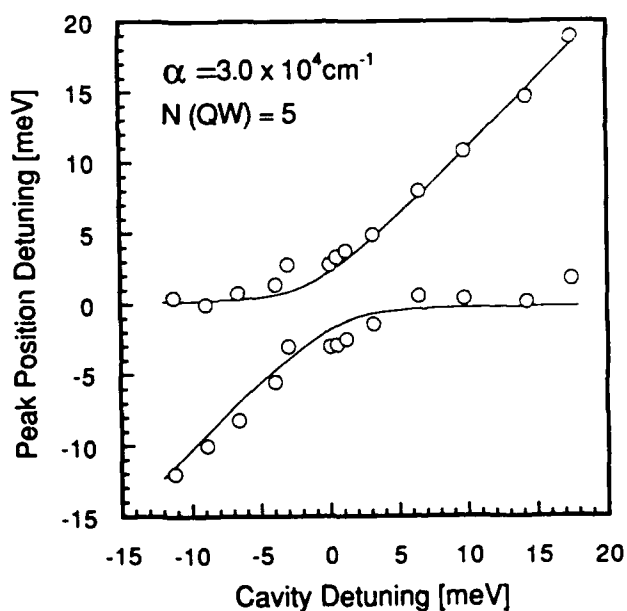
Figure 2 : Variation of the reflectivity peak positions as various points on the sample are tested, allowing various values of the detuning between excitons and cavity photons

Threshold Dependence on Cavity Length and Mirror Reflectivity in Fabry-Perot Microcavity Semiconductor Lasers with High Contrast Mirrors

D.L. Huffaker, D.G. Deppe, C.J. Pinzone, T.J. Rogers, B.G. Streetman, and R.D. Dupuis

Microelectronics Research Center
Department of Electrical and Computer Engineering
The University of Texas at Austin, Austin, Texas 78712-1084
Phone: (512) 471-4960

There is currently a great deal of interest in the use of small optical cavities to control the spontaneous emission characteristics from semiconductor light emitting diodes and lasers. Predictions of the magnitude to which the effect may be realized range from novel forms of lasers having "zero-threshold", to skepticism as to whether controlled spontaneous emission may impact practical devices at all since it simply represents "filtering". Therefore, experimental investigations which elucidate the role controlled spontaneous emission may play in present day realizable device structures are needed.

Recent calculations and predictions suggest that even in room-temperature Fabry-Perot semiconductor microcavity lasers, controlled spontaneous emission may play a significant role in setting lasing threshold.[1,2] The degree to which the cavity will influence the light emission properties of the gain region depends on the cavity length and mirror reflectivity. The effective cavity length is sensitive to the mirror design. We present data of experimental studies of various Fabry-Perot semiconductor microcavity lasers, which investigate the threshold dependence of lasing on cavity length, mirror reflectivity, and transverse loss in the laser cavity.

Assuming the optical gain of the semiconductor active region must equal the photon loss from the cavity, the threshold gain, g_{th}, can be expressed as

$$g_{th} = \alpha_{tr} - (1/2l_g)\ln(R_1 R_2), \qquad (1)$$

where l_g is the gain path length, R_1 and R_2 are the mirror reflectivities of the cavity and α_{tr} is the transverse loss of the lasing mode. The transverse loss is sensitive to cavity length through diffraction losses. We have investigated the lasing characteristics of two different epitaxial structures. The layer design allows laser fabrication on the same wafer of cavities with two different lengths, onto which high-contrast mirrors of varying number of pairs of CaF/ZnSe are deposited. The first layer structure consists of a $\lambda/2$ thick GaAs active region with etch stop layers to allow fabrication of either a λ-spacer (~0.28μm) or a 40λ-spacer (~10μm) on the sample. The second layer structure contains a GaAs-InGaAs three quantum well (QW) active region with etch stop layers of to fabricate either a λ-spacer or a 18λ-spacer cavity on the same sample. Design of the epitaxial layers is directed towards achieving identical optical pumping of the comparison cavities using a mode-locked Ti:Al$_2$O$_3$ laser. Processing of the laser structures is similar to that published previously.[3] Fabricating comparison cavities on the same sample insures identical mirror characteristics on the long cavities when compared to the short cavities, as well as nearly identical active regions. By fabricating the short cavities in 100μm "pits", long cavity lasers can be compared with short cavity lasers which are separated by only a few hundred microns in distance on the epitaxial film. The lasers are characterized while varying mirror reflectivity from low values in which lasing is not achieved (~3 pairs on each side) to high reflectivity

saturated by mirror loss. Lateral loss due to diffraction is measured by varying the excitation spot size from the Ti:Al$_2$O$_3$ pump laser.

Reduced threshold is found in the short cavity lasers versus the long cavity lasers in all structures measured. Ratios of the long-to-short cavity thresholds vary with the pump spot size and mirror reflectivity values, but saturate for large spot sizes (~50μm diameter) and high reflectivity (6 pairs on each side). Despite a 60% longer gain path in the long cavity with the GaAs active region, the threshold ratio of the long-to-short cavity saturates at a factor of ~2. For the InGaAs-GaAs QW active region, the long-to-short cavity threshold ratio saturates at a factor of ~4. For the cavity with the GaAs active region, little difference is measured in the integrated spontaneous emission, while significant increase is found for the cavity with the InGaAs-GaAs QW active region. Possible reasons for this will be suggested. The talk will focus on differences in the spontaneous emission characteristics from the laser cavities, lateral loss effects, mirror loss effects, heating effects, and overlap of the gain spectrum with the cavity modes.
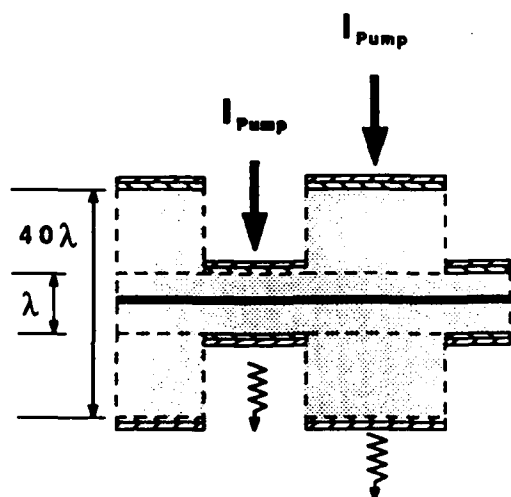
Fig.1 Schematic illustration of the the processed structures for long and short comparison cavities for the GaAs/AlGaAs microcavity.
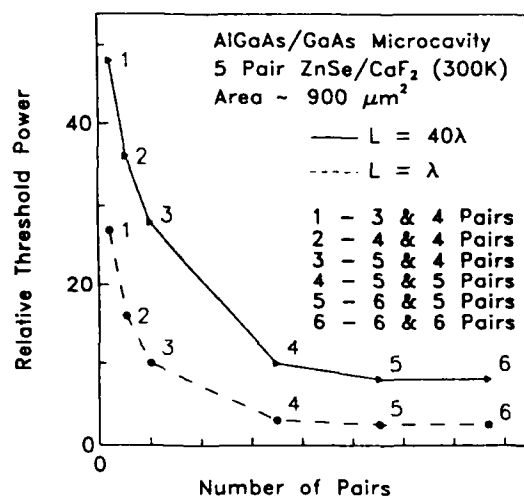
Fig. 2 Plot of relative threshold pump power for the long (solid line) and short (dashed line) GaAs/AlGaAs Fabry-Perot microcavities. For all samples of varying mirror reflectivity and pump area short cavity lasers are found to have lower thresholds by at least a factor of ~2.

1.   D.G. Deppe, T.J. Rogers, and B.G. Streetman, 48th Annual Device Research Conference, June 26, 1990, Santa Barbara, post-deadline paper VB-3.

2.   D.G. Deppe and C. Lei, Appl. Phys. Lett. **60**, 527 (1992); C.Lei and D.G. Deppe, J. Appl. Phys. **71**, 2530 (1992).

3.   D.L. Huffaker, C. Lei, D.G. Deppe, C.J. Pinzone, J.G. Neff, and R.D. Dupuis, Appl. Phys. Lett. **60**, 3203 (1992).

Asymmetric Gain in a Vertical-Cavity Surface-Emitting Laser

F. Brown de Colstoun, C. W. Lowry, G. Khitrova, H. M. Gibbs

Optical Sciences Center, University of Arizona, Tucson, Arizona 85721, (602) 621 4903

A. E. Paul

Department of Physics, University of Arizona, Tucson, Arizona 85721

S. W. Koch

Department of Physics and Optical Sciences Center, University of Arizona, Tucson, Arizona 85721

T. M. Brennan, B. E. Hammons

Division 1164, Sandia National Laboratories, Albuquerque, New Mexico 87185

The gain spectrum of a semiconductor can be locally modified by a strong nearly resonant laser field through population pulsations.[1,2] Rayleigh-gain, an asymmetric modification of the gain profile of an atom, has been investigated previously.[3,4] Laser diode longitudinal modes have been used to show gain asymmetry[1,5], but the mode spacing (75 GHz[5]) has limited the observation to the periphery of the curve. Mapping the more closely spaced gain peak and dip is important because they can significantly modify the output spectrum of a laser (creating new lasing lines at the new gain peak and extinguishing the original lasing with the gain dip). Pump/probe experiments in traveling wave amplifiers (TWA)[6] have shown the gain to be asymmetric, but the gain peak and dip were broadened because the injected signal grew in power (from $\simeq 87\mu$W to 4.4mW[6]) during propagation. Using a high Q vertical-cavity surface-emitting laser (VCSEL) as the gain medium we have intracavity powers at the injected frequency that do not grow with propagation and are much higher than the TWA experiments (up to 75 mW in a 5 μm spot), pushing the gain peak as far as 36.5 GHz from the injected frequency. Rather than using longitudinal modes to probe discretely the gain asymmetry, when the gain extrema are within 10 GHz of the injected frequency we directly observe localized dips and peaks in the continuous ouput spectrum of the VCSEL. As increased injected power pushes the gain extrema out further, we observe modification of the line shape and pushing of the lasing. We find that the detuning of the gain extrema from the injected frequency increases linearly with the intracavity intensity at the injected frequency (in contrast with relaxation oscillations and other effects that scale with the field level). Understanding local modifications of the cw gain profile is of crucial importance to elucidate instabilities in semiconductors lasers.

We used an electrically pumped VCSEL that lased at 830 nm with a threshold of 5.6 mA. This sample was grown by MBE at Sandia National Laboratories. In our experiment, the VCSEL was operated just above threshold (output power = 100 μW), and the lasing line (dotted, on Fig. 1 and 3) was 7.2 GHz FWHM (the line narrows to $\simeq 1$ GHz with increased pumping). Gain asymmetry is seen in the modification of the continuous emission spectrum of the VCSEL; we directly measure the frequencies of the gain peak and dip and their evolution with increased injected power. In Fig. 1 the injected signal is at $\nu_{inj} = \nu_{vc}$-3.6 GHz, with intracavity power at the injection frequency in the 1 to 20 mW range (solid lines). A region of the VCSEL lasing is reduced on the high frequency side of the injected signal, with minima ranging from $\nu-\nu_{inj}$=1.4 to 4 GHz. At the same time, a region of the VCSEL lasing line is enhanced on the low frequency side of the injected signal, with a narrow peak appearing at $\nu-\nu_{inj}$= -2 GHz. For the two curves corresponding to the two lowest injected powers, the gain modification is localized (≤ 8 GHz wide), leaving edges of the lasing lines largely unaffected.

With higher injected power the gain dip becomes deeper and moves to higher frequency. Note that both the localized asymmetry and movement of the dip to higher frequency lead us to believe that the gain asymmetry cannot be explained by a red shift of the lasing brought on by total carrier-density reduction. Rather it is a local modification of effective gain.
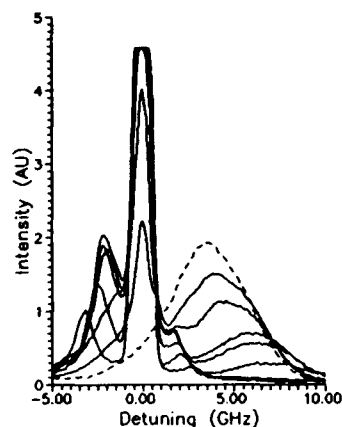

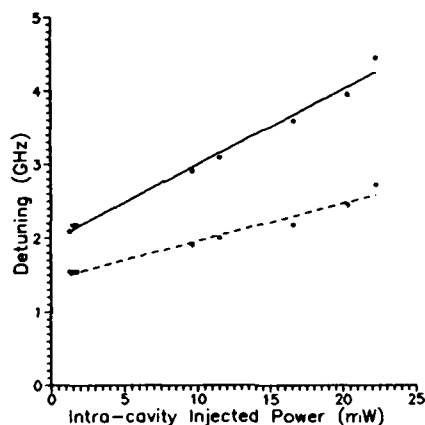**Fig. 1:** *The original VCSEL spectrum (dashed) is modified (solid) by increased injection power.*

Fig. 2: *Detunings of the gain peak (solid) and dip (dashed) are linear with intracavity injected power.*
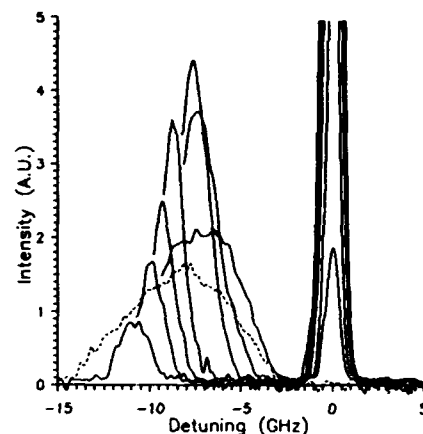
Fig. 3: *A gain peak appears at v_{inj}-7 GHz and is pushed to lower frequencies with increased injection.*

Lasing at the new peak of the gain curve can be pushed away from the injected frequency, proportional to the intracavity power at the injected frequency. As the injected power is increased, Fig. 1, the gain peak and dip increase in magnitude and spread out linearly in frequency. In Fig. 2 we show measured detunings and calculation from a corresponding quantum mechanical theory[2]. The intracavity power at the injected frequency was obtained by integrating the VCSEL output spectrum near the injected frequency and dividing by the VCSEL mirror transmittance, $T \simeq 0.005$. Detunings greater than the width of the VCSEL lasing were measured by tuning the injected frequency [Fig. 3] such that the gain peak fell within the VCSEL lasing line. As the injected power was increased, first pulling and then pushing of the lasing peak was seen. The detuning was pushed out by high injected powers to 36.5 GHz.

In summary, we have injected a cw laser beam into the Fabry-Perot peak of a cw VCSEL. Within the broad lasing line of the VCSEL pumped just above threshold we have seen dips in the lasing spectrum on the high energy side of the injected frequency and lasing peaks on the low energy side, giving strong evidence for asymmetric modification of the gain. We have measured detunings of the gain dips and peaks to be proportional to the intracavity power at the injected frequency which agrees with our analysis of recent gain asymmetry theory. The gain peak has been pushed out to 36.5 GHz from the injected frequency, further than theoretical and experimental results of the past.

References:
1.   A. P. Bogatov, P. G. Eliseev, and B. N. Sverdlov, IEEE J. Quant. Electr. QE-11, 510 (1975).
2.   A. E. Paul, M. Lindberg, S. An, and M. Sargent III, Phys. Rev. A 42, 1725 (1990).
3.   S. Haroche and F. Hartman, Phys. Rev. A 6, 1280 (1972).
4.   G. Khitrova et. al. and M. T. Gruneisen et. al., J. Opt. Soc. Am. B 5, 160 and 123 (1988).
5.   S. R. Chinn, App. Phys. Lett., 59 1673 (1991).
6.   K. Inoue, T. Mukai and T. Saitoh, Appl. Phys. Lett. 51, 1051 (1987).

Modulators 1

QWB 10:30am–12:00m
Oleander Room

David A. B. Miller, *Presider*
AT&T Bell Laboratories

Interleaved-contact electroabsorption modulator using doping-selective electrodes with 25 °C to 95 °C operating range

K.W. Goossen, J.E. Cunningham, W.Y. Jan, and D.A.B. Miller

AT&T Bell Laboratories, room 4B-519, Crawfords Corner Rd., Holmdel, NJ 07733

(908)949-6979   fax:(908)949-2473

As the number and bandwidth requirements of connections to integrated circuit chips approach thousands and hundreds of megahertz, respectively (which is occurring now), the capability of standard electrical chip input/output becomes strained. For this reason optical input/output to chips is being explored by a number of groups.[1] In modulator systems, an off-chip laser would be split into an array of beams that illuminates an array of surface-normal modulators. The modulators would be switched by the on-chip electronics to imprint information on the reflected beams. Multiple quantum well (MQW) modulators are attractive because they can produce large enough absorption changes in surface-normal devices with good yields, low intrinsic power dissipation and apparently good reliability. Since the modulators are p-i-n type devices they are also efficient input detectors. 64x64 arrays of operational modulators have been demonstrated.[2] Reliable modulators have also been demonstrated on silicon.[3]

A problem with such modulators, however, is their narrow usable wavelength range, which results in a small operating temperature range. The optical bandwidth is set by how far the exciton shifts due to the quantum-confined Stark effect.[4] The exciton can shift up to 30 nm without significant broadening, but this requires fields greater than 20 volts/μm.[5] Since for reasonable reflectivity changes the i region must be about 1 μm thick, this results in prohibitively large voltage requirements. Furthermore such high voltages (V) would result in large heat dissipation ($P=V \cdot I_p$) from the photocurrent (I_p). Here we present a solution to this problem. The i region may be made thinner, reducing voltage requirements, if several diodes are stacked (a n-i-p-i....), and electrically driven in parallel. The optical path length, and hence the reflectivity change, may be made large by increasing the number of i regions. This does result in a higher capacitance, which leads to systems designers' choice of trade-offs between voltage, temperature and wavelength operating range, and capacitance. We estimate the capacitance of our device would be 200 fF for a typical 10x10 μm mesa. Such a capacitance is still easy to drive electronically and is much less than the capacitance's of conventional electrical bond pads and interconnections.

There are five MQWs in our device (Fig. 1) consisting of 20 periods of 95 Å GaAs wells and 50 Å $Al_{0.4}Ga_{0.6}As$ barriers. The doped layers consist of $Al_{0.4}Ga_{0.6}As$ with a central 200 Å p^+ layer clad on either side by 200 Å p^- layers. The contacting scheme has been previously demonstrated by us for a surface-normal refractive modulator, which also requires high fields.[6] 200x200 μm mesas with sloping sidewalls were etched down to the mirror. Then AuZn and AuSn electrodes were deposited along the sidewalls as shown, and annealed at 420 °C. for 1 minute. Since Zn(Sn) is a p(n)-type dopant in AlGaAs, a $p(n)^+$ region is formed under the AuZn(Sn) contact, resulting in an ohmic contact with all the p(n)
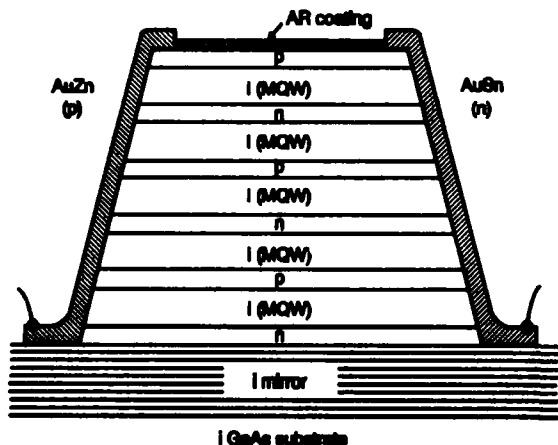

Fig. 1: Schematic of our modulator. A $p^+(n^+)$ region forms under the AuZn(AuSn) electrodes, forming selective contacts to the p(n) layers. Each MQW consists of twenty periods.
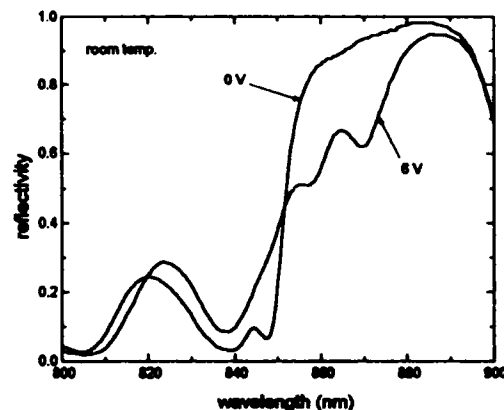

Fig. 2: Reflectivity spectra for sample at 0V and 6V p-n reverse bias. The heavy-hole exciton shifts from 848 nm at 0V to 870 nm at 6V.

layers and a rectifying contact with the n(p) layers. The p-n conduction shows clear diode behavior, albeit with some leakage under reverse bias (90 μA at 4V and 0.5 mA at 6V). This is probably due to tunneling current from the $p^+,(n^+)$ regions under the electrodes to the $n^+(p^+)$ contact layers.

The reflectivity (Fig. 2) of the sample was measured with a lamp/monochromator. This is shown in Fig. 3 for room temperature. The reflectivity of the mirror extends from 900 nm to shorter wavelengths and is reduced near 848 nm for 0 V by the heavy-hole exciton. Upon applying a reverse bias of 6V the heavy-hole exciton shifts more than 20 nm. This shift is consistent with that previously observed for the same fields in p-i-n samples.[4] The reduction in strength of the exciton with field is also consistent with earlier observations. A change in

Fig. 4: Change in reflectivity for a 0 to 6 volt swing as a function of wavelength for different temperatures.

reflectivity > 20 % is obtained over a bandwidth of 20 nm. Note that larger changes in reflectivity may be achieved at the same voltage by increasing the number of intrinsic regions, albeit with an increase in capacitance. In Fig. 3 we show the change in reflectivity for a 0 to 6 V swing at different temperatures from 25 °C to 95 °C. The wavelength for which maximum ΔR is achieved at 25 °C or 95°C is 875.9 nm, shown by the arrow. The insert of Fig. 3 shows ΔR as a function of temperature for this wavelength. Greater than 22 % ΔR is achieved from 25 °C to 95 °C, with a maximum of 37 % ΔR at 47 °C.

In conclusion, we have demonstrated an interleaved-contact n-i-p-i electroabsorption modulator. This modulator allows broad operating wavelength or temperature ranges without requiring high voltage drive. It relies on using several thin MQW absorbing regions, each operating at high field with consequent large absorption edge shifts. We have shown > 22 % change in reflectivity for a 0 to 6 volt swing for either a 25 °C to 95 °C temperature range at 875.9 nm or for a 15 nm wavelength range at 25 °C. Operating voltage could be reduced by using thinner intrinsic regions. Alternatively, if voltage was kept constant this would result in increased wavelength or temperature range because of larger Stark shifts. Reflectivity change could be increased by using more intrinsic regions. In all cases the trade-off is higher capacitance and a more complex, thicker structure. It appears that the capacitance of a small device is still low by normal electrical output standards, and we are not near any limit in the thickness or complexity of crystal growth, so the outlook for such further improved designs is promising.

REFERENCES

[1] For a compilation of recent work, see the proceedings of the 1992 Topical Meeting on Smart Pixels, Optical Society of America publications, Washington DC.

[2] A.L. Lentine, F.B. McCormick, R.A. Novotny, L.M.F. Chirovsky, L.A. D'Asaro, R.F. Kopf, J.M. Kuo, and G.D. Boyd, "A 2 kbit array of symmetric self-electrooptic effect devices," IEEE Photon. Technol. Lett., vol. 2, p. 51, 1990.

[3] K.W. Goossen, G.D. Boyd, J.E. Cunningham, W.Y. Jan, D.A.B. Miller, D.S. Chemla, and R.M. Lum, "GaAs-AlGaAs multiquantum well reflection modulators grown on GaAs and silicon substrates," IEEE Photon. Technol. Lett., vol. 1, p. 304, 1989.

[4] D.A.B. Miller, D.S. Chemla, T.C. Damen, A.C. Gossard, W. Wiegmann, T.H. Wood, and C.A. Burrus, "Electric field dependence of optical absorption near the band gap of quantum well structures," Phys. Rev. B, vol. 32, pp. 1043-1060, 1985.

[5] A.M. Fox, D.A.B. Miller, G. Livescu, J.E. Cunningham, and W.Y. Jan, "Quantum well carrier sweep out: relation to electroabsorption and exciton saturation," IEEE J. Quantum Electron., vol. 27, pp. 2281-2295, 1991.

[6] K.W. Goossen, J.E. Cunningham, and W.Y. Jan, "GaAs-AlAs low-voltage refractive modulator operating at 1.06 μm," Appl. Phys. Lett., vol. 57, p. 744, 1990.
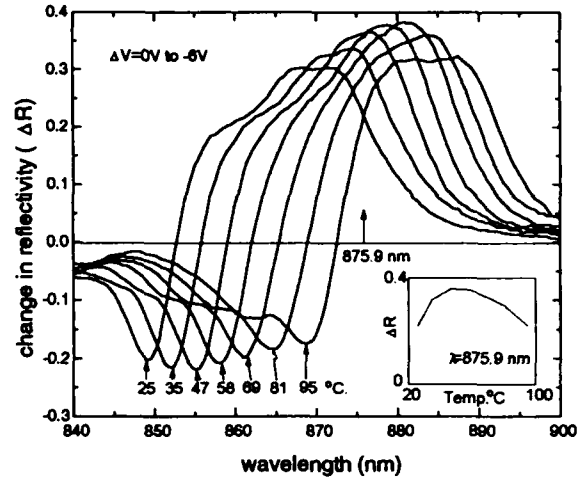
Functionally All-Optical Bistable *p-i-p-i-n* Device with Asymmetric GaAs/AlAs Coupled Quantum Well Absorption Layers and an AlAs Resistive Layer

Yasunori Tokuda, Yuji Abe, and Noriaki Tsukada
Central Research Laboratory, Mitsubishi Electric Corporation,
8-1-1, Tsukaguchi Honmachi, Amagasaki, Hyogo, 661 Japan
TEL +81-6-491-8021   FAX +81-6-497-7288

Optical bistabilities have been receiving considerable attention for potential application in future ultra-high performance information processing. Especially an all-optical bistable function, which can be achieved at low input power, seems to be very promising.[1]

In this work, we demonstrated a functionally all-optical bistable device by using a novel *p-i-p-i-n* structure. The operation mechanism is explained in terms of the bistable response of a coupled quantum well (CQW) photodiode with an inner feedback region by making good use of the built-in voltage, i.e., a non-biased self-electro-optic effect device (SEED)[2] without any external feedback element. The experiments on optical measurements were made at 77 K by using cw light from a titanium:sapphire laser pumped by an argon ion laser.

First we considered a way of making the SEED operate without any bias supply. The open circles in Fig. 1 show the applied-voltage dependence of the wavelength and intensity of the longest-wavelength absorption peak of a *p-i-n* photodiode with the asymmetric CQW elements, which consist of 60- and 100-Å-thick GaAs wells separated by 8-Å-thick AlAs barriers. The data were taken from the photocurrent spectra. As a reference, solid circles denote the data of an uncoupled quantum well photodiode. It should be noticed that the larger changes of the absorption characteristics in both the peak wavelength and intensity are obtained for the CQW diode. The results can be interpreted in terms of a resonance around - 0.2 V of the lowest
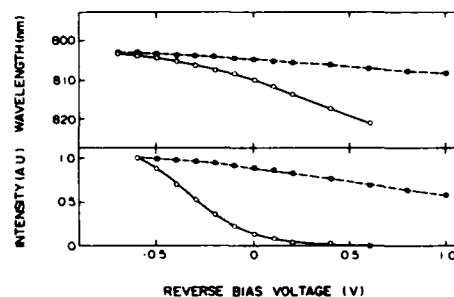

FIG. 1 Bias dependence of wavelengths and intensities of the longest-wavelength absorption peaks in a *p-i-n* photodiodes with coupled (open circles) and uncoupled (solid circles) quantum well absorption layers. The reverse bias is positive.
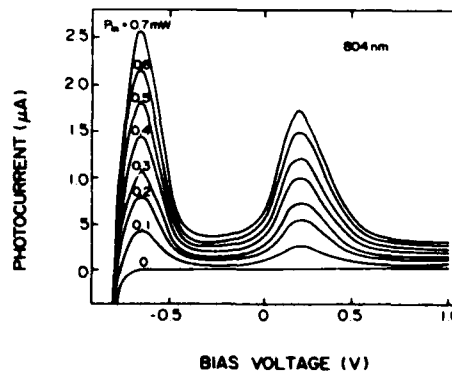

FIG. 2 Photocurrent-bias characteristics of the CQW *p-i-n* photodiode for various optical input powers, P_{in}. The incident light wavelength is 804 nm. The appearance of two current bumps is due to the anticrossing.

quantized electron levels in the respective quantum wells, i.e., an anticrossing of the optical transitions.[3]

These remarkable interwell coupling effects can multiplicatively modulate the electroabsorption characteristics, and thus induce a sharp photocurrent bump in the forward bias region for the incident light of appropriate wavelengths, as shown in Fig.2. By taking advantage of the characteristics of the present CQW photodiode, we could obtain a bistable responses with no bias supply only by using a resistive load.

Next we investigated a means of vertical integration of an effective feedback element into the CQW photodiode. For the present material system, we consider to utilize an intrinsic AlAs layer as a resistor-like load layer. A p-i-p-i-n sample as shown in Fig. 3 was prepared by molecular beam epitaxy on an n-type GaAs substrate. The upper intrinsic layer embedded in the p-type $Al_{0.33}Ga_{0.67}As$ region consists of 1000-Å-thick AlAs, whereas twelve pairs of the similar asymmetric CQWs, which are composed of 60- and 100-Å-thick GaAs wells
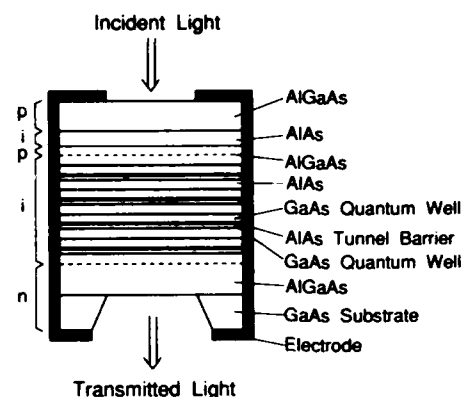

FIG. 3 A p-i-p-i-n device with asymmetric CQW optical absorption layers and an AlAs resistive layer.
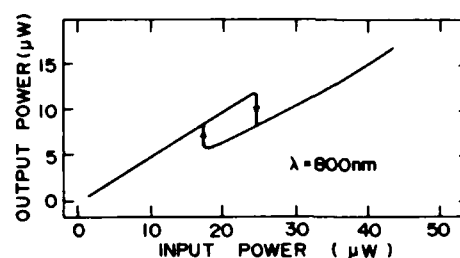
FIG. 4 Output power as a function of input power for the incident wavelength of 800 nm.

separated by 4-Å-thick AlAs barriers, are inserted in the lower intrinsic region between the p- and n-type $Al_{0.33}Ga_{0.67}As$ layers. The substrate was selectively etched away. The upper and lower electrodes with ~ 800 $\mu m\phi$ optical windows electrically connect through the side facet by a conductive paste.

Figure 4 shows the optical output power as a function of the optical input power for the incident wavelength of 800 nm. A clear optical bistable region was obtained at the input power range between as low as 17.5 and 25 μW. The result is due to the fact that the intrinsic AlAs layer acts as a resistive layer for holes.

To conclude, we demonstrated an all-optical bistable device with a p-i-p-i-n structure. The features such as the low power operation and the planer structure seem to be attractive for the two-dimensional optical data processing. In addition, the bistable operation at room temperature could be achieved for a similar device in our recent work.

REFERENCES

1. H. M. Gibbs, Optical Bistability: Controlling Light with Light (Academic, New York, 1985).

2. D. A. B. Miller et al., IEEE J. Quantum Electron. QE-21, 1462 (1985).

3. Y. Tokuda et al., Appl. Phys. Lett. 54, 1232 (1989); Phys. Rev. B41, 10280 (1990).

Visible Wavelength LEDs and Reflection Modulators with

AlGaAs/AlAs Quantum Wells

B. Pezeshki, J. A. Kash
IBM T. J. Watson Research Center, Yorktown Heights, NY 10598 (914) 945-1443

Daxin Liu, S. M. Lord, and J. S. Harris Jr.
Solid State Laboratories, Stanford University, Stanford, CA 94305-4055

Since most direct gap semiconductors have bandgaps in the infra-red, there is considerable effort in extending the operation of devices into the visible. In this work we show how indirect gap AlGaAs/AlAs quantum wells (QWs) can be suitable for the fabrication of reflection modulators and LEDs. We demonstrate a modulator with a 30% reflectivity change and a room temperature LED.

Though these QWs have an indirect bandgap, the indirect absorption is far weaker than the higher energy direct excitonic absorption. Consequently, large absorption changes can be obtained by shifting the excitonic absorption using the quantum-confined Stark effect[1,2]. We show that these QWs can be suitable for the fabrication of asymmetric Fabry-Perot modulators[3], despite the difficult material and growth characteristics[4]. Using an in-situ reflectivity monitoring scheme[5], we fabricate a reflection modulator with $Al_{0.45}Ga_{0.55}As/AlAs$ QWs in the active region and $Al_{0.6}Ga_{0.4}As/AlAs$ quarter wave layers as the back mirror. The position of the Fabry-Perot resonance was adjusted by etching the cavity after device fabrication. The reflectivity spectrum is shown in Fig. 1. The performance of the device is limited by a low back mirror reflectivity and quantum well interface roughness, both of which can be improved by using thin smoothing layers.

The LED structure is a simple p-i-n diode with 35 x 75 Å $Al_{0.4}Ga_{0.6}As$ quantum wells and AlAs barriers. The 300K electro-luminescence spectrum displayed a bright orange peak at 625 nm (Fig. 2). The band diagram in Fig. 3 shows that the strong luminescence originates from the direct bandgap in the AlGaAs, even though the lowest electron energy state is lower by 160 meV in the AlAs X valley.

The low temperature photoluminescence spectrum, shown in Fig. 4, is similar to previous results[6]. Since the carriers are generated in the direct gap and take a picosecond to scatter to the lower energy X minima, both direct and indirect gap luminescence is present. The temperature dependence of these peaks (Fig. 5) shows a strong increase in the direct gap recombination at higher temperatures.

This unusual increase in luminescence can be explained by the thermal excitation of electrons from the low energy X valley to the higher energy direct gap state. The efficiency of this process is much greater than expected since the carrier lifetime is very much longer in the indirect minima than in the quantum well. Thus the AlAs X minima act as reservoirs for the radiative recombination in the direct gap. Since our sample was grown at a low temperature, the scattering to trap states seriously limited our carrier lifetime and efficiency. We measured the lifetime to be reduced to 30 nS at room temperature yielding a calculated efficiency of about 3%. This number can be substantially improved by optimizing the growth parameters.

In conclusion, we have demonstrated that indirect gap AlGaAs/AlAs quantum wells can be suitable for room temperature optoelectronic devices such as reflection modulators and LEDs, with the current performance limited by the material quality.

(1) K. W. Goossen, R. H. Yan, J. E. Cunningham, and W. Y. Jan, Appl. Phys. Lett. **59** (1991) 1829.
(2) B. Pezeshki, S. M. Lord, T. B. Boykin, B. L. Shoop, and J. S. Harris Jr., Electron. Lett. **27** (1991) 1971.
(3) R. H. Yan, R. J. Simes, L. A. Coldren, A. C. Gossard, Appl. Phys. Lett. **56** (1990) 1626.
(4) M. T. Asom, M. Geva, R. E. Leibenguth, S. N. G. Chu, Appl. Phys. Lett. **59** (1991) 976.
(5) K. Bacher, B. Pezeshki, S. M. Lord, and J. S. Harris Jr., Appl. Phys. Lett. **61** (1992) 1378.
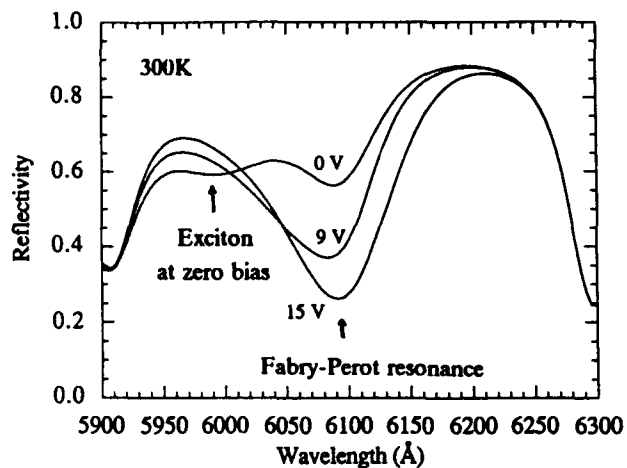(6) J. Feldman et al., Phys. Rev. B. **42** (1990) 5809.

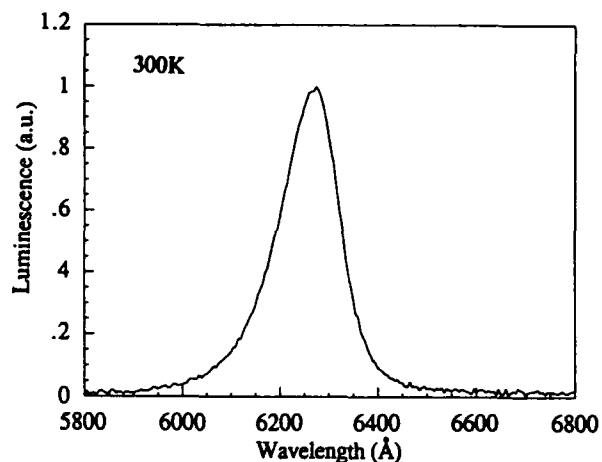Fig. 1: Normalized reflectivity of modulator at various reverse bias voltages
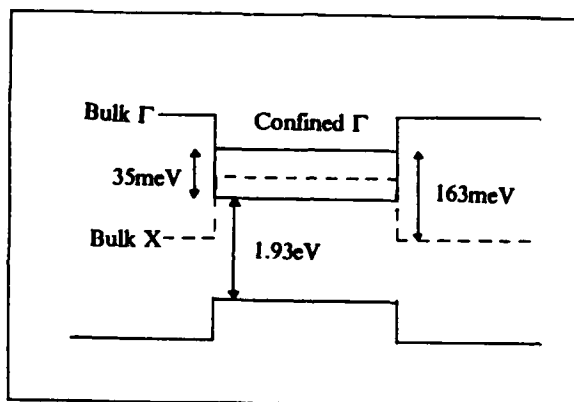

Fig. 2: Electro-luminescence of AlGaAs/AlAs QWs

Fig. 3: Approximate 300K band diagram of Al$_{0.4}$Ga$_{0.6}$As/AlAs QWs
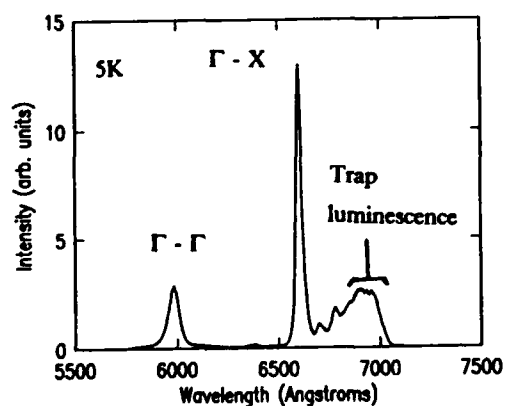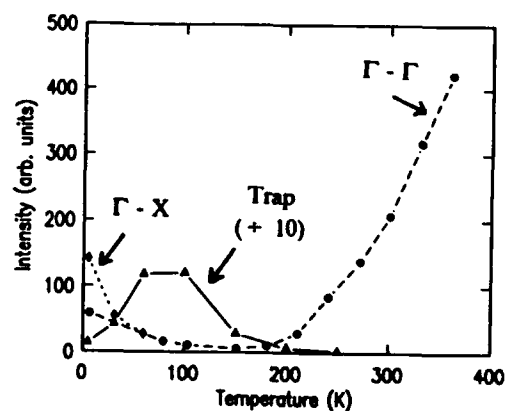

Fig. 4: Low temperature PL spectra

Fig. 5: Temperature dependence of PL peaks

Responsivity and Excitonic Electroabsorption in Proton-Implanted GaAs/AlGaAs Multiple Quantum Well Modulators

T. K. Woodward[a], B. Tell[b], W. H. Knox[a], J. B. Stark[b], M. T. Asom[c]

AT&T Bell Laboratories

[a] *Holmdel, NJ 07733,* [b]*Murray Hill, NJ 07974,* [c]*Breinigsville, PA 18031*

Heavily implanted MQW structures have not been examined as a function of applied bias in a *pin* geometry. Such studies address the interesting physical question of whether phenomena such as sharp excitons and quantum confined stark effect (QCSE), normally associated with ultra-clean material can persist amid the controlled introduction of defects.[1] We have studied several such MQW *pin* samples, each of which was grown on a quarter-wave dielectric reflecting stack mirror consisting of $Al_{0.11}Ga_{0.89}As$ and AlAs layers. Devices contained 60 periods of GaAs quantum wells 100 Å thick with 60 Å $Al_xGa_{1-x}As$ barriers having mole fractions of x=0.3, 0.45, and 1.0. Devices were implanted with roughly 130 keV protons, focusing the damage into the intrinsic regions, to dose levels of $1 \times 10^{12}\,cm^{-2}$, $1 \times 10^{13}\,cm^{-2}$, and $1 \times 10^{14}\,cm^{-2}$. Large-area mesa devices were then fabricated from these structures via standard lithographic techniques. We have previously reported the behavior of x=0.3 barrier samples.[2]

In accord with previous studies of proton implanted materials, we have found that the carrier lifetime is significantly reduced in implanted samples.[3, 4] Measurements of x=0.3 barrier samples show lifetimes of 65 ps, 6 ps, and 300 fs in the samples implanted to $1 \times 10^{12}\,cm^{-2}$, $1 \times 10^{13}\,cm^{-2}$, and $1 \times 10^{14}\,cm^{-2}$, respectively. The effect of this reduction in carrier lifetime is a suppression of the carrier collection efficiency, as measured by reduced responsivity of these *pin* devices when viewed as detectors. This has significant implications for electrically addressed modulators.[5] This suppression of responsivity is summarized in Fig. 1, which plots the peak 10 V responsivity as a function of implant dose in antireflection coated versions of the three samples. As can be seen, responsivity is strongly affected by both implant dose and Al mole fraction, which suggests that the origin of the effect is recombination of carriers in the quantum wells of the device, since quantum well escape times depend on barrier height.[6] Thus, quantum confinement is critical to suppressing responsivity in these structures. We focus now on the AlAs barrier sample.
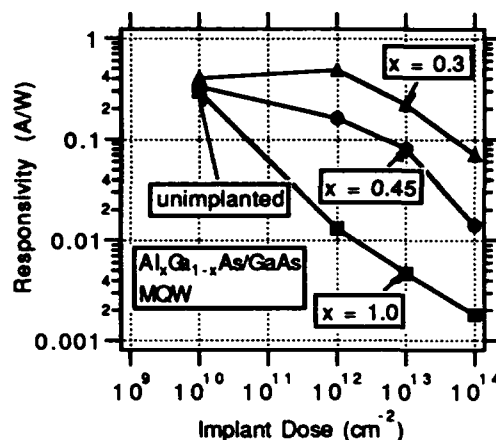

Figure 1: The peak longer-wavelength AR-coated responsivity of samples with $Al_xGa_{1-x}As$ barriers of x = 0. 3, 0. 45, and 1. 0, as a function of implant dose at 10 V.

Reflectivity spectra of AR-coated AlAs barrier samples are shown in Fig. 2. Two features of these graphs are compelling. Initially, we note that the zero-bias absorption feature is essentially unchanged until an implant dose of $1 \times 10^{14}\,cm^{-2}$ is reached, somewhat at variance with earlier data, in which noticable broadening could be observed at $1 \times 10^{13}\,cm^{-2}$.[3] This may be due to the use of AlAs barrier material, as opposed to the earlier x=0.29 case. Secondly, we note that excitonic electroabsorption, or QCSE, persists, even to the $1 \times 10^{14}\,cm^{-2}$ implant dose, as seen in the 12.5 V data. However, 12.5 V data show considerable broadening that increases with implant dose. We speculate that it arises from inhomogeneous effects caused by: 1) microscopic random fields in each well introduced by charged trap centers, and/or 2) variation in the field distribution in the intrinsic region of the device.

To investigate this phenomena, as well as to determine whether the responsivity suppression evidenced in Fig. 1 is saturable, we measured the re-
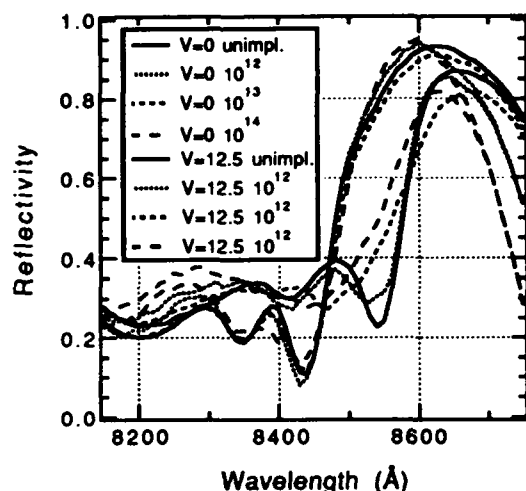
Figure 2: Reflectivity spectra for AlAs barrier devices implanted to levels of 0, $1 \times 10^{12} \, \text{cm}^{-2}$, $1 \times 10^{13} \, \text{cm}^{-2}$ and $1 \times 10^{14} \, \text{cm}^{-2}$.

flectivity and responsivity of the AlAs-barrier sample as a function of incident intensity. To avoid thermal effects, studies were performed with low duty cycle gain-switched semiconductor laser pulses (10 ns pulses with 1000 ns repetition rates). Responsivities did not increase with intensity to at least 60 kW/cm^2. In fact, they showed a decrease because of exciton saturation effects. Exciton saturation intensity was determined by measuring the reflectivity of the device as a function of incident power, at a bias level which brought the exciton peak into alignment with the laser. For both unimplanted and $1 \times 10^{13} \, \text{cm}^{-2}$ implanted devices, this bias level was 8 V. In Fig. 3, we plot a fit through over 500 points of reflectivity vs. incident power for these two devices. Clearly, reflectivity begins to deviate from its low intensity value at a much lower level in the unimplanted device than the implanted device. Further Analysis of this data determines the saturation intensity in the unimplanted device to be 4 kW/cm^2, and in the implanted device to be 45 kW/cm^2. Unimplanted saturation intensities are comparable to thick (65 Å) high (x=0.4) barrier samples while, with implantation, they are as large as those reported for thin (65 Å), low (x=0.2) barriers.[6]
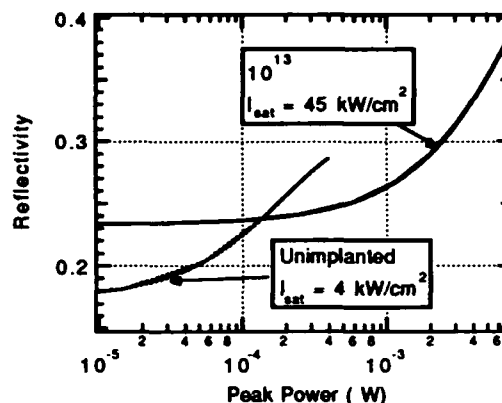
Finally, we note that when these devices are AR-

Figure 3: Fit to reflectivity data as as function of incident power for implanted ($1 \times 10^{13} \, \text{cm}^{-2}$) and unimplanted AlAs barrier samples at 8V and 849 nm.

coated, we find there to be only minor changes in the reflectivity properties of the samples, to implant doses of at least $1 \times 10^{13} \, \text{cm}^{-2}$. We believe that this is because the Fabry-Perot resonances present in uncoated devices dominate the reflectivity spectra, provided exciton broadening does not become extreme. This significant result has major potential device utility, and is the subject of a submission to the Photonic switching topical meeting co-located with Quantum Optoelectronics.[5]

[1] D. A. B. Miller, D. S. Chemla, T. C. Damen, A. C. Gossard, W. Wiegmann, T. H. Wood, C. A. Burrus, *Phys. Rev. Lett.* **53**, 2173 (1984).

[2] T. K. Woodward, B. Tell, W. H. Knox, J. B. Stark, *Appl. Phys. Lett.* **60**, 742 (1992).

[3] P. W. Smith, Y. Silberberg, D. A. B. Miller, *J. Opt. Soc. Am. B.* **2**, 1228 (1985).

[4] M. Lambsdorff, J. Kuhl, J. Rosenzweig, A. Axmann, J. Schneider, *Appl. Phys. Lett.* **58**, 1881 (1991).

[5] T. K. Woodward, B. Tell, W. H. Knox, M. T. Asom, J. B. Stark, submitted to Photonics in Switching Topical Meeting, 1992.

[6] A. M. Fox, D. A. B. Miller, G. Livescu, J. E. Cunningham, W. Y. Jan, *IEEE J. Quant. Electronics* **27**, 2281 (1991).

Nonlinear optical properties in infrared region in quantum well
---- an application of intersubband transitions

J. B. Khurgin and Shaozhong Li

Department of Electrical and Computer Engineering

The Johns Hopkins University

Baltimore, MD 21218

Substantial effort has been recently dedicated to the study of the infrared nonlinear optical properties of the intersubband transitions (IST) in different quantum well structures [1-5]. The large oscillator strength of IST gives it a great potential application in infrared nonlinear optical devices, such as detection and frequency conversion. In this work, we extensively investigated the nonlinear optical susceptibilities due to the IST's in different bands and the comparison with band-to-band transition is also made.

Most of the research of IST nonlinearities are based on nothing but the saturation of the IST transition. Therefore the high insertion loss is inherent in the devices based on resonant IST's and their speed is determined by the intersubband relaxation time (a few picoseconds). We have studied the nonlinearities near the two-photon resonance in conduction band, i.e. the linear absorption and thus the insertion loss is small, while the response time is determined by the detuning. It is very easy to derive that the third order susceptibility near the two-photon resonance is

$$\chi^{(3)}(\omega;-\omega,\omega,\omega)=\frac{N_s e^4}{\epsilon_0 L \hbar^3 \omega_{fg}^2 (\omega_{fg}-2\omega-i\Gamma)} \sum_f | <g\,|(z-\bar{z}_0)^2\,|f> |^2 \qquad (1)$$

where $\bar{z}_0 = <g\,|z\,|g>$ and N_s is 2D density.

Our calculation shows that $\chi^{(3)}$ reaches $10^{-7} \sim 10^{-6}\,esu$ below the two-photon resonance where the absorption is small. The results of $\chi^{(3)}$ is at least two order of larger than the most bulk materials. The operating wavelength is above $20\mu m$ for GaAs/AlGaAs quantum well structures due to the limitation of the band offset. To extend the operating wavelength to the useful $10\mu m$ region, we considered the two-photon absorption between confined and continuum state. we found the nonlinear refractive index is up to $10^{-9}\,cm^2/W$ while the nonlinear absorption is extremely small in the $10\mu m$ region.

In most second harmonic generation (SHG) experiments for III-V compounds, the observed SHG efficiency is very low even the waveguide structure is used, due to the diagonal nature of the tensor of $\chi^{(2)}(2\omega)$ near the $\Gamma-point$ of the conduction band and the lack of means for the phase matching. The new and effective method for SHG in the surface-emitting waveguide was proposed [6,7]. The method relies on the existence of $\chi^{(2)}_{zz}$ which is usually zero for conduction band. However, in the valence band, the situation is quite different because of the band mixing effect. Our theory shows that the mixing makes it possible to have a non-zero $\chi^{(2)}_{zz}$ because there is indeed the oscillator strength for both normal to the plane (z) IST's and for the in-plane (x) IST's, due to the geometrical symmetry of the wavefunctions of the original heavy and light holes. The calculation gives the efficiency of SHG of the order of 1% per watt of fundamental power, which is sufficient for many practical applications.

Finally, the comparison between the intersubband and band-to-band non-linearities in quantum wells. Using a simple $\mathbf{k \cdot p}$ theory, we concludes with a surprising result, contrary to the prevailing consensus, that the IST and band-to-band transition have almost equal in terms of the magnitude of optical response. But IST offers greater flexibility in the choice of material and operating wavelength.

In summary, the interesting nonlinear optical properties due to the IST's have a great potential for application of infrared optical devices.

References

[1] L. C. West and S. J. Eglash, Appl. Phys. Lett. 46, 1156 (1985)

[2] B. F. Levine, R. J. Malik, J. Walker, K. K. Choi, C. G. Bethea, D. A. Kleinman and J. M. Vandenberg, Appl. Phys. Lett. 50, 273 (1987)

[3] M. K. Gurnick and T. A. DeTemple, IEEE J. Quantum Electron. QE - 19, 791 (1983)

[4] M. M. Fejer, S. J. B. Yoo. R. L. Byer, A. Harwit, and J. S. Harris, Phys. Rev. Lett., 62 1041 (1989)

[5] E. Rosencher, P. Bois, J. Nagle, E. Costard, and S. Delaitre, Appl. Phys. Lett. 55, 1597 (1989)

[6] R. Normandin and G. I. Stegeman, Opt. Lett. 4, 58 (1979)

[7] D. Vakhshocri, M. C. Wu and S. Wang, Appl. Phys. Lett. 52, 422 (1988)

Intersubband Transitions in High Indium Content InGaAs / AlGaAs Quantum Wells Grown on GaAs with a Graded InGaAs Buffer

H. C. Chui, S. M. Lord, and J. S. Harris, Jr.
Solid State Laboratory, Stanford University, Stanford, CA 94305

M. M. Fejer
Ginzton Laboratory, Stanford University, Stanford, CA 94305

Large intersubband transition energies are interesting for applications in quantum well infrared photodetectors (QWIPs) and nonlinear optical frequency conversion devices. QWIPs have recently been a topic of interest for applications in high speed detector arrays.[1] By using large energy intersubband transitions in quantum wells, the useful range of these QWIPs can be extended to the 3-5μm atmospheric window. With the demonstration of large nonlinear optical susceptibilities in quantum wells,[2] application of large intersubband transition energies to frequency conversion devices is also of interest. Large intersubband transition energies have been observed in GaAs / AlAs (E_{16} = 434meV)[3] as well as InGaAs / InAlAs on InP quantum wells (E_{12} = 400meV for strained, E_{12} = 295meV for unstrained).[4,5,6] By using pseudomorphic InGaAs / AlGaAs quantum wells, the conduction band offset ΔE_c is further extended.[7] However, the lattice mismatch of InGaAs and AlGaAs typically limits the range of indium content available. By using a compositionally graded buffer, Lord, et. al.[8] have demonstrated that high quality In(0.5)Ga(0.5)As / AlGaAs quantum wells can be grown on a GaAs substrate. Using this novel growth technique, we report the first observation of intersubband transitions in high indium content InGaAs / AlGaAs quantum wells.

In(0.11)Ga(0.89)As	200Å
Al(0.45)Ga(0.55)As	80Å
In(0.3)Ga(0.7)As	40Å
In(0.11)Ga(0.89)As Graded Buffer 16% / μm GaAs	6000Å
GaAs	500Å
GaAs SI substrate	

x 50.5

(a) y = 0.3

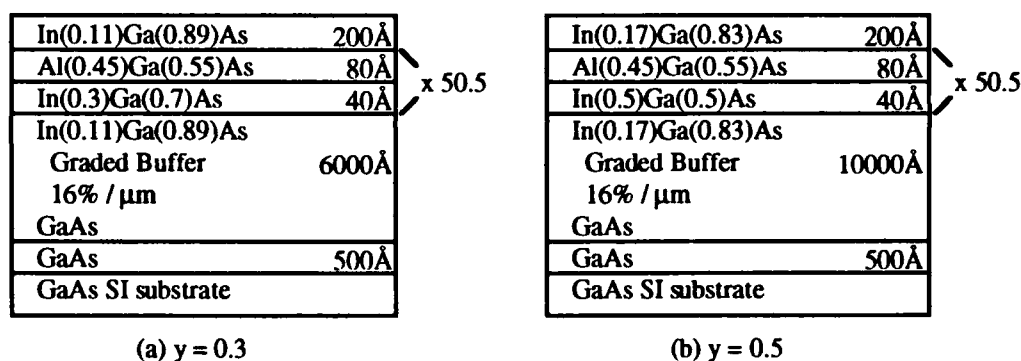| In(0.17)Ga(0.83)As	200Å
Al(0.45)Ga(0.55)As	80Å
In(0.5)Ga(0.5)As	40Å
In(0.17)Ga(0.83)As Graded Buffer 16% / μm GaAs	10000Å
GaAs	500Å
GaAs SI substrate	

x 50.5

(b) y = 0.5

Figure 1. Targeted MBE grown MQW structures

The multiple quantum well (MQW) structures were grown by molecular beam epitaxy (MBE) in a Varian Gen-II system using As_2. The samples were grown at 480°C on a semi-insulating GaAs substrate. Two n = $3.5e18 cm^{-3}$ well doped In(y)Ga(1-y)As / Al(0.45)Ga(0.55)As MQW structures were grown with well compositions y = 0.3 and 0.5. The targeted structures are shown schematically in Figure 1. The InGaAs buffer was linearly graded at rate of 16% indium / μm from GaAs to near the average indium composition of the MQWs. In the same growth run, two 1μm thick InGaAs samples were grown at the same composition as the y = 0.3 and 0.5 wells. X-ray diffraction measurements of these thick InGaAs samples determined that the actual well compositions in the MQW samples were y = 0.28 and 0.51.

The intersubband transition energies were measured using a Fourier transform infrared spectrometer (FTIR) at room temperature with the samples mounted at Brewster angle to TM polarized light. The FTIR spectra for the two MQW samples are shown in Figure 2. The absorption peaks for the 1-2 transitions were found to be 311meV and 351meV with FWHM linewidths of approximately 22meV and 40meV for the y = 0.3 and 0.5 samples, respectively. These intersubband transition energies are among the largest ever reported.[3-6] These transition energies are comparable to the theoretical value of approximately 330meV for both the y = 0.3 and 0.5 MQWs (Figure 3) estimated using a

single band effective mass model.[9] Nonparabolicity was included by using an energy dependent effective mass derived from the conduction band dispersion.
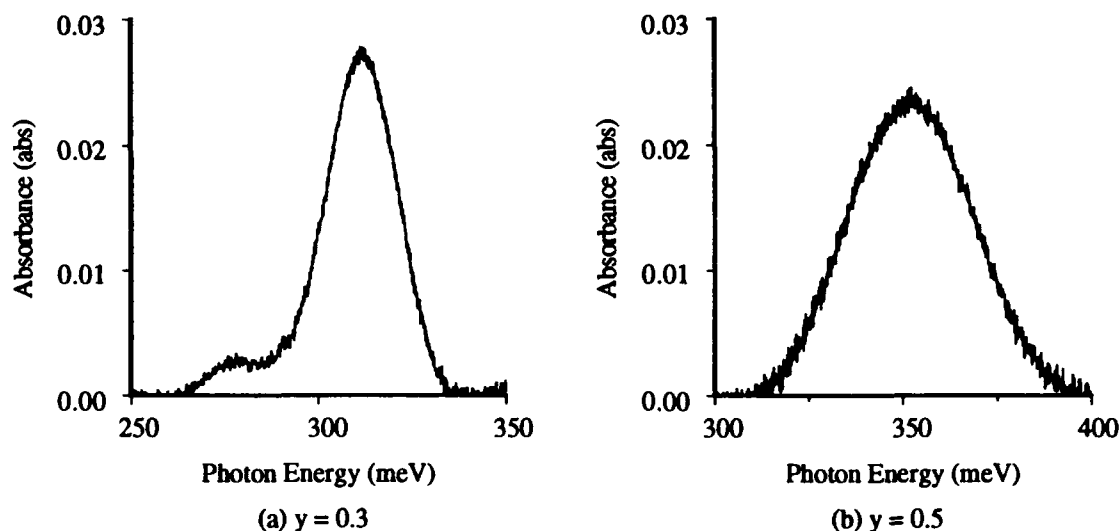

(a) y = 0.3

(b) y = 0.5

Figure 2. FTIR spectra of the y = 0.3 and 0.5 MQW structures

In summary, we report the first observation of intersubband transitions in high indium content InGaAs / AlGaAs quantum wells. The 1-2 intersubband transitions were measured by FTIR for y = 0.3 and 0.5 well indium compositions to be 311meV and 351meV, among the largest intersubband transitions ever demonstrated. Since ΔE_c = 820meV for the y = 0.5 MQW sample, even larger intersubband transition energies should be possible with InGaAs / Al(0.45)Ga(0.55)As MQWs, and with AlAs barriers, ΔE_c = 1.25eV can be achieved.[3] Further studies on extending InGaAs / AlGaAs MQWs to larger intersubband transition engeries are in progress and will be presented.
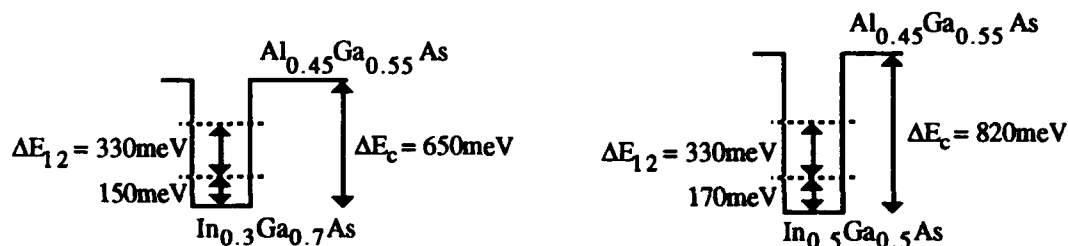

Figure 3. Conduction band diagrams of MQW samples with theoretically estimated subband energies

[1] C.G. Bethea, B.F. Levine, V.O. Shen, R.R. Abbott, S.J. Hseih, IEEE Electron Devices, 38, 1118 (1991).
[2] M.M. Fejer, S.J.B. Yoo, R.L. Byer, A. Harwit, and J.S. Harris, Jr., Phys. Rev. Lett., 62, 1041 (1989).
[3] J.L. Pan, L.C. West, S.J. Walker, R.J. Malik, and J.F. Walker, Appl. Phys. Lett., 57, 366 (1990).
[4] H. Asai and Y. Kawamura, Appl. Phys. Lett., 56, 746 (1990).
[5] B.F. Levine, A.Y. Cho, J. Walker, R.J. Malik, D.A. Kleinman, D.L. Sivco, Appl. Phys. Lett., 52, 1481 (1988).
[6] S.D. Gunapala, B.F. Levine, D. Ritter, R. Hamm, and M.B. Panish, J. Appl. Phys., 71, 2458 (1992).
[7] X. Zhou, P.K. Bhattacharya, G. Hugo, S.C. Hong, and E. Gulari, Appl. Phys. Lett., 54, 855 (1989).
[8] S.M. Lord, B. Pezeshki, and J.S. Harris, Jr., Electron. Lett., 28, 1193 (1992).
[9] G. Bastard, Wave Mechanics Applied to Semiconductor Heterostructures (les éditions de physique, France, 1988), Chapter 2.

Fundamental Processes

QWC 1:30pm–3:00pm
Oleander Room

Yoshihisa Yamamoto, *Presider*
NTT, Japan

Quiet Electrons, Noisy photons: Quantum Statistical Effects

in Wave Guide Transport

M. Büttiker

Institut für Physik, Universität Basel, Klingelbergstr. 82, CH-4056 Basel, Switzerland,

phone 041-61-267-3690 and

IBM T. J. Watson Res. Ctr., P. O. Box 218, Yorktown Heights, N. Y. 105492, U.S.A.,

phone 001- 914-945-2513.

Fluctuations of the current at the contacts of a small phase-coherent conductor are compared with fluctuations of the intensity at the contacts of a photon wave guide [1]. The electronic conductor and the photon wave guide are viewed as a target at which carriers incident from the reservoirs (balck body radiators) connected to the contacts are reflected or transmitted into another reservoir. The spatial separation between reservoirs is assumed to be so small that transmission from one contact to another is phase-coherent. We are interested in the fluctuations of the current and the intensity away from their steady state average. Of principal interest are properties of the fluctuations which are directly related to the statistics of indistinguishable quantum particles. Such effects are a consequence of the symmetry of the wave-function under exchange of two carriers. Experiments with photon beams in free space were pionered by Hanburry Brown and Twiss almost forty years ago. In contrast to experiments with beams of light or beams of electrons in free space, experiments in conductors or wave guides have the advantage that a much higher degree of occupation of available states can be achieved. At kT=0 in a conductor, all states below the Fermi energy are occupied. Despite this advantage a clear demonstration of quantum statistical effects in conductors is lacking.

If the potential provided by the wave guide is assumed to be fixed only two sources of noise remain: (a) There is thermal noise due to the fluctuation in the occupation numbers of the incident states; (b) Even at zero temperature there is a

shot noise if an incident carrier has more than one final state available. The shot noise vanishes [2] if the final state is reached with probability 1 (perfect transmission channel). Examples of conductors with highly transmissive channels are quantum point contacts and quantum Hall conductors. Surprisingly, even if propagation in the wave guide is diffusive, a fraction of the transmission channels remains open and leads to a shot noise which is smaller than the naively expected result [3].

The theory finds that the low frequency fluctuation properties are given by exchange amplitudes which can be expressed in terms of the global scattering matrix of the wave guide. At equilibrium all cross-correlations are negative independent of statistics. In the presence of transport cross-correlations in a Bose system can change sign, in agreement with Hanburry Brown and Twiss, but Fermi cross correlations remain negative [1].

To elucidate the role of exchange we propose an experiment on a four probe wave guide in which photons or electrons are incident from two contacts and in which the cross-correlation is measured at the two remaining contacts [1]. It is shown that this cross-correlation is not the sum of the two correlations which would be measured if one of the currents were switched off but in addition contains a contribution which arises from the quantum mechanical impossibility to distinguish identical carriers. In this experiment the exchange amplitude is a periodic function of a quantum mechanical phase. The possibility of tuning this phase with the help of an Aharonov-Bohm flux is discussed [4].

[1] M. Büttiker, Phys. Rev. Lett. 65, 2901 (1990);Phys. Rev. B46, 12845 (1992).

[2] G. B. Lesovik, JETP Lett. 49, 592 (1989).

[3] C. W. J. Beenakker and M. Büttiker, Phys. Rev. 46, 1889 (1992).

[4] M. Büttiker, Phys. Rev. Lett. 68, 843 (1992); Physica B 175, 199 (1991).

Squeezing With Input State of Large Phase Uncertainty

I. Lyubomirsky, M. Shirasaki* and H. A. Haus

Department of Electrical Engineering and Computer Science
Massachusetts Institute of Technology,
Cambridge, Massachusetts   02139
(617) 253-2585
* is also with Fujitsu Laboratories Ltd.

Noise suppression in an interferometer, employing a nonlinear Mach-Zehnder squeezer, was proposed[1] and experimentally confirmed[2,3]. The noise characteristics of this squeezer were derived for a coherent state input[4]. It may be advantageous to put the squeezer directly into a modelocked laser resonator where higher power pulses may be utilized. In this case the light acquires a large phase uncertainty. Thus, it is of interest to analyze squeezing with an input state of large phase uncertainty. One approach is to expand the input state in terms of coherent states[5]. Another approach is to use number states, which have total phase uncertainty and also present some interesting quantum features.

The output field operators of the squeezer $\hat{f}$ and $\hat{g}$ (Fig. 1) are simplified by making the approximation $\kappa^2 n \ll 1$ (κ is the coefficient of nonlinearity and n is input photon number):

$$\hat{f} = \exp(i\kappa \hat{b}^+ \hat{b})\,[\hat{\mu}\hat{a} + \hat{\nu}\hat{a}^+], \qquad \hat{g} = \exp(i\kappa \hat{b}^+ \hat{b})\,\hat{b}$$

where

$$\hat{\mu} = 1 + \frac{i\kappa}{2}\hat{b}^+ \hat{b}, \qquad \hat{\nu} = \frac{i\kappa}{2}\hat{b}^2$$

In the case of a coherent state input we may linearize the $\hat{f}$ operator, replacing the operators $\hat{\mu}$ and $\hat{\nu}$ by their c-number averages[1]. But when the input has large phase uncertainty, we must retain the nonlinear form of the operators.

Noise in the output of Fig. 1 is obtained from the matrix elements of $\Delta\hat{n}$ and $\Delta\hat{n}^2$. In number state basis, we get:

$$\langle m|\Delta\hat{n}|n\rangle = 0$$

$$\langle m|\Delta\hat{n}^2|n\rangle = \delta_{mn}\{n + \frac{\kappa^2}{4}(2n^3 - 3n^2) - \kappa(n^2 - n)\,Sin2\psi - \frac{\kappa^2}{2}(n^3 - 2n^2)\,Cos2\psi\}$$

In our approximation we have ignored terms of order $\kappa^4 n^2$.

Using the above matrix elements, we can calculate the noise for any input state. In particular, the noise of a number state input is given by the diagonal matrix element. When $\kappa^2 n \ll 1 \ll \kappa n$, the minimum noise occurs for $2\psi = \arctan(2/\kappa n)$:

$$\langle n|\Delta n^2|n\rangle = 1/\kappa^2 n + \kappa^2 n^2/4$$

This is the same result as the minimum noise for a coherent state input[4] if we replace n by the average photon number. Figure 2 shows plots of normalized noise $\langle n|\Delta\hat{n}^2|n\rangle/n$ as a function of the phase bias, and minimum noise as a function of nonlinearity.

There is an important distinction between the cases of a coherent and number state input. For a coherent state, the output of the squeezer produces squeezed vacuum. On the other hand, with a number state input, one may visualize the operation of the squeezer by assigning to each phase component its own "probability ellipse." This results in modulated vacuum: a superposition of many probability ellipses with different orientations of major axes. The modulated vacuum and the local oscillator are phase correlated, so that the minimum noise is still extracted from each ellipse by the homodyne detection.
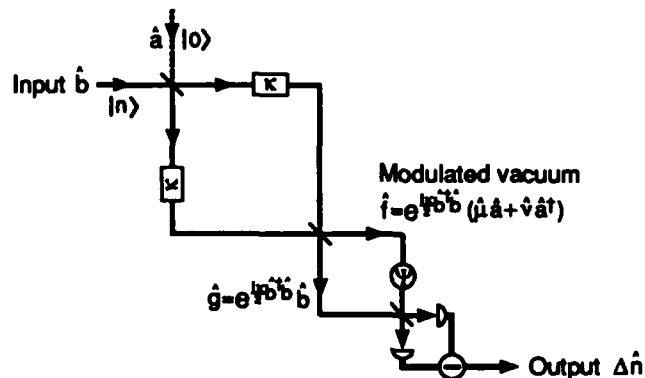
Fig. 1 Nonlinear Mach-Zehnder squeezer with homodyne detection
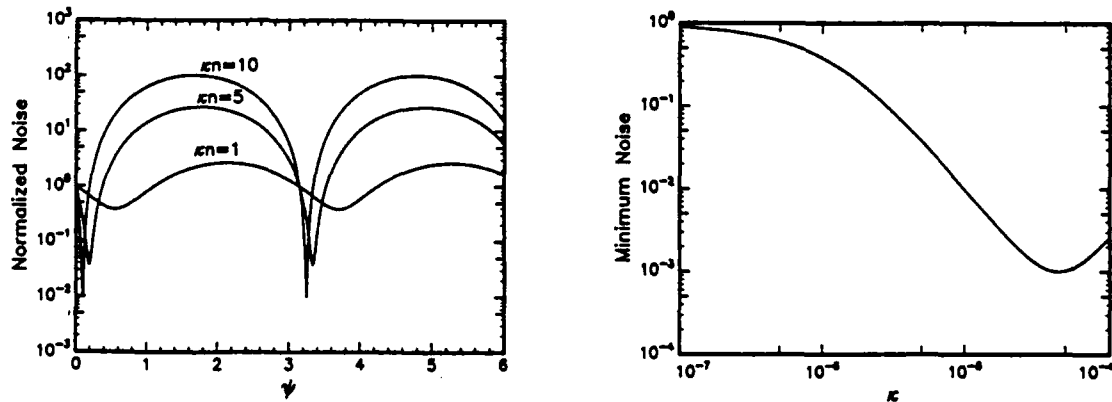
Fig. 2 Noise characteristics for n=10⁶

References
1. M.Shirasaki and H.A.Haus, J.Opt.Soc.Am.B, 7, 30 (1990)
2. K.Bergman and H.A.Haus, Opt.Lett., 16, 663 (1991).
3. M.Rosenbluh and R.M.Shelby, Phys.Rev.Lett., 66, 153 (1991)
4. M.Shirasaki, Opt.Lett., 16, 171 (1991).
5. M.Shirasaki and H.A.Haus, International Quantum Electronics Conference, paper PWe048 (1992)

Quantum Non-Demolition Measurement of Photon Number using a Mesoscopic Electron Interferometer

Akira Shimizu

Institute of Physics, University of Tokyo, Komaba, Tokyo 153, Japan
Fax:+81-3-3467-1281, Phone:+81-3-3467-1171 ext. 426

Quantum phenomena in low-dimensional electron systems have been attracting much attention of semiconductor physicists and engineers for the last few decades. However, most discussions concern either electron transport or responses to classical electromagnetic fields. On the other hand, non-classical effects of light are a subject of growing interest in quantum optics. In this case, however, electronic systems are usually limited to either atoms or effective media (which are phenomenologically described to induce photon-photon couplings). The purpose of this talk is to give a brief introduction to "fully-quantum optoelectronics," in which electrons confined in low-dimensional semiconductors are assumed to interact with quantized electromagnetic fields.

Up to now two types of approaches to the fully-quantum optoelectronics have been reported. One is light emitters using cavity quantum electrodynamics in low-dimensional semiconductors, which may be presented in this meeting by Professor Yamanishi and by Dr. Jewell. We will present the other type: light detectors with a striking function. Conventional photodetectors absorb photons, i.e., they alter the photon number from a finite value to zero. In quantum-mechanical terms, these detectors are "demolition" detectors which destruct the distribution of the observable of interest, i.e., the photon number. By contrast, we will present photodetectors which preserve the distribution of the photon number. Such detectors are generally called quantum non-demolition (QND) detectors [1].

Consider first the composite device shown in Fig.1. The incident light beam is divided by the 1:1 beam splitter. One of the divided beam is detected by a conventional photodetector (such as a photodiode), and double of its intensity is regarded as the intensity of the original incident beam. The other of the divided beam is doubly amplified by an optical amplifier, and the output beam from the amplifier has the same intensity as the original incident beam. Hence, the net function of the composite device is an "absorption-free" photodetector. However, this device is *not* a QND photodetector; the device only preserves the *classical* intensity. In fact, we can easily show for the input and output states (which are denoted by subscripts *in* and *out*, respectively) that $\langle n \rangle_{out} = \langle n \rangle_{in}$ and $\langle \delta n^2 \rangle_{out} = \langle \delta n^2 \rangle_{in} + \langle n \rangle_{in}$. That is, the photon number distribution is broadened by the device, and only the mean value is preserved. Moreover, we can also show that the measurement error of the device always exceeds $\sqrt{\langle n \rangle}$ (even when the photodiode is an ideal error-less one). Such a device cannot be used as receivers in a future *quantum* optical communication system in which information is encoded into a photon-number distribution, and many receivers read the information subsequently. The information would be contaminated by each receiver and thus the signal-to-noise ratio (SNR) will be helplessly degraded after passages through many receivers. Moreover, the measurement error would be too large to make full use of the quantum optical communication

system. By contrast, if QND photodetectors are used for receivers, the SNR is completely preserved and also the measurement error can be made small enough – at least in principle.

We will present the QND photodetector shown in Fig.2, which uses a quantum-wire electron interferometer as a quantum probe of the photon states [2]. Physical meaning of the device is briefly discussed from the viewpoint of the general theory of QND measurements which was developed recently [3]. Possible uses of other mesoscopic interferometers will also be discussed.
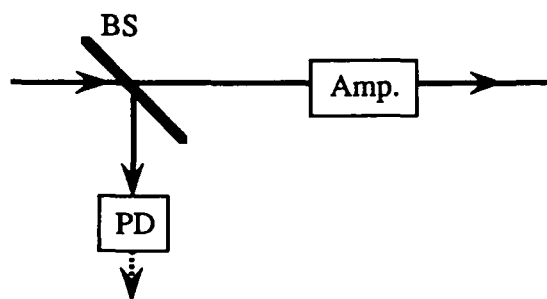
Fig.1 A classical abosorption-free photodetector, which does *not* work as a QND detector.
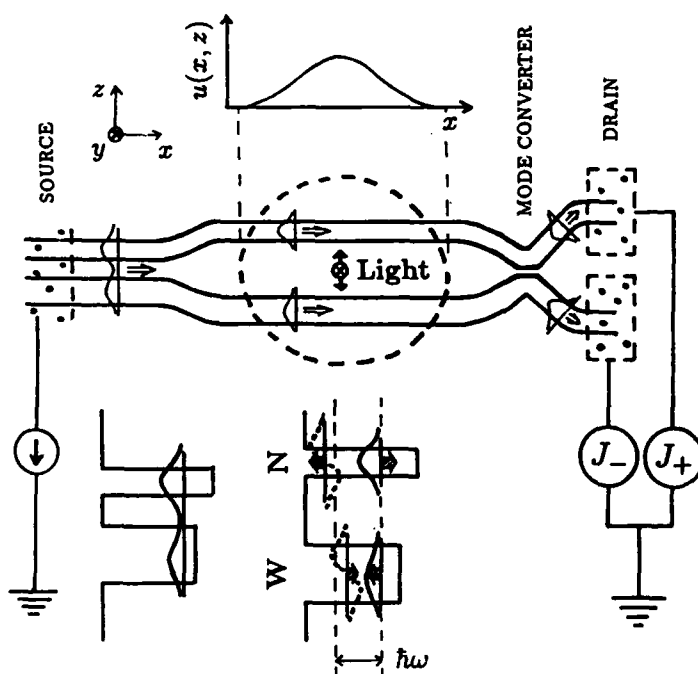
Fig.2 A QND photodetector using an electron interferometer composed of two quantum wires, N and W. The lowest subband energies (of the z-direction confinement) ϵ_a^N and ϵ_a^W of the wires are the same, but the second levels ϵ_b^N and ϵ_b^W are different. Electrons occupy the lowest levels only. A z-polarized light beam of photon energy of $\epsilon_b^W - \epsilon_a^W < \hbar\omega < \epsilon_b^N - \epsilon_a^N$ hits the dotted region, and the electrons are excited "virtually." After the light beam passes through the interferometer, the photon number distribution returns to its initial distribution, whereas the electron wavefunction undergoes a phase shift between the amplitudes in the two wires. This phase shift modulates the interference currents J_+ and J_-, from which we can deduce the photon number of the light beam.

[1] V.B. Braginsky et al., Science **209** (1980) 547; C.M. Caves et al., Rev. Mod. Phys. **52** (1980) 341; A. La Porta, R.E. Slusher, and B. Yurke, Phys. Rev. Lett. **62**, 28 (1989).

[2] A. Shimizu, Phys. Rev. **A43** (1991) 3819.

[3] A. Shimizu and K. Fujita, Proc. *Quantum Control & Measurement*, Saitama, Japan, 1992, Edited by H. Ezawa and Y. Murayama (Elsevier, to be published).

Semiconductor Laser with Dispersive Loss: Quantum Noises and Amplitude squeezing

R.F. Nabiev *

E.L. Ginzton Lab., Stanford University
Stanford, CA 94305
Tel.: (415) 723-0219

In the recent paper [1] semiclassical treatment of semiconductor laser (SL) with dispersive loss element (DLE) inside the cavity was presented. In SL with frequency dependent photon life time τ_p ($\tau_p^{-1} = \tau_{p0}^{-1} + 2C\varphi$, φ is the slowly varying phase of an electromagnetic field) phase and amplitude noises were shown to be decreased $(1+C\alpha)^2 / (1+\alpha^2)$ and $(1+C\alpha)^2 / (1+C^2)$ (α is the linewidth enhancement factor) times, respectively, comparing to the conventional SL (C=0). At the same time, he low frequency portion of current modulation response is unchanged. Possible values of parameter C [1] can be ~10 and some dozens in the case of atomic absorption cell and the weak coupling of SL to an external high-finesse Fabry-Perot etalon, respectively.

Following the technique developed by Y. Yamamoto [2] we carried out a comprehensive quantum mechanical treatment of SL with DLE and obtained power spectra of the fluctuating operators of amplitude and phase of the field inside ($P_{A\alpha}$ and P_φ) and outside (P_{Ar} and P_ψ) the cavity. The linewidth of laser emission calculated in this way is determined P_ψ and occurs to be equal to the one obtained in semiclassical approach [1]. Amplitude noises (AN) of output flux depend on whether output wave does not pass through DLE (case a) or does (case b). Near threshold, we have suppressing of low frequency AN of both internal and output field what agrees with results of Ref. [1]. The results on AN far above threshold can be separated into two groups and for the case $C\alpha \gg 1$ they are:

1. The case of usual pumping. At low frequencies AN power of internal field $P_{A\alpha}$ is n_{sp} (inversion parameter) times higher than the one for conventional SL. Output flux AN power P_{Ar} at low and high frequencies is approximately equal to $1/2+n_{sp}$ and 1/2 (case a), and 1/2 and $n_{sp}(C\alpha)^2$ in the case (b). Note that for the conventional SL $P_{Ar} \sim 1/2$ in all frequency region, and this value of AN coincides with a shot noise limit (SNL) of an ideal laser [2].

2. The case of the noise suppressed pumping (it was proposed by Y. Yamamoto et al [3] to get amplitude squeezing (AS) in conventional SL). At small and high frequencies $P_{Ar} \sim n_{sp}(1+\alpha^{-2})$ and ~1/2 (case a), and $P_{Ar} \sim n_{sp}(\tau_{p0}\Omega)^2 / \alpha^2$ and $\sim n_{sp}C^2$ in the case (b). Table shows briefly these data for low and high frequency limits of AN in the both cases of pumping. Figures represent the spectra of external field AN power $P_{Ar}(\Omega)$ at different

normalized pumping rates R for the both cases. Solid lines correspond to the case C=0, dashed lines (C=10), and dashed-dotted lines (C=100). Long-dashed line indicates SNL P_{Ar}=1/2. It is seen that that in the case (a) DLE aggravates considerably noise properties of SL with noise suppressed pumping. At $C \neq 0$ AN is much higher in the low frequency region than the one at C=0. In the case (b) we have an opposite situation and AN in low frequency region in SL with DLE is less than the one for conventional SL by the factor α^2 / n_{sp}. For α=4, and n_{sp}=1.5 DLE decreases the AN level 5 times. At the same time the frequency region of AS is increased by the same factor, what is the most important from the experimental point of view, especially at moderate values of pumping level (see Fig. (b), R=10).

In conclusion, the quantum mechanical analysis shows that the use of DLE can decrease the amplitude noises of SL α^2 / n_{sp} times, and the frequency region of amplitude squeezing is α^2 / n_{sp} times broader than in the conventional SL.

1. A.Yariv, R. Nabiev, K. Vahala. Optics Letters, 15, 1359 (1990).
2. Y. Yamamoto, N. Imoto. IEEE J. of Quant. Electr., QE-22, 2032 (1986).
3. Y. Yamamoto, S. Machida, O. Nilsson. Phys. Rev., 34A, 307 (1986).
   * On leave from P.N. Lebedev Physics Inst., Moscow, Russia.

Table: Amplitude Noise P_{Ar} limits:

	Usual pumping		Pump suppressed pumping	
	(a)	(b)	(a)	(b)
Low freq.	$1/2+n_{sp}$	1/2	$n_{sp}(1+\alpha^{-2})$	$n_{sp}(\tau_{p0}\Omega)^2 / \alpha^2$
High freq.	1/2	$n_{sp}C^2$	1/2	$n_{sp}C^2$

(a)

(b)
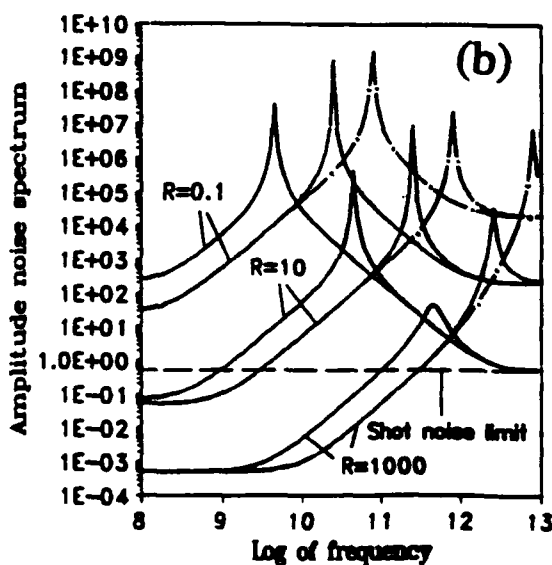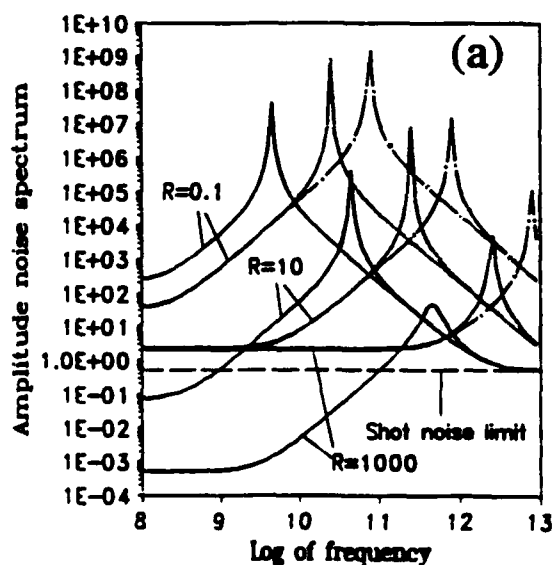
Quantum Well Lasers

QWD 3:30pm–5:00pm
Oleander Room

H. Temkin, *Presider*
Colorado State University

Multi-Quantum Barrier (MQB)
— Is It a Good Spice for Semiconductor Laser Performances ? —

K. Iga

Tokyo Institute of Technology
4259 Nagatsuta, Midoriku, Yokohama, Japan 227
Fax +81-45-921-0898

1. Introduction

We use the double heterostructure (DH) in most of current semiconductor lasers for the purpose of confinement of both optical field and carriers as well[1]. In order to prevent electrons from leaking over the hetero-barrier of a p-type cladding, it is known that more than 300 meV of built-in potential difference is usually required[2]. But in some cases such as high power and high temperature operations, much higher barrier height is preferable. However, enough barrier height is not sometimes available due to the material limitation, e.g., in short wavelength GaAlInP based red-orange lasers and II-VI based blue-green ZnCdSSe or blue ZnMgSSe systems[3].

We have to pay attention not only to the active *engine* of semiconductor lasers, but also to the cladding layer to achieve high performance devices. One of the ways to increase the effective barrier height is to dope high to p-cladding, and another is to use the quantum effect, i. e., multi-quantum barrier (MQB)[4]. The MQB is a semiconductor super-lattice which can reflect electrons by interference.

2. Principle

We first introduce the basic concept and design rules of MQB which is formed by a chirped semiconductor super lattice to reflect electron waves as shown in **Fig. 1**. Basically, the MQB consists of a quarter de Broglie wavelength stacks of semiconductors with different effective masses. The MQB was proposed in 1986 to enhance the carrier confinement of the double heterostructure laser diodes (LD) by a virtual potential barrier utilizing the interference of the quantum reflection of electron waves from the stacked superlattices[4]. The MQB concept is now recognized as being effective for enhance the barrier height of heterojunction, whereas most of super lattices in the past are for the purpose of focused on resonant tunneling.
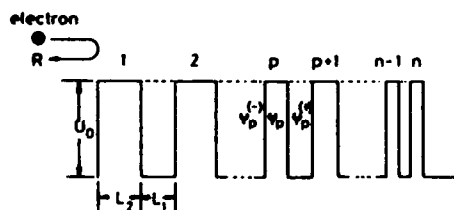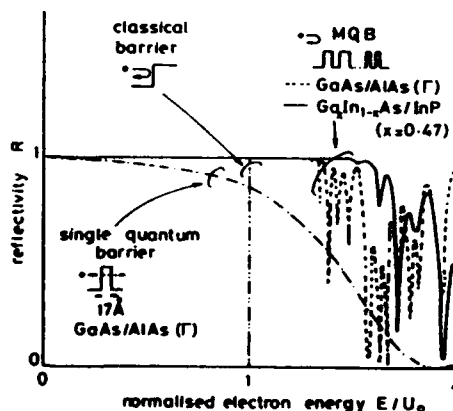
Fig.1 A model of MQB

Fig. 2 The reflectivity of MQB

The reflectivity of electron waves in conduction band against various energies at the MQB super lattice is one of the most important measure. This is obtained the transfer matrix method developed be Esaki and Tsu[5]. The boundary condition at each well (denoted by W) and barrier (denoted by B) is the continuity of wave functions and quantum currents, i. e.;

$$\psi_W = \psi_B \tag{1}$$

$$\frac{1}{m^*_W} \frac{d\psi_W}{dz} = \frac{1}{m^*_B} \frac{d\psi_B}{dz} \tag{2}$$

The resonance condition, on the other hand, is written as

$$(\sqrt{2m^*_W E} / \hbar) \times 2L_W = (2m-1)\pi \quad (m=1, 2, 3,) \tag{3}$$

$$(\sqrt{2m^*_B (E-U_0)} / \hbar) \times 2L_B = (2n-1)\pi \quad (n=1, 2, 3,) \tag{4}$$

Here, E is electron energy, m^*_W and m^*_B are the well and barrier effective mass, U_0 is classical barrier height, and L_W and L_B are the thicknesses of well and barrier, respectively. The reflectivity can be obtained by calculating the transfer matrices and given by

$$R = | B_{1(-)} / A_{1(-)} |^2 \tag{5}$$

where $B_{1(-)}$ and $A_{1(-)}$ are the amplitude of reflected and incident electron wave functions, respectively. These can be deduced by employing the matrix method.

3. GaAlAs/GaAs System

We have made the design of MQB for GaAlAs/GaAs system first. It is found that the effective barrier height could be 50 % higher than the classical barriers[1] as shown in **Fig. 2**. We confirmed its effectiveness for the first time by photoluminescence (PL) experiment by using MBE grown GaAlAs/GaAs MQB[6]. It was found that the PL intensity did not saturate so much at high excitation levels as shown in **Fig. 3**. We have also demonstrated the superior carrier reflection by the MQB over the bulk barrier in the n-GaAs/i-barrier/n-GaAs tunneling diode structure[8] as shown in **Fig. 4**.
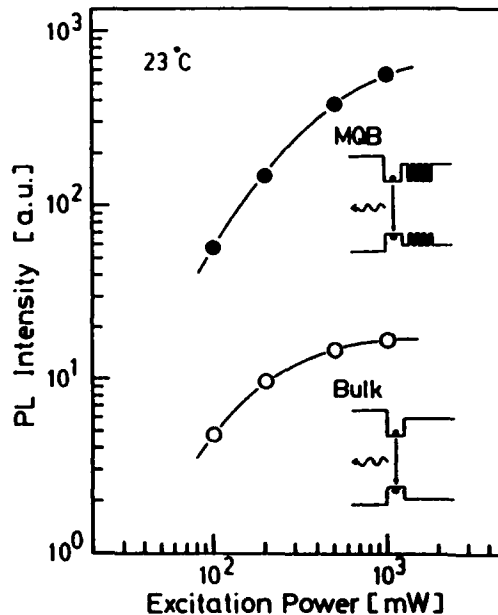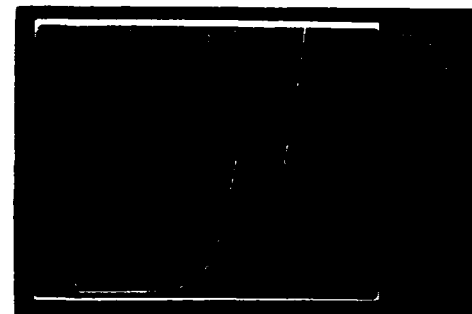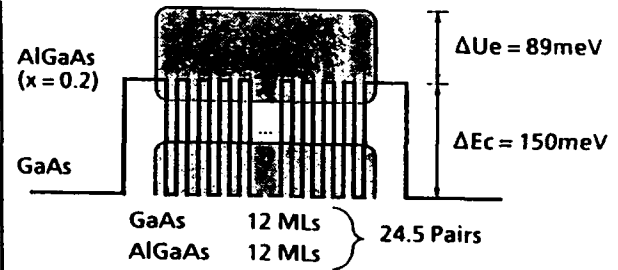

Fig. 3 PL intensity of MQB sample

Fig.4 MQB tunneling diode and I-V

4. GaAllnP/GaInP System

The MQB will become more important for reducing the carrier leakage over the p-type hetero-barrier of semiconductor lasers, particularly in short wavelength and high output powers. The model of MQB is shown in **Fig. 5**. The most preferable reflectivity is shown in **Fig. 6**, where the well and barrier number is 6 and 4, respectively[6,8,9,10,11]. In order to get much higher barrier height a modified MQB is proposed. In this scheme we use narrower bandgap material for the wells as shown in **Fig. 7**. The optical loss is not substantial, since the quantum state in wells can be higher than that of active region. By this configuration we could achieve 300 meV for artificial barrier height[6].

Several other groups are developing semiconductor lasers loaded by MQB[7,12,13,14]. It has been pointed out that the T_0 can be higher[7], and the operating temperature of visible GaAllnP/GaInP lasers, orange to red, can be raised up by 20 K by employing the MQB to the p-cladding.

5. GaInAsP/InP System

Its application to long wavelength lasers and surface emitting lasers is under consideration. We have designed the MQB for the long wavelength system and the result is already shown in Fig. 2. From more optimized design, the reflectivity can be as high as 200 % of the classical one. Also we fabricated a tunneling diode by chemical vapor deposition (CBE) and confirmed that the interference occurs in this system[15]. By utilizing wider bandgap material for barrier, e. g., a tensile stressed AlInAs as shown in **Fig. 8**, we can construct an MQB providing 1.2 eV of effective barrier which is good for preventing hot electrons from leaking through the p-cladding[16]. This will be advantageous for high temperature operation of quaternary lasers, if realized.

6. Conclusion

In this paper we have reviewed the progress of MQB for semiconductor lasers and tunneling diodes. It is recognized that the design procedure is almost established. We can say that the MQB is a good SPICE (Scheme of Periodic Interference for Conducting Electronwaves) and this structure will become very important for the improvement of semiconductor lasers, in particular, surface emitting lasers, where a much higher barrier is required.

Acknowledgments

References

1. I. Hayashi, M. B. Panish, P. W. Foy, S. Sumski: Appl. Phys. Lett. 17, 109 (1970)
2. H. C. Casey, Jr., M. B. Panish: Heterostructure Lasers , Academic Press, New York, (1978)
3. H. Kukimoto, 13th IEEE Semiconductor Laser Conf., Takamatsu, A-3, (1992)
4. K. Iga, H. Uenohara and F. Koyama, Electron. Lett., 22, 1008, (1986); Trans. IEICE of Jpn., J70-C, 851, (1987)
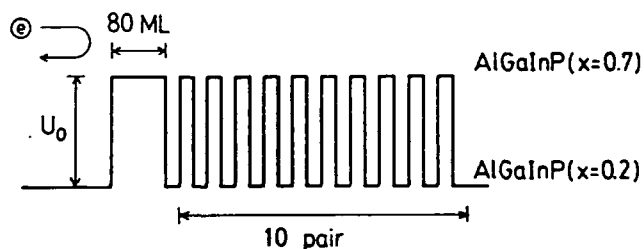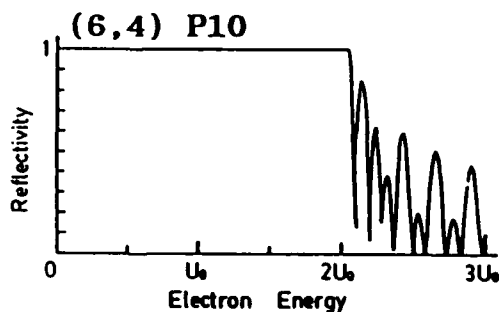
Fig. 5 GaAllnP MQB

Fig. 6 Its reflectivity

5. K. Iga, F. Koyama, and H. Uenohara , US Patent, 5091756 (Feb. 1992)
6. T. Takagi, F. Koyama and K. Iga, IEEE J. Quant. Electron., 27, 1511, (1991)
7. K. Kishino, A. Kikuchi, Y. Kaneko and I. Nomura, Appl. Phys. Lett., 57, 1822, (1991)
8. T. Takagi, F. Koyama, and K. Iga, Trans. IEICE of Jpn., J.74-C-1, (Dec. 1991)
9. T. Takagi, F. Koyama, and K. Iga, Appl. Phys. Lett., 59, 2877, (1991)
10. T. Takagi, F. Koyama, and K. Iga, Electron. Lett., 27, 1081, (1991)
11. T. Takagi and K. Iga, 18th Internt'l Quantum Electron. Conf. (IQEC'92), MoE3, 18 (1992)
12. J. Rennie, M. Okajima, M. Watanabe, and G. Hatakoshi, 13th IEEE Semicond. Laser Conf., Tech,. Digest. No. G-4, 158, (1992)
13. T. Kamizono, S. Arimoto, H. Watanabe, K. Kadoiwa, E. Omura, S. Kakimoto, and K. Ikeda, 13th IEEE Semicond. Laser Conf., Tech,. Digest. No. D-30, 94, (1992)
14. H. Hamada, K. Tominaga, M Shono, S. Honda, K. Yodoshi, and T. Yamaguchi, Electron. Lett., 28, 1834, (1992)
15. Y. Inaba, T. Uchida, N. Yokouchi, F. Koyama and K. Iga, Jpn J. Appl. Phys., submitted (1992).
16. M. Irikawa, Y. Sasaki, M. Iwase, and K. Iga, Jpn J. Appl. Phys., 31, L1351 (1992)
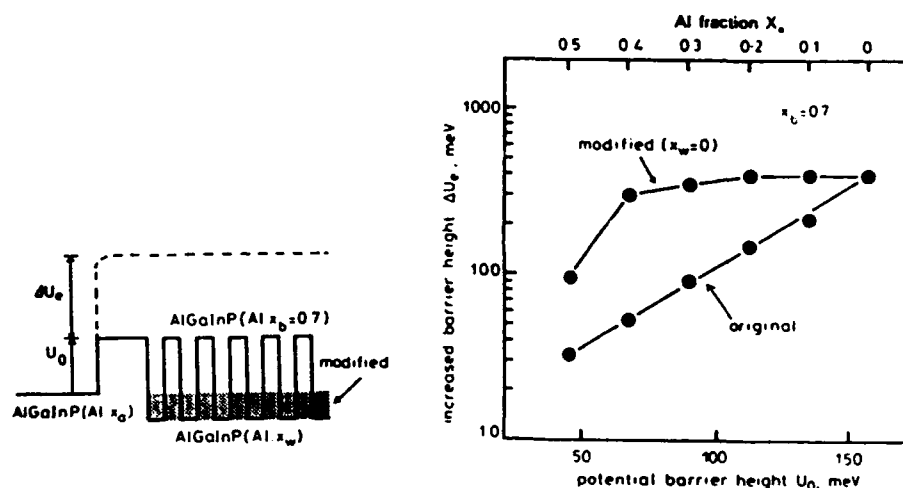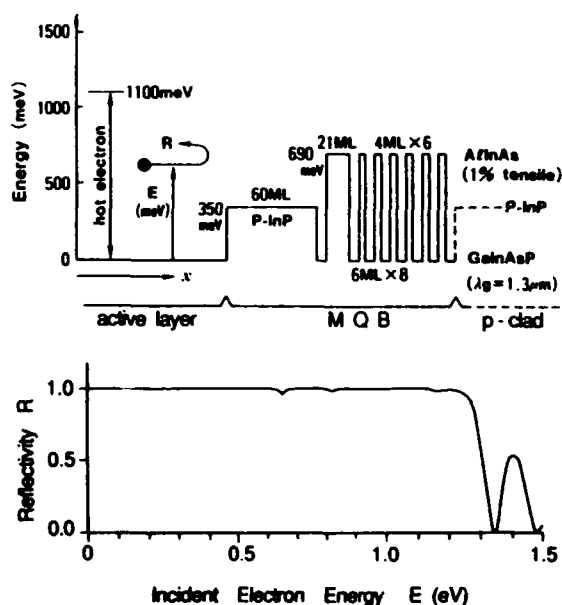
Fig. 7 Modified MQB

Fig. 8 MQB consisting of GaInAsP/ AlInAs

Optimum Strained MQW Structure in 680 nm AlGaInP Laser Diodes for Low Threshold and High Power

T. Tanaka, S. Kawanaka, H. Yanagisawa, S. Yano, and S. Minagawa

Central Research Laboratory, Hitachi Ltd.,
1-280 Higashi-koigakubo, Kokubunji, Tokyo 185, Japan
TEL : +81-423-23-1111 EXT 3013

It has recently been shown that various important laser characteristics are improved by adopting the strained MQW (SMQW) structure. In the case of visible AlGaInP lasers for use in the optical disk systems, high-power operation of the fundamental transverse-mode is an important requirement. Stable high output around 30 mW has already been attained using compressively strained QWs [1][2]. Compressive strain is introduced by increasing the In content of the GaInP alloy. This brings about a decrease in bandgap energy of the active region, which causes a large potential barrier that confines the injected carriers. In fact, the wavelength red-shift caused by the compressive strain can reduce threshold currents [3].

However, there have been few attempts to reduce threshold currents without a change of lasing wavelength. The quantum size effect in thin QWs shortens the wavelength to around 670 to 680 nm in the unstrained DH lasers. In thinner QWs, the threshold injected carrier density tends to be high and the carrier overflow is enhanced, although the required low optical density for high-power can be attained. Therefore, there is a trade-off between the design of thin QWs and low-threshold. The authors examined the optimum SMQW structure needed to satisfy both low threshold and stable operation at more than 30 mW at wavelengths around 680 nm. We also separately studied the effects of the alloy composition and the strain on the laser characteristics. The former mainly influences the better carrier confinement caused by the large potential barrier and the latter mainly decreases the threshold injected carrier density through the reduction in the effective masses of electrons and holes. Figure 1 shows that photoluminescence (PL) peak wavelengths from the GaInP DHs shift as much as 30 nm for the lattice mismatch of +1.0%. In the MQW structure, PL wavelengths can be controlled in the same range and the large lattice mismatch up to +2.0% without misfit dislocation can be used in thin QWs as shown in Fig. 2. We tried to determine which factor of the alloy composition or strain-induced effective mass reduction is dominant for decreasing threshold current density J_{th}. Dependence of J_{th} on the QW width is calculated when the lasing wavelength and the effective mass are independently taken into account as shown in Figs. 3 and 4, respectively. Here the linear interpolation to estimate the effective masses is used, and the hole mass in the case of +2.0% strain is assumed to be half of the unstrained. The values of J_{th} are calculated as the total current density due to the net threshold injected carriers and the excess overflow carriers. The results suggest that the red-shift of the lasing wavelength leads mainly to low J_{th} compared with the decrease of effective mass. It is, however, expected that the J_{th} of MQW LDs can be reduced by the small effective masses due to a large strain in thin QWs which can retain the wavelength. Figure 5 shows that J_{th} decreases even when the optical confinement factor Γ becomes as small as 0.05 without a change of lasing wavelength. Along with the reduction of Γ, the maximum output power increases even at 50°C without thermal saturation due to lower J_{th} as shown in Fig. 6. Comparing the experimental data with the calculated two-dimentional optical density in the active region, the power density of these lasers is around 4 MW/cm^2.

[1] K. Nitta et al., Electron. Lett., 27, pp.1660-1661(1991).
[2] Y. Ueno et al., Electron. Lett., 28, pp.860-861(1992).
[3] S. Kawanaka et al., Extended Abstracts of the Inter. Conf. on SSDM, pp.240-242(1992).
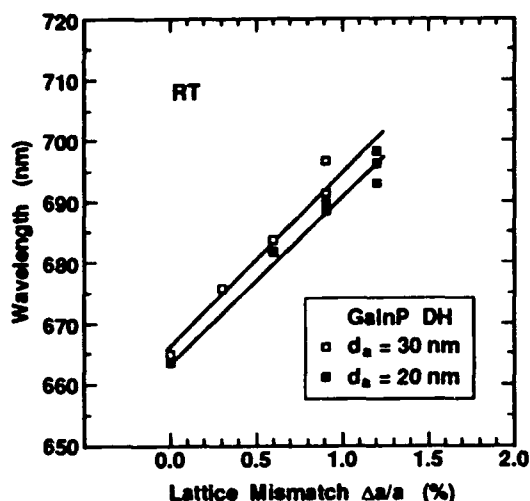
Fig. 1 Dependence of PL peak wavelengths on the lattice-mismatch introduced in GaInP DHs.
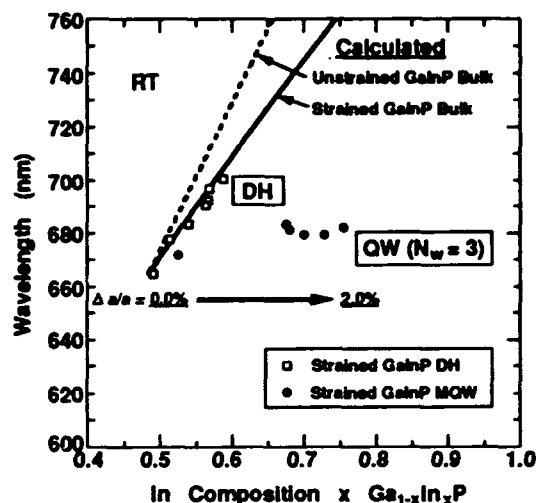

Fig. 2 Relationship between PL peak wavelengths and In composition of Ga₁₋ₓInₓP in strained DHs and MQWs.
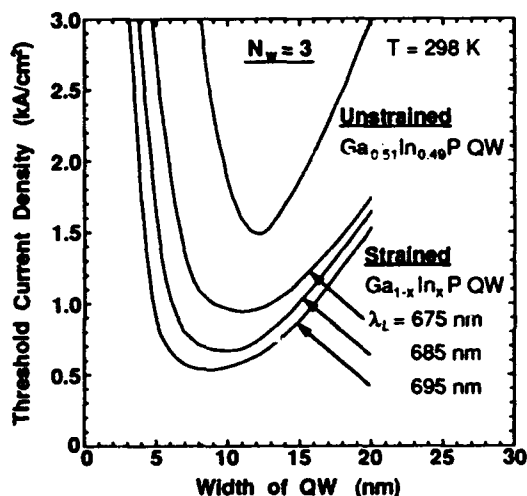

Fig. 3 Calculated dependence of the threshold current density on the different oscillation wavelengths of unstrained and strained GaInP MQWs.
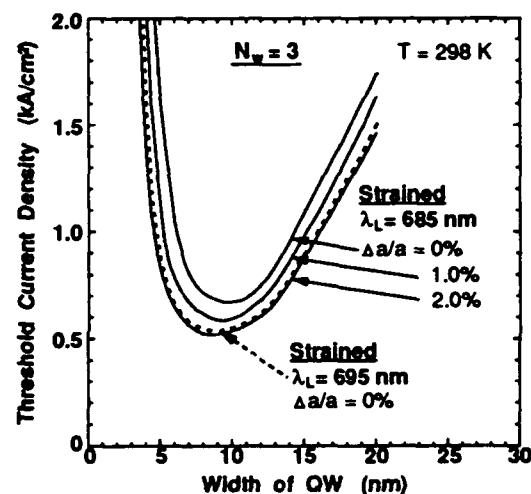

Fig. 4 Comparison of calculated results for threshold current density which depends on oscillation wavelengths and net compressive strains induced by lattice-mismatch in strained MQWs.
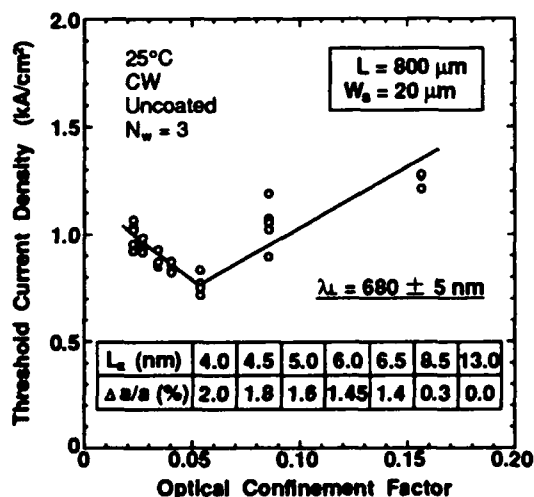

Fig. 5 Threshold current density for several strained MQW LDs related to optical confinement factor in the same oscillation-wavelength range.
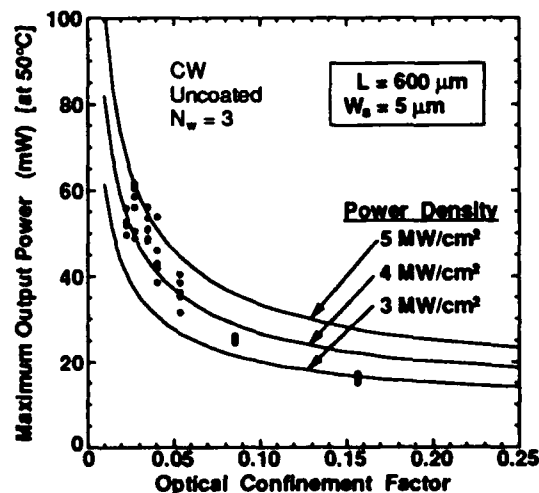

Fig. 6 Dependence of the maximum output power at a temperature of 50°C on optical confinement factor of narrow-stripe strained MQW LDs.

Narrow Linewidth Long Wavelength Phase-Locked Laser Array with Mode Controlling Grating Filter

Jie DONG, Shigehisa ARAI, and Tetsu IKEDA

Department of Physical Electronics, Tokyo Institute of Technology
2-12-1 O-okayama, Meguro-ku, Tokyo 152, Japan
Tel: +81-3-3726-1111 ext.2512. Fax: +81-3-5499-4791

Single-longitudinal-mode (DSM) semiconductor lasers have been widely investigated for achieving low chirping and narrow linewidth characteristics. Various schemes such as corrugation-pitch-modulated distributed feedback lasers[1], DBR[2] or DR[3] lasers with passive regions and quantum wire or box lasers with small α parameter[4] have been reported. High power and small spontaneous emission factor further reduce the spectral linewidth. For achieving high power and small spontaneous emission factor, phase-locked laser arrays[5,6] are attractive as well as for narrow beam operation. We report in this paper a single mode and narrow linewidth characteristics of a five-element $1.5\mu m$ GaInAsP/InP phase-locked laser array with a mode controlling grating filter (GFA).

The GFAs with a compressive strained MQW (CS-MQW) active layer were fabricated with four steps LP-OMVPE growths. Figure 1 schematically shows the GFA structure, which consists of a five-element positive-index-guided phase-locked array region with corrugation over each array element and a common laterally unguided region with a grating filter. The grating filter is used to distinguish different lateral array modes which have different spectral compositions in the Fourier space[5] because of its narrowband-reflecting behavior.

Figure 2 shows the light-current characteristic of a three-pair CS-MQW GFA with step-OCL measured under pulsed condition. The threshold current, maximum power and external differential quantum efficiency from the front facet were 330mA, 150mW and 17%, respectively. The power ratio from the front facet to the rear facet was about 3:1, which meant that large fraction of light was reflected by the grating filter and the external differential quantum efficiency was increased. In order to investigate the mode characteristics, its far-field patterns and spectra are shown in Fig.3. Stable single lobe (FWHM=4.7°) and single-longitudinal-mode (SMSR≥30dB) operation were obtained at 100mW. This indicated the GFA oscillated in the in-phase array mode and the wavelength was determined by the Bragg condition.

Linewidth characteristic of a five-pair CS-MQW GFA with GRIN/STEP-OCL is shown in Fig.4 with that of a previously reported DR laser[3] for comparison. The Bragg wavelength was detuned to shorter wavelength with respect to the gain peak in the order of 10nm. Measurement was made at $-40°C$ in order to get CW operation. The threshold current and maximum power were 130mA and 50mW, respectively. Narrow linewidth of 203kHz was achieved at 25mW output power. In order to see the influence of temperature on the linewidth, measurement was also made at $5°C$. Within single mode operation range, the linewidth characteristic was similar to that measured at $-40°C$. This narrow linewidth property was considered to be due to small spontaneous emission factor.

References: [1] M.Okai, T.Tsuchiya, and N.Chinone, Tech. Dig. Conf. Lasers and Electro. Optics (CLEO'91), CPDP40-1, 1991. [2] R.F.Kazarinov and C.H.Henry, IEEE J. Quantum Electron., vol. QE-23, pp.1401-1409, 1987. [3] J.I.Shim, T.Nomaguchi, K.Kudo, and S.Arai, Electron. Lett., vol.28, pp.741-742, 1992. [4] Y.Miyake and

M.Asada, Jpn. J. Appl. Phys., vol.28, pp.1280-1281, 1989. [5] J.Dong, T.Ikeda, S.Arai, and K.Komori, IEEE Photon. Technol. Lett., vol.4, pp.491-494, 1992. [6] K.-Y.Liou, A.G.Dentai, E.C.Burrows, R.P.Gnall, C.H.Joyner, and C.A.Burrus, 13th IEEE Int. Semicon. Laser Conf., paper D-27, pp.88-89, Takamatsu, Japan, 21-25 Sept. 1992.
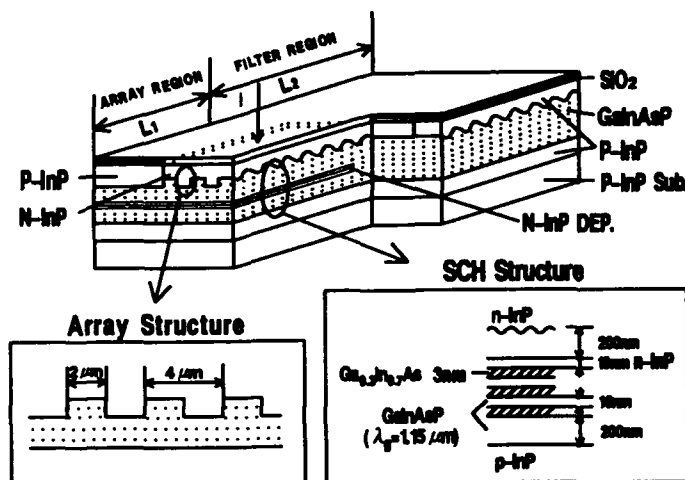
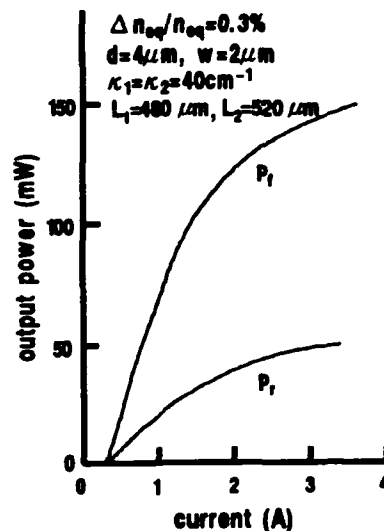Fig.1 Schematic structure of a five-element CS-MQW GFA.

Fig.2 Light-current characteristics from the front and rear facets of a three-pair CS-MQW GFA at pulsed condition.
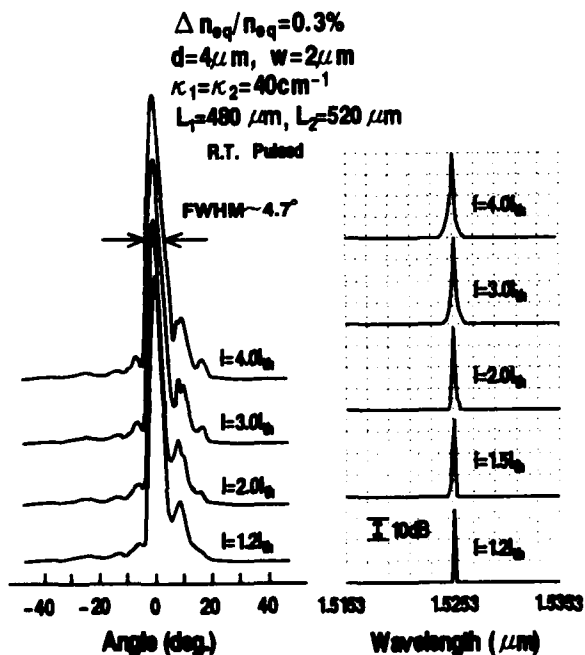
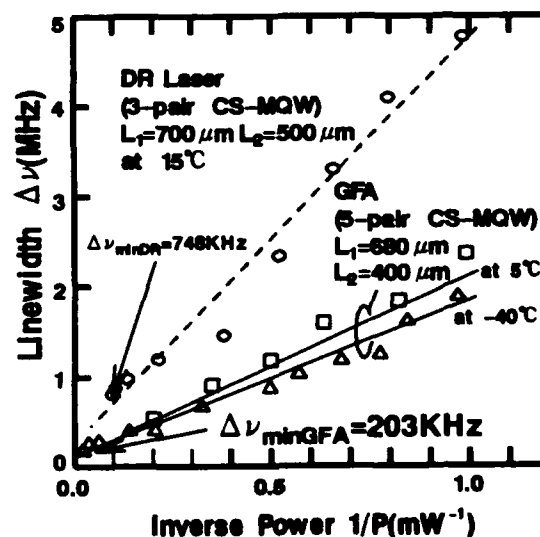Fig.3 Far-field patterns and spectra at various injected levels. Single mode operation was obtaind up to 100mW.

Fig.4 Linewidth characteristic of a five-pair CS-MQW GFA measured at $-40°C$ and $5°C$. Narrow linewidth of 203kHz was achieved at 25mW.

Highly Non-degenerate (>1THz) Four-Wave Mixing in Multi-Quantum Well Laser Structures.

M.C.Tatham, G.Sherlock & C.P.Seltzer

BT Laboratories, Martlesham Heath, Ipswich IP5 7RE. U.K. +44 473 643210

Carrier dynamic processes in semiconductor lasers, such as spectral hole-burning and dynamic carrier heating, give rise to nonlinear gain. This affects many of the important static and dynamic laser characteristics, including the bandwidth and damping of high speed lasers. Recent time-domain pump-probe experiments[1] have shown that several ultrafast processes contribute to nonlinear gain in InGaAs/InGaAsP laser structures with time-constants varying from sub-100fs to 1ps, but these are not yet fully understood. Here we describe measurements of ultrafast carrier dynamic processes in InGaAs/InGaAsP laser amplifiers using the technique of highly non-degenerate four-wave mixing[2,3] (FWM), with pump-probe detunings of >1THz capable of measuring effects with time-constants of <200fs. We have used the technique to make quantitative measurements of both the time-constants and nonlinear gain parameters for the dominant processes.

In the experiments, light from two tuneable, narrow linewidth lasers, with frequencies f_1 and f_2, is coupled into the quantum well traveling wave amplifier (TWA) through the end facet. The light is amplified as it propagates through the TWA and generates conjugate beams at $(2f_1-f_2)$ and $(2f_2-f_1)$. The output intensities of the pump, probe and conjugate beams are measured either by direct detection using an optical spectrum analyser, or by heterodyne measurement. The efficiency of FWM is measured as a function of the pump-probe detuning, with the pump beam frequency maintained close to the gain peak of the TWA.

Figure 1 shows the dependence on pump-probe detuning frequency of the ratios (P_1'/P_1) and (P_2'/P_2) for a 4-well InGaAs/InGaAsP TWA, where P_1, P_2 are the output intensities of the pump and probe beams, and P_1', P_2' the intensities of the conjugate beams. For detunings up to ~100GHz, the conjugate beams show a 2nd-order roll-off resulting from carrier density 'population pulsations' in the TWA, with a characteristic time-constant τ_1 ~80ps, corresponding to the effective carrier lifetime (including stimulated emission).

The clear departure from this roll-off (dotted line) above ~100GHz reveals the presence of fast nonlinear gain effects, giving rise to a second roll-off. The characteristic frequency of this second roll-off at ~320GHz indicates a time-constant τ_2 for the nonlinear gain process of 0.5ps, and from the ratio (P_1'/P_1) at frequencies below $1/2\pi\tau_2$ we find the nonlinear gain parameter, ε, to be ~0.4×10^{-17}cm^3. The solid lines in the figure show the response predicted using a multi-wave solution to the propagation equations, with the above parameters.

Figure 2 shows a similar plot of the ratios (P_1'/P_1) and (P_2'/P_2) against pump-probe detuning, but for a strained-layer 16-well InGaAs/InGaAsP TWA, with ~1% compressive strain in the wells. The
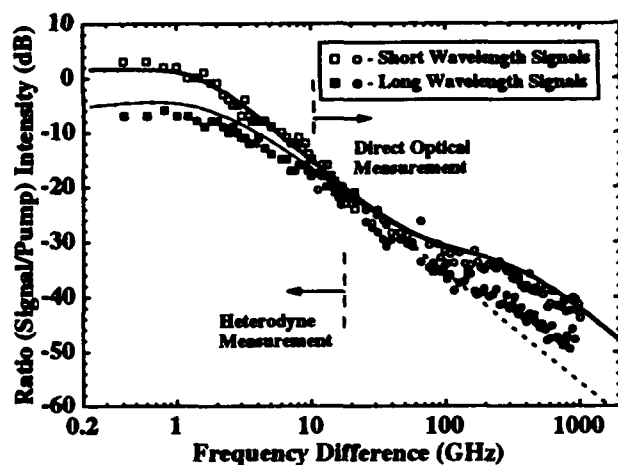
Fig.1: Ratios of conjugate to pump beam intensities for a 4-well quantum well TWA.

Fig.2: Ratios of conjugate to pump beam intensities for an 16-well strained-layer TWA.

dependence on detuning is almost identical, showing a departure from the 2nd-order roll-off (dotted line) above ~100GHz resulting from fast nonlinear gain effects. Again, the time-constant τ_2 for the nonlinear gain process is 0.5ps, $\varepsilon \sim 0.4 \times 10^{-17} cm^3$.

For both the lower frequency roll-off (population pulsations) and the higher frequency roll-off (nonlinear gain), the FWM results from both real and imaginary parts of the susceptibility. For population pulsations, the ratio $Re(\chi)/Im(\chi)$ is given by the 'linewidth enhancement factor', α. The corresponding ratio (which we call β) for the nonlinear gain effects depends strongly on the nature of the effect: for spectral hole-burning $\beta \ll 1$, whereas for carrier heating $\beta \sim \alpha$ (ref. 3). The phases of the conjugate beams generated by FWM depend on α and β; when $\alpha \neq \beta$, interference effects are predicted to arise in the FWM close to the frequency at which the contributions from population pulsations and nonlinear gain are equal. The absence of such interference effects in the data indicates that in fact $\beta \sim \alpha$.

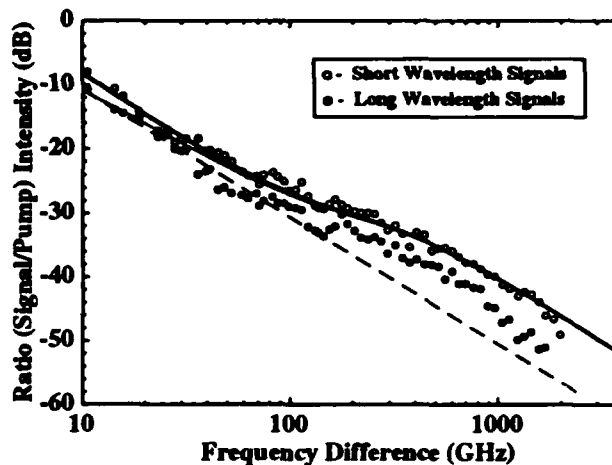That spectral hole-burning is *not* the nonlinear gain effect observed is established by

two observations: (1) the value of $\beta \sim \alpha$, as described above, and (2) the measured time-constant of 0.5ps is too long for this process, under high density conditions ($>5 \times 10^{18} cm^{-3}$). The effect is, however, consistent with dynamic hot carrier effects, although it is extremely difficult to predict a simple time constant for this effect under such conditions.

In conclusion, we have used the technique of highly non-degenerate four-wave mixing in quantum well laser structures to make quantitative investigations of ultrafast carrier dynamics. The results show an almost identical effect in strained and unstrained structures with a characteristic time-constant of 0.5ps. This effect was shown not to be spectral hole-burning, but was consistent with dynamic hot carrier effects.

References

[1] K.Hall, Y.Lai, E.P.Ippen, G.Eisenstein and U.Koren, Appl. Phys. Lett. **57**, 2888, 1990.

[2] L.F.Tiemeijer, Appl. Phys. Lett. **59**, 499, 1991.

[3] K.Kikuchi, M.Kakui, C.-E.Zah and T.-P.Lee, IEEE J. Quantum Electron. **28**, 151, 1992.

Optical Properties of Tensile and Compressively Strained (GaIn)P–(AlGaIn)P Multiple Quantum Wells

Martin D. Dawson and Geoffrey Duggan

Sharp Laboratories of Europe, Ltd.
Edmund Halley Road, Oxford Science Park, Oxford OX4 4GA, United Kingdom
Tel: Int. +44 865 747711

(AlGaIn)P bulk and quantum well heterostructures, grown on GaAs substrates, are being intensively studied for visible laser diode and LED applications, because of the large room-temperature direct energy gaps (up to ~2.3eV) which they offer. Early effort has concentrated on the lattice–matched $Ga_{0.52}In_{0.48}P-(Al_yGa_{1-y})_{0.52}In_{0.48}P$ system. In this case[1], laser action has typically been achieved at ~660 to 680nm at room temperature, with threshold current densities of at best $0.2 - 0.4$ kA cm^{-2}. These lasers have commonly shown rapid degradation in threshold current density as the temperature is increased above 294K. Recently, in an effort to improve performance and shorten the operating wavelength, laser structures with (GaIn)P quantum well active regions *under coherent strain* on the GaAs substrate have been produced. Both[1] compressively and tensile strained active layer lasers have been investigated, with strain of up to ~1% in each case.

Device design and development has, however, been hampered by the lack of studies of the basic physical properties of this material with strain. Indeed, only recently has a consensus been emerging on the fundamental physical parameters of the lattice–matched material, because of complicating effects associated with spontaneous ordering on the Group III sub–lattice[2] during growth by metal–organic vapour phase epitaxy (MOVPE). In an attempt to address these problems, we have undertaken a detailed study of the (AlGaIn)P system, with bulk and quantum well structures grown at high temperature (~750°C) on substrates misoriented from (100), conditions chosen to minimise the effects of alloy ordering. Low temperature photoluminescence (PL) and photoluminescence excitation spectroscopy (PLE) are combined with envelope function approximation modelling of the observed excitonic transitions. We briefly summarise our findings on the lattice–matched material, including strong evidence in support of a conduction band discontinuity, ΔE_c, of ~$0.67\Delta E_g$ in this case. Results on compressively–strained $Ga_{0.45}In_{0.55}P$ (+0.5% strain) and $Ga_{0.4}In_{0.6}P$ (+0.9% strain), and tensile–strained $Ga_{0.6}In_{0.4}P$ (–0.6% strain) structures are presented and general trends extracted.
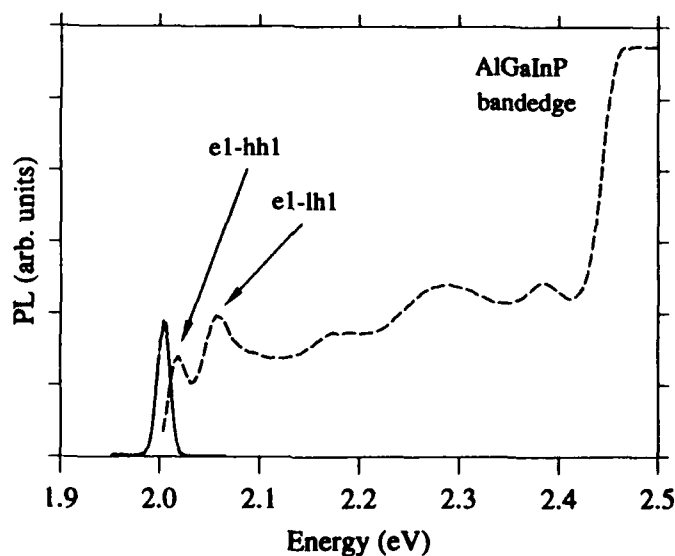

Fig.1. 5K PL and PLE spectra for a 50Å $Ga_{0.45}In_{0.55}P$ MQW structure.

Fig.1 shows an example of 5K PL and PLE spectra taken for a $Ga_{0.45}In_{0.55}P$ 5-period 50Å multiple quantum well (MQW) structure. The e1-hh1 and e1-lh1 splitting (39meV in this case) is clearly resolved, with the PL line Stokes-shifted from the e1-hh1 PLE peak by 14meV. The "absorption" edge of the $(Al_{0.7}Ga_{0.3})_{0.52}In_{0.48}P$ confinement layers in the structure is also clearly visible above 2.4eV.

The e1-hh1 and e1-lh1 transitions measured by PLE, and corresponding PL energies, for a series of samples of the same nominal composition, but differing well-width, are shown in Fig.2. Well widths were determined directly from transmission electron microscopy (TEM) measurements performed on the structures.[3] Also shown in the figure is a "fit" (see below) to the observed excitonic transitions assuming a constant In mole-fraction of 54%. We see that the e1-hh1/e1-lh1 splittings are well accounted for. The small error in the actual energetic positions of the transitions for the larger well widths most likely originates in either the uncertainty in absolute well width obtained from the TEM measurements, or a slight variation (~2 atomic %) in the composition for these separately grown structures. X-ray diffraction measurements indicate an indium mole-fraction of ~57% for the 300Å structure, indicating that the latter explanation is the most likely.
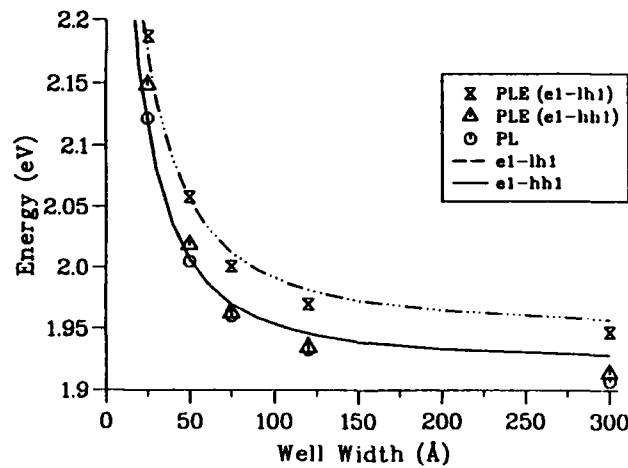

Fig.2. 5K e1-hh1 and e1-lh1 transition energies vs. well width and envelope function fitting for ~0.5% compressively strained structures.

The expected interband transition energies shown by the fitting curves in Fig.2 were calculated within the envelope function approximation, using boundary conditions requiring continuity of the envelope function F and $(1/m^*)(dF/dz)$ at the $(GaIn)P/(AlGaIn)P$ interfaces. Here, z denotes the growth direction of the epitaxial layer. Necessary input parameters included the hydrostatic and shear deformation potentials, elastic moduli, electron-, heavy hole-and light-hole effective masses and spin-orbit splitting, all determined as a function of indium fraction. These were extrapolated from literature values for the appropriate binary end-members, GaP and InP. Also required was the variation of the 5K unstrained gap E_0 with indium fraction (x), which is taken to be[4]:

$$E_0(eV) = 1.421 + 0.73(1-x) + 0.7(1-x)(1-x).$$

The success of this model in generally describing the measured transition energies for all the tensile and compressive strain structures is described.

1.   D. P. Bour et al., Appl. Phys. Lett. **60**, 1927 (1992) and references therein.
2.   A. Gomyo, T. Suzuki, and S. Iijima, Phys. Rev. Lett. **60**, 2645 (1988).
3.   M.D. Scott and P. Rees (private communication).
4.   T.Y. Wang et al., J. Appl. Phys. **68**, 3356 (1990).

Microcavity and Vertical Emitters 2

QThA 8:30am–10:00am
Grand Ballroom East

Kenichi Iga, *Presider*
Tokyo Institute of Technology, Japan

Microcavity VCSELs

J.L. Jewell[1], A. Scherer[2], B. Van der Gaag[2], L.M. Schiavone[2],

J.P. Harbison[2] and L.T. Florez[2]

[1]*Photonics Research Inc., 4840 East Pearl Circle, Boulder, CO 80301*
(303) 541-9292
[2]*Bellcore, 331 Newman Springs Rd., Red Bank, NJ 07701*

Microcavity lasers potentially will have ultra-low thresholds in the micro ampere range or even lower. The vertical-cavity surface-emitting laser (VCSEL) structure represents the most straightforwardly produceable device which can scale down to ultra-small cavity dimensions and active material volumes. By a simple scaling, one can calculate that a single-quantum-well (SQW) microcavity VCSEL, given a 100 A/cm^2 threshold current density, would have a 200 nA threshold if scaled down to a 0.5 μm diameter. This calculated threshold does *not* rely on any enhancement of spontaneous emission, which could further reduce the threshold. The spontaneous emission factor in a GaAs/AlAs microcavity VCSEL of this diameter is predicted to be greater than 0.1, even at room temperature, compared to ~10^{-4} for conventional laser diodes [1], or ~10^{-2} for cryogenic-temperature planar microcavity VCSELs [2]. It is questionable, however, whether such a device is feasible. A SQW microlaser cavity must have extremely low loss, well under 1 % per pass. At some minimum diameter, almost certainly above 0.2 μm, diffraction and scattering due to sidewall roughness and the mirror-layer interfaces will cause losses to be excessively high. For an ultra-small microlaser to be electrically pumped with practical efficiency formidable fabrication challenges must be overcome.

Experiments have shown that GaAs/AlAs microresonators of less than 0.5 μm diameter still have the high finesse required for lasing [3]. A 0.4 X 0.4 μm square microcavity VCSEL, optically pumped with ~10 ps pulses from a mode-locked dye laser, produced laser emission with 2 pJ incident pump energy (Fig's. 1,2). Considering the pump efficiency (1-5 %), the estimated energy absorbed in the spacer was 20-100 fJ, and the carrier density was thus not greatly above the density required for transparency. It is concluded therefore that the optical losses in this microcavity are very small. Furthermore this device was the smallest one tested and it had the lowest pump energy threshold, indicating the possibility of even smaller devices maintaining low loss. Since devices 0.2 μm or smaller will have excessive waveguide losses, the experiments have closely approached the lower feasibility limit of diameter for SQW microlasers. The most important interpretations of this experiment are: 1) high finesse is maintained at extremely small diameters; and therefore 2) the calculations of enhanced spontaneous emission for such structures can be meaningful in real devices.

With the physically feasibility of ultra-small microcavity VCSELs established, attention can turn to reducing effective cavity length by using mirror materials with larger refractive index differences, improving electrical pumping efficiency [4], and suppressing carrier surface recombination at the sidewalls. Fabrication must also be extemely precise since waveguide dispersion causes the cavity resonance to be highly dependent upon device diameter at these small sizes [5].
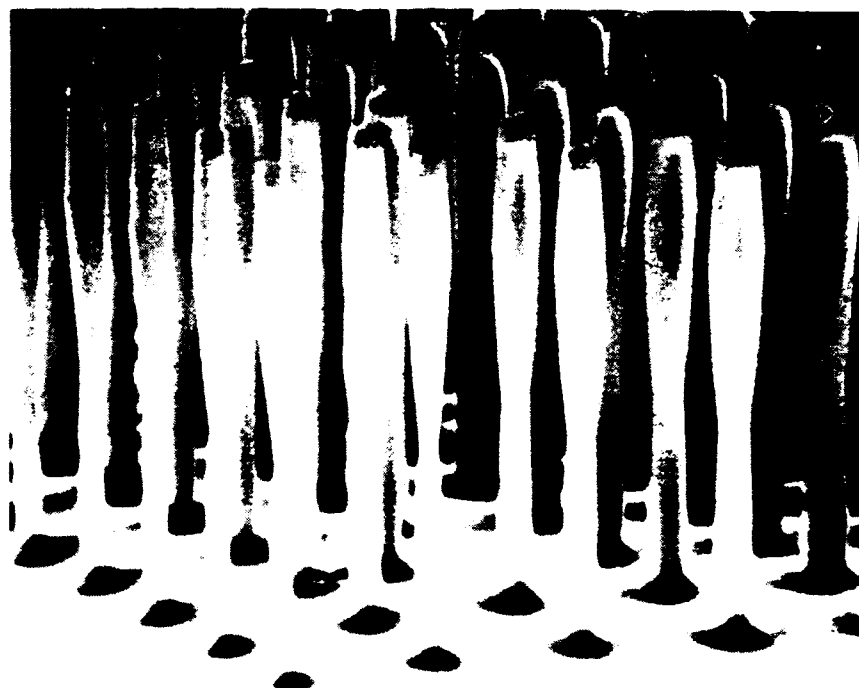
Fig. 1. Scanning electron micrograph of the smallest microcavity VCSELs: 0.4 μm wide by 8 μm tall.
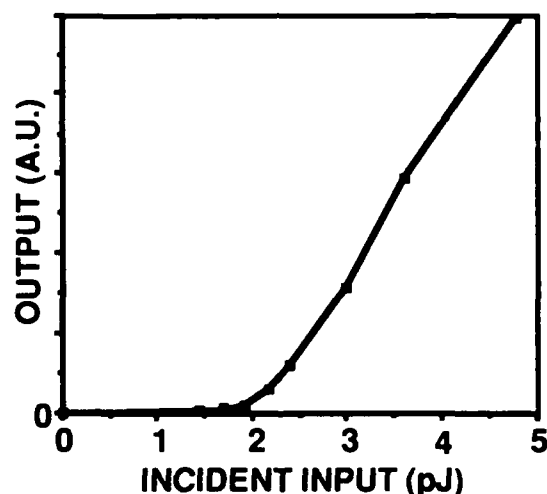

Fig. 2. Output vs. input for the smallest size microcavity VCSEL tested.

[1] Baba, T., Hamano, F., Koyama, F., and Iga, K., IEEE J. Quantum Electron. **27**, 1347 (1991).

[2] Horowicz, R.J., Heitmann, H., Kadota, Y., and Yamamoto, Y.,Appl. Phys. Lett. **61**, 393 (1992).

[3] Jewell, J.L., Scherer, A., Van der Gaag, B., McCall, S.L., Harbison, J.P., Florez, L.T., and Schiavone, L.M., Topical Meeting on Quantum Optoelectronics, Optical Society of America, Salt Lake City, Utah, March 11-13, 1991, Postdeadline Paper PdP3.

[4] Scherer, A., Jewell, J.L., Walther, M., Harbison, J.P., and Florez, L.T., Electron. Lett. **28**, 1224 (1992).

[5] Jewell, J.L., McCall, S.L., Scherer, A., Houh, H.H., Whitaker, N.A., Gossard, A.C., and English, J.H., Appl. Phys. Lett., **55**, p. 22 (1989).

Threshold Reduction of 1.3 μm GaInAsP/InP Surface Emitting Laser by a Maskless Circular Planar Buried Heterostructure Regrowth

T. Baba, K. Suzuki, Y. Yogo, K. Iga and F. Koyama

Tokyo Institute of Technology, P & I Lab.
4259 Nagatsuta, Midori-ku, Yokohama, 227 Japan
Tel. +81-45-922-1111 Ext. 2026, Fax. +81-45-921-0898

By a maskless PBH (planar buried heterostructure) LPE regrowth technique, we improved the hetero-interface of GaInAsP/InP circular BH structure. In this report, we demonstrate a low threshold 1.3 μm BH type surface emitting laser using this technique. We call this type of device circular PBH surface emitting laser (CPBH-SELD).

Recently, the room temperature pulsed operation of GaInAsP/InP SELD has been realized by several device structures[1-4]. However, most of them do not satisfy the condition for the room temperature cw operation, i.e., a low threshold current, low device resistance, and effective heat sinking. The BH seems to be the best structure not only for these requirements but also for reducing the surface recombination problem and extracting ultimate quantum optoelectronic performance of microcavity SELD.

Our device structure is shown in Fig. 1. To achieve efficient carrier confinement and heat sinking, the circular active region is buried by p- and n-InP blocking layers and additionally covered with a p cladding layer. Owing to the almost planarized epitaxial surface, we can also expect a high reflectivity laser mirror formed on it. Previously, we reported a similar structure, the FCBH SELD, fabricated by a 2-step LPE regrowth[5]. Although it recorded a low threshold (4.2 mA) at 77 K, there still remains a problem of relatively defective hetero-interface which appears as pinholes around the mesa after the regrowth and the leakage current remarkable against both forward and reverse bias. In this study, we introduce a single step maskless PBH regrowth[6] to overcome this problem. We prepared a DH wafer having 0.7 μm thick p-GaInAsP active layer. After forming a circular mesa of 2 μm in height by a chemical etching, the blocking layers (each of them are 1 μm thick), cladding layer, and quaternary cap layer are successively grown without masks. From the direct observation of the cross-section of grown structure near the circular mesa, we confirmed that blocking layers do not grow on the mesa of less than 12 μm in diameter. It should be noted that, in this process, most of pinholes around the mesa disappeared and the leakage current decreased especially against the reverse bias.

So grown wafers were processed into a newly optimized device structure. As shown in Fig. 1, the cap layer just above the active region was removed to eliminate the large free-carrier absorption loss of this layer[7]. In spite of the complicated current injection from such window cap structure, homogeneous spontaneous emission was observed from a 12 μm diameter active region. This result coincides with the almost uniform current injection predicted by the SPICE simulation based on the model of Fig. 2(a). This window cap permits to individually design the thickness of cap layer d_{cap} for the reduction of device resistance r, apart from the limitation coming from the design of laser cavity. As illustrated in Fig. 2(a), the current injected from the ring electrode flows through the cap layer and concentrates to the active region. We found in the simulation that r decreases as d_{cap} increases. As shown in Fig. 2(b), r was reduced typically from 45 Ω to 10 Ω by increasing d_{cap} from 0.3 μm to 1 μm.

Fig. 3 shows lasing characteristics of fabricated devices at 77 K under cw condition. The minimum threshold current obtained was 2.2 mA. This is the lowest value that has ever been reported by BH-type devices. This reduction seems to be primarily attributed to the reduction of leakage current and the elimination of absorption loss at the cap layer. Since this threshold still includes the leakage current of about 0.6 mA, which does not contribute to the emission, the threshold will be much lower by further improving the regrowth process. Room temperature operation and higher temperature cw operation will also be expected. In addition, the quantum optoelectronic effect of microcavity, i.e., spontaneous emission control and photon recycling, may be obtained by further reducing the device size and deeply etching

the surrounding region to be a post-shape cavity.

References

1) A. Kasukawa, Y. Imajo, S. Kashiwa, T. Fukushima and H. Okamoto, *Proc. 48th Device Res. Conf.*, VB-II, 1990.

2) H. Wada, D. I. Babic, D. I. Crawford, J. J. Dudley, J. E. Bowers, E. L. Hu and J. L. Merz, *IEEE Photon. Technol. Lett.* **3**, 977, 1991.

3) S. Kubota, F. Koyama and K. Iga, *Proc. Conf. Laser and Electro-Optics.*, JThD5, 1992.

4) T. Tadokoro, H. Okamoto, Y.Kohama, T. Kawakami and T. Kurokawa, *IEEE Photon. Technol. Lett.* **4**, 409, 1992.

5) T. Baba, K. Matsuoka, F. Koyama and K. Iga, *Dig. Optoelectronic Conf.*, 16C2-3, 1992.

6) I. Mito, M. Kitamura, K. Kobayashi, S. Murata, M. Seki, Y. Odagiri, H. Nishimoto, M. Yamaguchi, and K. Kobayashi, *IEEE/OSA J. Lightwave Technol.* **LT-1**, 195, 1983.

7) N. Yokouchi, T. Uchida, T. Miyamoto, Y. Inaba, F. Koyama and K. Iga, *Jpn. J. Appl. Phys.* **31**, 1255, 1992.
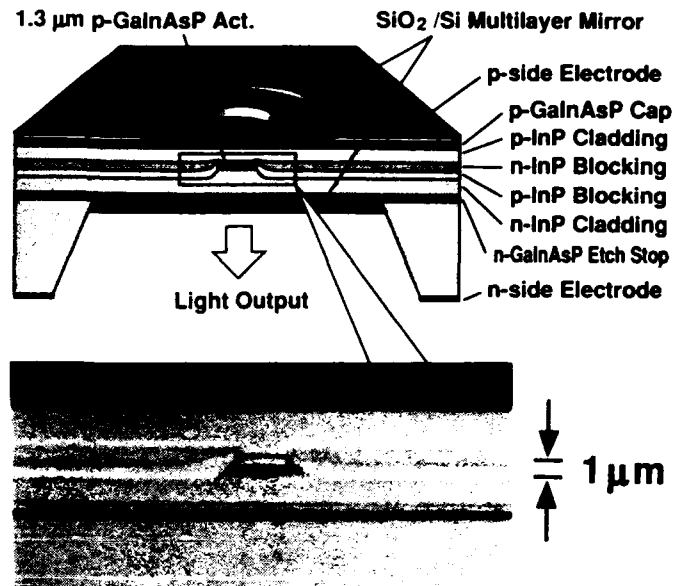

Fig. 1 Schematic of GaInAsP/InP CPBH-SELD and cross-sectional view of grown structure cleaved near center of circular active region. The photo includes etch stop layer which will be removed in fabrication process.
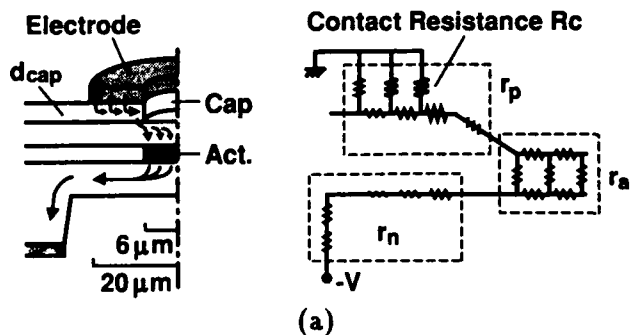

Fig. 2 Current flow and device resistance of CPBH-SELD. (a) Analysis model and (b) theoretical and experimental results versus thickness of cap layer.
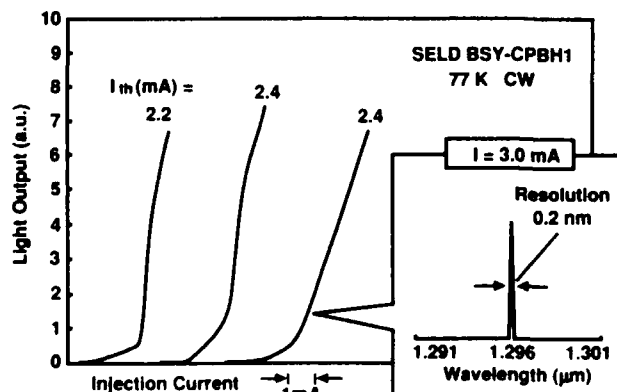

Fig. 3 Lasing characteristics of fabricated devices at 77 K under cw operation.

Pixels Consisting of a Single Vertical-Cavity Laser-Thyristor and a Double Vertical-Cavity Phototransistor

Hideo Kosaka, Ichiro Ogura, Hideaki Saito, Mitsunori Sugimoto,

Kaori Kurihara, Takahiro Numai, and Kenichi Kasahara

Opto-Electronics Research Laboratories, NEC Corporation,

34 Miyukigaoka, Tsukuba, Ibaraki 305, Japan

Phone: +81-298-50-1172, FAX: +81-298-56-6140

Abstract

Bi-directionally cascadable optical pixels comprising low-threshold (1mA) high-efficiency (0.25W/A) surface-emitting laser-thyristors and wide-bandwidth (50Å) high-photocurrent-gain (230A/W) double vertical-cavity phototransistors are described.

1. Introduction

Vertical-cavity surface-emitting lasers (VCSELs) are promising for two-dimensional optical interconnections and information processing. Furthermore, integrating photodetector function with them enables bi-directional or cascadable interconnections [1-3]. A p-i-n photodetetor alone, without any support of transistor amplifier such as an HBT or FET, is insufficient for driving VCSELs, while a heterojunction phototransistor (HPT) has the ability to drive VCSELs directly. However, the fabrication process for integrating VCSELs and HPTs is not easy due to structural differences.

In this work we propose a pixel consisting of a VCSEL-thyristor and a Double Vertical-Cavity HPT (DVC-HPT), using the same structure, as shown in Fig. 1. This pixel features that the VCSEL-thyristor and DVC-HPT are formed by the same layer structure as VC-VSTEP [1], except for a spacer layer inserted into the lower DBR of the DVC-HPT. The schematic diagram of the unit circuit is shown in Fig. 2. The VCSEL-thyristor is switched electrically or optically, and then functions as a VCSEL modulated by the light incident on

the HPT. To obtain low laser threshold, active layers in the VCSEL-thyristor consist of InGaAs quantum-well layers, which act also as photo-absorption layers in the DVC-HPT. Absorptivity in the HPT sections is enhanced through resonant-cavity effect. Using the same high-Q cavity as VCSEL, however, the absorption bandwidth is so narrow that we have introduced a spacer layer in the lower DBR of the HPT to obtain wide absorption bandwidth together with high absorptivity. The DVC-HPT structure provides enough bandwidth to tolerate the wavelength change of the laser by heating, and makes precise wavelength control unnecessary [4,5]. Besides, the junction-side down configuration is preferable for good heat dissipation.

2. Device Structure and Fabrication

A wafer for the pixel is prepared using a molecular beam epitaxy (MBE) regrowth; the first growth up to the spacer layer and the second growth comprising pn-pn structure. The spacer layer ($\lambda/2$-thickness) in the VCSEL section is removed by wet-etching and desorption before starting the second growth. The active layer is made of three 100-Å undoped $In_{0.2}Ga_{0.8}As$ strained quantum wells inserted into the pn-pn structure, and positioned at the peak of the electric-field standing-wave pattern inside 3λ-separated distributed Bragg reflectors (DBRs) with alternating $\lambda/4$ AlAs/GaAs layers. Upper DBR (14.5 pairs) is p-doped (Be: $3\times10^{18}cm^{-3}$) and lower DBR (22.5 pairs) is n-doped (Si: $2\times10^{18}cm^{-3}$). The lower npn layers in the pn-pn structure for VCSEL-thyristor are used for collector, base, and emitter for DVC-HPT, respectively.

3. Results

Figure 3 shows calculated absorption bandwidth and threshold gain for the VCSEL. To obtain low lasing-threshold gain, the layer number of the bottom DBR should be larger than 20 pairs. The absorption bandwidth with the same structure is narrow, when the same DBR structure is used. Figure 4 shows calculated absorption spectrum of the DVC-HPT together with the experimental photocurrent spectrum. The layer number of the bottom is changed keeping the total number of the middle and bottom DBR to be 23 pairs. In the case of the

7.5 pair-bottom DBR, the bandwidth and the peak absorptivity are about five times larger than that of the single vertical-cavity structure without the spacer. The bandwidth of 50 Å permits a temperature change of 80°C in the laser section, assuming the temperature dependence of the lasing threshold to be 0.63Å/°C. Typical I-V characteristics for the HPT are shown in Fig. 5 as a function of the incident-light power. The photocurrent gain of 230 A/W is obtained with 10 μW incident-light power. Typical L-I and I-V characteristics for the VCSEL-thyristor are shown in Fig. 6 [6]. The lasing threshold is 1 mA, and the slope efficiency is 0.25 W/A. After the VCSEL-thyristor is switched on, the HPT drives the VCSEL with the optical gain of 57.5.

4. Conclusion

In conclusion, we have demonstrated pixels consisting of single vertical-cavity laser-thyristors and double vertical-cavity phototransistors using the same pnpn structure, which have high optical gain (57.5) and wide spectral bandwidth (50Å). Their simplicity of the implementation makes them attractive for high-density 2-D optical interconnections and information processing.

References

[1] T. Numai, M. Sugimoto, I. Ogura, H. Kosaka, and K. Kasahara, Appl. Phys. Lett. 58 (1991) 1250.

[2] I. Ogura, H. Kosaka, T. Numai, M. Sugimoto, and K. Kasahara, Appl. Phys. Lett. 60 (1992) 799.

[3] H. Kosaka, K. Kurihara, M. Sugimoto, and K. Kasahara, Jpn. J. of Appl. Phys. 30 (1991) L1172.

[4] I. J. Fritz, J.F. Klem, and J.R. Wendt, Appl. Phys. Lett. 59 (1991) 753.

[5] H. Kosaka, I. Ogura, M. Sugimoto, H. Saito, T. Numai, and K. Kasahara, SSDM '92, Tsukuba, Japan, (1992) B-5-2.

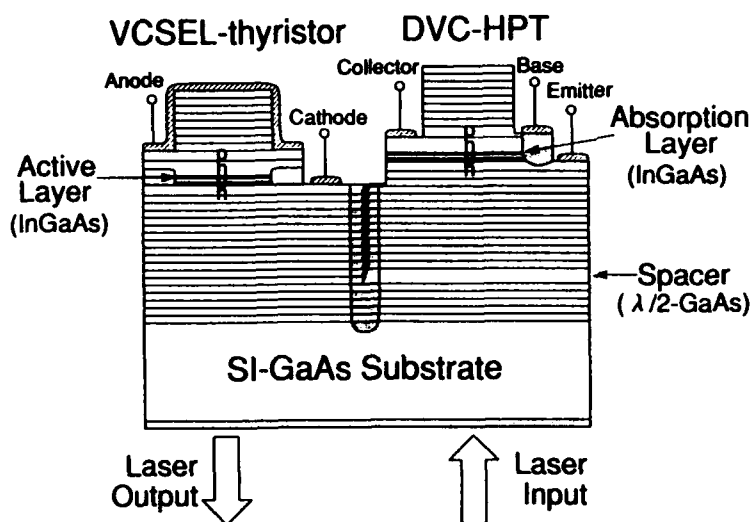[6] K. Kurihara, T. Numai, I. Ogura, H. Kosaka, M. Sugimoto, and K. Kasahara, SSDM '92, Tsukuba, Japan, (1992) B-5-3.

Fig. 1. Integrated VCSEL-thyristor/Double Vertical-Cavity HPT device structure.
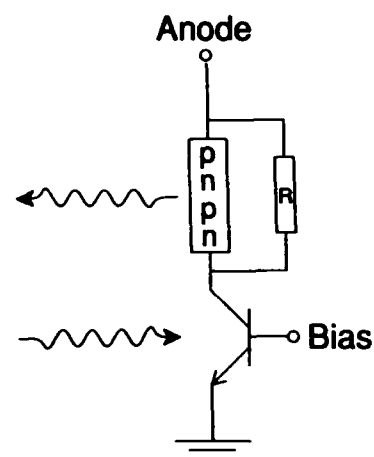

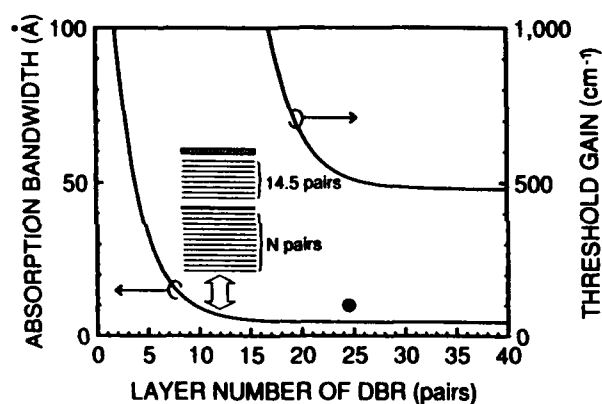**Fig. 2.** Schematic diagram of the unit circuit.

Fig. 3. Calculated absorption bandwidth and threshold gain versus layer number of lower DBR in the VCSEL. Closed circle shows the experimental bandwidth.
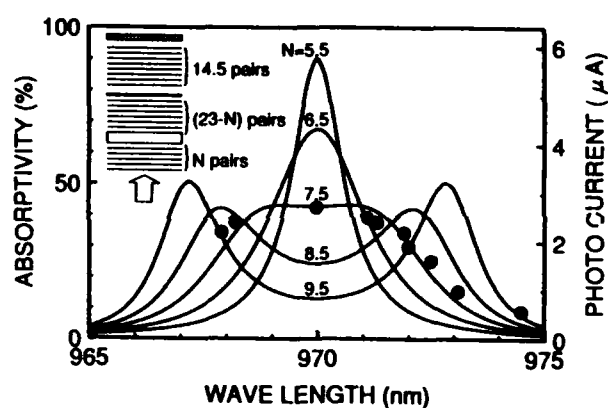

Fig. 4. Calculated absorptivity spectrum of the Double vertical-cavity HPT with the bottom DBR consisting of different layer number. Closed circle shows the experimental photocurrent at 7.5 pairs.
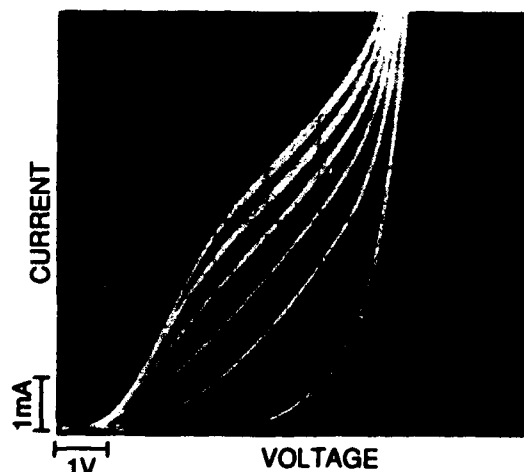

Fig. 5. I-V characteristics of the HPT under different incident-light intensities (10 μW/ step).
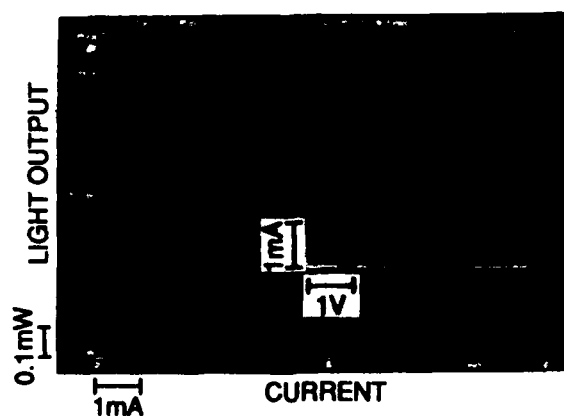

Fig. 6. L-I characteristics for the VCSEL-thyristor. The inset shows I-V characteristics.

Intensity Modulation Bandwidth Limitations of Vertical-Cavity Surface-Emitting Laser Diodes

M.G. Peters, M.L. Majewski[†], L.A. Coldren

ECE Dept., University of California, Santa Barbara
Santa Barbara, CA 93106 : (805) 893-8154
[†]on leave from the University of Queensland, Australia

Vertical-Cavity Surface-Emitting Lasers (VCSELs) are seen as major candidates for optical interconnections. This is due to their extremely low threshold currents, easy on-chip integration of multiple devices, and high-efficiency fiber coupling. Important to most practical applications of VCSELs is the ability to operate these devices at high data rates (up to several Gbit/sec) which requires their intensity modulation bandwidths to be in the GHz frequency range.

It has recently been reported by several authors[1,2] that the modulation bandwidth of VCSEL structures which drive current through the semiconductor DBR mirror stacks may be severely limited because of high electrical and thermal resistances of the mirrors. Therefore, in order to be able to quantitatively analyze the effects of the external (extrinsic) parasitic components, especially the DBR mirrors, on the intensity modulation bandwidth we introduce for the first time a simple small-signal equivalent circuit model for a VCSEL device.

The device structure[3] and the proposed equivalent circuit model are shown in Fig. 1. It can be noted that some other parasitic components outside the device, i.e. packaging, test equipment, etc. have been ignored for simplicity. R_{SUB} and R_C are the substrate and contact resistances and are on the order of a few ohms. R_{M1} and R_{M2} are the n-type and p-type mirrors resistances, respectively, which are current dependent and are much greater than the other components so $R \approx R_M(I) = R_{M1}(I)$ and $R_{M2}(I)$. R_A and C_A are used to model the carrier transport effects in the spacer and active regions and are combined into a time constant $\tau_A = R_A C_A$ (used as a fitting parameter). The "intrinsic laser diode" in Fig. 1(b) models the response of the multiple quantum-well (MQW) active region. This intrinsic response can be evaluated based on relative intensity noise (RIN) measurements of the device and the ultimate achievable 3dB modulation bandwidth of a structure can be determined[4]. The overall 3dB modulation bandwidth, however, is a product of the intrinsic and parasitic responses. The following page shows the formulas developed for estimating each the extrinsic (1) and intrinsic (2) effects.

To determine the resistive characteristics of the DBR mirrors, R_M, separately grown n-type and p-type mirror stacks were MBE grown and tested. The results were scaled for a 6μm device and are shown in Fig. 2 along with the light output curve of the single-mode 6μm VCSEL used in this experiment. Figure 3 shows the results of RIN measurement of the 6μm device. The saturation of the resonance peak frequency, f_r, and the structure of the damping factor, Γ_r, are typical to MQW structures and have been theoretically analyzed[5,6]. Because of low optical powers, gain compression effects were not included.

The intrinsic and extrinsic modulation responses for three different bias currents are shown in Fig. 4 and in each case the parasitics limit the modulation response. An estimated C of 0.1pF and an assumed τ_A of 180ps (with $C/C_A \ll 1$) was used. The remaining parameters were determined from Figs. 2&3. A comparison between measured and calculated modulation responses (at 2.0 mA current) is shown in Fig. 5. The agreement between the characteristics is satisfactory despite the simplicity of the model. Using this model, improvement in modulation response for lower resistive and capacitive structures as well as different active regions can be estimated.

[1] Gamelin, J., Lin., S., Hong, M., and Mannearts, J.P., CLEO '92, paper JThD2, 424, 1992

[2] Dziura, T.G., Yang, Y.J., Fernandez, R., and Wang, S.C., *Appl. Phys. Lett.*, **59**, 1147, 1991

[3] Geels, R.S., Corzine, S.W., and Coldren, L.A., *IEEE J. Quantum Electron.*, **27**, 218, 1990

[4] Fukushima, T., Nagarajan, R., Bowers, J.E., Logan, R.A., Tanbin-E.T., IEEE Phot. Tech. Lett., **3**, 691, 1991

[5] Lee, J. and Vassell, M.O., *IEEE J. Quantum Electron.*, QE-28, 624, 1992

[6] Zhao, B., Chen, T.R., and Yariv, A., *Appl. Phys. Lett.*, **60**, 313, 1992

$$A_{extr}(f) = \frac{f_o^2}{\sqrt{(f_o^2 - f^2)^2 + (f\Gamma/2\pi)^2}} \quad (1)$$

$$f_o = 1/(2\pi \sqrt{(\tau_A \tau)})$$

$$\Gamma = 1/\tau_A + (1 + C/C_A)/\tau$$

$$\tau_A = R_A C_A \; ; \tau = RC \; ; \; R \approx R_M$$

$$A_{intr}(f) = \frac{f_p^2}{\sqrt{(f_p^2 - f^2)^2 + (f\Gamma_i/2\pi)^2}} \quad (2)$$

$$f_p, \Gamma_i \text{ derived from RIN measurements}$$

$$A_{tot}(f) = 20\log(A_{intr}) + 20\log(A_{extr})$$

Fig.1
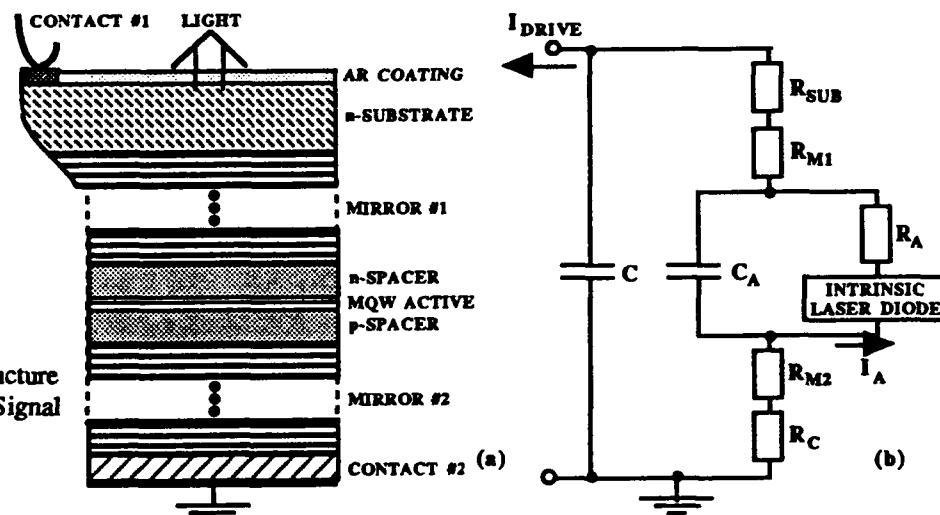(a) VCSEL Device Stucture
(b) Equivalent Small-Signal Circuit Model
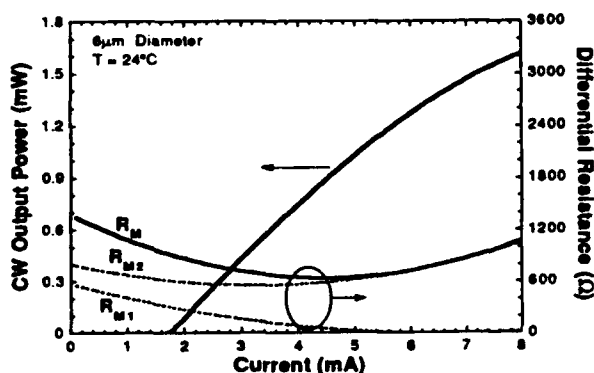
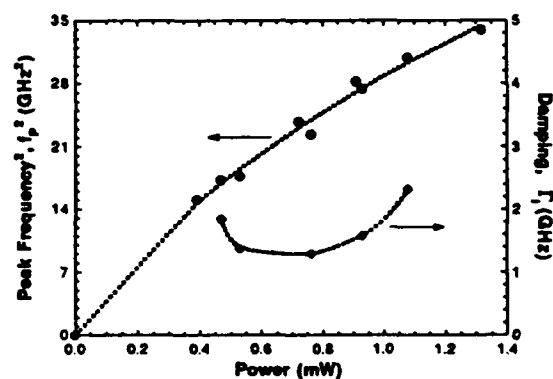**Fig.2** LI Curve and DBR mirror resistance characteristics of 6µm diameter single-mode VCSEL

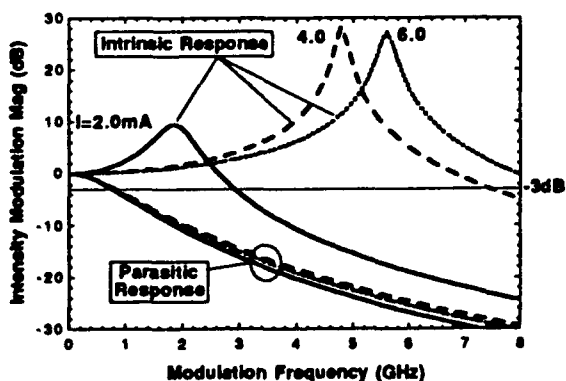**Fig.3** Relaxation resonance frequency, f_p, and damping factor, Γ_i, of 6µm VCSEL extracted from RIN data

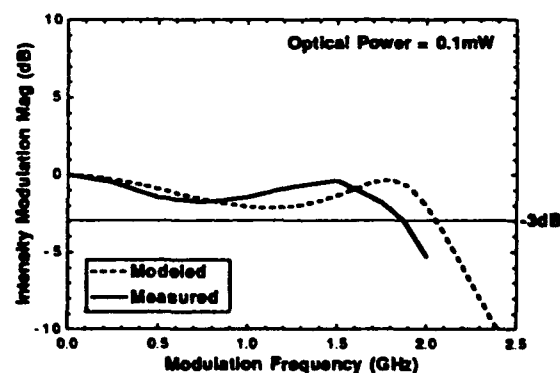**Fig.4** Calculated intrinsic (using RIN data) and extrinsic (measured parasitics) response of 6µm VCSEL.

Fig.5 Total calculated (intrinsic + extrinsic) and measured response of 6µm VCSEL at 2.0mA current.

Modulators 2

Analog Differential Self-linearized Quantum Well Self-Electrooptic Effect Modulator

E.A. De Souza, L. Carraresi, G.D. Boyd and D.A.B. Miller

AT&T Bell Laboratories, 101 Crawfords Corner Road
Holmdel, New Jersey 07733-3030

We demonstrate a new mode of operation for quantum well self-electrooptic-effect devices (SEEDs) using their *analog* features, and our results shows that this device is potentially useful for analog systems. This device was recently proposed as a new analog SEED circuit operating with differential pairs of light beams[1]. It uses the *difference* in two light beam powers to represent an analog value. Normally, processing such bipolar values is difficult with optics. This new circuit allows many different analog functions to be performed, including addition, subtraction, and differentiation of images, correlation, and optically controlled bipolar matrix-vector multiplication[2]. In general, such operations operate on and generate both positive and negative values; this circuit allows full use of such values in analog systems, and, since it was fabricated using the symmetric SEED array process[4], it is compatible with being fabricated in large two-dimensional arrays. We demonstrate the linear performance of this circuit from 50 nW to 3 mW optical powers.

The key to this device is the use of a negative feedback "self-linearized" mode of simple SEED circuits, extended here to a novel circuit with two quantum well modulator/detector diodes in series. The negative feedback arises when the absorption in the diode rises with increasing voltage. As discussed previously, when we drive a single, illuminated quantum well diode with a current source, the voltage across the diode adjusts itself to generate just enough absorption to give a photocurrent equal to the drive current[3]. The absorption changes result from quantum-confined Stark effect electroabsorption in the quantum wells. For example, if the diode was generating too little photocurrent, the net current would charge up the diode, increasing its absorption and hence its photocurrent. Since these diodes give one electron of current for every photon absorbed, the absorbed power is linearly proportional to drive current.

The present circuit (Fig. 1) extends the use of this mode to a *pair* of quantum well diodes reverse-biased electrically in series, and with a current I_c injected into the center between the two diodes. In this case, applying the above "self-linearizing" principle together with conservation of current, we can deduce that the difference in the absorbed power in the two diodes is proportional to the drive current into the center. This mechanism works for either an electrical (Fig. 1(a)) or optoelectronic source for I_c (Fig. 1 (b)).
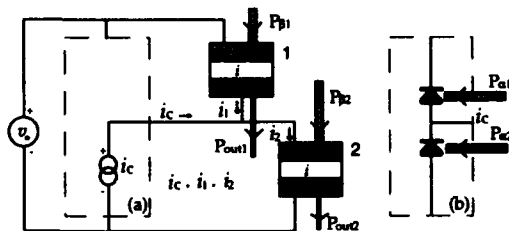

Fig. 1. Self-linearized differential modulator. (a) with current source. (b) with two conventional photodiodes providing a current proportional to the difference in input powers.

In the case of the photodiode pair current source in Fig. 1(b), a current I_c flows out of the center point of the two conventional input photodiodes. The photocurrent in these diodes is essentially independent of reverse bias voltage and is therefore proportional to the *difference* in the absorbed powers in the two diodes. If the power $P_{\alpha1}$ is larger than the power $P_{\alpha2}$, a positive current flows out of the center point. By conservation of the current, in the steady state the difference in absorbed power in the two quantum well diodes is linearly proportional to the difference in the incident powers on the two conventional diodes.

We characterized this circuit both using a current source and using two conventional diodes as a current generator, as shown in Fig 1. For simplicity, we use equal input power shining on the quantum well diodes, ($P_{\beta1} = P_{\beta2}$). Then the difference in the output powers P_{out1} and P_{out2} is proportional to the difference in input powers $P_{\alpha1}$ and $P_{\alpha2}$. It is easy to see how such a circuit can be used to perform image subtraction and spatial derivatives of images.

In the case of the electrical current source, by scanning the source current between positive and negative current values we obtained a curve of the difference between the two output beams ($D_{out} = P_{out1} - P_{out2}$) from the quantum well diodes as a function of the current flowing in to the center point. The Fig. 2 shows these results; the family of curves represents different power levels shining on the quantum well diodes.
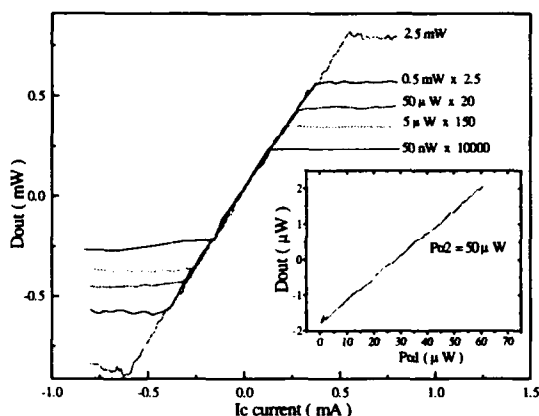
Fig.2 . Difference between the output from the two quantum well diodes as a function of the source current flowing in the center point for various powers incident on the quantum well diode. The operating wavelengh is 856 nm. For the lower powers, the scales on both axes are modified by the factor shown. The insert shows operation with optical drive.

As can be seen from Fig. 2, the absorbed power in the quantum well diode is linearly proportional to the drive current over a range of more than four orders of magnitude within the central operating region. Assuming that each photon absorbed in the quantum well generates one electron of current, the slope should be equal to hv/e, where h is a Planck's constant, v the light frequency and e the electron charge. The slope of experimental curves is 1.48 V, which is close to the theoretical value, hv/e = 1.45.V.

Another feature of this device is the fact that the slope is independent of the power level shining on the quantum well diodes; the range of linearity does increase with increasing the power level. The limits of the linear range arise when one or other diode reaches its maximum or minimum absorption; for the data shown here, the limits occur when one of the diodes goes into forward bias.

In the case of optical drive, we used two "conventional" diodes as a source of current. In our case, we actually used two other quantum well diodes as the "conventional" diodes; when illuminated with short wavelength (~780 nm), their responsivity is essentially independent of reverse bias voltage. The insert on Fig. 2 shows the curve of D_{out} as a function of the (~780 nm) incident power on one "conventional" diode. We maintained a constant power on the other "conventional" diode. In this case, the difference in the output beams, D_{out}, is proportional to the difference between the input beams, $(P_{\alpha 1} - P_{\alpha 2})$, shining on the "conventional" diodes.
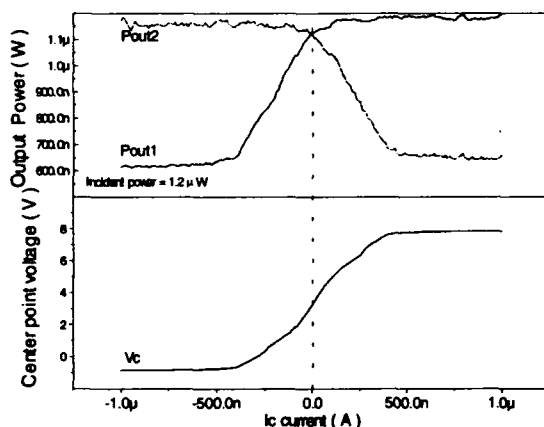

Fig 3 Output power from the quantum well diodes and voltage applied on them as a function of the drive current. The operating wavelength is 856 nm.

Fig. 3 shows the individual output powers (P_{out1} and P_{out2}) from this circuit, and the voltage at the center between the two quantum well diodes, as a function of the drive current. These curves represent the physical performance of this circuit. When the voltage (Vc curve) in the center between the two quantum well diodes is low, the quantum-confined Stark effect shifts the absorption edge of the quantum well diode 1 to long wavelengths, increasing its optical absorption (P_{out1} curve). The same happens with quantum well diode 2 when the voltage in center between the two quantum well diodes is high (P_{out2} curve). Note that when we look at these individual powers, these powers are not linear with drive current over the operating range (in this case +/- 400 nA), even though the difference, D_{out}, is linear.

In conclusion, we have demonstrated the concept of the self-linearized differential modulator, we have shown linearity over more than four orders of magnitude, and have shown that the circuit can be driven both electrically and optically, directly demonstrating the ability to subtract two optical powers. It should now be possible to construct two-dimensional arrays of devices for a variety of analog optical processing applications.

[1] D.A.B. Miller, Smart Pixels Conference, Santa Barbara, August 10, (1992) Paper WB3.

[2] D.A.B. Miller, IEEE J. Quantum Electron. Special Issue on Smart Pixels , to be published, December (1992)

[3] D. A. B. Miller, D.S. Chemla, T.C. Damen, T.H.Wood, C.A. Burrus Jr, A.C. Gossard, and W. Wiegmann, IEEE J. Quantum Electron. QE-21, 1462, (1985)

[4] L. M. F. Chirovsky, L.A. D'Asaro, C.W. Tu, A.L. Lentine, G.D. Boyd, and D.A.B. Miller, Proceedings of the OSA Topical Meeting on Photonic Switching, March1-3, 1989, Salt Lake City

AlGaAs/InGaAs/GaAs Multiple Quantum Well Voltage Tunable Bragg Reflector with Inter-digitated Contacts

O. Blum,
University of California, Berkeley, CA 94720, (510) 643-9862
J. E. Zucker
AT&T Bell Laboratories, Holmdel, NJ 07733, (908) 949-1077
X. Wu, K. Gulden, T. K. Gustafson
University of California, Berkeley, CA 94720, (510) 643-3139

Future developments in optical communications, interconnects and information processing rely on availability of integratable, tunable, surface-normal geometry mirrors and filters. In this paper, we present the first tunable multiple quantum well (MQW) distributed Bragg reflector (DBR) with inter-digitated contacts. This contacting scheme, shown in Fig. 1, allows us to apply large fields across MQW $\lambda/4$ layers producing electro-refraction and electro-absorption associated with the quantum confined Stark effect. Compared to our previous MQW DBR [1], where the applied voltage dropped across the entire mirror stack, in this work we obtain similar changes in reflectivity with nearly 20 times lower voltages .

The DBR consists of 30.5 pairs of bulk $\lambda/4$ $Al_{.7}Ga_{.3}As$ layers alternating with MQW $\lambda/4$ layers. The MQW $\lambda/4$ layer contains 4 $In_{.15}Ga_{.85}As$ quantum wells and 3 GaAs barriers. Fig. 2 shows the measured zero bias reflection spectrum along with the calculated response. The theoretical curve is calculated using the transmission matrix method and absorption and refractive index spectra obtained from a control sample that contained only the quantum wells. Both the magnitude and the position of the reflectivity stop band, as well as the position of the fringes are in good agreement with the measured response. We obtain reflectivity of 98% at 1.06 μm indicating that this material system is ideal for YAG based system applications.

In Fig. 3 we show the measured changes in reflectivity, $\Delta R/R$ for both positive and negative applied voltages. For -3 V applied the maximum $\Delta R/R$ of 10% is measured near 990 nm. Application of +1 V produces $\Delta R/R$ of 12% at 950 nm. These changes in reflectivity are caused by shifts of the excitonic absorption edge in InGaAs quantum wells and the attendant changes in refractive index and are predicted by our model. We find that the inter-digitated contacts produced by the shadow masking growth technique [2] allow small voltages to produce large electric fields across the MQW layers, with extremely low leakage currents, on the order of hundreds of nA.

This type of low-voltage driven DBRs is promising for implementation of tunable Fabry-Perot cavities and thus tunable surface emitting lasers. Furthermore, these devices would provide much needed surface normal active elements for applications in opto-electronic integrated circuits.

[1] O. Blum, J. E. Zucker, T.H Chiu, M. D. Divino, K. L. Jones, S. N. G. Chu, T. K.Gustafson, Appl. Phys. Lett., 59, 2971, 1991

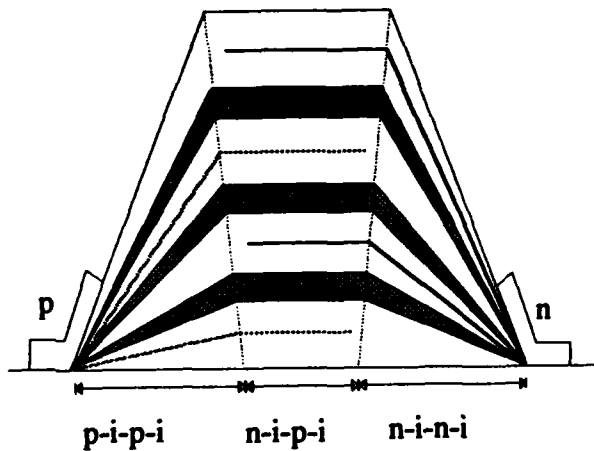[2] G. H Dohler, G. Hasnain, J. N. Miller, Appl. Phys. Lett. 49, 704, 1987

Fig. 1 Inter-digitated contact structure. White regions are the AlGaAs bulk layers, 840 Å thick, cross hatched regions are the MQW InGaAs/GaAs layers, with 4 100 Å InGaAs wells and 3 70 Å GaAs barriers. δ doped contact layers are the thin lines in the middle of the bulk AlGaAs layers.
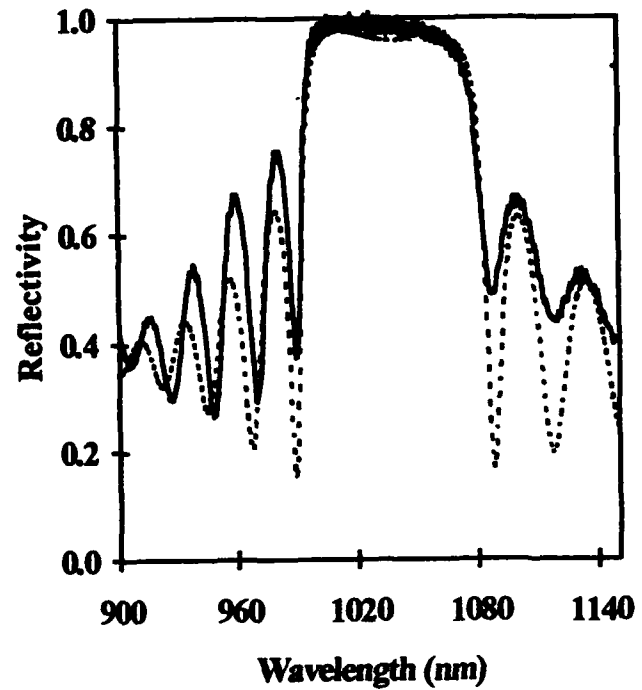

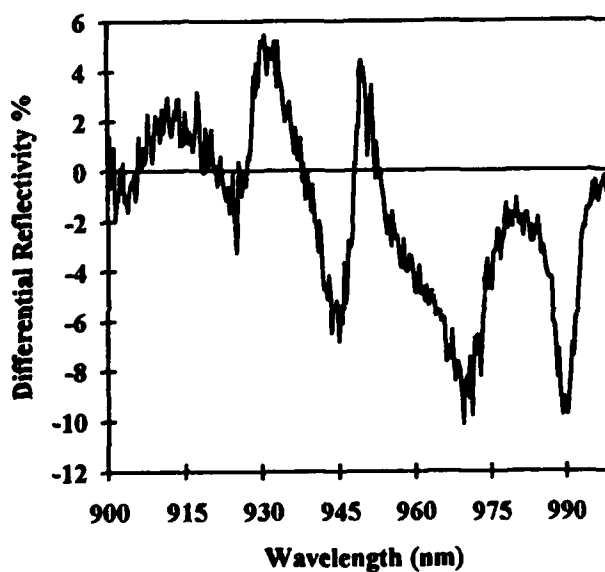Fig. 2 Zero bias reflectivity: measured (solid line) and calculated (dashed line)
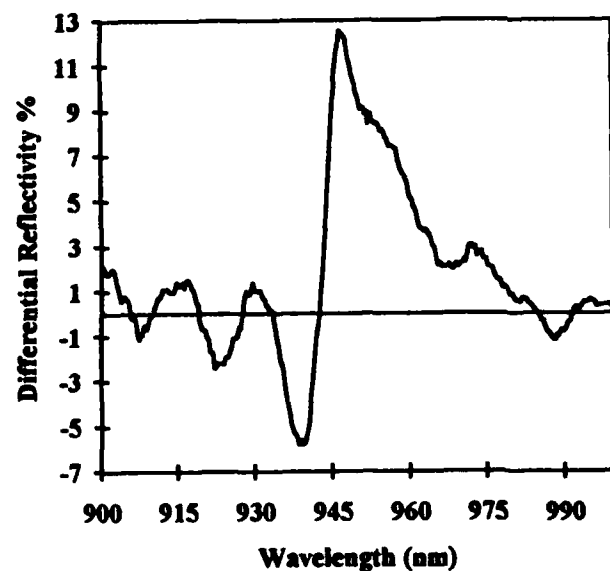

Fig. 3a Measured ΔR/R for -3V applied

Fig. 3b Measured ΔR/R for +1V applied

Large, Low Voltage Absorption Changes and Absorption Bistability in Novel, Three-Step Asymmetric Quantum Wells.

J. A. Trezza, M. C. Larson, S. M. Lord, and J. S. Harris, Jr.

Solid State Laboratories, Stanford University, Stanford CA 94305, (415) 723-1926

Optoelectronic devices which use large absorption changes in quantum wells typically use the Quantum Confined Stark Effect (QCSE).[1] Negative differential absorption modulation (NDAM), which entails high absorption at zero field and lower absorption at large bias, is limited by the shifting of light hole excitons. Although the excitons are quenched with high bias, the devices require very high electric fields to produce any substantial absorption drop. Here we demonstrate a method for obtaining a higher degree of NDAM than is obtainable through the QCSE and at a far lower voltage than is typically required by the QCSE. In addition, at other wavelengths the same device displays positive differential absorption modulation (PDAM). Finally, the devices can display absorptive bistability. These characteristics make it uniquely suited for use in vertical cavity modulators[2], self electro-optic effect devices (SEEDs)[3], and waveguide devices, as well as a whole host of new devices.

To first order, exciton absorption is proportional to the overlap integral of the electron and hole envelope wavefunctions.[2] A structure which, under bias, affects the overlap of the two particles will affect the strength of the dipole element between them and hence the magnitude of the optical absorption. In contrast to the QCSE, this mechanism does not require the exciton resonance wavelength to shift. If an applied bias decreases the overlap integral for an exciton, the absorption will also decrease at that exciton's resonant wavelength. Conversely, absorption will rise if the overlap increases.

To realize this modulation effect, we designed three-step asymmetric quantum wells. The device was grown by molecular beram epitaxy with a band structure shown in Figure 1. The active area consisted of 20 coupled wells, each one containing a 50Å GaAs well and a 20Å $In_{0.2}Ga_{0.8}As$ well separated by a 10Å $Al_{0.33}Ga_{0.67}As$ barrier. 200Å $Al_{0.33}Ga_{0.67}As$ barriers separated adjacent wells. These coupled wells were contained in the intrinsic region of a *p-i-n* structure.

The absorption spectrum at low voltage can be seen in Figure 2. We measured photocurrent and normalized our data to account for quantum efficiency fluctuations. This normalized data is proportional to the absorption spectrum. Photocurrent at 8175Å drops to 30% of its maximum value for an applied bias of 4 volts (72kV/cm). In addition, an exciton resonance at 8125Å increases its absorption by 70% with an applied bias of 6V (109kV/cm), demonstrating PDAM. At 8175Å, the ratio of percentage change in absorption to applied field is 96 µm/KV where this 'efficiency ratio' is $[(\alpha_{high}-\alpha_{low})/\alpha_{high}]/E_{max}$. Here α_{low} and α_{high} are obtained from the minimum and maximum photocurrent values and E_{max} is the field applied to achieve this modulation. In contrast, when the QCSE is used, absorption typically drops to around 50% of maximum for fields near 300kV/cm.[4] The efficiency ratio of such devices is 17 µm/kV. We thus obtain substantially improved NDAM performance at a significantly lower voltage than is realizable using the QCSE. In addition, at the wells' PDAM wavelength, the efficiency ratio is 38 µm/KVwhich is viable for device applications.

While at low biases the changes in absorption at the two wavelengths of interest are dominated by the change in overlap integral, the QCSE begins to affect the behavior of the excitons at higher biases as shown in Figure 3. Here the exciton which displayed PDAM at low bias begins to red shift with applied field. The benefit of such an effect is demonstrated in Figure 4. At 8160Å, for example, the photocurrent at 0V and at 11V is quite large while at 6V we have a minimum in photocurrent. Similarly, at 8125Å absorption is low at 0V and at 11V and becomes large for intermediate voltages. This absorptive-bistability is ideally suited to many optical switching situations.

In conclusion, we have created a three-step asymmetric quantum well which is better suited for negative differential absorption modulation than are devices based upon the QCSE.

Our method also allows for positive differential absorption modulation and shows absorptive bistability. We believe this to be the first such device produced. Our structure has many applications for both vertical cavity and waveguide optical modulators as well as for bistable latching switches.

1. D. A. B. Miller, D. S. Chemla, T. C. Damen, A. C. Gossard, W. Weigmann, T. H. Wood, and C. A. Burrus, Phys. Rev. B. **32**, 1043 (1985).
2. B. Pezeshki, S. M. Lord, T. B. Boykin, and J. S. Harris, Jr., Appl. Phys. Lett **60**, 2779 (1992).
3. D. A. B. Miller, D. S. Chemla, T. C. Damen, A. C. Gossard, W. Wiegmann, T. H. Wood, and C. A. Burrus, Appl.. Phys. Lett. **45**, 13 (1984).
4. K. W. Jelley, R. W. H. Engelmann, K. Alavi, and H. Lee, Appl. Phys. Lett **55**, 70 (1989).
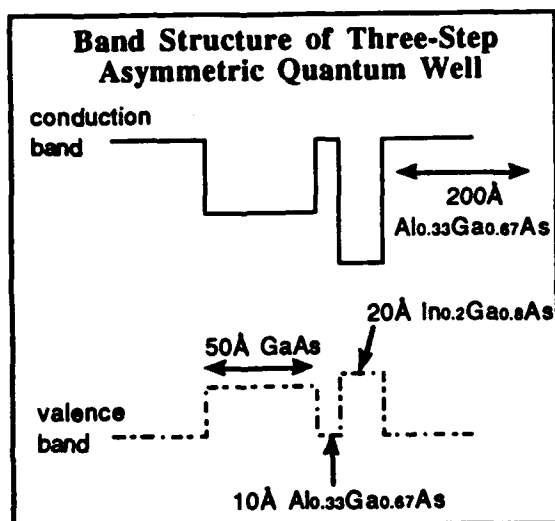
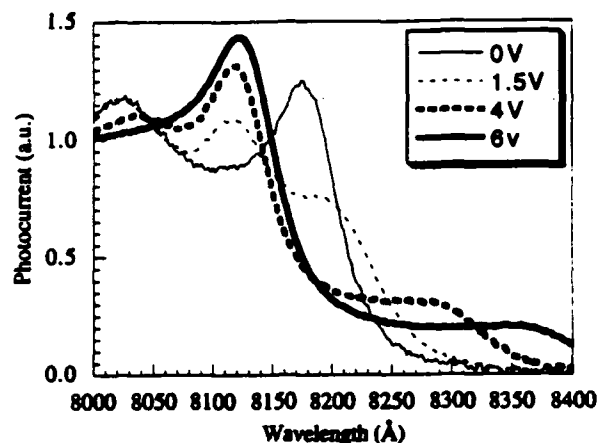Figure 1: Schematic band diagram of the MBE-grown structure.

Figure 2: Photocurrent measurements for the structure shown in Figure 1 at various low applied biases where the overlap integral changes dominates absorption changes.
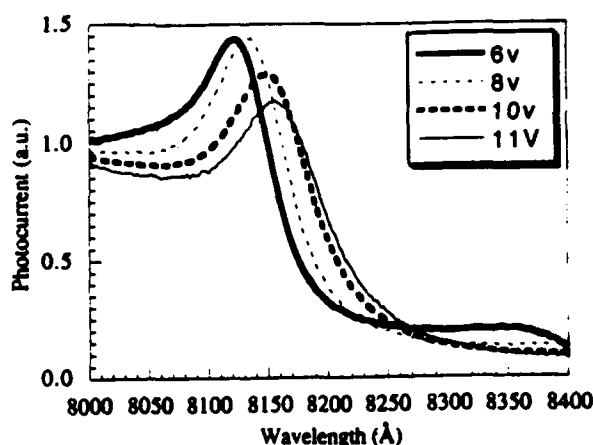

Figure 3: Photocurrent measurements at higher bias where the Quantum Confined Stark Effect dominates.
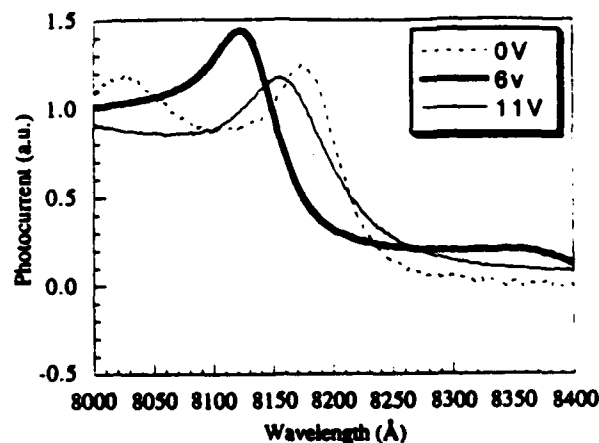

Figure 4: Photocurrent at low, intermediate, and high bias. Here bistable absorption is seen near 8125Å and 8175Å.

High Contrast, All-Optical GaAlInAs/AlInAs Multiple Quantum Well Reflection Modulator at 1.3 μm

M.F. Krol and R.K. Boncek
Rome Laboratory Photonics Center, RL/OCPA, 25 Electronic Pky
Griffiss AFB, NY 13441-4515, (315) 330-4456

T. Ohtsuki, G. Khitrova, B.P. McGinnis, H.M. Gibbs, and N. Peyghambarian
Optical Sciences Center, University of Arizona, Tucson, AZ 85721

Recently, there has been considerable research interest in multiple quantum well (MQW) light modulators which utilize reflective nonlinear asymmetric Fabry-Perot etalons to achieve extremely high contrast ratios with both electrical and optical control.[1-3] Here, we demonstrate the first all-optical, high-contrast GaAlInAs MQW asymmetric reflection modulator for operation at 1.3 μm.

The asymmetric reflection modulator investigated consists of a 65 period 69 Å $Ga_{0.376}Al_{0.094}In_{0.53}As$ well/89 Å $Al_{0.48}In_{0.52}As$ barrier MQW nonlinear spacer on top of a 24 period 936 Å $Ga_{0.3}Al_{0.18}In_{0.52}As$/1003 Å $Al_{0.48}In_{0.52}As$ quarter-wave stack back mirror. This structure is grown lattice-matched on a semi-insulating InP substrate by molecular beam epitaxy. The etalon front mirror is formed by the air/spacer interface and has a value of $R_f \approx 0.31$, and the quarter-wave stack back mirror has a reflectance of $R_b \approx 0.92$. The total spacer thickness is L = 1.027 μm. The modulator was designed such that the Fabry-Perot resonance is located on the long wavelength side of the heavy-hole exciton peak to take advantage of large, pump-beam induced absorptive and refractive nonlinearities. In the absence of the pump, the absorption near the heavy-hole exciton is high and thus results in a balanced cavity and near zero reflectance at resonance. When the pump is present, the photo-generated electron and hole populations saturate the absorption near the heavy-hole exciton and result in an increase in the reflectance at resonance by unbalancing the Fabry-Perot cavity. There is also a considerable shift in the Fabry-Perot resonance due to the change in refractive index related by the Kramers-Kronig transformations to the pump induced absorption change.

The nonlinear behavior of the modulator was investigated in a pump/probe geometry. The nonlinear reflectance spectra at pump intensities of 0.0, 6.62, and 41.22 kW/cm² are shown in Fig. 1(a). In the linear spectrum (no pump) shown by curve 1 in Fig. 1(a), the minimum reflectance occurred at a wavelength of 1314.3 nm, with a value of 0.00055. As the pump intensity is increased to 41.22 kW/cm², the reflectance at the initial cavity resonance increased to a value of 0.7. As can be seen from curve 3 of Fig. 1(a), the increased reflectance is the result of the combined absorptive and refractive nonlinearities associated with saturating the heavy-hole exciton as indicated by the increase in reflectance and the shift of the resonance to shorter wavelengths. The measured reflectance at the resonance wavelength of 1314.3 nm as a function of pump intensity is shown in Fig. 1(b). As can be seen in the figure, the reflectance rapidly increases from a value of 0.00055 at zero pump intensity to a value approaching 0.72 as the pump intensity is increased. Assuming the device begins to enter saturation when the instantaneous slope of the transfer characteristic is less than unity, the saturation reflectance value for the modulator is approximately 0.6. This value of reflectance corresponds to an on/off contrast ratio of 1060:1 and an insertion loss of 2.2 dB at a pump intensity of only 30 kW/cm²,

corresponding to a carrier density of 4.5×10^{17} cm^{-3}.

The recover, dynamics of the modulator was measured in a time-resolved pump/probe geometry. The measured response of the modulator with carrier density of 1.4×10^{16} cm^{-3} is shown in Fig. 2. The fast turn-on of the modulator is the result of the generation of electron-hole pairs by the pump pulse. The modulator recovers exponentially with a time constant of τ $\approx$ 725 ps as determined by the calculated fit (dashed curve in Fig. 3). The fast recovery of the modulator allows for use in optical processing systems where bandwidths approaching 1 GHz are required.

In summary, by using the combined absorptive and refractive nonlinearities associated with saturating the heavy-hole exciton resonance, an on/off contrast ratio of 1060:1 and an insertion loss of 2.2 dB have been achieved at a carrier density of 4.5×10^{17} cm^{-3}. The recovery time-constant of the modulator was measured and found to be 725 ps.

1. K. K. Law, M. Whitehead, J. L. Merz, and L. A. Coldren, *Elec. Lett.* 27 1863 (1991).

2. K. Hu, L. Chen, A. Madhukar, P. Chen, K. C. Rajkumar, K. Kaviani, Z. Karim, C. Kyriakakis, and A. R. Tanguay, *Appl. Phys. Lett.* 59 1108 (1991).

3. R. Jin, G. Khitrova, H. M. Gibbs, C. Lowry, N. Peyghambarian, *Appl. Phys. Lett.* 59 3216 (1991).
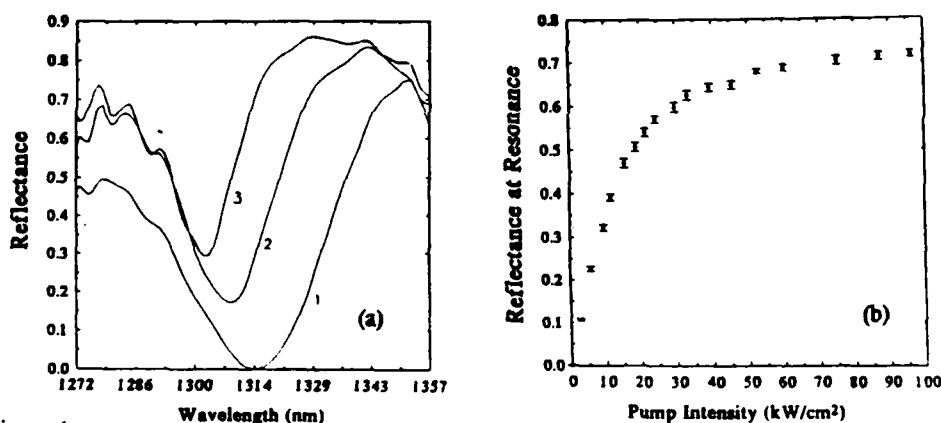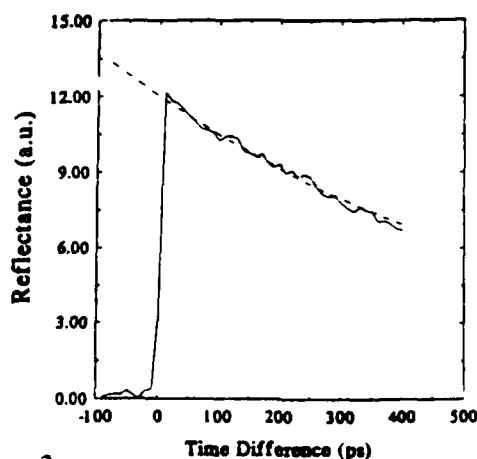
Figure 1

Figure 2

Mixing of Electronic States and Control of Optical Transitions in Asymmetric Triple Quantum Well Structures

N. Sawaki, S. Fukuta, and H. Goto,
Nagoya University, Dept. of Electronics,
Chikusa-ku, Nagoya 464-01, Japan
(tel. +81-52-781-5111, fax. +81-52-782-9145)
T. Suzuki, H. Ito, and K. Hara
Nippondenso Co., Ltd., Research and Developement Dept.,
Showa-cho, Kariya, Aichi 448, Japan
(tel. +81-566-25-6976, fax. +81-566-25-5588)

The resonance of electronic states, or the mixing of wave functions in semiconductor coupled quantum wells has attracted much attention, because of the physical interest as well as a possibility attaining novel functional devices in electro-optical applications[1,2]. In this paper, we will study the mixing of the electronic states in coupled triple quantum well structures(TQW's). The coupling of the electronic states is a strong function of the external field applied perpendicular to the heterointerface, which enables us to control the optical oscillator strength.

Two types of TQW's were grown by MBE on semi-insulating(001)GaAs substrates. The widths of the three GaAs quantum wells are (Sample #166) 5, 5.5, and 6nm or (Sample #140) 6, 15, and 5nm, which were separated by 2nm-$Al_{0.3}Ga_{0.7}As$ barrier layers. The TQW's were embeded in 100nm-$Al_{0.3}Ga_{0.7}As$ cladding layers. In order to apply electric fields, the bottom electrode was made with a Si δ-doped layer(sheet density 1×10^{12} cm^{-2}) and the top layer with a Si doped 100nm-GaAs.

Using appropriate parameters, we have calculated the wave functions and the energy levels of electrons and holes in TQW's. In these samples, three electronic states (ground states) localized in each quantum well are almost at the resonance (in 15nm well of sample #140 we use the first excited state). It was found that the degree of resonance or the mixing of these states is a strong function of the applied electric field, i.e., the maximum of the electron wave function of a particular states shifts from one well to the other. As the result, the oscillator strength for optical transition due to corresponding state varies abruptly as shown in Fig.1, which demonstrates that the intensities of three emission or absorption peaks exchange by increasing or decreasing the fields. Similar calculation has been done for a double quantum well structure, but the change was not so abrupt as in TQW's.

Figure 2 shows the photoluminescence(PL) spectra of sample #166 at 77K. Obviously,
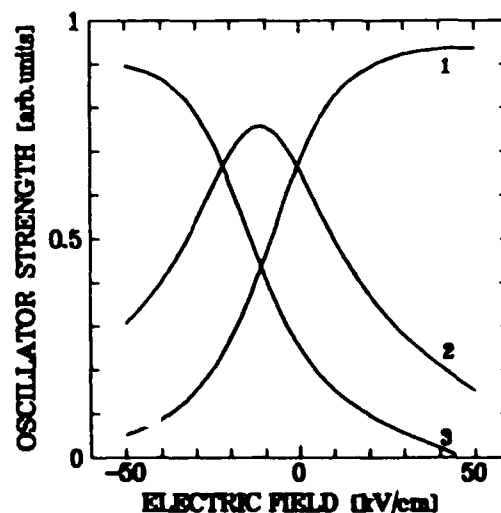

Fig.1. Oscillator strength of three levels in TQW
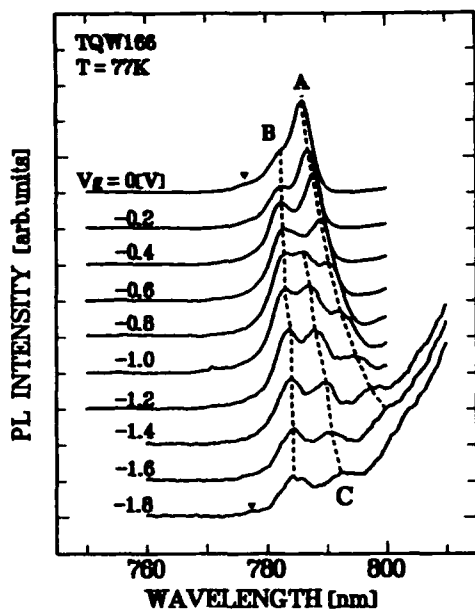
Fig. 2. The PL spectra of TQW
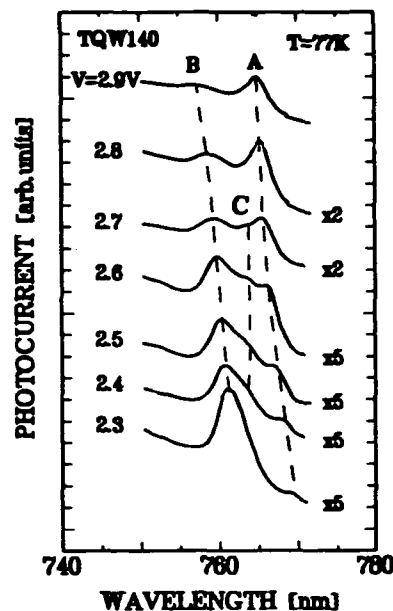   (sample #166) at 77 K.

Fig. 3. The PC spectra of TQW
         (sample #140) at 77 K.

there are three peaks and their intensities exhibit the behaviour as expected, i.e., peak A decreases by increasing the field while peak B increases, and peak C shows increase followed by decrease. Figure 3 shows photo-current(PC) spectra of the sample #140 at 77K. There appeare three peaks in the corresponding wave lengthes, one of which (A) is enhanced in high fields, while the peak (B) is enhanced in lower fields, in agreement with the theoretical results.

Above results prove that the probability of optical transition at a wavelength is strongly influenced by the electric field, and the switching of the absorption occurs by the field applied to the quantum wells. The use of the resonance or the anti-crossing phenomena does enhance the variation. It is notable that the switching of the absorption occurs with the field as low as 30 kV/cm.

Alternatively, the electric field could be applied by the charges created by optical absorption itself[1]. In sample B, e.g., the absorption of a light in the 5 nm quantum well will produce electron and hole pairs within the well. In a little while, however, the electrons will escape to the 15 nm wide well by tunneling process, leaving holes in the original well, since the hole tunneling time is much longer[3]. This changes the internal field in TQW's, which, in turn, will change its absorption coefficient. We will realize an optical nonlinearity and/or all optical switching device, which will be functional at picosecond time scale or the tunneling time of electrons and holes. The feasiblity of the new type of optical nonlinearity to apply to a kind of optical computing system will be discussed.

[1] A.M. Fox etal: Phys. Rev. B42(1990) 1841, ibid. B44(1991) 6231.
[2] Y. Tokuda et al: Appl. Phys. Lett. 56(1990) 116, ibid. 56(1990) 2166, Phys. Rev. B43(1991) 7170.
[3] N. Sawaki et al: Appl. Phys. Lett. 55(1989) 1996.

Saturation and carrier sweep-out in electro-absorptive GaAs/GaAlAs MQW diodes

D.J.Goodwill, J.S.Massa, G.S.Buller, S.J.Fancey

Heriot-Watt University, Edinburgh, U.K.

Tel. (44) 31-449 5111

A.Wachlowski

Alcatel Austria Elin Research Centre, Vienna, Austria

While the speed at which a SEED device may be switched is limited fundamentally by carrier vertical transport times and RC effects, in a practical parallel processing system it is likely to be limited by the ratio of incident optical power and device switch energy. Since high speed SEED operation is desirable for a high processing rate, it is important that the device performance is not degraded at high incident power. One of the important mechanisms which result in this degradation is the build-up of a carrier density in the quantum wells (QWs). This carrier density weakens the excitonic absorption feature, resulting in a reduction of the reflectivity contrast ratio. In references [1] and [2] several QW structures were compared and the saturation effects were found to decrease as the sweep-out time [3] was reduced by either lowering or thinning the barrier between wells. An MQW consisting of 100Å GaAs wells and 35Å $Ga_{0.7}Al_{0.3}As$ barriers was therefore developed in [1] and for this structure, at the intensities used in that work, no saturation effects were observed. We have extended the results by examining a similar structure and measuring the saturation of the responsivity and reflectivity at incident intensities up to 40kW/cm² (1400µW in a spot with 2.1µm $1/e^2$-$1/e^2$ intensity). Thermal effects were also observed. Using time resolved photoluminescence (TRPL) we have directly measured carrier sweep-out times and so have been able to calculate the carrier densities generated in the saturation experiments.

The diode was a reflection type device designed to have the room temperature hh1-e1 excitonic absorption peak at 848nm. The MQW consisted of 71.5 periods of 100Å undoped GaAs wells and 35Å undoped $Ga_{0.7}Al_{0.3}As$ barriers (total undoped region thickness 0.96µm). This was grown on a n-GaAlAs/AlAs mirror stack on a n-GaAs substrate, and had a p-GaAlAs overlayer. A mesa had been formed, ohmic contacts put down and a dielectric anti-reflection coating applied to the 20x40µm window.

The device used was a test device on a commercially available Logic-SEED chip from AT&T. Measurements were made at room temperature using a cw beam from a Ti:Sapphire laser and an I-V characterizer. The incident and reflected power were calibrated using a power meter which had an accuracy of ±10%.

Fig. 1 shows the responsivity spectra at different reverse bias voltages (V) for (a) $P=45µW$ and (b) $P=670µW$ where P is the incident power. In Fig. 1(a) (low intensity) the $V=0$ hh1-e1 exciton peak is clearly visible at 847.5nm. The peak red-shifts and broadens as V is increased. Fig. 1(b) shows the responsivity spectra for $P=670µW$. At $V=0$ the hh1-e1 exciton peak is now much less sharp and is lower than for the low power case,

and has moved to almost 849nm. Once again, the exciton peak red-shifts and broadens as V increases. Complementary behaviour to the responsivity spectra is observed in the reflectivity spectra (not shown). The reflectivity contrast ratio extracted from this data is shown in Table 1. Over the wavelength range in which the device might be used in an S-SEED, a clear reduction in the contrast ratio is seen at the higher power level. This reduction is much less at 860nm, where the device might be used as a spatial light modulator.

λ (nm)	P (µW)	Contrast ratio R_{10V}/R_{0V}	Contrast ratio R_{15V}/R_{0V}
846	45	2.02	2.25
	670	1.51	1.72
848	45	3.19	3.88
	670	1.68	1.91
850	45	1.09	1.46
	670	1.26	1.56
860	45	1/3.19	1/2.00
	670	1/2.61	1/2.06

Table 1. Reflectivity contrast ratios

To investigate the carrier sweep-out times, TRPL measurements were performed, using a 10µm diameter spot size and a 10ps pulse from a 780nm diode laser [4]. The time-correlated single photon counting technique was used and the system gave a temporal resolution of 10ps after iterative reconvolution analysis. The pulse energy of 1.1pJ is calculated to produce an initial carrier density of $8x10^{16}cm^{-3}$ carriers. Filters were used to select only the PL photons with wavelength within 5nm of the bias-dependent exciton peak. Measured TRPL curves are shown in Fig.2 for different bias voltages. At $V\sim0.8V$ forward bias, the flat band condition is reached and the TRPL decay is due only to recombination and hence is slow (PL decay constant ~3ns). At $V=0$ and for all reverse bias conditions the decay is due to carrier sweep-out and is much faster (350ps at $V=0$, 20ps at $V=10V$). The values agree well with those in [1] where they were measured by a pump/delayed probe transmission experiment.

The origin of the saturation of the responsivity at high intensity may now be understood via a calculation of the carrier density generated in the wells. At the densities created, radiative recombination may be ignored. The steady state carrier density N is given by $N = I_{AV}A\tau/L$ $\hbar\omega$

where $I_{AV} = P/\pi r_0^2$ is an 'average' incident intensity of the Gaussian spot, r_0 is the spot radius, $A=(1-R)$ is the fraction of the incident light which is absorbed by the quantum wells, R is the reflectivity, $L=0.71µm$ is the total length of absorbing QW material, $\hbar\omega$ is the photon energy and

$$\frac{1}{\tau} = \frac{1}{\tau_{SWEEP}} + \frac{1}{\tau_{NR}} + \frac{1}{\tau_{RAD}}$$

For $V\geq0$, $\tau_{SWEEP} \ll \tau_{NR}, \tau_{RAD}$ and hence $\tau \sim \tau_{SWEEP}$.

Our experimental data shows that for the low intensity case with incident power $P=45\mu W$ ($I_{AV}=1.30kW/cm^2$) and $V=0$, the reflectivity is 0.105 and the responsivity is 0.465A/W at 848nm. Hence $A=0.895$ and the photo-generated carrier density is $N=2.5\times10^{16}cm^{-3}$. For the high intensity case, at $P=670\mu W$ ($I_{AV}=19.3kW/cm^2$) and $V=0$, the reflectivity is increased to 0.183 and the responsivity is reduced to 0.39. Now $A=0.817$ and $N=3.3\times10^{17}cm^{-3}$. Since the radiative lifetime is in both cases much longer than the carrier sweep-out time, it is clear that the saturation of the responsivity is not due to the onset of radiative recombination.

Data from [5] shows that in similar QWs with no electric field present, the absorption coefficient α at the hh1-e1 exciton peak reduces by a factor of 1.25 as the carrier density increases over this range. From our measured values of A, we calculate $\alpha=1.6\times10^4cm^{-1}$ at low power and $\alpha=1.2\times10^4cm^{-1}$ at high power. The ratio of these values is 1.33, consistent with [5]. We therefore conclude that the reduction in responsivity, absorption and contrast ratio as the power is increased is due to saturation of the exciton transition by the build up of photo-excited carriers in the quantum wells. The presence of the photocarriers is not however expected to shift the

peak in wavelength. Hence the observed 1.5nm red-shift at $V=0V$ must be thermally induced. A shift of 1.5nm corresponds to a spot-centre temperature rise of 6°C.

We have measured the performance of a QW modulator up to very high incident intensities and used TRPL to investigate the dynamics of carrier sweep-out. The reflectivity contrast ratio was found to be maintained remarkably well even at an average incident intensity of $20kW/cm^2$. The experiments reported here used a 2.1μm diameter laser spot, as opposed to the 4μm spot normally used in circuit demonstrators at Heriot-Watt. Since the red-shift of the absorption features due to thermal effects is washed-out by the carrier density induced broadening, it is reasonable to assume that similar contrast ratios would be maintained in a 4μm spot, which would correspond to an optical power in a single beam of 2.5mW.

We will present further results concerning the reduction in lifetime and quantum efficiency due to surface recombination in devices with smaller mesas.

[1] A.M.Fox et al. IEEE J.Quantum Electron. 27 2281 (1991)

[2] G.D.Boyd et al. Appl.Phys.Lett. 57 1843 (1990)

[3] G.Livescu et al. Semicond.Sci.Tech. 5 549 (1992)

[4] G.S.Buller et al. Rev.Sci.Instrum. 63 2994 (1992)
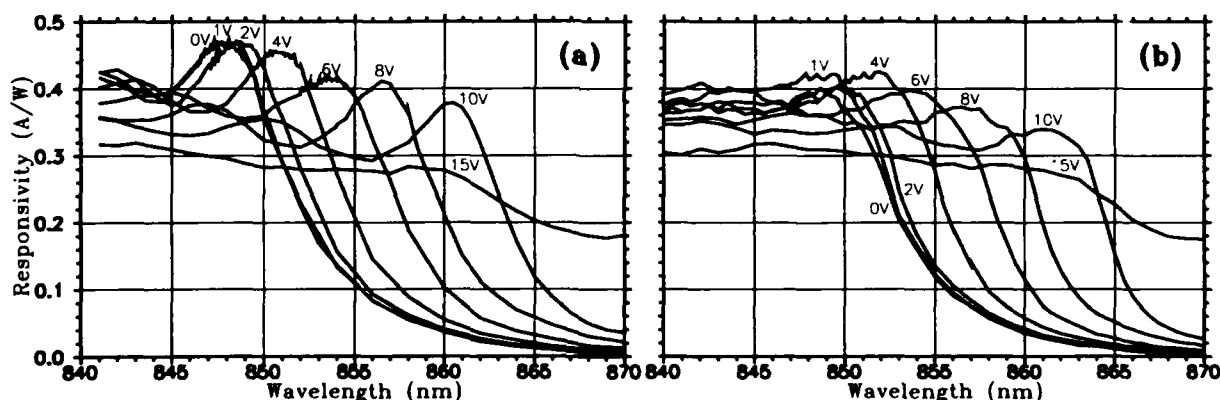
[5] S.H.Park et al. Appl.Phys.Lett. 52 1201 (1988)

Fig.1 QW diode responsivity spectra under different bias conditions for incident power of (a) 45μW, (b) 670μW.
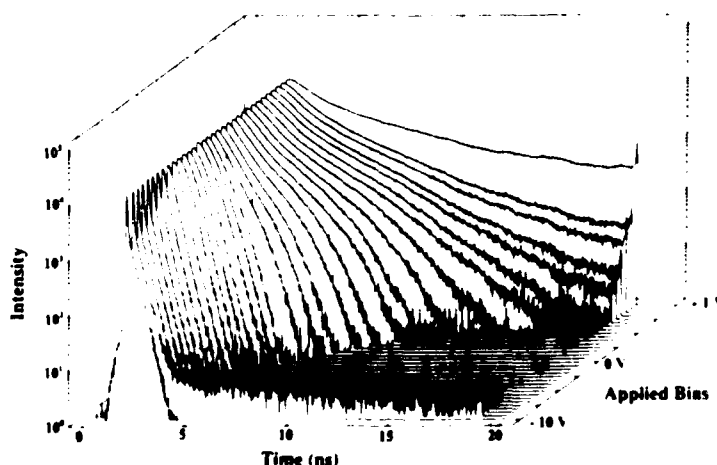

Fig.2 TRPL decays under different bias conditions.

High Contrast Reflection Electro-Absorption Modulator With Zero Phase Change

J. A. Trezza, B. Pezeshki[a,] M. C. Larson, S. M. Lord, and J. S. Harris, Jr.
Solid State Laboratories, Stanford University, Stanford CA 94305, (415) 723-1926
[a]Currently at IBM T.J. Watson Research Center, Yorktown Heights NY, 10598 (914) 945-1443

Vertical cavity quantum-well optical modulators utilizing the quantum-confined Stark effect (QCSE) are being increasingly investigated for use in optical communication and computing.[1] Reflection modulators based upon large absorption changes in quantum wells have shown high contrast ratios[2] while exhibiting lower parasitic phase modulation than conventional waveguide modulators.[3] Since quantum wells are capable of large absorption changes ($\Delta\alpha$), they also exhibit large refractive index changes (Δn).[4,5] Understanding the role of quantum well excitons and phase is crucial for high speed optical switching since such switching will be critically limited by Δn induced pulse broadening. The ratio of phase shift to absorption is typically reported through the chirp parameter where a low chirp parameter is desirable for low-dispersion amplitude modulation. Here we describe how parasitic Δn can be eliminated in a novel, optimized structure thus yielding a pure reflection modulator with a zero chirp parameter. At the operating wavelength, such a device would exhibit a high reflectivity change and zero phase change when switched between two bias points. We have designed and developed such devices by analyzing excitonic lineshapes, numerically simulating our structures including quantum well absorption and dispersion effects, and creating a flexible modulator design which allows for optimization after growth. We note that our theory also applies to eliminating Δn in waveguide modulators which rely upon the QCSE.

The Kramers-Kronig relation can be used to calculate Δn given $\Delta\alpha$. By looking at the change in absorption between two bias points versus wavelength, we can extract Δn versus wavelength at an applied voltage. At wavelengths far longer than the exciton resonance, for a given bias, absorption changes little with wavelength and the calculated refractive index enhancement due to the exciton will be small. However, because well defined excitons have a strong resonance with a nearly symmetric absorption lineshape around their peak, at wavelengths near this peak, refractive index change due to the exciton will be small as well. This can be understood by noting the anti-symmetry in the Kramers-Kronig relation. Hence, if we operate a device at a wavelength which is far from the zero Volt absorption maximum, but near the absorption maximum at another bias, we can obtain a situation where $\Delta n=0$ and $\Delta\alpha$ is large. This is ideal for a pure reflection vertical cavity modulator. To make such a modulator, we need to simultaneously have a Fabry-Perot (F-P) dip at the appropriate wavelength, the correct $\Delta\alpha$ to achieve the matching condition for high contrast, and the correct bias to achieve $\Delta n=0$ for zero phase shift. Figure 1 shows the absorption and relative index change for an optimal F-P cavity at 8375Å.

To obtain numerical simulations of device performance, we developed a thin-film program which calculated reflection, transmission, and absorption as a function of bias. To model changes with voltage, we used absorption spectra for 75Å GaAs/35Å AlAs quantum wells that we previously characterized.[6] By using the Kramers-Kronig relation, we were also able to incorporate the dispersion of these wells into the program.

To confirm our theoretical predictions and our simulated results, we grew a structure with 92 quantum wells with the aforementioned characteristics. The wells were placed between a bottom quarter wave stack of 25.5 periods $AlAs/Al_{.33}Ga_{.67}As$ and a top mirror consisting of 6 periods of $AlAs/Al_{.33}Ga_{.67}As$. We then placed an additional quarter wave layer of $Al_{.33}Ga_{.67}As$ on the top surface as an anti-reflection coating. By etching this top layer, we could change the top mirror reflectivity from about 5% to 77%. This etching gave us the ability to exactly tune the matching condition. Hence, after we shifted the exciton to obtain $\Delta n=0$ at our F-P wavelength, we could adjust our front mirror reflectivity to give us the maximum reflectivity change for the available $\Delta\alpha$ at that bias. Once the structure was grown, the simulation was adjusted to account for fluctuation in the molecular beam epitaxial growth to obtain the optimal

etch depth. The top was etched 190Å and a top mirror reflectivity of 31% was obtained. Experimental results of the total reflectivity versus wavelength are shown in Figure 2. Reflectivity changes from 94% to 6% were obtained at 8375Å. Simulations show agreement within 2% at wavelengths near the F-P minimum. As the exciton shifts toward the F-P minimum, that minimum shifts to longer wavelength since the refractive index is raised by the exciton. At the $\Delta n=0$ bias, the F-P dip is again at the same wavelength as at zero bias.

Figure 3 shows reflectivity and phase versus bias at 8375Å. The phase increases as the exciton approaches the F-P dip, as we expect, but drops to zero when it is at the F-P wavelength. This occurred at about 34V bias. The experimental curves agree quite closely with the phase values predicted by our simulation. The figure also confirms that etching accurately placed the reflectivity minimum at this same bias.

In conclusion, we have laid the theoretical basis for the optimal design of zero-chirp high contrast reflection modulators. Our theory for eliminating Δn is applicable to quantum wells in waveguide modulators. We have also created a device with reflectivity change from 94% to 6% while retaining zero phase shift between the two bias points. We believe this to be the first such optimized device.

1. D. A. B. Miller, Proceedings of the SPIE--The International Society of Optical Engineering 1389, 496 (1991). (and references therein)
2. M. Whitehead, A. Rivers, G. Parry, J. S. Roberts, and C. Button, Electron. Lett. 25, 984 (1989).
3. B. Pezeshki, G.A. Williams, and J. S. Harris, Jr., Appl. Phys. Lett 60, 1061 (1992).
4. J. E. Zucker and T. L. Hendrickson, Appl. Phys. Lett. 52, 945 (1988).
5. T. Hausken, R. H. Yan, R. J. Simes, and L. A. Coldren, Appl. Phys. Lett. 55, 718 (1989).
6. B. Pezeshki, S. M. Lord, T. B. Boykin, and J. S. Harris, Jr., Appl. Phys. Lett. 60, 2779 (1992).
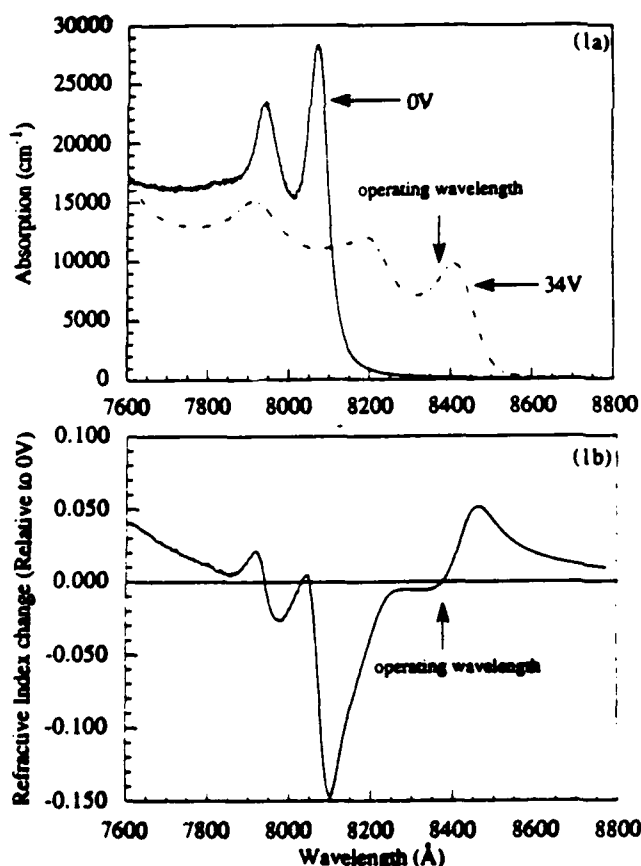
FIGURE 1: a) Absorption Spectrum at 0V and 34V and b) the change in refractive index of the system due to the applied voltage. As can be seen, at 8375Å, the refractive index change is zero while the change in absorption is high. This is optimal for a reflection modulator.
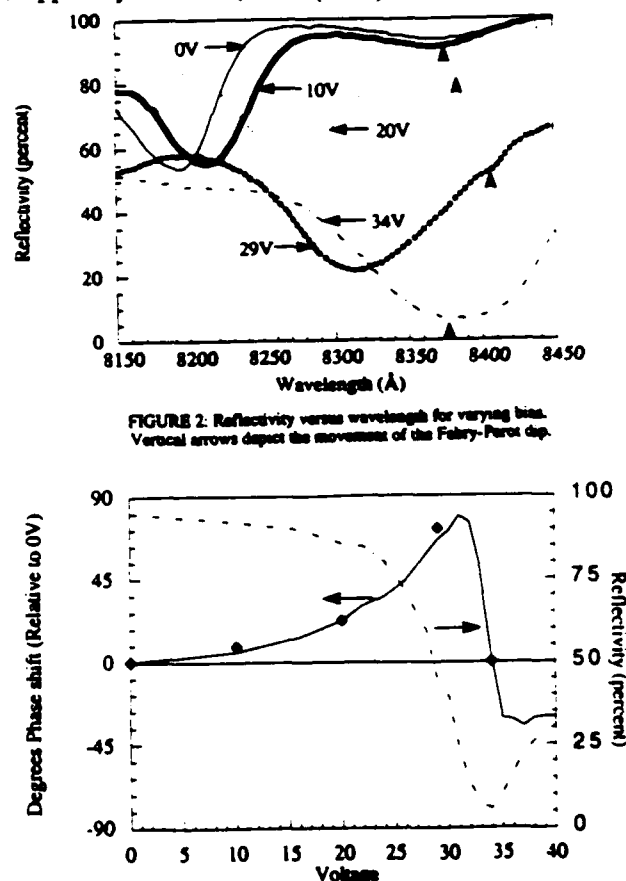

FIGURE 2: Reflectivity versus wavelength for varying bias. Vertical arrows depict the movement of the Fabry-Perot dip.

FIGURE 3: Phase and reflectivity versus bias at 8375Å. Reflectivity changes from 94% to 6% as bias changes from 0 to 34 volts. The device exhibits zero phase shift between these two bias points. Dots are simulated phase shift at the voltages of figure 2.

Exciton and Carrier Dynamics 1

QThC 1:30pm–3:00pm
Grand Ballroom East

Wayne H. Knox, *Presider*
AT&T Bell Laboratories

Coherent Exciton Effects in Quantum Wells

E. O. Göbel[*]
Philipps-Universität Marburg
Physics Department and Material Science Center
Renthof 5, 3550 Marburg, Fed. Rep. Germany

Resonant excitation of excitons by short optical laser pulses creates a macroscopic polarization which decays in the simplest case with a constant rate described by the dephasing time T_2. In semiconductors and semiconductor quantum well structures this dephasing time is of the order of 1ps. Thus, subpicosecond time resolution is required to study coherent exciton effects in quantum wells. We have applied femtosecond Four-Wave-Mixing (FWM) spectroscopy in our studies. As more than one exciton state is excited simultaneously, the coherent dynamics and interaction of these exciton states can be studied. This may reveal specific properties of quantum well excitons, which are not accessible otherwise. As will be illustrated more specificly by the following 3 examples:

(i) Quantum beats and polarization interference in GaAs/AlAs quantum wells; it will be demonstrated that transient FWM with time resolved detection of the nonlinear signal by means of a femtosecond optical sampling technique allows to decide whether different exciton transitions have electronic states in common or not.

(ii) Photon echo in GaAs/AlAs superlattices; in short period superlattices homogeneous broadening of the exciton transitions leads to the occurence of photon echos, which allows the determination of the homogeneous exciton line width. In addition, different exciton transitions like free and bound excitons which are hidden by the large inhomogeneous broadening in linear spectroscopy can be resolved in the photon echo and their coherent dynamics and interaction has been studied.

(iii) Quantum beats of excitons in different growth islands; the localization of excitons within different growth islands with monolayer thickness fluctuations results in slightly different exciton energies, which is reflected in a beating behaviour of the FWM signal. We demonstrate that this beating is caused by a coherent coupling of the excitons in different islands. Possible mechanism for this coherent coupling like dipol-dipol interaction are discussed.

Time Resolved Optical Orientation Used to Examine Coulomb Screening and Phase Space Filling in Quantum Well Excitonic Saturation

M. J. Snelling, P. Perozzo, R. Bambha, and A. Miller
Center for Research in Electro-Optics and Lasers
University of Central Florida, Orlando FL32826
Tel:407-658-6800

D. C. Hutchings
Department of Electronics and Electrical Engineering
University of Glasgow

Picosecond pulses from a mode locked dye laser were used in an excite-probe configuration (figure 1) with excite and probe beam powers of 200uW and 20uW respectively. Both beams were polarised to produce either mutually orthogonal linear polarisations (linear-linear), the same circular polarisation (same-circular), or opposite circular polarisation (opposite-circular). The sample was fabricated by MBE with a p-type background doping of $10^{16}cm^{-3}$, etched to remove the GaAs substrate, and consisted of 120 periods of 65Å quantum wells with 212Å $Al_{0.4}Ga_{0.6}As$ barriers.

The laser wavelength was tuned to the heavy hole maximum and excite-probe scans were performed with the beams in each of the three different polarisation configurations. (A-C figure 2). These were repeated with the wavelength tuned to the low energy side of the heavy hole exciton (D-F figure 2).

Excitation by right or left handed circularly polarised light at the heavy hole energy results in the promotion of either $m_J=1/2$ or spin $m_J=-1/2$ electrons to the conduction band, quantised with respect to the direction of laser light propagation. With linear-linear beams (B figure 2) equal amounts of spin up and spin down electrons are created and the initial increase in transmission is due to exciton saturation caused by both phase space filling (PSF) and coulomb screening (CS). Given same-circular beams the excite pulse selectively populates only one spin state which is then examined by the probe (A figure 2). The probe experiences twice the PSF over the linear-linear case and causes a greater initial increase in transmission which is subsequently reduced as the spins relax. The converse is true for the opposite-circular scan. In each case the effect of CS is the same as the number of carriers remains unchanged.

This interpretation is confirmed by the off resonance scans, (D-F figure 2) Any effect due to CS is now detected as excitonic broadening and causes a decrease in transmission. After the initial decrease the relative form of the curves is the same as for the resonant scans which verifies that they are produced by PSF. Thus from curves A-C in figure 2, in which the effect of CS is manifest as a transmission increase, it can be seen that the contributions to exciton saturation from CS and PSF are almost equal.

This measurement is in broad agreement with calculation[1] (figure 3). In addition our measured spin relaxation time of 50ps is longer than the value of 12ps obtained by Tackeuchi[2] et al in a 45Å GaAs-$Al_{0.51}Ga_{0.49}As$ multiple quantum well. This follows the trend, seen at liquid helium temperatures,[3,4] in which the spin relaxation time becomes longer with increasing well width.

References

1   *Transient Grating Studies of Excitonic Optical Nonlinea-*   J. Opt. Soc. Am. B   *A. Miller, R. J. Manning, P. K. Milsom,*
    rities in GaAs/AlGaAs Multiple Quantum Well Structures   4 (6) 1989   *D. C. Hutchings, D. W. Crust and*
                                                                                            K. Woodbridge

2   *Direct Observation of Picosecond Spin Relaxation of*   Appl. Phys. Lett   *A. Tackeuchi, S. Muto, T. Inata and*
    Excitons in GaAs/AlGaAs Quantum Wells Using   56 (22) 1990   *T. Fujii*
    Spin-Dependent Optical Nonlinearity

3   *Spin Relaxation in Excitonic and Degenerate n and p*   In preparation   *M. J. Snelling and R. T. Harley*
    Doped Quantum Wells

4   *Time-Resolved Spin-Polarisation Spectroscopy in*   Surface Science   *Ph. Roussignol, P. Rolland,*
    GaAs/AlGaAs Quantum Wells   360 (267) 1992   *R. Ferreira, C. Delande, G. Bastard,*
                                                                                            A. Vinattieri, L Carraresi, M. Colocci
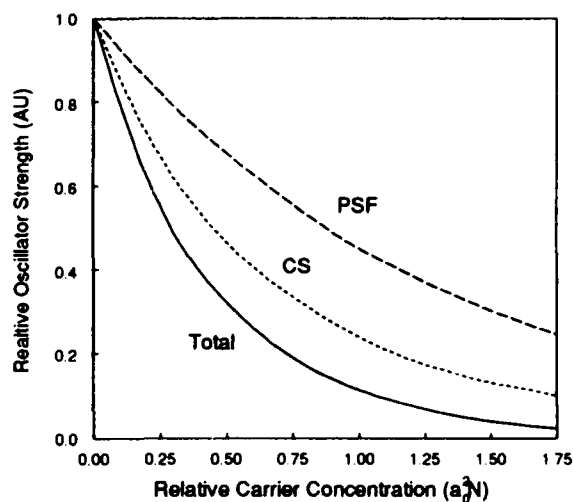   *and B. Etienne*

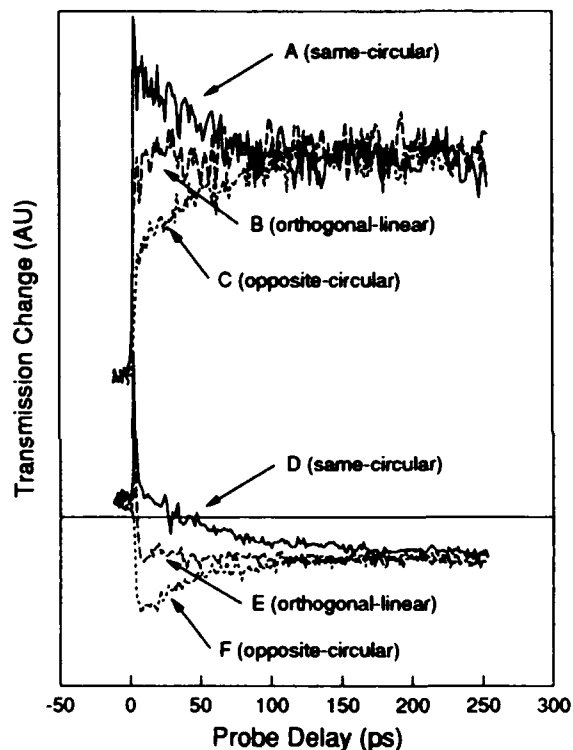## Figures
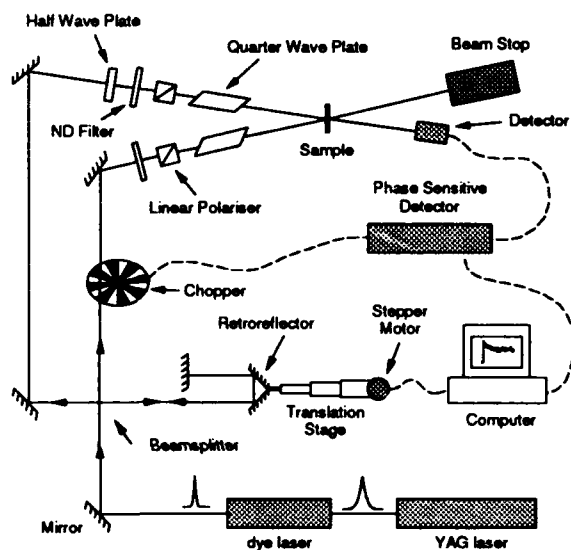
Figure 1. The experimental configuration

Figure 2. Excite-probe scans for a variety of beam polarisa-
tion. Curves A-C were performed at heavy hole resonance
while curves D-F were taken on the low energy side of the
exciton.

Figure 3. Theoretical prediction of the relative components of
PSD and SC involved in exciton saturation.

QUANTUM MECHANICAL OSCILLATIONS OF
THE ELECTRON CAPTURE TIME IN QUANTUM WELLS

B. Deveaud, D. Morris, A. Regreny
France Telecom, CNET 22300 Lannion FRANCE
Tel (33) 96 05 32 13, Fax: (33) 96 05 32 39

M. Barros, P. Becker
AT&T Bell Laboratories,
Murray Hill   NJ 07793   USA

When a quantum well is surrounded by large barriers (i.e. larger than the mean free path of the electrons) the capture mechanisms are dominated by diffusive motion of the electrons in the barriers. This is the situation governing the capture process for example in a separate confinement heterostucture laser [1]. In working conditions, the limiting times correspond to the slow diffusion of holes.

On the contrary, in multi-quantum well systems with narrow enough barriers, the quantum mechanical description should prevail. In such a case, the capture process corresponds to the scattering mechanism from a level having an energy above the barrier, to a level with an energy below the barrier. Such a scattering is dominated in most cases by LO phonon scattering through Fröhlich interaction : as such it depends on both the q vector of the emitted phonon, and the overlap of the initial and final enveloppe wavefunctions. Both contributions should give rise to very deep resonances when the energy difference between the two levels of interest equals the energy of an LO phonon [2,3]. Contribution of ionized impurity scattering reduces the contribution of the antiresonances where LO phonon scattering is forbidden (less than one LO phonon between two levels) [4]. This explains why the capture times in multi quantum well systems is always short (never more than a few ps).

We have observed strong resonances of the electron capture time in quantum wells by two different experimental techniques on two series of samples with different structures. In each case, the resonance is indeed observed when the energy separation of the electron levels involved in the transition is close to the energy of the LO phonons.

The first series of experiments is pump-probe spectroscopy with femtosecond resolution [5]. A set of quantum wells is excited resonantly at the barrier energy with a 100 fs laser pulse. The recovery time of the bleached signal gives the electron capture time. Three samples have been studied with well width of 40,60 and 80 Å (all have 30% AlGaAs barriers). A 500 fs capture time is observed at resonance for a well width of 60 Å, and capture times of 2 ps about on either side of the resonance. These measurements are carried out at room temperature which allows to get rid of the contribution of holes, but renders the time at resonance a bit longer than

expected at low temperatures. As a matter of fact, the thermal spreading of the electrons in the barrier states has a tendancy to wash out the very sharp resonance.

In the second series of experiments, samples with barriers modified by edge spikes are studied using luminescence with subpicosecond resolution [6]. The spikes consist of 22 Å wide 50% AlGaAs, and are used to diminish the overlap of the wavefunctions by a factor of about 20. Electron and hole capture times are monitored through the decay of the barrier luminescence and the rise of the well luminescence at temperatures below 100 K. No resonances are observed for the hole capture (presumably because the expected resonances are too sharp). Electron capture resonances are observed, once again for an energy separation of the levels corresponding to the LO phonon energy. The energy separation of the different levels involved is monitored by the luminescence spectrum at very short time. An example of such a spectrum is shown on Fig 1 for a sample off resonance. The $n=1$ and $n=2$ transitions in the well are clearly resolved as well as the barrier luminescence. The electron capture time, deduced from a fit with coupled rate equations for electrons and for holes, is 40 ps about for well widths below resonance, shows a minimum of 1.5 ps for a well width of 60 Å, and goes up again to 25 ps for larger wells.
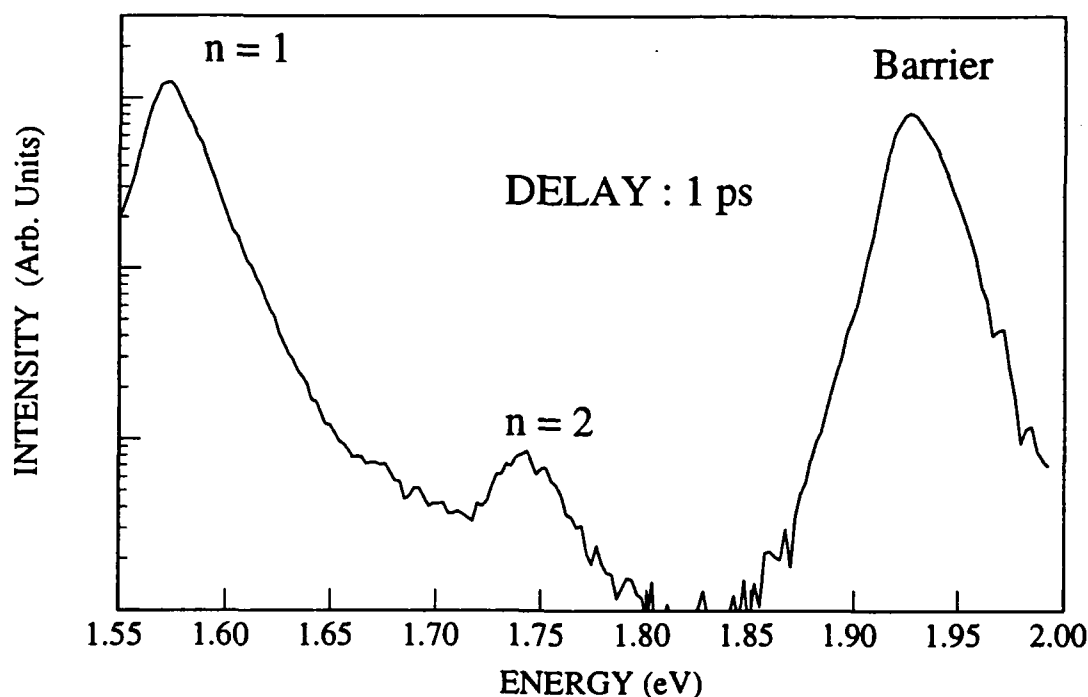
References :
[1] S. Morin, B. Deveaud, F. Clérot, A. Regreny, K. Fujiwara, *IEEE, J. Quantum Electron.*, **QE27**, 1669 (1991)
[2] J.A. Brum, G. Bastard, *Phys. Rev.*, **B33**, 1420 (1985)
[3] M.Babiker, B.K. Ridley, *Superlatt. and Microstruct.*, **2**, 287 (1986)
[4] B. Deveaud, D. Morris, A. Chomette, A. Regreny, *Solid State Commun.* (to be published)
[5] M. Baros, P. Becker, D. Morris, B. Deveaud, A. Regreny, F. Beiser, to be published
[6] D. Morris, B. Deveaud, A. Regreny, 21th Int. Conf On the Physics of Semiconductors, Beijing (1992)

AC-Stark shift of the Fermi edge singularity in modulation doped quantum wells

I. Brener, W.H. Knox, J.E. Cunningham

AT&T Bell Laboratories, Holmdel, NJ 07733, USA

Tel: (908) 949-430

D.S. Chemla,

Physics Department, University of California at Berkeley, and Material Sciences Division, Lawrence Berkeley Laboratory, Berkeley, CA 94720.

AC-Stark shifts of the electronic states are observed when a semiconductor is excited by ultrashort, below band-gap laser pulses. So far, all the studies have been performed in undoped samples [1,2], and the effect has been called "excitonic AC-Stark effect". It has been explained by means of the interaction of "virtual" excitons created by the pump beam with the real excitons created by the weak probe beam [3]. In this talk, we will describe our work on the AC-Stark shifts observed in the absorption spectra of modulation doped quantum wells (MDQW). This effect occurs in a new regime, as the absorption edge in MDQW samples at low temperatures is governed by the "Fermi edge singularity" (FES).

We study GaAs/Al$_{0.3}$Ga$_{0.7}$As MDQW samples of various widths and with carrier concentrations of n=1-3x10^{11} cm^{-2}. We also use reference undoped samples in order to illustrate the peculiarities of this new effect. The AC-Stark effect is measured by recording the femtosecond transient changes in absorption induced by an intense below band gap excitation pulse. Both pump and probe beams are derived from white-continuum pulses generated with an amplified Ti-sapphire laser pulse focused in an ethylene-glycol jet with a time resolution of ~100fsec. The inset in Fig. 1 shows the linear absorption of a 11nm MDQW with n=2.5x10^{11}cm^{-2} at T=8K together with the pump spectrum used to record the differential spectra. The sharp feature around 1.53 eV is the FES, and it rapidly smears out as the temperature is raised above 20K. Also shown in Fig. 1 is the time evolution of the differential transmission for below gap excitation and at the same temperature. The AC-Stark shift is measured as an instantaneous signal which lasts only for the duration of the pump pulse.

In order to analyze the details of the AC-Stark effect in this new regime, we show in Fig. 2 the modified absorption spectra when the pump is present at two different time delays. We also compare the MDQW sample with an undoped QW and with a similar well width. A similar AC-Stark shift is measured both for doped and undoped QWs. However, the bleaching behavior is markedly different. For the *same blue shift*, the MDQW sample exhibits a very small bleaching of the FES. On the contrary, the 1S *hh* exciton in the undoped QW is considerably bleached. In the interacting *e-h* picture, the bleaching and blue shift behavior seen in the ACSE can usually be explained by the interaction of the virtual carriers with the carriers generated by the probe beam. In undoped QWs, there exists a clear relationship between the blue-shift and the bleaching of the absorption as both mechanisms share the repulsive terms due to Pauli exclusion principle. In 2D

systems a relationship of the form: $\dfrac{\Delta E}{E_{1S}} \propto \dfrac{\Delta F}{F}$ holds, where E is the blue shift of the 1S exciton

and F its bleaching. Hence, simple scaling arguments are clearly not sufficient to explain the influence of virtual carriers on the FES and other experimental observations. A correct many body treatment of the problem needs to be accounted for. We will also describe other experiments which show the peculiarities of the AC-Stark effect in this strongly correlated regime.
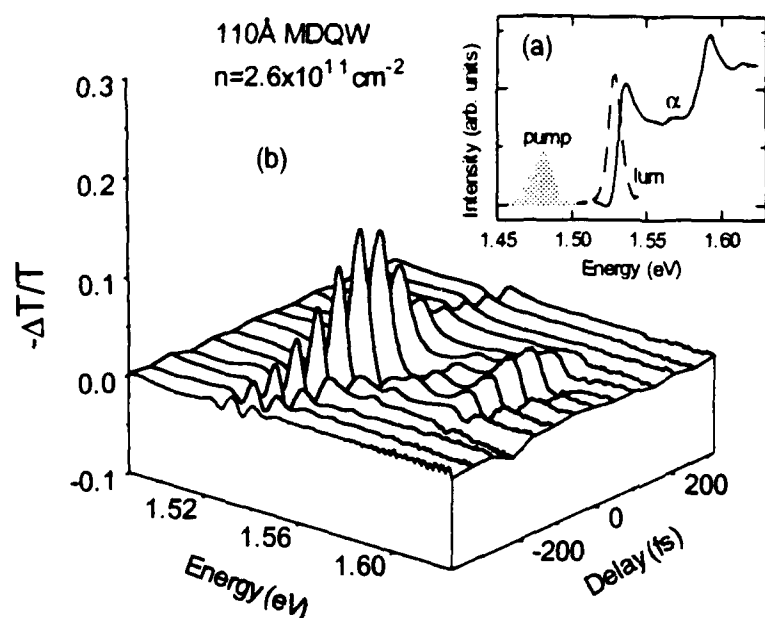

Fig. 1: (a) Absorption and luminescence of the MDQW sample, together with the pump spectrum used to record the spectrum (b) which shows the measured AC-Stark effect of the Fermi-edge singularity.
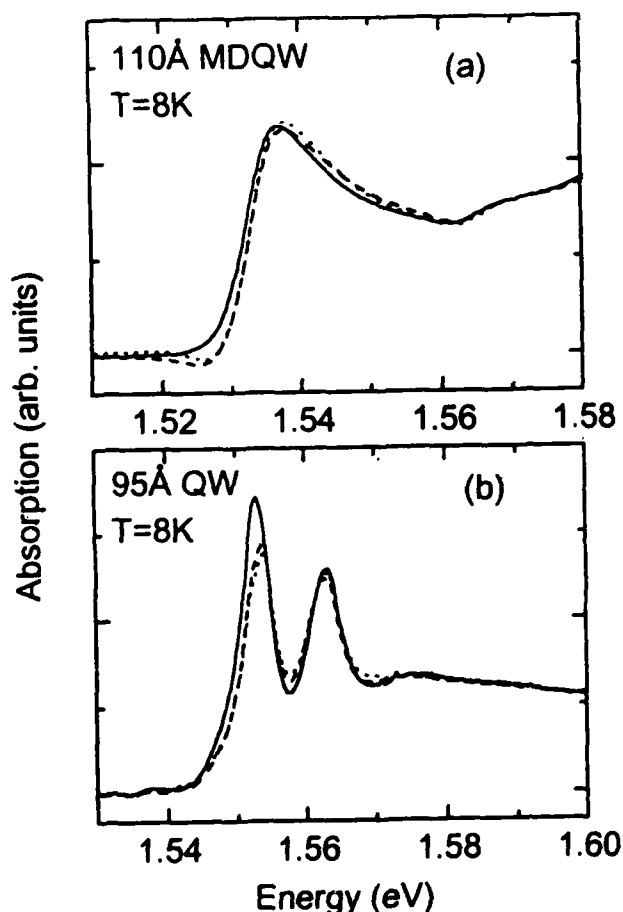
Fig. 2: Linear absorption without pump (solid lines) with pump present at $\Delta t=-50$ fs (dashed lines) and at $\Delta t=0$ (dotted lines) for the doped sample (a) and the undoped one (b)

References

[1] A. Mysyorowicz, D. Hulin, A. Antonetti, A. Migus, W.T. Masselink and H. Morkoc, Phys. Rev. Lett. **56**, 2748 (1986); A. von Lehmen, D.S. Chemla, J.E. Zucker and J.P. Heritage, Opt. Lett. **11**, 609 (1986).

[2] W.H. Knox, D.S. Chemla, D.A.B. Miller, J.B. Stark, S. Schmitt-Rink Phys. Rev. Lett **62**, 1189 (1989).

[3] S. Schmitt-Rink, D.S. Chemla, H. Haug, Phys. Rev. **B37**, 941 (1988).

Exciton and Carrier Dynamics 2

QThD 3:30pm–4:45pm
Grand Ballroom East

Benoit Deveaud, *Presider*
CNET, France

Femtosecond Dynamics of Room-Temperature Excitons in II-VI Multiple Quantum Wells

Anthony M. Johnson[a], Philippe C. Becker[b], Donghan Lee[a],
Miriam R. X. de Barros[b], Robert D. Feldman[a], Alan G. Prosser[b],
Richard F. Austin[a], and Robert E. Behringer[a]

[a] AT&T Bell Laboratories, Room 4D-431, 101 Crawfords Corner Road
Holmdel, NJ 07733
Tel: 908-949-6764   FAX: 908-949-6010
[b] AT&T Bell Laboratories, Murray Hill, NJ 07974

In semiconductors, with increasing carrier densities, excitons are screened and eventually lose their oscillator strengths [1]. As a result, the excitonic absorption will be greatly reduced or bleached. One interesting question is: How strongly can excitons, which are electrically neutral but consist of electrons and holes, self-screen the exciton? In bulk GaAs, Fehrenbach et al. [2] observed that the screening of excitons by excitons is very weak, compared to the screening of excitons by free carriers. Recently, Knox et al. [3] found that the bleaching effect of excitons on excitons was stronger than that of the same density of "warm" free carriers in GaAs multiple quantum wells (MQWs). This behavior is qualitatively well explained by the theory of Schmitt-Rink et al. [4], in which only the effects of the Pauli exclusion principle (phase space filling and exchange interaction) are considered for the bleaching of excitons by both excitons and free electron-hole (e-h) pairs, assuming long-range Coulomb screening is very weak in quasi-two-dimensional (2D) QWs. This assumption could be best tested by measuring the bleaching strength of "cold" free e-h pairs which are supposed to screen the exciton most strongly in bulk [1].

The present II-VI CdZnTe/ZnTe MQWs provide a unique situation, in which the exciton binding energy ($E_X^b \approx 23$ meV) and LO-phonon energy (≈ 25 meV) are comparable, in addition to providing a well-defined room-temperature (RT) excitonic absorption peak (n=1-hh, Fig. 1) [5]. In this case, the ionized e-h pair from the resonantly created exciton is initially "cold," with an excess energy of ≈ 2 meV. Additionally, at RT ($kT_L \approx 26$ meV), the ionized carriers are "cool" in units of kT/E_X^b at equilibrium, in contrast to "hot" free carriers ($kT/E_X^b \approx 3-10$) in III-V MQWs. For $kT/E_X^b \approx 1$, a theoretical estimate suggests that the bleaching of excitons by "cold" excitons is much less effective, by a factor of 0.5, than that by "cool" free e-h pairs [4].

We have found, using the femtosecond pump-probe technique, that the bleaching strength of resonantly created excitons is, surprisingly, 1.8 times that due to the same number of "cool" free e-h pairs. The bleaching strength determined here goes in the opposite direction to the estimate of 0.5, calculated in the limit of T = 0 K and T = ∞ K and sketched between them [4]. This result is indicated in the time-resolved, differential transmission at the excitonic resonance, shown in Fig. 2. In this RT measurement, only excitons are created initially by the 80 fs pump pulse, and the free e-h pairs are created only through the ionization of excitons. The change of transmission induced by the

created carriers is traced by the broadband 14 fs probe pulse, as a function of delay. Our result does strongly support the assumption that long-range Coulomb screening is negligible in quasi-2D MQWs, since otherwise the bleaching due to "cool" free carriers (which are supposed to screen most strongly in bulk) would overwhelm that due to excitons.

Additionally, we have measured a very fast exciton ionization time, ≈ 110 fs, which agrees extremely well with measurements of the homogeneous exciton linewidth broadening. This supports a model of thermal broadening due to the ionization of excitons through LO-phonon scattering. This exciton ionization time is significantly faster than that reported in III-V MQWs (≈ 300 fs), reflecting the stronger exciton-LO-phonon interaction in this wide-gap II-VI MQW system.

References

[1] H. Haug and S. Schmitt-Rink, J. Opt. Soc. Am. B 2, 1135 (1985).

[2] G. W. Fehrenbach, W. Schafer, J. Treusch, and R. G. Ulbrich, Phys. Rev. Lett. 49, 1281 (1982).

[3] W. H. Knox, R. L. Fork, M. C. Downer, D. A. B. Miller, D. S. Chemla, C. V. Shank, A. C. Gossard, and W. Wiegmann, Phys. Rev. Lett. 54, 1306 (1985).

[4] S. Schmitt-Rink, D. S. Chemla, and D. A. B. Miller, Phys. Rev. B 32, 6601 (1985).

[5] D. Lee, A. M. Johnson, J. E. Zucker, R. D. Feldman, and R. F. Austin, J. Appl. Phys. 69, 6722 (1991).
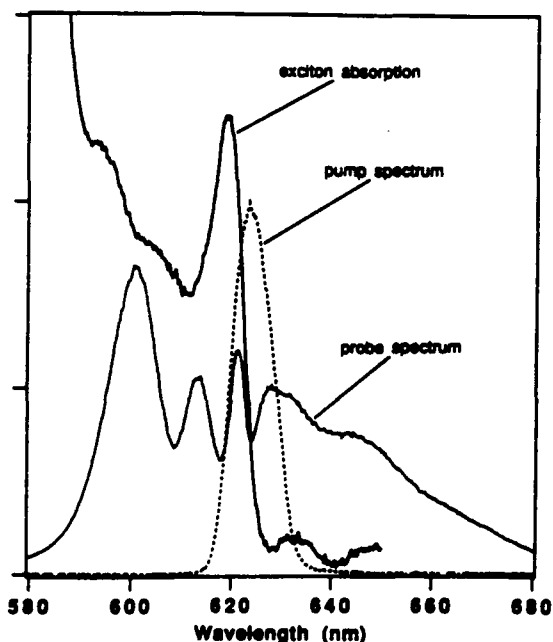
Fig. 1. Room-temperature absorption spectrum of the CdZnTe/ZnTe quantum-well sample (smooth curve) and the spectra of the 80-fs dump pulse (dashed curve) and the 14-fs probe pulse used for the pump-probe measurements (dotted curve).
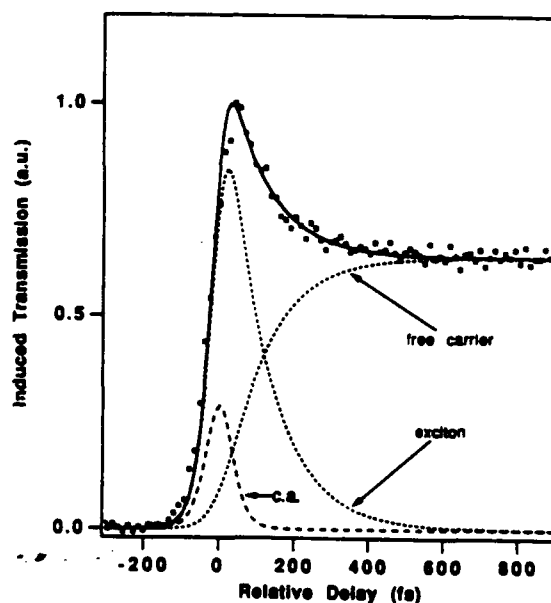
Fig. 2. Room-temperature pump-probe response measured at 620 nm. Experimental (dots) and calculated (smooth curve) pump-probe response. The separate contributions of excitons and free carriers are shown as dashed lines. The coherent artifact (c.a.) term is shown separately.

Femtosecond Dynamics of Exciton Gain

in (Zn,Cd)Se/ZnSe Quantum Wells

M. Hagerott, J. Ding, and A.V. Nurmikko

Division of Engineering and Department of Physics

Brown University, Providence, RI 02912

(401)863-2869

Y. Gan, D. Grillo, J. Han, H. Li, and R.L. Gunshor

School of Electrical Engineering

Purdue University, West Lafayette IN 47907

The recent proof-of-concept demonstration of a blue-green diode laser in 1991 [1],[2] relied in part on the useful optical properties of the (Zn,Cd)Se/ZnSe and (Zn,Cd)Se/Zn(S,Se) quantum wells. These included large exciton effects to room temperature and beyond [3], a particularly unusual circumstance in wide gap II-VI semiconductors, given the large exciton-LO phonon interaction. However, due to quantum confinement, the binding energy in a ZnCdSe QW can exceed the LO-phonon energy so that excitons can in principle dominate also spontaneous emission to device temperatures. So far, most of the characterization of the new diode lasers has been performed at T= 77K, a

temperature where the 2D excitons are particularly robust. The role of excitons in providing gain has been argued by us to be a physical reality in the ZnCdSe/ZnSe system [4], a feature which takes additional potential significance in terms of future diode laser design and development.

In this paper we discuss results of femtosecond experiments in which the excitonic nature of gain and its dynamics of formation are unambiguously demonstrated at T = 77K. Two types of experiments were performed, initially in the temperature range from 10 to 77K: (i) pump-probe experiments where the modification of the n = 1 HH absorption was probed under resonant excitation, and (ii) degenerate four-wave mixing experiments (DFWM) the purpose of which was to study the exciton phase and energy relaxation in the high electron-hole density environment. Figure 1(a) shows the experimental schematic of the pump-probe arrangement, including the possibility of observing stimulated emission through cleaved end facets of a QW sample. The samples contained 3 to 6 QWs with well thicknesses ranging from 30 Å to 90 Å. Figure 1(b) shows the relationship between the exciton n = 1 HH absorption resonance, the fsec pulse spectrum, and the stimulated emission spectrum from a sample with L_w = 30 Å at T = 77K.

Figure 2 displays the result of a pump-probe experiment where the absorption/gain spectrum through the QW section is graphed at 300 fsec and 10 psec delay with respect to the pump pulse. The appearance of gain on the low energy side of the exciton is unambiguously demonstrated (and accurately measured) at 10 psec delay, while the major portion of the exciton resonance remains in the absorptive state. We have recently constructed a phenomenological model in which the state filling of excitons within the

inhomogeneously broadened resonance can be calculated to provide the observed gain. Note in the figure how the stimulated emission spectrum is consistent with the spectral position of the gain. The laser emission also occurred after a time delay on the order of 10 psec relative to the pump pulse.

An example of the spectrum of the degenerate four wave mixing experiments is shown in Figure 3. The experiments were conducted in the two-beam configuration and had the aim of eludicating the phase and energy relaxation in the ZnCdSe QWs in the presence of a high density ($\sim 10^{11}$ cm^{-2}) exciton population. Our indications are that the phase relaxation itself is very fast and beyond the system resolution ($T_2 < 300$ fsec). Unusually, however, the spectrum of the DFWM signal, under near resonance excitation ($\Delta E \approx 10$ meV), can show a distinctly two-peaked form. The signature of the DFWM 'excitation spectrum' shows rather complex variations with the wavelength tuning of the pump beams, and can be reduced to a single resonantly enhanced DFWM feature when the excitation is coincident with the exciton absorption peak.. From a combination of spectral and temporal observations, we argue that this behavior reflects the presence of a strong energy dependent variation in the energy relaxation process with the 2D excitons. In particular, the presence of a "mobility edge" to separate excitons in localized states (low energy portion of the inhomogeneous resonance) from those in the extended states (high energy) is expected to give a large, relatively abrupt change in T_1 (E).

References:

[1]   M. A. Haase, J. Qiu, J.M. Depuydt, and H. Cheng, Appl. Phys. Lett. **59**, 1272 (1991);
H. Jeon, J. Ding, W. Patterson, A. V. Nurmikko, W. Xie, D. C. Grillo, M. Kobayashi,
R. L. Gunshor, Appl. Phys. Lett. **59**, 3619 (1991)

[2]   J. DePuydt, M. Haase, J. Qiu, and H. Cheng 1992, *Proc. Conf. on Blue-Green Lasers*,
Albuquerque NM (Optical Society of America); H. Jeon, J. Ding, Patterson, A. V.
Nurmikko, W. Xie, D. C. Grillo, M. Kobayashi, R. L. Gunshor, *App. Phys. Lett.* **60**,
2045 (1992), and *Optics Letters* (in press)

[3]   N. Pelekanos, J. Ding, A.V. Nurmikko, H. Luo, N. Samarth, and J.K. Furdyna, Phys.
Rev. **B45**, 6037 (1992)

[4]   J. Ding, H. Jeon, T. Ishihara, M. Hagerott, A.V. Nurmikko, H. Luo, N. Samarth, and
J.K. Furdyna, *Phys. Rev Lett.* **69**, 1707 (1992); Phys. Rev. **B** (in press)

Figure 1: (a) Schematic of the experimental arrangement; (b) The absorption spectrum near the n = 1 HH exciton resonance of the (Zn,Cd)Se/ZnSe QW, pump laser spectrum, and laser emission from a QW structure at T = 77K, respectively.
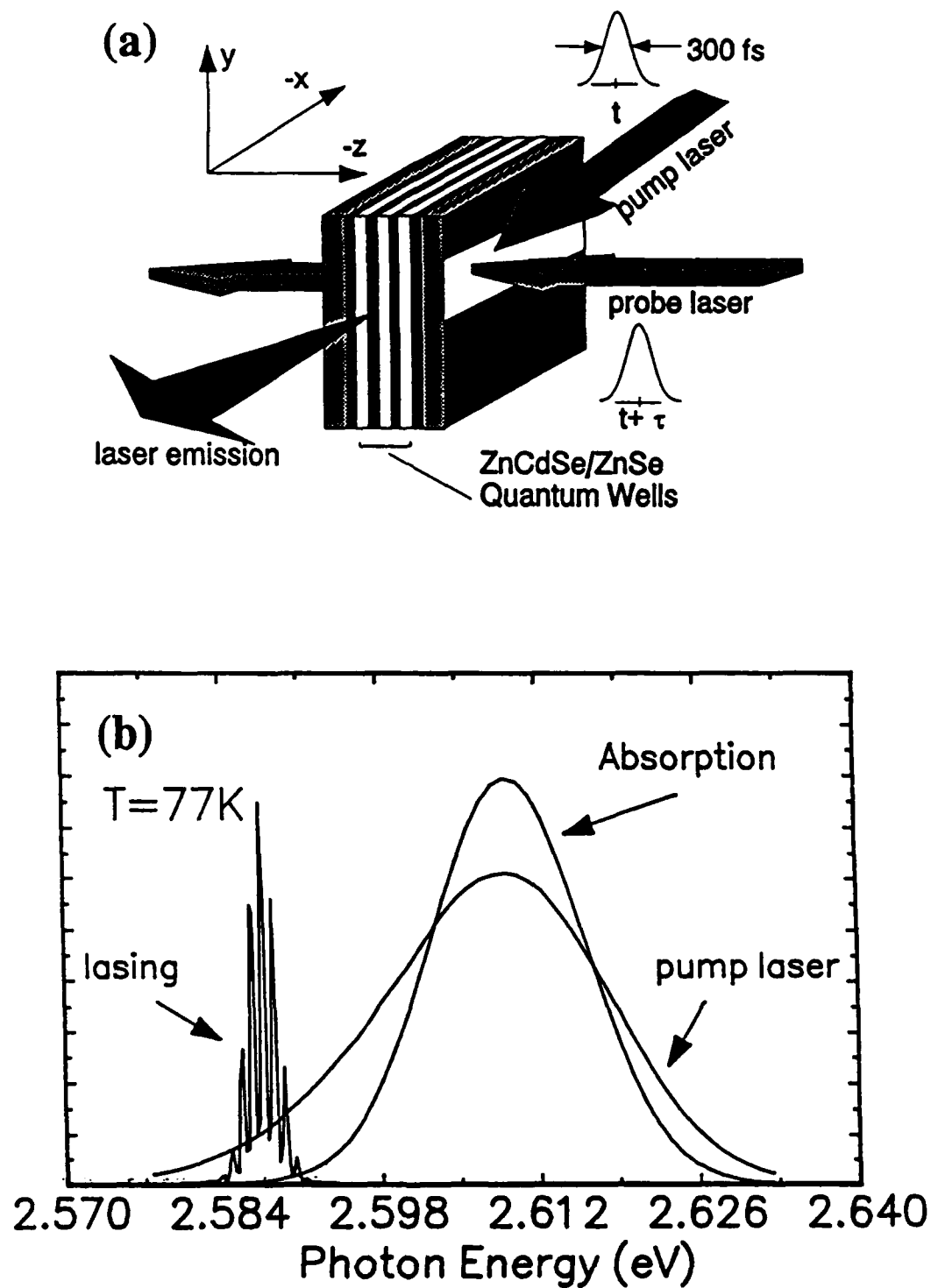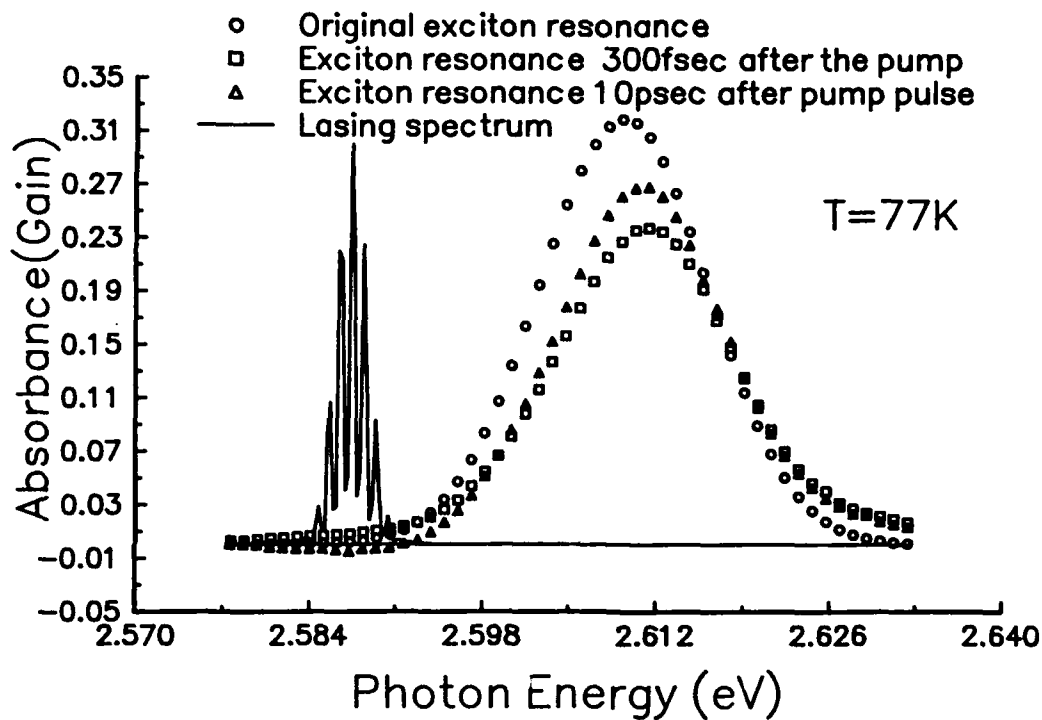
Figure 2: The n = 1 HH exciton absorption resonance at T = 77 K without photoexcitation (circles), and 300 fsec (squares) and 10 psec (triangles) after the photoexcitation. The QW laser emission spectrum is also included.
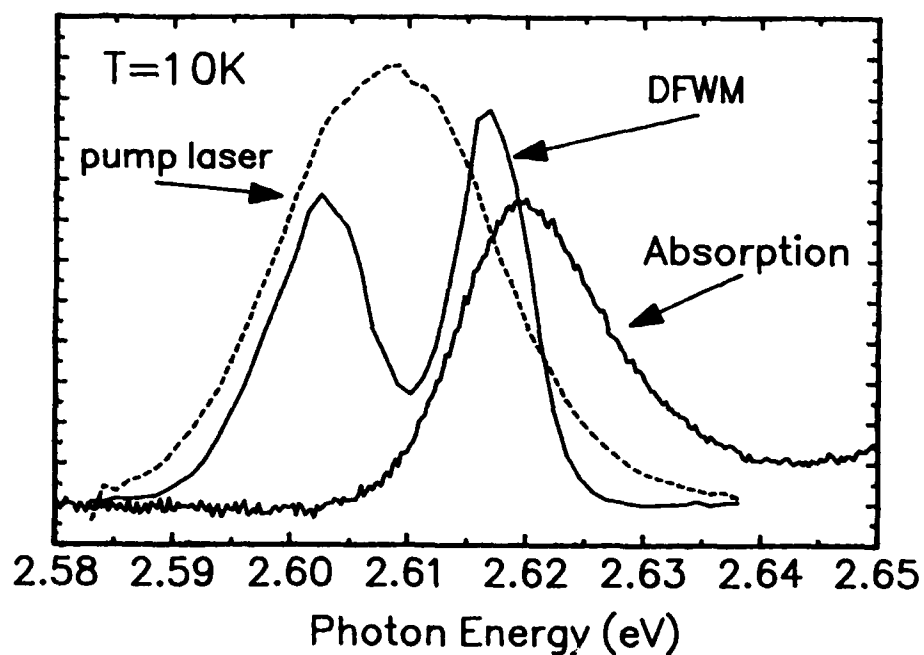
Figure 3: The spectrum of the DFWM taken with ≈500 fsec time delay between the excitation pulses at T = 10K. For reference, the figure also shows the pulse spectra and the n = 1 exciton absorption resonance.

Femtosecond Studies of Ultrafast Large-Angle Polarization Rotation in GaAs/Al$_x$Ga$_{1-x}$As Multiple Quantum Wells Under Uniaxial Stress

M. Wraback,[a†] H. Shen,[a‡] J. Pamulapati[a], M. Dutta[a], P. Newman[a],
and Y. Lu[b]

[a]U. S. Army Research Laboratory, Electronics and Power Sources Directorate
AMSRL-EP-EF, Fort Monmouth, New Jersey 07703-5601, (908) 544-3584

[b]ECE Department, Rutgers University, Piscataway, New Jersey 08855-0909

Due to symmetry considerations, polarization rotation is not possible for light incident normal to a lattice matched or pseudomorphic multiple quantum well (MQW) structure. However, it has been shown[1] that a uniaxial stress applied in the plane of the structure breaks the rotation symmetry, which should result in an anisotropic excitonic absorption due to the mixing of the heavy and light hole states in the MQW. In this paper we show for the first time that the bleaching of this absorption creates an ultrafast large-angle polarization rotation which may have applications in the field of high speed, high contrast ratio spatial light modulators (SLM).

A p-i(MQW)-n structure grown on (100) GaAs in which the intrinsic region consists of a 100 period, 150Å GaAs/ 60Å Al$_{0.1}$Ga$_{0.9}$As MQW was employed in this study. The structure was removed from the GaAs substrate by epitaxial lift-off and bonded to a LiTaO$_3$ substrate cut such that one of the in-plane thermal expansion coefficients (y-axis) matched that of the MQW while its orthogonal counterpart (x-axis) did not. The sample temperature was lowered to 150K, creating a compressive uniaxial strain of ~0.15%. Pulses of 200fsec duration and 83MHz repetition rate were obtained from a self-mode-locked Ti:sapphire laser[2]. Conventional pump-probe geometry was used, with the pump pulse polarization horizontal, while that of the probe pulse was vertical and oriented at 45° wth respect to the x and y axes of the LiTaO$_3$. A phase compensator and high quality polarizer were used to analyze the probe light transmitted through the sample, which was subsequently dispersed by a monochromator placed before the detector. The polarizer was oriented for the minimum probe transmission at the heavy hole exciton transition energy for the configuration in which the probe pulse preceeds the pump When the probe pulse is delayed with respect to the pump, the anisotropic excitonic absorption is bleached by the excitation pulse and an increase in transmission of the probe is measured due to the rotation of its polarization.

Figure 1 shows the change in this probe transmission ΔT during the first 3psec after excitation with the pump pulse. A sharp peak is observed at time $t = 0^+$ psec corresponding to a dynamic polarization rotation of $\Delta\theta \sim 25°$ and a maximum contrast ratio $CR = \Delta T(0^+)/\Delta T(-t)$ in excess of 100:1, where $\Delta T(-t)$ is the probe transmission at a delay such that the probe preceeds the pump. This onset decays within 1psec to a plateau which decreases very slowly over our measurement range of 2nsec. The subpicosecond decay may be related to the evolution of a nonlinear susceptibility enhanced by the temporal coincidence of the pulses in the sample and is currently under further investigation. The lack

of background signal at negative delay times indicates that the slow decrease is completely finished within the 12nsec period of the laser pulses. This decay in our shallow well sample at low temperature and 0 bias voltage is consistent with that of other researchers[3] and is most likely due to LO phonon-assisted tunneling to unconfined continuum states.

After the initial rapid decay, $\Delta\theta \sim 10°$ at the onset of the slower decrease. The contrast ratio of $\sim 28:1$ obtained in this case is compared with that resulting from absorption alone (effect of polarizer absent) in figure 2. Even for this smaller $\Delta\theta$ the rotation enhanced contrast ratio is more than 5 times larger than that found for the simple absorption case. Further improvement can be attained for stronger bleaching of the excitonic absorption by the pump pulse. In this case, however, the rotation does not turn off within 12nsec in the absence of a bias voltage, perhaps due to screening of the electron-LO phonon interaction at higher excitation densities. Contrast ratios in excess of 200:1 have been found when the pump is completely blocked in the off state. Impression of a bias voltage upon the structure should result in a high speed, high contrast ratio device which may find application as a SLM.

References

†   NRC-EPSD Research Associate.

‡   Also at Geo Centers, Inc., Lake Hopatcong, New Jersey 07849.

1.   J. Lee, C. Jagannath, M. O. Vassell, and E. S. Koteles, *Phys. Rev.*, **B37**, 4164 (1988)

2.   D.E. Spence, P.N. Kean, and W. Sibbett, *Optics Lett.*, **16**, 42 (1991).

3.   J. Feldmann, K.W. Goossen, D.A.B. Miller, A.M. Fox, J.E. Cunningham, and W.Y. Jan, *Appl. Phys. Lett.* **59**, 66 (1991).
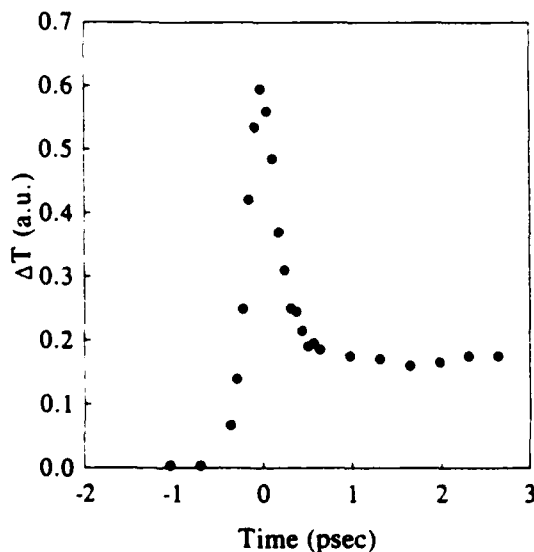
Fig. 1: Photoinduced change in probe transmission ΔT in the first 3psec after photoexcitation in the MQW structure described in the text.
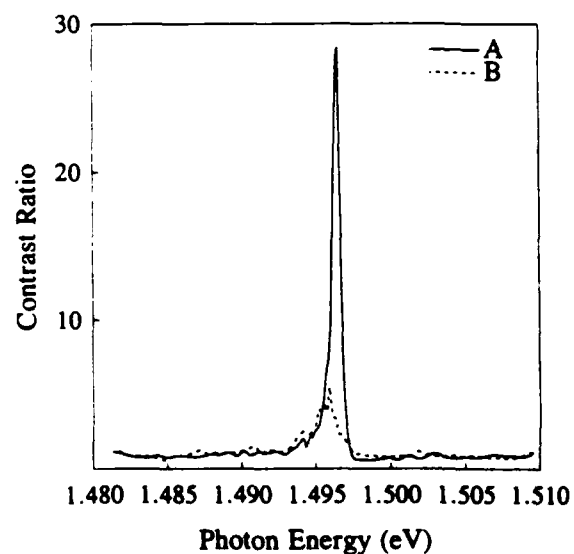
Fig. 2: Contrast ratio in the MQW structure A)with 10° polarization rotation enhancement; B) without enhancement.

Fast optical switching and amplification in a multiple quantum well vertical microcavity

R. Raj, J. L. Oudar and M. Bensoussan

FRANCE TELECOM
Centre National d'Etudes des Télécommunications, Paris B
Laboratoire de Bagneux
BP 107, 92225, Bagneux, France
Fax: (33 1) 42 53 49 30
Tel: (33 1) 42 31 72 88

SUMMARY

A major advance in the processing of optical signals in recent years has been the development of innovative devices based on vertical microcavity structures such as surface emitting lasers, bistable optical switches and modulators. These devices have attracted a lot of attention as they are highly suitable for bidimensional integration allowing fast parallel processing of information[1]. However such a bidimensional optical processing could be performed much more easily if another important function i.e amplification could be achieved in a practical way.

Indeed, semiconductor optical amplifiers based on stimulated emission are now widely considered for use in photonic switching systems[2], due to their ability to regenerate optical signals with a high bandwidth, and also to act as gated amplifiers with subnanosecond temporal resolution. They operate in a waveguide geometry[3], usually with antireflection coatings in order to achieve a high gain in a single-pass travelling-wave regime. This approach however, is not directly applicable to bidimensional integration, due to the complexity in the fabrication process and their low degree of miniaturization. On the other hand, optical modulation transfer through the modulation of the electrical current in a vertical cavity surface emitting laser have been proposed recently[4] and have been demonstrated but for limited modulation widths up to a few GHz.

In this letter we demonstrate that vertical microcavities can be used effectively as optical amplifiers with a bandwidth of 2 THz, and with the capability of acting as gated amplifiers, with a time resolution better than 20 ps. As opposed to waveguided amplifiers, this device actually benefits from the optical cavity resonance that gives rise to a multipass operation. Due to the very short cavity length, the intrinsic mode bandwidth is still relatively large, and can easily amplify multi-GHz signals. In addition we show that the use of oblique incidence allows to achieve a high gain (typically larger than 10 dB) in the gain-switched regime. This implies that angle-multiplexing can be used to amplify simultaneously several channels incident on the same active device. Such a high gain is achieved transiently *before* the usual laser emission actually takes place. As this laser emission is directed perpendicular to the mirrors, the amplified signals are spatially distinct from it, and therefore can be easily discriminated through spatial filtering. Further, using a vertical cavity FP array with a variable spacer within the cavity it is possible to envisage a perfectly adapted monolithically integrated amplifier for the vertical cavity laser arrays emitting different wavelengths.

The sample studied is composed of active an medium of 130-period GaAs/Al$_{0.3}$Ga$_{0.7}$As multiple quantum wells with 10nm/10nm nominal layer thickness sandwiched between a pair of Bragg reflector mirrors. The reflectivities of the back mirror R$_b$ and front mirror R$_f$ at the Bragg wavelength are 97.2 and 91.7% respectively. The experiments were performed at room temperature using two independently tunable beams from LiO$_3$ optical parametric generators, pumped by frequency doubled Nd:YAG delivering pulses with 18ps duration, 1nm spectral width and with typically a few μJ energy. Two beams, a strong pump beam and a weak test beam travelling parallel to each other were focussed by a single lens to a spot size of 30μm and intersect the sample at an angle of 30° and 20° respectively.

The linear as well as nonlinear reflectivity spectra are displayed in figure 1. The linear spectrum (full line) was traced by scanning the wavelength of the test beam (100pJ/cm^2) from 780nm to 860nm, in the absence of the pump beam. The linear spectrum displays the Fabry-Perot peaks in the absorption and transparent regions. Nonlinear spectra obtained by pumping the sample with beam intensity of 90 mJ/cm^2 and monitoring the reflected intensity of the test beam is depicted in figure 1. Only a small portion of this intensity is effectively used for pumping the active medium as the sample is not optimised for optical pumping. The pump wavelength is fixed at 782nm, where the active medium is absorbant. When the sample is pumped we see that the FP peaks in the absorption region switch into peaks with reflectivities greater than one. This is due to the test beam being strongly amplified by stimulated emission in the active layers of the cavity. Under similar pumping conditions a gain of as much as 8 dB has been observed. The spectral width of the gain peaks point to the gated amplification of THz optical signals.
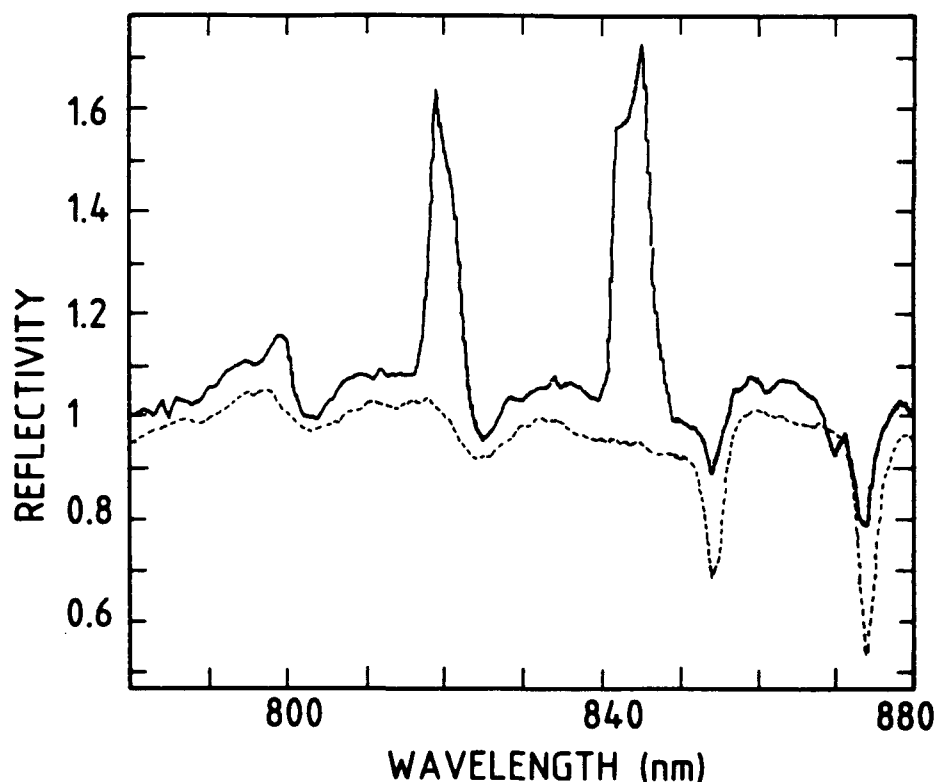
Figure 1. Spectra in the absence and presence of optical pumping. *Dashed line:* linear spectrum (slightly displaced for visual comfort). *Full line:* spectrum of the test beam in the presence of a pump at 782nm with an intensity of 15μJ/cm^2

A fair picture of the amplification process is given by a simple model which yields for the reflectivity of the microcavity the following expression:

$$R = \frac{I_{reflected}}{I_{incident}} = \frac{(R_f - R_\alpha)^2/R_f + 4R_\alpha \sin^2 \phi}{(1 - R_\alpha)^2 + 4R_\alpha \sin^2 \phi} (1)$$

where $R_\alpha = \sqrt{R_f R_b} \exp(-\alpha L)$, R_f being the reflectivity of the front mirror, R_b the reflectivity of the back mirror, $\alpha = \frac{4\pi K}{\lambda}$, $\phi = \frac{2\pi n L}{\lambda}$, with λ the wavelength of the weak beam, L the cavity length, n being the refractive index of the medium which governs the cavity resonance and α, depending on the sign, is the absorption or the gain coefficient averaged over the active medium length.

A plot of the reflectivity as a function of ϕ for several values of α (not is shown here) describes qualitatively the experimental observation: the onset of saturation, and the gain for different carrier densities corresponding to different pumping intensities. By plugging in all the measured parameters in equation (1), a 10 dB gain is estimated for a carrier density of $1.5 \times 10^{12}/cm^2$, close to the measured gain of 8 dB. The model used for calculating the reflectivity gives us an overall understanding of the process in play as well as helps us determine certain parameters of optimisation such as the reflectivities of mirrors which can lead to far higher gains than the ones observed.
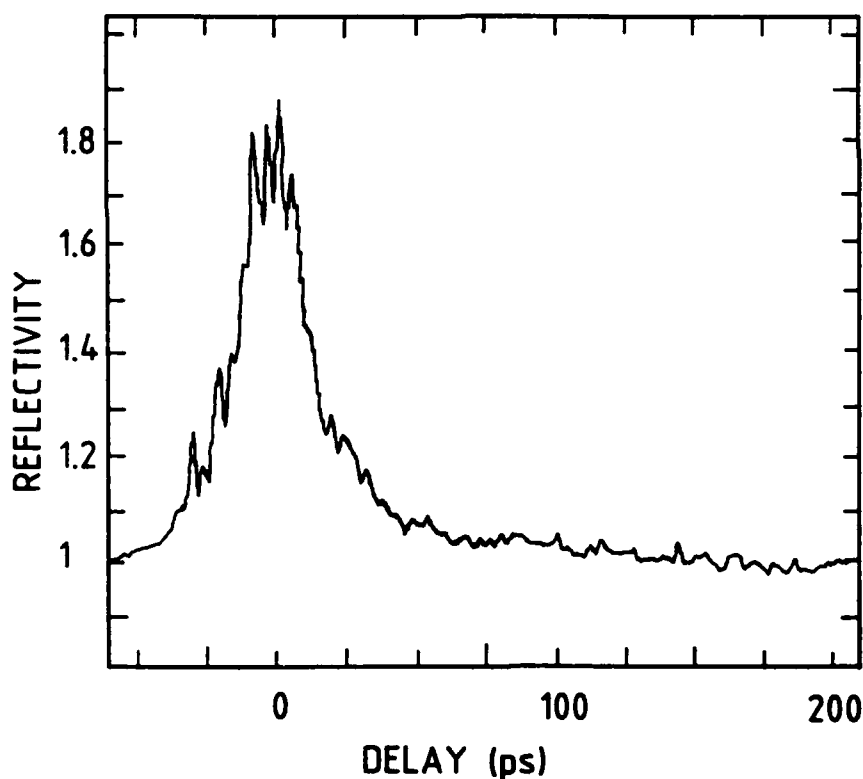
Figure.2 Temporal response of the amplified signal at 843nm.

The temporal response of the system obtained by varying the optical path between the two beams showed that the amplification of the weak beam lasts for only 18ps (i.e. the duration of the pump pulse) as shown in figure 2 where the pump wavelength and intensity are those of figure 1 and the weak-beam wavelength is 843 nm. For the pumping energies used in this experiment, the laser emission depletes the sytem to such an extent that the amplification lasts

only for 18ps. This short a duration of amplification suggests the use of the vertical cavity laser as an amplifying optical switch with very broad modulation bandwidth exceeding 10 GHz. The modulation and amplification may be obtained by varying the carrier density so as to switch the system from the absorptive state to an amplifying state. The rapidity of the switching is mainly dictated by the rapidity with which the carrier density is varied. And by combining amplification with modulation insertion loss is eliminated while maintaing a good contrast. Remembering that the incident angles of the test and pump beams were 20° and 30°, devices based on this amplification can be driven above the lasing threshold and as the laser emission is directed vertically, it does not interfere with the amplified signals which propagate at oblique angles.

In conclusion we have experimentally demonstrated that a vertical cavity works as an efficient and fast optical switch. The time response of such a switch in our experiment is mainly limited by the pulse duration. As this optical switch is based on structures which have proved extremely successful for the performance of several other optical functions, it constitutes a promising element towards integration in parallel optical processing of information.

REFERENCES

[1] J. L. Jewell, S. L. McCall, Y. H. Lee, A. Scherrer, A. C. Gossard and J. H. English, Appl. Phys. Lett., 54, 1400, (1989).

[2] I. W. Marshall, M. J. O'Mahony, D. M. Cooper, P. J. Fiddyment, J. C. Regnault and W. J. Devlin, Appl. Phys. Lett., 53, 1577, (1988).

[3] T. Saitoh and T. Mukai in Coherence, Amplification and Quantum effects in Semiconductor Lasers, ed Y.Yamamoto (Wiley, New York, 1991), Chap 7.

[4] M. W.Maeda, C. Chang-Hasnain, A. Von Lehmen, Chinion Lin, H. Izadpanah and M. Z. Iqbal CLEO postdeadline CPDP3-1/575 (1991).

[5] R. Raj, M. Bensoussan, J. L. Oudar and A. Levenson, French Patent pending.

Wires and Dots

QFA 8:30am–10:00am
Grand Ballroom East

C. Weisbuch, *Presider*
Thomson CSF-LCR, France

Characterization Studies and Luminescence of Quantum Wires and Dots

Jean-Yves Marzin
CNET, BP 107
Bagneux, France

Summary not available at time of printing.

Effects of Size Fluctuation on the Optical Properties of Very Narrow InGaAs/InP Quantum Well Wires

S. Nojima, M. Notomi, M. Nakao, and T. Tamamura

NTT Opto-electronics Laboratories
3-1 Morinosato-Wakamiya, Atsugi, Kanagawa 243-01, Japan
Phone +81 462 40 2827: Fax +81 462 40 4305

The authors have succeeded in fabricating very narrow InGaAs/InP quantum well wires (QWWs with cross sections down to 50 Å×100 Å) by combining electron beam lithograhpy, reverse-mesa wet etching, and the subsequent overgrowth onto bare QWW structures.[1] Moreover, the authors reported several optical properties of the QWWs thus fabricated which manifested the one dimensional confinement of the electron-hole system.[1,2] In order to adequately draw on the potential of QWWs, it is essential, in addition to the fundamental qualities described above, to reduce the QWW size fluctuation.[3] This is because great size-fluctuation leads to pronounced fluctuation in quantum levels and the resultant broadening of the otherwise sharp density of state spectrum. Considering this, it is urgent that the relationship between the size fluctuation and the characteristics of QWWs be clarified.

This presentation reports the experimental and theoretical studies for QWWs performed to date in our Labs., putting a stress on the latest subject shown in the title.

To evaluate the size fluctuation, we carried out for the first time the direct measurement of the QWW lateral size using Atomic Force Microscopy (AFM). The AFM technique has the advantage of minute three-dimensional mapping compared with a conventional technique such as scanning electron microscopy. An example of a direct AFM image of QWWs is shown in Fig. 1, the lateral size of which is approximately 200 Å. The fabricated wires are located on the tops of the ridges. The numerical data on the AFM image permits us to calculate two kinds of standard deviations for the lateral size fluctuaions, σ_{intra} and σ_{inter}, which are defined for the fluctuation within a wire (intra-wire) and among the wires (inter-wire), respectively. In Fig. 2, the σ_{intra} and σ_{inter} values are plotted as a function of the average lateral size (Ly). The σ_{intra} values are averaged at about 6 Å while σ_{inter} about 15 Å. Surprisingly low σ_{intra} values appear to be achieved primarily by the reverse-mesa wet etching process, because the fluctuation in the mask pattern in this etching process reveals a large standard deviation value of about 20 Å (not shown in Fig. 2; this will be discussed at the meeting). This is one of the advantages of the present QWW fabrication method. The relatively large σ_{inter} values may be created by some fluctuations in the electron beam lithography. The lateral size fluctuation among the wires is thus known to be crucial compared with that within a wire. In the succeeding paragraphs, we discuss the effects of the size fluctuation on the optical properties of QWWs, on the basis of the fluctuation actually evaluated in Figs. 1 and 2.

First, we performed the photoluminescence (PL) measurements. Figure 3 shows the band-edge PL intensity spectrum measured at 2 K (solid lines) for QWW with Lx=50 Å and Ly=100 Å, together with that of QWF (single QWF) with Lx=50 Å (and Ly=∞) for reference. The large peak-energy shift (about 35 meV) clearly indicates enhanced confinement due to decreased lateral size (Ly) from ∞ to 100 Å. The spectrum width of the QWW is much wider (about 5 times) than that of the QWF. This fact is contrary to our general expectation that the QWW must reveal a narrower PL spectrum because of its sharper density of state. An attempt was made to explain this spectrum broadening using a model that takes into account the evaluated lateral size fluctuation. The dashed line indicates the PL spectrum calculated assuming the fluctuation described by a Gaussian distribution of σ_{inter}=15 Å and the line shape function with a carrier relaxation time of 0.1 ps. As is clearly shown in Fig. 3, the inter-wire fluctuation explains the measured PL spectrum for this narrowest of QWWs. This spectrum is much broader than one calculated assuming no size fluctuation (shown by a dash-dotted line). The small discrepancy between the theory and the experiment may result from some other broadening factor such as impurities. It is thus clear that the inter-wire fluctuation must be reduced to obtain a sharp PL spectrum.

Second, we studied the polarization anisotropy of the light emitted from QWWs. Figure 4 shows the TM/TE intensity ratio (i.e., Ix/Iy) of the electroluminescence emitted from the QWW edge (see the inset) as a function of the lateral size (Ly) for a fixed Lx of 150 Å. The TM/TE ratio increases with decreasing Ly and approaches the value of 1.0, which is expected for QWWs having a symmetrical cross section (Lx=Ly=150 Å). This is clear evidence of the two- to one-dimension (2D to 1D) transition of the electron-hole system due to decreasing the lateral size (Ly) from

600 to 200 Å. The solid line in Fig. 4 indicates the corresponding optical-transition-matrix-element ratio calculated using the k.p method which has taken the six-valence-band mixing into account.[4] The region sandwiched between the two dashed lines indicates the band in which this ratio is within its standard deviation (here, $\sigma_{inter}=15$ Å is again employed as the lateral size fluctuation). As is clear from Fig. 4, the size fluctuation does not greatly alter the interpretation of the polarization anisotropy. Note, in particular, that most of the experimental points are located within the fluctuation band. These results can thus be undoubtedly regarded as evidence of the 2D to 1D transition of the electron-hole system.

[1] M. Notomi, M. Naganuma, T. Nishida, T. Tamamura, H. Iwamura, S. Nojima, and M. Okamoto, Appl. Phys. Lett. 58, 720 (1991).

[2] M. Notomi, M. Okamoto, S. Nojima, H. Iwamura, and T. Tamamura, 19th Int. Conf. on Gallium Arsenide and Related Compounds, Karuizawa, Japan (1992).

[3] Y. Arakawa, T. Takahashi, and K. Vahala, 16th Int. Conf. on Quantum Electronics, Tokyo, Japan (1988): H. Zarem, K. Vahala, and A. Yariv, IEEE J. Quantum Electron. QE-25, 705 (1989).

[4] S. Nojima, Jpn. J. Appl. Phys. 31, L765 (1992).
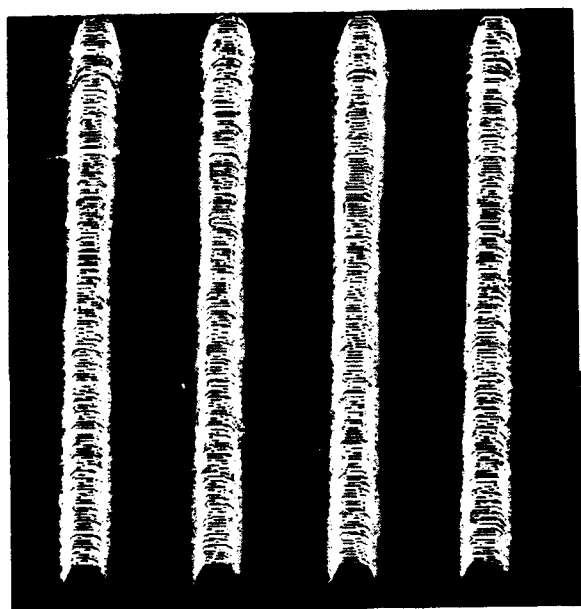
Fig. 1. AFM image of QWW array.　　1000 Å

Fig. 2. Standard deviation for size fluctuation vs. Ly.

Fig. 3. PL spectra of QWW and QWF (reference).
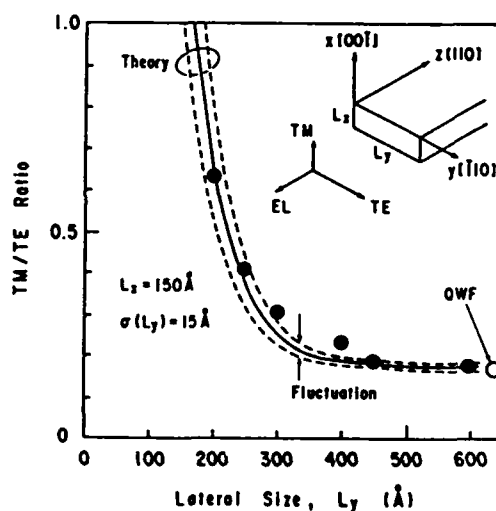
Fig. 4. TM/TE ratio for edge-emitted EL vs. Ly.

Fabrication of GaAs Quantum Wires (~ 10nm) by MOCVD Selective Growth

S. Tsukamoto[1], Y. Nagamune[2], M. Nishioka[1], and Y. Arakawa[1,2]

[1]Institute of Industrial Science, [2]Research Center for Advanced Science and Technology,
University of Tokyo
7-22-1 Roppongi, Minato-ku, Tokyo 106, Japan
Telephone: +81-3-3478-1139, Fax: +81-3-3402-5078

Low dimensional semiconductor structures such as quantum wires have recently received great attentions since new physical phenomena with applications to semiconductor lasers and other functional optical devices are expected[1,2]. To fabricate these quantum microstructures, selective growth on patterned substrates is one of the most attractive techniques[3-5]. In order to obtain *real* quantum wire devices, the structures with lateral width less than 15nm must be achieved. In this paper, we report a successful fabrication of the GaAs triangular-shaped quantum wires with ~10nm lateral width, showing both photoluminescence(PL) measurement and a high-resolution scanning electron micrograph(SEM) observation. The fabrication technique employed here is based on the MOCVD selective growth technique which we have developed recently[6].

By changing the growth time of GaAs material for the quantum wires, we obtained the quantum wires with various lateral widths. Figure 1 shows high-resolution SEMs of the quantum wires with the lateral widths of ~10, ~15, ~25, ~35nm, respectively and their illustration. Each quantum wire smoothly connects to quantum well layers with ~2, ~3, ~5, ~7nm thickness. As shown in this photograph, the quantum wire with Lx~10nm was obtained by systematic change of the growth time.
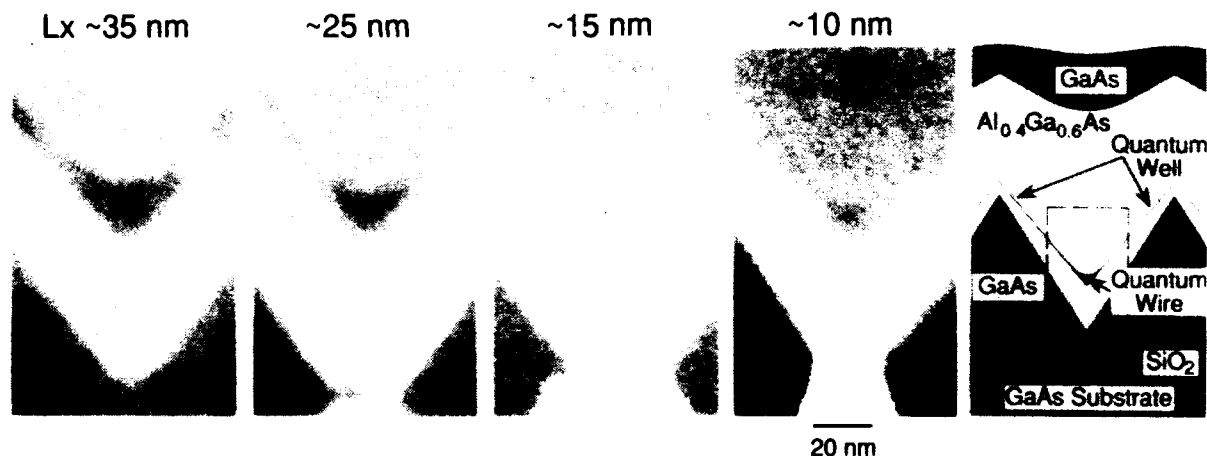
Fig. 1   High-resolution scanning electron micrographs of the part of the quantum wires with lateral wire widths of ~10, ~15, ~25, ~35 nm, respectively and their illustration.

The PL spectra from the quantum wire structures were measured as a function of the lateral wire widths of 0, ~7, ~10, ~15, ~25, ~30, ~35nm at 20K are given by the traces in Fig. 2(a). The lateral width of 0nm is a structure without the quantum wires. Note that the dimension of Lx~7nm was determined by both the growth time condition and the PL peak position of the quantum wires. In this figure, the hachured PL peaks are corresponding to the quantum wires. For example, in the PL spectra with Lx~35nm, the peak at 1.528eV is corresponding to the quantum wire and the other peaks come from GaAs bulk, the quantum well regions and AlGaAs regions.

Figure 2(b) exhibits the energy shift ΔE of the PL peak of the quantum wires versus the lateral wire width Lx which is determined by SEM observation for open circles. The position of open triangle is determined by the growth time condition and the PL peak position of the quantum wires. ΔE is defined as the energy difference between the PL peaks of the GaAs bulk (1.513eV) and the

quantum wires As shown in this figure, the blue shifts occur systematically with decreasing Lx, which is due to enhancement of the two-dimensional quantum confinement effect. The solid curve in the figure is the result of the Kronig-Penney calculation, taking the relationship[7] of the dimensions between triangular- and rectangular-shaped quantum wires into account. These results indicate that a strong lateral confinement is achieved in the quantum wire structures with $Lx \sim 10nm$.
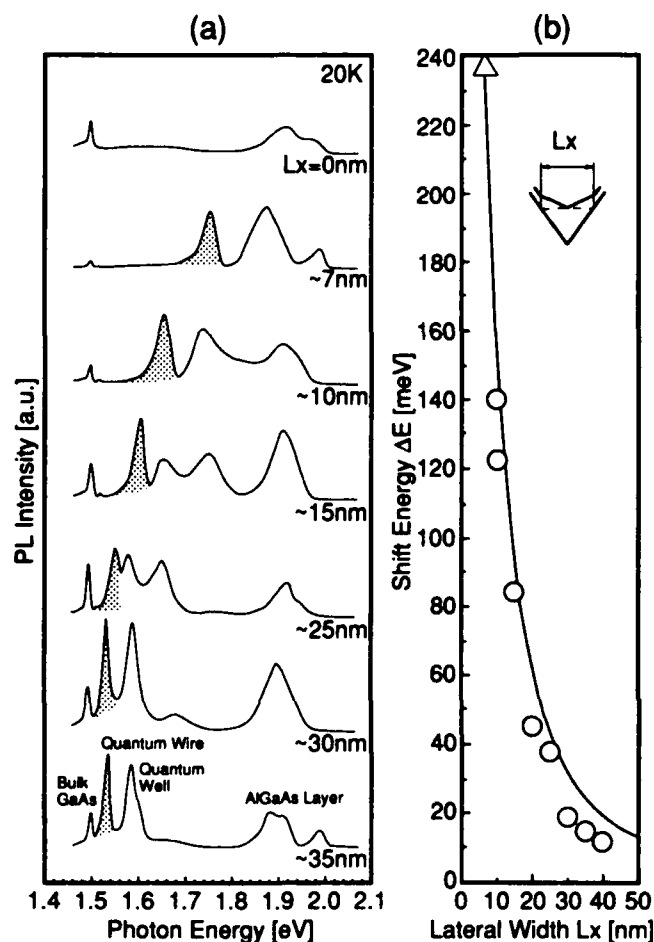
Figure 3 shows the integrated PL intensities of the quantum wires versus the lateral width Lx. As shown in this figure, the PL intensities of the quantum wires are not decreasing even when the lateral width is reduced. This result demonstrates that the high interface quality in the quantum wires are achieved here by our in-situ growth techniques.

Fig. 3   PL intensities of the quantum wires versus the lateral width Lx.

Fig. 2   (a) Photoluminescence(PL) spectra from the quantum wire structures measured as a function of the lateral widths of 0, ~7, ~10, ~15, ~25, ~30, ~35 nm at 20K. The lateral width of 0nm is a structure without the quantum wires. (b) The energy shift ΔE of the PL peak of the quantum wires versus the lateral width Lx which is determined by scanning electron micrographs observation for open circles. The position of open triangle is determined by the growth time condition and the PL peak position of the quantum wires.

References

[1] Y.Arakawa and H.Sakaki, Appl.Phys.Lett., 40, 939 (1982).

[2] Y.Arakawa, K.Vahala, and A.Yariv, Appl.Phys.Lett., 45, 950 (1984).

[3] T.Fukui, S.Ando, and Y.K.Fukai, Appl.Phys.Lett., 57, 1209 (1990).

[4] C.S.Tsai, J.A.Lebens, C.C.Ahn, A.Nouhi, and K.J.Vahala, Appl.Phys.Lett., 60, 240 (1992).

[5] E.Kapon, K.Kash, E.M.Clausen,Jr., D.M.Hwang, and E.Colas, Appl.Phys.Lett., 60, 477 (1992).

[6] S.Tsukamoto, Y.Nagamune, M.Nishioka, and Y.Arakawa, J.Appl.Phys., 71, 533(1992).

[7] T.Tanaka, T.Yamauchi, and Y.Arakawa, the 52th Autumn Meeting of Japan Society of Applied Physics, Okayama, October 1991.

GaInAs/InP Long-Wavelength Quantum-Wires and Boxes:
Fabrication Technology and Lasers

Shigehisa ARAI
Department of Physical Electronics
Tokyo Institute of Technology
2-12-1 O-okayama, Meguro-ku, Tokyo 152, Japan
Phone: +81-3-3726-1111 ext. 2512 Fax.: +81-3-5499-4791

Improvements in the regrowth process of a low-pressure OMVPE and the usage of p-type InP substrate enabled to obtain a room temperature CW operation of GaInAs/InP quantum-wire laser. Approaches to high performance lasers consisting of low-dimensional quantum-well structures will be presented.

Even though low-dimensional quantum-well structures have higher differential gain and lower linewidth enhancement factor[1], a certain density of quantum-wires and boxes is required for high performance operation. As can be seen in Fig.1 for lattice-matched GaInAs/InP system, the product of number of quantum-wells and the space filling factor along the in-plain direction, $n \cdot \rho$, should be larger than 2 for quantum-wire laser and 0.5 for quantum-box lasers from the viewpoint of high efficiency operation.

We have investigated the fabrication process of GaInAs/InP quantum-wires and -boxes by employing 2-step LP-OMVPE growth and wet-chemical etching[2], and observed quite large field-induced refractive index variations[3],[4], however a room temperature operation of a laser was not obtained due to poor regrowth process[5]. Introduction of a thin (~3nm) InP layer prior to the growth of GaInAsP layer in the regrowth as well as a pre-heating in pure hydrogen atomosphere reduced the threshold of quantum-well lasers with 70-140nm wide wire-like active region to almost a half that by a conventional process[6]. And an usage of p-type InP substrate reduced again to a half that, this might be attributed to an elimination of potential barrier against holes in the valence band[7].

By combining these as well as employing EBX direct writing of 70nm periodic line pattern, GaInAs/InP 3-quantum-well lasers with the active region width of 10-30nm were fabricated[8]. Figure 2 shows an SEM view of stain etched cross section of the BH laser. A room temperature CW operation was obtained with I_{th}=82mA (J_{th}=5.9KA/cm^2 for L=700μm), such a high threshold might be caused by poor optical confinement factor of quantum-wires (ξ ~0.6%, g_{act} ~2300cm^{-1}) because I_{th}~50mA (J_{th}=2.6KA/cm^2) was obtained only by putting HR-coated InP substrate on one facet. By comparing the EL peak wavelength of quantum-wire samples with that of quantum-film samples both fabricated on the same wafer, a blue-shift of ~20nm was observed.

Aiming at higher performance quantum-wire lasers as well as larger tolerance in the fabrication due to lower effective mass of holes[9], compressively strained quantum-well lasers with wire-like active region (Fig.3) were made with the period of 100nm. A RT-CW operation was also obtained with I_{th}=53mA (J_{th}=2.9kA/cm^2 for L=910μm). Though the active region was much wider (30-60nm) than that of lattice-matched one, a blue-shift of ~40nm was observed, that indicates reduced effective mass of holes as well as the effective wire width of ~30nm. In temperature dependences of the threshold current as shown in Fig.4, we did not observe noticeable difference between samples with/without wire-like active region both fabricated on the same wafer.

CONCLUSION: A room temperature CW operation of GaInAs/InP quantum-wire laser was achieved by employing 2-step OMVPE growth and wet-chemical etching. An introduction of a compressively strained quantum-well structure to

quantum-wire lasers was attempted for higher performance operation as well as larger fabrication tolerance.

REFERENCES

[1] Y.Miyake and M.Asada: Jpn. J. Appl. Phys., vol.28, no.7, pp.1280-1281, Sept. 1989.

[2] Y.Miyamoto et al.: Jpn. J. Appl. Phys., vol.26, no.4, p.L225-227, Apr. 1987.

[3] K.G.Ravikumar et al.: Appl. Phys. Lett., vol.58, no.10, pp.1015-1017, Mar. 1991.

[4] T.Aizawa et al.: IEEE Photon. Technol. Lett., vol.3, no.10, pp.908-909, Oct. 1991.

[5] M.Cao et al.: Trans. IEICE, vol.E73, no.1, pp.63-70, Jan. 1990.

[6] Y.Miyake et al.: IEEE Photon. Technol. Lett., vol.3, no.3, pp.191-192, Mar. 1991.

[7] Y.Miyake et al.: IEEE Photon. Technol. Lett., vol.4, no.9, pp.957-960, Sept. 1992.

[8] Y.Miyake et al.: 13th IEEE Int'l Semicon. Laser Conf., Takamatsu, Japan, M-4, pp.234-235, Sept. 1992.

[9] S.Ueno et al.: Jpn. J. Appl. Phys., vol.31, no.2A, pp.286-287, Feb. 1992.
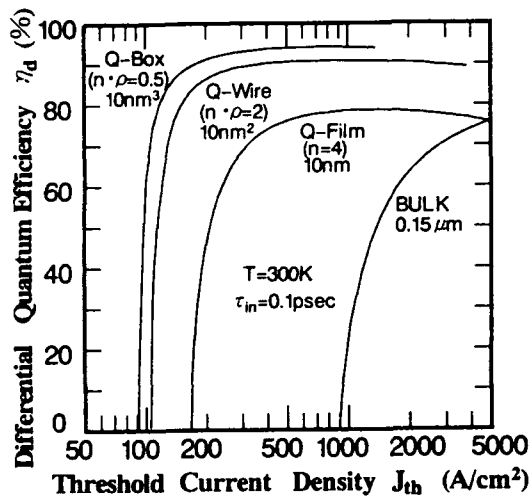
Fig.1 Relation between differential quantum efficiency and threshold current density, for lattice-matched GaInAs/InP bulk, Q-film, Q-wire, and Q-box lasers.

Fig.2 Schematic structure of GaInAs/InP 3-layered quantum-wire laser which operated in CW at room temperature, and cross-sectional SEM view of quantum-wire laser

Fig.3 Schematic structure of $Ga_{0.3}In_{0.7}As/InP$ GRIN-SCH 5-layered compressive strained quantum-well laser with wire active region.
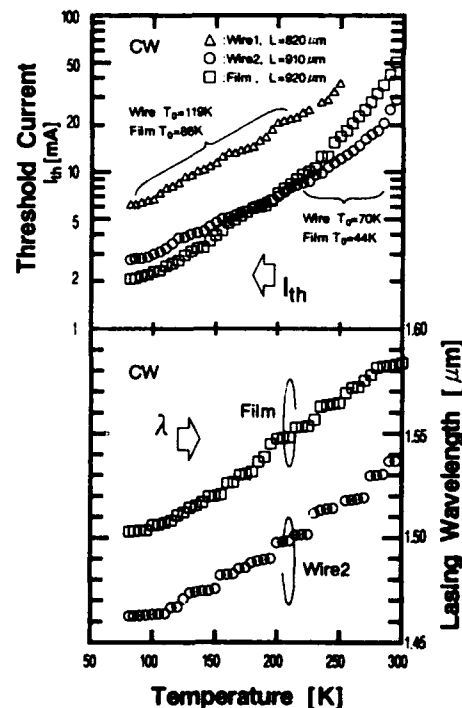
Fig.4 Temperature characteristics of $Ga_{0.3}In_{0.7}As$ /InP GRIN-SCH 5-layered compressive strained quantum-well laser with wire active region.

Optics and Transport in Reduced Dimensionality

QFB 10:30am–11:45am
Grand Ballroom East

Manfred Pilkuhn, *Presider*
Universitat Stuttgart, Germany

PROS AND CONS OF REDUCED ENERGY RELAXATION AT LOW DIMENSIONS FOR OPTOELECTRONICS DEVICES

H. BENISTY

Laboratoire de Physique des Solides, Tour 13-E2
Université Paris 6, F-75252 Paris Cedex 05, France

Unlike the early recognition of the improved performances of quantum wells in optoelectronic devices, there is still no clear demonstration of similar gains from quantum wires, as one would expect from this further step in the spectral concentration of the oscillator strength. It is even far worse for quantum boxes where a universal collapse of the photoluminescence (PL) yield is observed for lateral sizes below ~100 nm, i.e. for quantization energies way below the ~20 meV required for improved room-temperature operation.

In this paper, we shall firstly trace the reason for these negative trends to the reduced energy relaxation in these systems[1] The need for such an *intrinsic* explanation is all the more strong as the maturity of nanostructure fabrication technology is now assessed by the many instances where narrow wires with acceptable optical properties are reported, evidencing a limited amount of fabrication defects. It becomes dubious, therefore, to systematically invoke these latter to account for the poor properties of quantum boxes. In a second part, we will show that the same phenomenon, the longer lifetime of excited carrier states can be extremely positive for devices relying on intersubband transitions, in the mid to large-infrared range.

We shall first discuss the generality of scattering reduction in low-dimensional systems and concentrate on the reduced electron-acoustic phonon relaxation in quantum-boxes, evidencing a critical level separation E^{crit} of the order of only 1 meV above which relaxation vanishes in the two-level case.

When considering today's quantum-boxes (diameter ~100 nm), carriers have to cascade down tens or hundreds of box levels to reach the ground state(s) of interest. Then, any level separation exceeding E^{crit} behaves as a bottleneck. To predict the overall effect of such bottlenecks and cast them into a single representative rate (Fig. 1), a statistical approach is presented, based on the Poisson distribution of neighboring level separations, allowing to extract the limiting bottleneck in the cascade of a box of given size. We next use the above results to determine a critical lateral size L_x^{crit} below which relaxation is strongly reduced. A similar critical size is found for quasi-wires (elongated boxes) with a simple aspect ratio dependence.
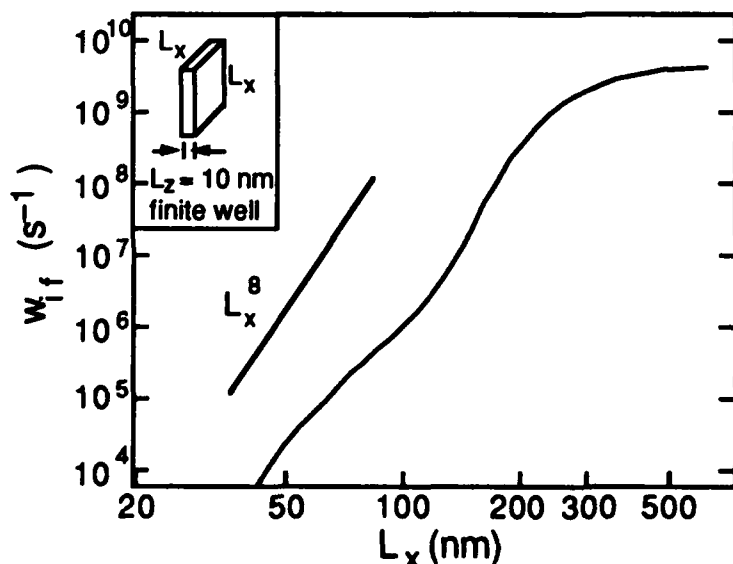

Fig. 1 : Statistically averaged electron scattering rate through a cascade of quantum-box levels within 30 meV of the ground-state in the InGaAs/InP system as a function of the lateral size L_x of the square box (see inset). The box is patterned in a 10 nm thick quantum-well. The effect of the "bottlenecks" is felt for L_x as large as 200-300 nm.

Turning to optoelectronic devices, a severe penalty is shown to affect the *interband radiative recombination* in quantum boxes, due to the combination of reduced relaxation with known orthogonality properties of quantum states and unavoidable nonradiative recombination. The corresponding collapse of the photoluminescence yield is well rendered in our statistical framework, below lateral sizes as large as 200-300 nm in the InGaAs/InP system (Fig. 2).

Experimental results evidencing such an interplay of reduced relaxation and optical properties show up through time-resolved experiments or, more strikingly, through the photoluminescence lines from excited state(s) in ordinary PL measurements.

Recent evidence for reduced electron-electron scattering in 0D systems will be discussed suggesting that, in spite of modified many-body effects in boxes, the reduction of carrier cooling has a general character in these systems, jeopardizing the feasibilty of the quantum-box lasers.

On the contrary, we will show in the second part of our paper that the longer lifetime of *intraband excited carriers* has a high potential for optoelectronic devices based on intersubband transitions in quantum wells (QW) such as infrared detectors and envisioned masers. Most figures of merit of the QW devices (responsivity, operating temperature, yield) are limited by the short (~10 ps) lifetime due to efficient intersubband phonon relaxation. Patterning these devices into boxes of moderately small size to get reduced inter- and/or intra-subband relaxation (~100 nm) will be shown to enhance dramatically these figures of merit (Fig. 3). The bottleneck of phonon relaxation through energy and momentum selection from 3D electron quantization is in this case very helpful as it takes place way before the occurence of room temperature electron quantization effects. Additional advantages for light-coupling applications make this investigation a very attractive one.

Reference

1. H. Benisty, C. M. Sotomayor-Torres and C. Weisbuch, Phys. Rev. **B44**, 10945 (1991).
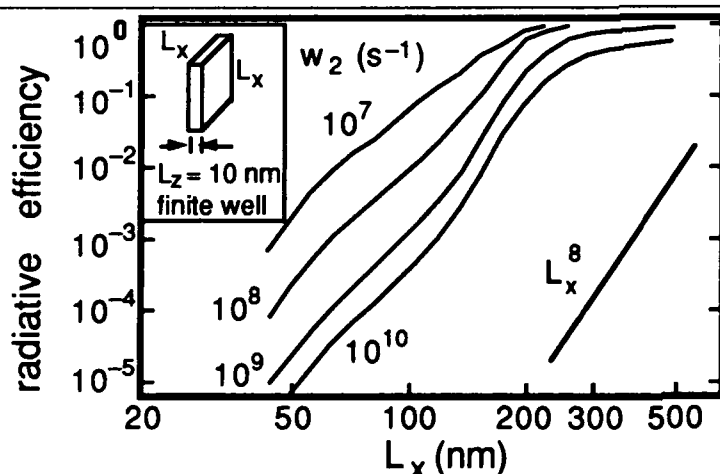
Fig. 2 : Photoluminescence internal yield for the same box as in Fig. 1 as a function of the lateral size L_x for various nonradiative recombination rate w_2 as indicated. The decrease remains steep even for a very slow w_2 value and the L_x value of the elbow is quite independent of w_2.
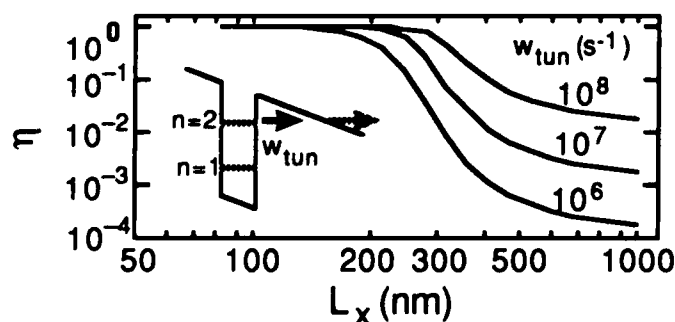

Fig. 3 : Improvement of the inetrnal yield of a photoconductive infrared detector based on a 30 nm thick InGaAs/InP quantum well upon patterning into boxes of lateral size L_x for various values of the tunneling rate from the n=2 level as indicated.

Thermal and Coherent Carrier Escape from Quantum Wells in an Electric Field

A. M. Fox and R. G. Ispasoiu
Department of Physics, University of Oxford
Clarendon Laboratory, Parks Road, Oxford OX1 3PU, U.K.
tel: +44 865 272207

C. T. Foxon
Department of Physics, University of Nottingham
University Park, Nottingham, NG7 2RD, U.K.

In this work we investigate the mechanism of carrier escape from GaAs/Al$_{0.33}$Ga$_{0.67}$As quantum wells in an electric field using CW photocurrent and photoluminescence (PL) techniques. The photocurrent generated with a fixed intensity light source depends strongly on both the applied field and the temperature (T). At low fields the photocurrent increases with T, as expected for a thermally-activated escape mechanism. At higher fields, however, the photocurrent actually *decreases* with T up to about 100K, and then starts to increase again. The most likely explanation of this is the reduction of a *coherent* component of the tunneling current, associated with a reduction in the wave function coherence length with increasing temperature.

Photocurrent is generated if the photogenerated carriers can escape from the quantum wells faster than they recombine. The magnitude of the photocurrent depends on the absorption coefficient and the photocurrent quantum efficiency, η (the ratio of the number of photoelectrons collected to the number of photons absorbed). In our measurements we chose the optical wavelength so that the absorbance varies only weakly with the field (F) and T. Hence the measured variations of the photocurrent are determined principally by $\eta(F,T)$. η is given by:

$$\eta = \frac{1}{1 + \tau_E/\tau_R} \tag{1}$$

where τ_E is the escape time of the carriers from the quantum wells, and τ_R is the recombination time. Since both τ_E and τ_R vary strongly with field and temperature [1], η itself is strongly dependent on both F and T.

The sample studied was a p-i-n structure grown by molecular beam epitaxy with an intrinsic region thickness of 1μm. The absorbing GaAs quantum
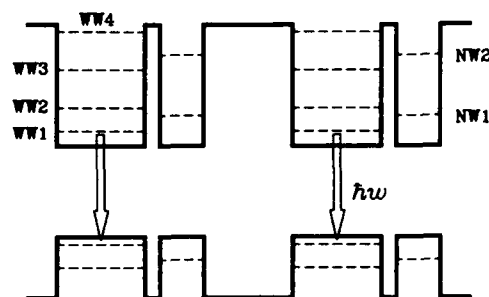
Figure 1: Schematic band diagram of the sample at zero field showing the optical transitions observed in photoluminescence.

wells were located in the intrinsic region, and consisted of 25 coupled asymmetric double wells. Fig. 1 shows a sketch of the band diagram of the sample. The thickness of the wide well (WW) and narrow well (NW) were 158Å and 79Å respectively, with a 17Å barrier separating them. The width of the 'thick' barrier separating each coupled well pair was 153 Å.

Fig. 2 gives a summary of our photoluminescence and photocurrent results. Positive voltage implies reverse bias. The photocurrent I-V curves were taken at 10K, 50K and 100K using filtered 725nm light from a tungsten bulb as the light source. Also shown is the wavelength integrated photoluminescence intensity versus voltage at 10K. The PL changes from being spatially direct to indirect around 1V. The integrated PL intensity changes relatively smoothly through this transition, which indicates that the non-radiative recombination rate is low. At 10K the photocurrent is very small at low voltages, while the PL is strong. However, at 4V the photocurrent increases strongly, while the PL
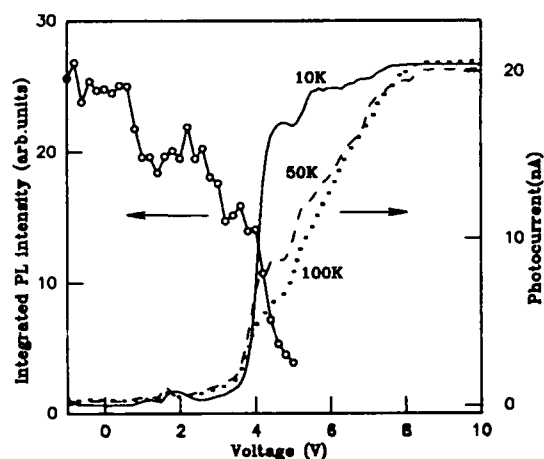
Figure 2: Photocurrent versus voltage at 10K, 50K and 100K, and wavelength-integrated PL intensity against voltage at 10K.

intensity drops to near zero. On increasing the voltage further, the current continues to increase slightly until reaching a saturation value. On increasing T, the low voltage photocurrent increases monotonically with T, whereas the photocurrent between 4V and 8V decreases up to 100K.

These results may be explained using Eq.(1) and from analysis of the energy levels of the structure. At low voltage and low temperatures, the escape from the wells is very inefficient. Hence η is small, and the photoluminescence efficiency is high. The probability of tunneling through the structure is very small, and any current collected is due to the thermal activation of the carriers over their confining barriers. The anomalous temperature-dependence of the photocurrent above 4V may be explained if we assume that the tunneling mechanism responsible for the current contains a substantial *coherent* component at 10K. Calculations show that the photocurrent peaks at 1.8V and 4.7V correspond to resonances aligning the NW1 electron level of one pair of wells with the WW3 and WW4 levels respectively of the next pair through the 'thick' 153Å barrier (see Fig. 3). This would give rise to an efficient escape mechanism, because it is the 'thick' barrier which limits the tunneling current. We propose that the reason for the decrease in current with T in this voltage range is that the wave function coherence length is reduced on increasing T, thereby reducing the effective transmission through the barrier. A decrease in photocurrent with increasing temperature has been seen before by other groups [2, 3]. Schnei-
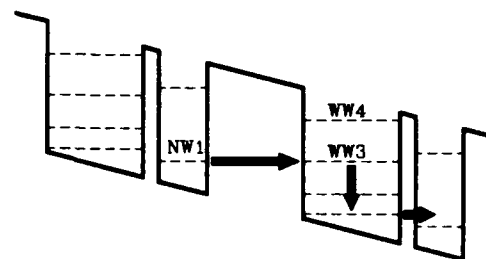
Figure 3: NW1 → WW3 resonant electron transport mechanism proposed to explain the data.

der *et al.* proposed an explanation based around a thermally-activated decrease in the recombination time τ_R due to non-radiative processes [3]. This explanation seems implausible in our case because it would not explain why we observe totally different behaviour for the temperature dependence of the photocurrent at low and high voltages.

The low voltage quantum efficiency at room temperature was close to unity. This shows that it is possible to sweep-out the carriers in GaAs/Al$_{0.33}$Ga$_{0.67}$As quantum wells at low voltages entirely by thermal processes. This finding is of relevance to GaAs/AlGaAs quantum well optoelectronic devices, such as modulators, self electro optic effect devices (SEEDs), and solar cells [1, 4]. In particular, it reinforces the previous conclusion that the best way to improve the speed and saturation performance of SEED devices and modulators is to use lower barriers to assist the thermal escape of the carriers at low voltages [1]

The sample was grown at Philips Research Laboratories, Redhill, and processed by T. Rivers at University College, London.

References

[1] A. M. Fox, D.A.B. Miller, G. Livescu, J.E. Cunningham and W.Y. Jan, IEEE J. Quantum Electron. **27**, 2281 (1991).

[2] R. T. Collins, K. v. Klitzing and K. Ploog, Appl. Phys. Lett. **49**, 406 (1986)

[3] H. Schneider, K. v. Klitzing and K. Ploog, Superlat. and Microstruct. **5**, 383 (1989)

[4] K.W.J. Barnham and G. Duggan, J. Appl. Phys. **67**, 3490 (1990)

Temperature Dependence of Electron and Hole Emission Rates from a Single Quantum Well with Asymmetric Barriers

R. Bambha, M.J. Snelling, P. Li-Kam-Wa, A. Miller
Center for Research in Electro-Optics and Laser, University of Central Florida, Florida 32816
Tel: (407) 658-6800   Fax: (407) 658-6880

J.A. Cavailles, D.A.B. Miller, J.E. Cunningham
AT & T Bell Laboratories, Crawfords Corner Rd, Holmdel, New Jersey 07733
Tel: (908) 949-6872   Fax: (908) 949-2473

In recent years, much attention has been focused on carrier emission rates and cross-well motion in semiconductor quantum well structures because the efficiency and response speed of many MQW optoelectronic devices depend on the dynamics of vertical carrier transport processes. Thermionic emission is believed to be the principal mechanism for the escape of the carriers from each individual quantum well. In most cases, measurements of the transport dynamics have been carried out in structures that contain multiple quantum wells. However in multiple well structures, effects such as resonant tunneling and carrier retrapping make it difficult to unambiguously separate the effects from one another. In recent measurements on single quantum wells with asymmetric barriers, we monitored electron and hole sweep-out rates simultaneously as a function of electric field[1], and showed that the carrier emission from the wells is thermionic in nature, but this preliminary analysis did not give very good quantitative agreement with the conventional thermionic emission model[2]. In this paper, we will present a study of the emission for both carrier types as a function of temperature and electric field in order to fully evaluate the applicability of the thermionic emission model to the process of carrier escape in a single quantum well.

Carrier transport measurements employing picosecond laser excite-probe techniques have relied on the transmission changes of the quantum wells associated with the exciton saturation due to the presence of photo-excited carriers in the wells and the quantum confined Stark shifting of the exciton due to the screening of the electric field caused by the sweep-out of the carriers in an electric field. Monitoring of the transmission changes in a direction perpendicular to the plane of the quantum wells have required a stack of several quantum wells. However, by performing similar measurements using a waveguide geometry, the investigation of carrier dynamics in a single well structure is made possible. Furthermore, growing structures with different barrier heights, the properties can be tailored in such a way that either the electrons or the holes can be made to escape faster from the quantum well.

In this work we utilize the excite-probe technique to study the transient transmission response of p-i-n waveguide structures which contain a single quantum well. The escape times of the electrons and holes relative to one another are controlled by the use of asymmetric quantum well barriers. Both types of optically generated carriers influence the absorption in the quantum well simultaneously through exciton saturation and the quantum confined Stark effect (QCSE)[3]. Exciton saturation results primarily from the presence of electrons in the quantum well through phase space filling[4]. The QCSE depends on the electric field across the quantum well, which is influenced by the presence of both types of carriers even after they have escaped from the quantum well. The simultaneous electron and hole emission rates have been studied in two asymmetric structures, one which allows the electrons to escape more quickly and the other which allows more rapid hole escape. The electric field dependence of the emission rates for different barrier heights were deduced by modeling the dynamics of the carrier transport. The results shown here were obtained from a device with a low barrier on the side of the well nearest the n-doped region in order to reduce electron escape time. The device is reverse biased to improve carrier sweep-out. A temperature regulated

heater is used to control the sample's temperature. Pulses of approximately 1.5 ps. were produced by a Styryl 9 dye laser synchronously pumped by an Nd:YAG mode locked laser. The laser output is cavity dumped to produce a repetition rate of 7.6 MHz. Time resolved transmission change is measured at different temperatures. Fig. 1 shows a representative excite-probe curve that was obtained from the device held at a temperature of 348K. The temporal change in transmission is modeled as a sum of contributions from the QCSE and the recovery of the exciton saturation. The time dependence of the electric field in the quantum well is calculated using an analytical model involving both electron and hole escape times. For small changes in the electric field the QCSE is assumed to be proportional to the field change. Exciton saturation is modeled as an instantaneous rise in transmission followed by exponential decay dependent on an electron escape time constant. Fitting this model to experimental measurements allows for the discrimination between electron and hole contributions.

Escape times for both electrons and holes are plotted logarithmically as a function of temperature in fig. 2. We observe that the time constants for both electrons and holes decay exponentially with increasing temperature. The time constants changed by a factor of ~2 over a 50 degree temperature change. This provides direct evidence that the emission is thermionic as previously hypothesized. Work is currently in progress to study a complementary sample which allows the holes to escape faster than the electrons.

References

1.   J. A. Cavailles, D. A. B. Miller, J. E. Cunningham, P. Li Kam Wa, A. Miller, IEEE J. Quantum Electron., vol. 27, no. 10, pp. 2486-2497, 1991.
2.   H. Schneider, K. v. Klitzing, Phys. Rev. B, vol. 38, pp. 6160-6155, 1988.
3.   D. A. B. Miller, D. S. Chemla, T. C. Damen, A. Gossard, W. Wiegmann, T. Wood, C. Burrus, Phys. Rev. B, vol. 32, no. 2, pp. 1034-1060, 1985.
4.   S. Schmitt-Rink, D. S. Chemla, D. A. B. Miller, Phys. Rev. B, vol. 32, pp. 6601-6609, 1985.
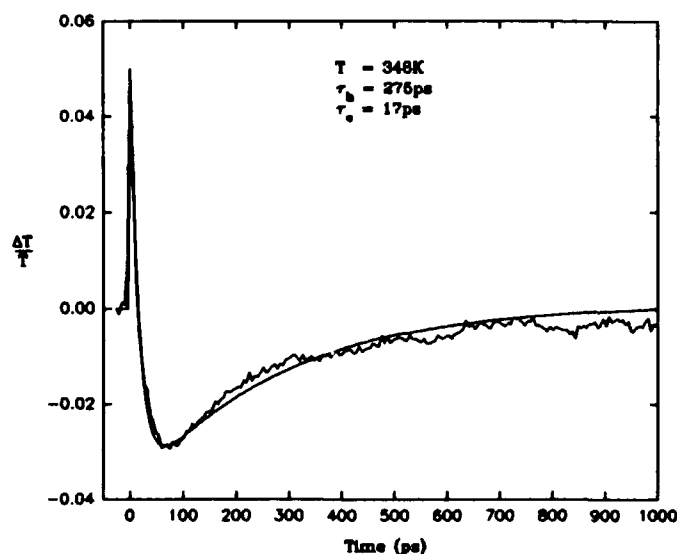
Fig. 1. Probe transmission change as a function of pump-probe delay.
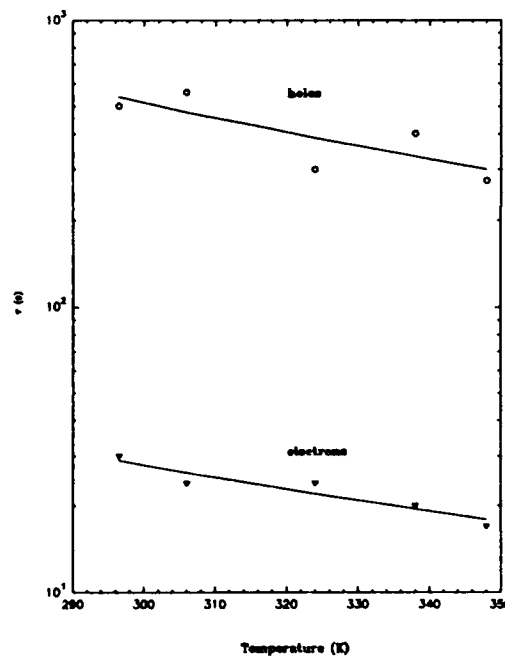
Fig. 2. Electron and hole escape times as a function of temperature.

Optical Nonlinearities Associated with Piezo-Electric Field
Screening in [111] Strained-Layer InGaAs/GaAs Quantum Wells

Arthur L. Smirl, D. S. McCallum, A. N. Cartwright, Thomas F. Boggess,
Center for Laser Science & Engineering, University of Iowa,
124 AMRF Oakdale, Iowa City, IA 52242
Tel: (319) 335 4580 Fax: (319) 335 4582

T. S. Moise, L. J. Guido, R. C. Barker
Center for Microelectronics Materials & Structures, Yale University,
P.O. Box 2157, Yale Station, New Haven, CT 06520
Tel: (203) 432 4240 Fax: (203) 432 7769

and B. S. Wherrett
Department of Physics, Heriot-Watt University, Edinburgh EH14 4AS, United Kingdom
Tel: 44 31 451 3039 Fax: 44 31 451 3136

Optical switching and logic devices require a large optical nonlinearity (absorptive or refractive) per absorbed photon, combined with a rapid excitation recovery time. The accumulated absorptive (or index) changes during a laser pulse are proportional to the shorter of either the pulse duration or the excitation lifetime. Optimally the two are matched, in which case the switching energy (power-time product) is determined primarily by the absorption (or refraction) cross-section; that is, the change in absorption coefficient per photogenerated carrier-pair. Any mechanism that is purported to enhance the cross-section is therefore of considerable interest. It has been suggested that the in-well screening of the piezoelectric field present in certain strained-layer quantum well structures could provide such an enhancement[1].

In this paper, we report the results of experimental studies of multiple-quantum-well InGaAs/GaAs structures. Growth in the [111] crystallographic direction produces in-well piezo-electric fields of order 10^7 Vcm^{-1} in that direction; consequently there are large Stark-shifts of the excitonic absorption features compared to those in [001]-grown structures in which there are no piezo-electric fields.

Our first results showed, in agreement with the measurements of Sela et al. on similar samples[2], an accumulated absorption change under cw excitation that is an order of magnitude larger for the [111] sample than for the [001]. Furthermore, measurements of photoluminescence following excitation of large carrier densities indicated a dominant nanosecond-timescale carrier recovery in both cases. At first sight then, these results seem to imply that we do indeed have a factor of ten enhancement in the cross-section of the [111]-material.

In order to confirm (or deny) the enhancement, it is important to perform measurements of the lifetime of the nonlinearity under excitation conditions as close as possible to those of the cw experiments. Parts a and b of Fig. 1 show the results of differential-transmission pump-probe experiments in which a tunable, 1.5 ps pulse-duration, synchronously mode-locked dye laser system was employed to monitor the decay of induced absorption changes. At the lowest pump fluences used (0.18 μJ/cm^2), the spectral signatures and the decays for the two samples are completely different.

For the [001]-sample, fairly symmetric differential absorption spectra are seen (Fig. 1a), decaying with a time-constant at all wavelengths of around 1 ns. These are consistent with a bleaching of the heavy-hole excitonic feature observed in the linear absorption and a recovery of the bleaching on the same timescale as observed for the photoluminescence decay. In contrast, for the [111]-sample (Fig. 1b) the differential spectra are asymmetric. This asymmetry is the signature for a spectral shift in the excitonic absorption. The shift is to the blue, as would be expected for the screening of the built-in piezo-electric fields in the quantum wells. Most strikingly the absorption change does not decay after 1 ns but is almost unchanged even 1 μs after the pump pulse.

The unfortunate implication is that the carriers responsible for the cw absorption change in [111] sample are much longer lived that those in the [100] sample and that the absorption change associated with the screening produced by a carrier pair is, if anything, less than that associated with

bleaching. This conclusion is backed-up by higher fluence picosecond experiments in which we show that the differential absorption is of similar magnitude, and is dominated by bleaching, in both samples.
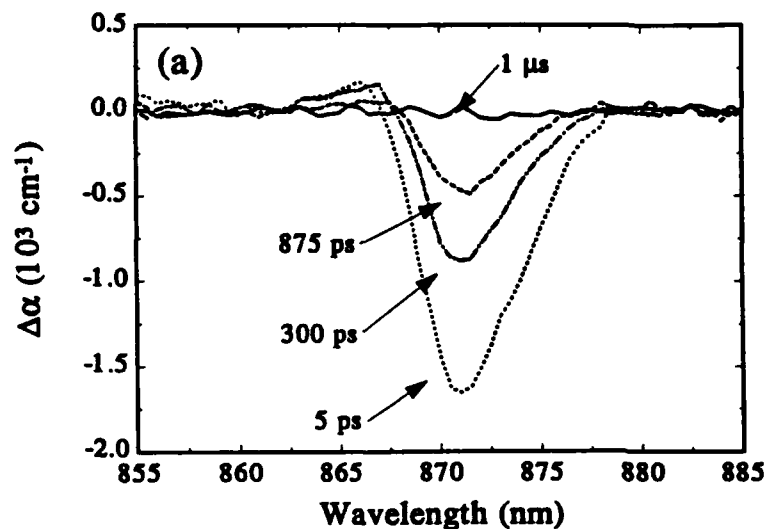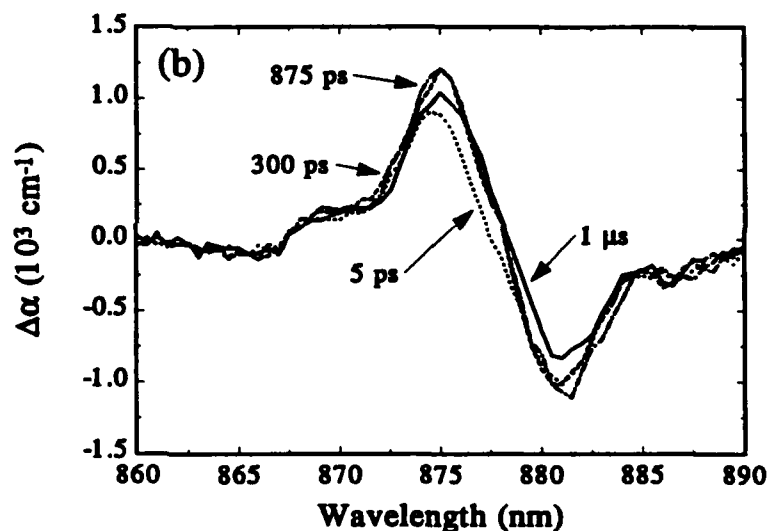

Fig. 1 The decay of the spectrally-resolved change in absorption coefficient, $\Delta\alpha$, of (a) the [001] sample and (b) the [111] sample at a fixed pump fluence of 0.18 $\mu J/cm^2$.

We present an argument that explains the mechanism for the long-lifetime of the [111]-sample carriers and the highly non-exponential nonlinearity decay that we observe. The argument is based upon the presence of a degree of mechanical clamping in the [111]-structure, as a consequence of which there is a long-range accumulated potential in the absence of carrier generation. Following excitation we believe that a fraction of the carriers escape from the wells and drift to the edges of the quantum-well region. These widely-separated electrons and holes screen the piezo-electric fields. Their subsequent recombination becomes successively more difficult at lower concentrations because the piezo-electric fields become re-established and prevent the two carrier species from diffusing back into contact with each other.

A series of picosecond differential-transmission experiments used to identify the mechanisms of the carrier dynamics and to demonstrate the non-exponential temporal response will be described.

References

1. D. L. Smith and C. Mailhiot, Phys. Rev. Lett. 58, 1264 (1987).
2. I. Sela, D. E. Watkins, B. K. Laurich, D. L. Smith, S. Subbanna and H. Kroemer, Appl. Phys. Lett. 58, 684 (1991).

Abe, Yuji — QWB2
Arai, Shigehisa — QWD3, QFA4
Arakawa, Yasuhiko — QWA3, QFA3
Asom, M. T. — QWB4
Austin, Richard F. — QThD1

Baba, T. — QThA2
Bambha, R. — QThC2, QFB3
Barker, R. C. — QFB4
Barros, M. — QThC3
Becker, P. — QThC3
Becker, Philippe C. — QThD1
Behringer, Robert E. — QThD1
Benisty, H. — QFB1
Bensoussan, M. — QThD4
Blum, O. — QThB2
Boggess, Thomas F. — QFB4
Boncek, R. K. — QThB4
Boyd, G. — QThB1
Brener, I. — QThC4
Brennan, T. M. — QWA5
Brown de Colstoun, F. — QWA5
Buller, G. S. — QThB6
Buttiker, M. — QWC1

Carraresi, L. — QThB1
Cartwright, A. N. — QFB4
Cavailles, J. A. — QFB3
Chang-Hasnain, Constance J. — QWA
Chemla, D. S. — QThC4
Chui, H. C. — QWB6
Coldren, Larry A. — QThA4
Cunningham, J. E. — QWB1, QThC4, QFB3

Dawson, Martin D. — QWD5
de Barros, Miriam R. X. — QThD1
De Souza, E. A. — QThB1
Deppe, D. G. — QWA4
Deveaud, Benoit — QThC3, QThD
Ding, J. — QThD2
Dong, Jie — QWD3
Duggan, Geoffrey — QWD5
Dupuis, R. D. — QWA4
Dutta, M. — QThD3

Fancey, S. J. — QThB6
Fejer, Martin M. — QWB6
Feldman, Robert D. — QThD1
Florez, L. T. — QThA1
Fox, A. M. — QFB2
Foxon, C. T. — QFB2
Fukuta, S. — QThB5

Gan, Y. — QThD2
Gibbs, H. M. — QWA5, QThB4
Göbel, E. — QThC1
Goodwill, D. J. — QThB6
Goossen, Keith W. — QWB1
Goto, H. — QThB5
Grillo, D. — QThD2
Guido, L. J. — QFB4
Gulden, K. — QThB2
Gunshor, R. L. — QThD2
Gustafson, T. K. — QThB2

Hagerott, M. — QThD2
Hammons, B. E. — QWA5
Han, J. — QThD2
Hara, K. — QThB5
Harbison, J. P. — QThA1
Harris, J. S., Jr. — QWB3, QWB6, QThB3, QThB7
Haus, H. A. — QWC2
Huffaker, D. L. — QWA4
Hunt, N. E. J. — QWA2
Hutchings, D. C. — QThC2

Iga, Kenichi — QWD1, QThA, QThA2
Ikeda, Tetsu — QWD3
Ishikawa, A. — QWA3
Ispasoiu, R. G. — QFB2
Ito, H. — QThB5

Jacobson, D. C. — QWA2
Jan, W. Y. — QWB1
Jewell, Jack Lee — QThA1
Johnson, Anthony M. — QThD1

Kasahara, Kenichi — QThA3
Kash, J. A. — QWB3
Kawanaka, S. — QWD2
Khitrova, G. — QWA5, QThB4
Khurgin, J. B. — QWB5
Knox, Wayne H. — QWB4, QThC, QThC4
Koch, S. W. — QWA5
Kosaka, Hideo — QThA3
Koyama, F. — QThA2
Krol, M. F. — QThB4
Kurihara, Kaori — QThA3

Larson, M. C. — QThB3, QThB7
Lee, Donghan — QThD1
Lee, Yong — QWA1
Li, H. — QThD2
Li, Shaozhong — QWB5
Li-Kam-Wa, P. — QFB3
Liu, Daxin — QWB3
Lord, S. M. — QWB3, QWB6, QThB3, QThB7
Lowry, C. W. — QWA5
Lu, Y. — QThD3
Lyubomirsky, I. — QWC2

Majewski, M. L. — QThA4
Marzin, Jean-Yves — QFA1
Massa, J. S. — QThB6
McCallum, D. S. — QFB4
McGinnis, B. P. — QThB4
Mendez, E. E. — QThB
Miller, A. — QThC2, QFB3
Miller, David A. B. — QWB, QWB1, QThB1, QFB3
Minagawa, S. — QWD2
Moise, T. S. — QFB4
Morris, D. — QThC3

Nabiev, R. F. — QWC4
Nagamune, Y. — QFA3
Nakao, M. — QFA2
Newman, P. — QThD3
Nishioka, M. — QWA3, QFA3
Nojima, S. — QFA2

Sponsored by
Optical Society of America

Technical Cosponsor
IEEE/Lasers and Electro-Optics Society

QUANTUM OPTOELECTRONICS
POSTDEADLINE PAPERS

RED (639-661 nm) InAlGaP/AlGaAs

VERTICAL CAVITY SURFACE EMITTING LASER DIODES[†]

J. A. Lott and R. P. Schneider, Jr.

Sandia National Laboratories
Compound Semiconductor Research Laboratory
P. O. Box 5800, Albuquerque, NM, 87185-5800

The first electrically injected visible InAlGaP/AlGaAs vertical cavity surface emitting lasers (VCSELs) are reported. The structures consist of an InAlGaP optical cavity active region surrounded by AlAs/AlGaAs distributed Bragg reflectors. Pulsed room temperature lasing is achieved from 639 to 661 nm with test devices fabricated on unrotated wafers. Beam divergence is 6.5° (full angle) and device on-resistance is less than 15 Ω. At 650 nm, a current threshold of 30 mA at 2.7 V is measured with peak output power exceeding 3.3 mW for devices with a 20 μm emitting diameter.

The lattice-matched epitaxial layers are grown by metalorganic vapor-phase epitaxy (MOVPE) on (n+) GaAs substrates[1]. The bottom Si-doped DBR consists of 55.5 periods of alternating AlAs and $Al_xGa_{1-x}As$ (x = 0.5) quarter-wave layers with x = 0.75 barrier reduction layers at each interface. An identical 36 period C-doped top coupling DBR is used and concludes with a (p+) GaAs layer to reduce contact resistance. The InAlGaP optical cavity contains three InGaP strained quantum wells in a step graded-barrier separate confinement heterostructure configuration. The wafers are unrotated during growth to increase the range of possible emission wavelengths. Injected carrier confinement and efficiency were improved by studying the performance of edge-emitting lasers with InAlGaP active regions and AlGaAs DBR cladding layers, and similarly constructed resonant cavity light-emitting diodes.

This first demonstration of InAlGaP/AlGaAs visible VCSEL diodes opens the door for advanced device applications such as laser pointers, plastic fiber communications, arrays for displays, interconnects, and holographic memories, telemetry, and as a compact replacement for HeNe lasers.

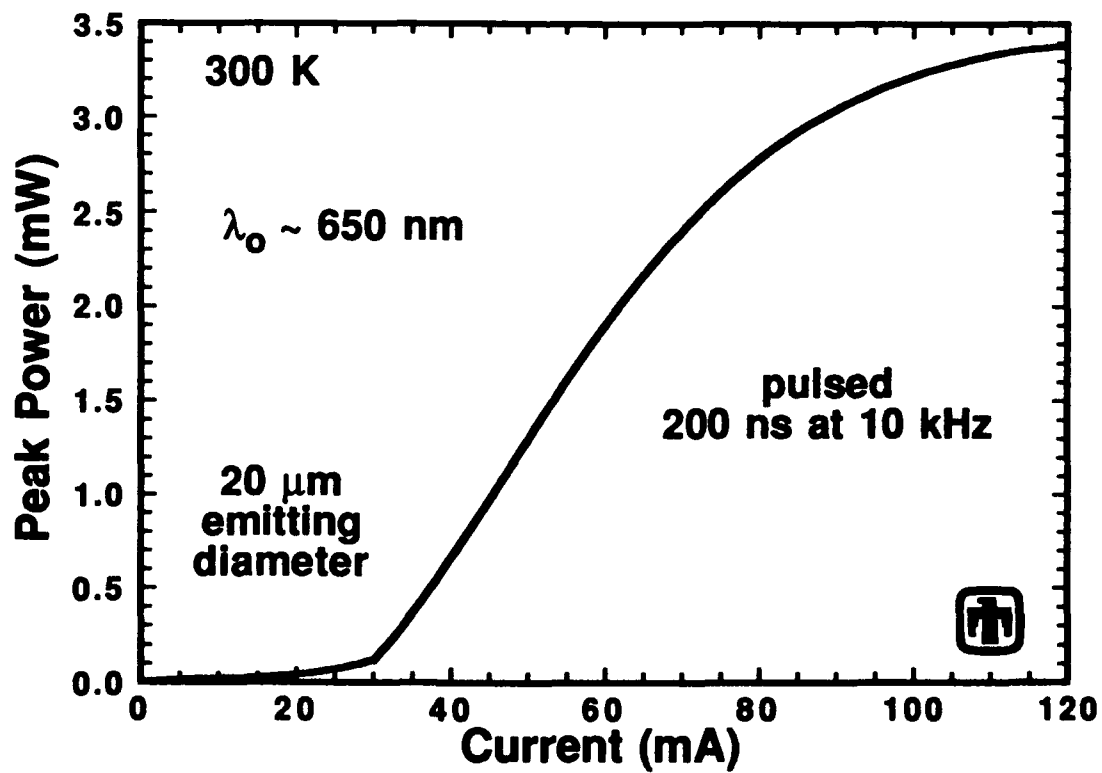1. R. P. Schneider, Jr., R. F. Bryan, J. A. Lott, and G. R. Olbright, Appl. Phys. Lett., **60** (15), p. 1830, 1992.
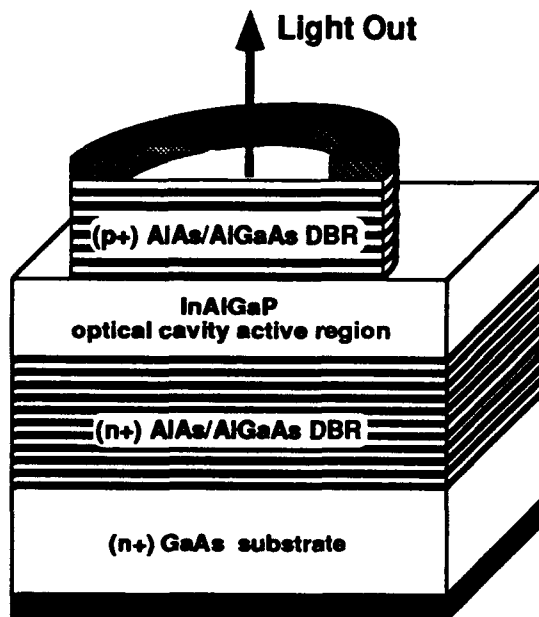
Schematic diagram of the visible VCSEL diode test structure.
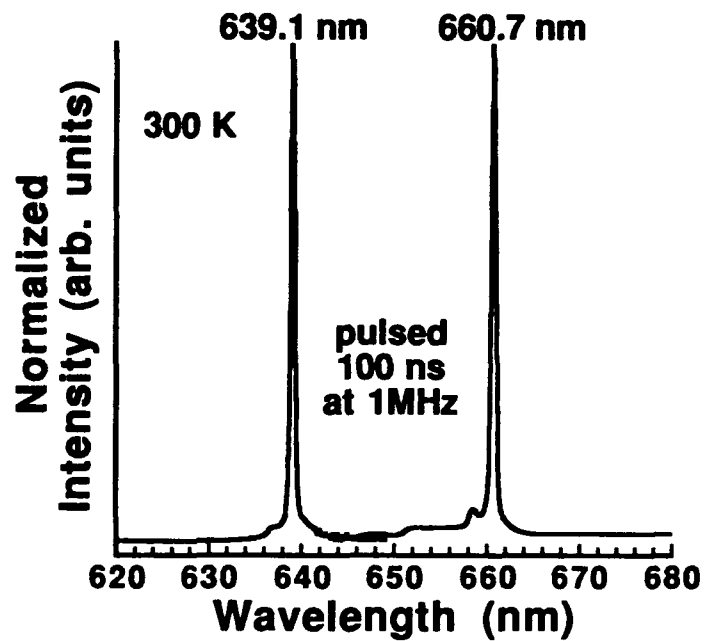
Visible VCSEL diode lasing spectra.

Light-current (L-I) characteristic for a visible VCSEL diode.

First Room Temperature CW Operation of GaInAsP/InP Surface Emitting Laser

T. Baba, Y. Yogo, K. Suzuki, F. Koyama and K. Iga

Tokyo Institute of Technology, P & I Lab.
4259 Nagatsuta, Midori-ku, Yokohama, 227 Japan

We have achieved the room temperature cw lasing operation in GaInAsP/InP vertical cavity surface emitting laser diodes for the first time. By employing a buried heterostructure with a 1.3 μm range circular active region[1] and a thermally conductive MgO/Si heat sink mirror, the cw lasing operation was obtained up to 14 °C, as shown in Fig. 1.

So far, the room temperature pulsed operation of GaInAsP/InP surface emitting lasers has been realized,[2-5] and a high temperature operation and a quasi-cw operation were also reported for photo-pumped devices.[6,7] However, the cw operating temperature for current injection devices was limited to −126 °C.[8] Very recently, we have reported cw operation at −31 °C by introducing a buried heterostructure named CPBH and a thermally conductive MgO/Si multilayer heat sink mirror.[9] Those were helpful for strong carrier confinement and efficient heat sinking. In this study, we further reduced the threshold level by increasing the mirror reflectivity and accelerated the heat sinking by bonding devices on a diamond heat sink.

The structure and the fabrication process of the device were very similar to those described previously.[1,9] The circular active region (1.3 μm of wavelength, 0.7 μm in thickness, 12 μm in diameter) was buried by current blocking layers and cladding layer through a maskless CPBH regrowth process. The series resistance was typically as low as 10 Ω owing to the smooth current flow in the thick contact layer with the aperture of 14 μm in diameter.[9] In this experiment, we enhanced the mirror reflectivity by adding a pair of dielectric multilayers to the previously reported ones, i.e. 8.5 pairs of MgO/Si for p-side and 6 pairs of SiO$_2$/Si for n-side in total. Both of them deposited on dummy InP wafers exhibited the reflectivity of 99.4 %, the accuracy limit of measurement. The devices were bonded p-side down on a Au-coated diamond heat sink with a Ga solder.

The minimum threshold current of measured devices at 77 K under cw condition was 0.42 mA. One of the device operated up to 14 °C and the threshold current at this temperature was still as low as 22 mA. Because of extremely high reflectivities of both heat sink mirror and output mirror, the output power level is estimated to be several μW. However, we can see a single mode spectrum above threshold with the spectral width of 0.2 nm, the resolution limit of used optical spectrum analyzer. From the observation of near field pattern, we found a circular spot profile. The far field divergence full angle was 4.2 degrees at half maximum.

Thus, we have successfully achieved the room temperature cw lasing in 1.3 μm GaInAsP/InP surface emitting lasers. High temperature operation and output power are the next targets. Those are only technical problems, which should be overcome by engineering.

134

References

1. T. Baba, K. Suzuki, Y. Yogo, K. Iga and F. Koyama, *Electron. Lett.*, **29**, 331, 1993.
2. A. Kasukawa, Y. Imajo, S. Kashiwa, T. Fukushima and H. Okamoto, *Proc. 48th Device Res. Conf.*, VB-II, 1990.
3. H. Wada, D. I. Babic, D. I. Crawford, J. J. Dudley, J. E. Bowers, E. L. Hu and J. L. Merz, *IEEE Photon. Technol. Lett.* **3**, 977, 1991.
4. S. Kubota, F. Koyama and K. Iga, *Proc. Conf. Laser and Electro-Optics.*, JThD5, 1992.
5. T. Tadokoro, H. Okamoto, Y.Kohama, T. Kawakami and T. Kurokawa, *IEEE Photon. Technol. Lett.* **4**, 409, 1992.
6. J. J. Dudley, M. Ishikawa, D. I. Babic, B. I. Miller, R. Mirin, W. B. Jiang, J. E. Bowers and E. L. Hu, *Appl. Phys. Lett.* **61**, 3095, 1992.
7. S. J. Yoo, R. Bhat, A. Scherer, K. Uomi, C. E. Zah, M. A. Koza, M. A. Wang and T. P. Lee, *Proc. LEOS Annual Meeting*, PD6, 1992.
8. T. Miyamoto, T. Uchida, N. Yokouchi, Y. Inaba, F. Koyama and K. Iga, *Proc. LEOS Annual Meeting*, DLTA13.2, 1992.
9. T. Baba, Y. Yogo, K. Suzuki, F. Koyama and K. Iga, *Dig. Opt. Fiber Commun. & Int. Opt. Opt. Commun. Conf.*, PD28, 1993.
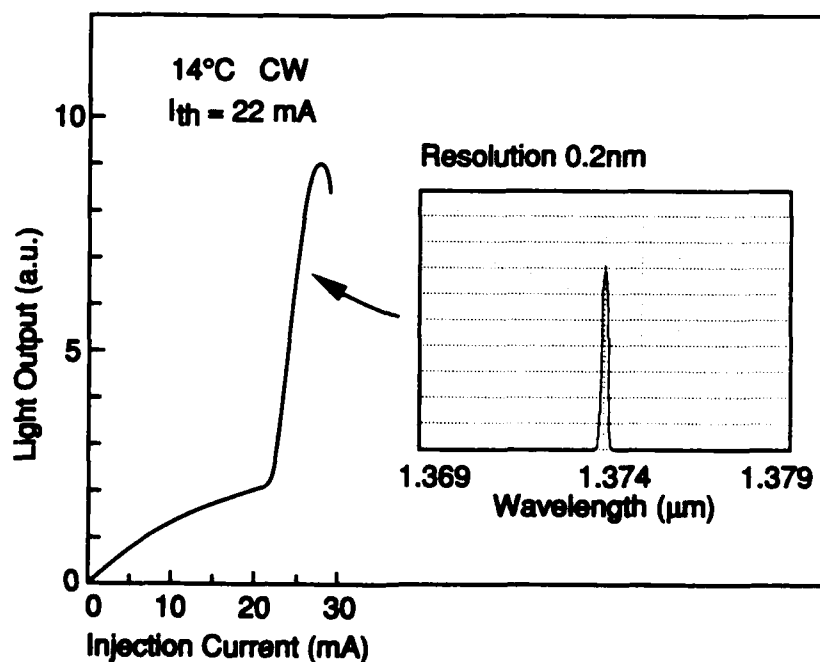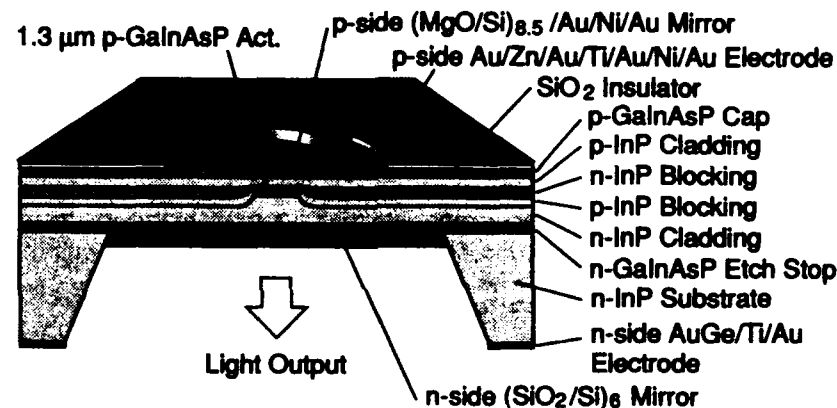
Fig. 1 Structure of GaInAsP/InP surface emitting laser
and room temperature cw lasing characteristics

The transition from photonic band gaps to microcavities, a one-dimensional unified model.

R. Houdré, R.P. Stanley, U. Oesterle, and M. Ilegems.

Institut de Micro- et Optoélectronique, Ecole Polytechnique Fédérale de Lausanne, CH1015, Switzerland

C. Weisbuch

Thomson-CSF, Laboratoire Central de Recherches, Domaine de Corbeville, F91404 Orsay cedex, France

Spontaneous emission can be controlled by reducing the number of allowed photon modes. One method suggested by Yablonovitch [1] and others [2], is to use three-dimensional periodic structures to create a Photonic Band Gap (PBG). Impurity states within the band gap can localise light and radically alter the emission characteristics of resonant luminescent centres. A second complementary approach followed by Yamamato [3] and Yokoyama [4] concentrates on microcavity structures, which quantize the photon modes by size effects.

The present work aims at comparing impurities in PBG and quantum microcavities. We use a well known physical system, the multilayer quarter-wave stack distributed Bragg reflector (DBR). By making one of the layers in the structure of variable width we can move continuously from a perfect PBG material to one with an impurity which localises light, to a microcavity. The modelled DBR has alternate $\lambda/4$ layers of GaAs and AlAs and air on both sides i.e. air/[GaAs/AlAs] x 20/GaAs 'impurity' (test) layer/[GaAs/AlAs] x 20/air. We choose the dimensions of the layers such that hc/λ = 1 eV except for the middle layer which is varied. We use the standard method of matrices to calculate the transmission of the stack and the field intensity throughout the structure.

The transmission of the structure with a $\lambda/4$ 'impurity' layer, for which the complete structure acts as a Bragg mirror is shown in Fig.1(b) (curve denoted $\lambda/4$). The transmission has a broad minimum or stop band from 0.93 to 1.07 eV. On either side of the stop band, there is a series of sidelobes, with maxima reaching unity transmission. At these energies light can propagate unimpeded through the structure. We call the two transmission peaks nearest to the stop

band, band edge modes. These represent the lowest (highest) energy photons that can propagate freely outside the stop band. For a $\lambda/2$ 'impurity' layer we satisfy the FP condition and a transmission maximum
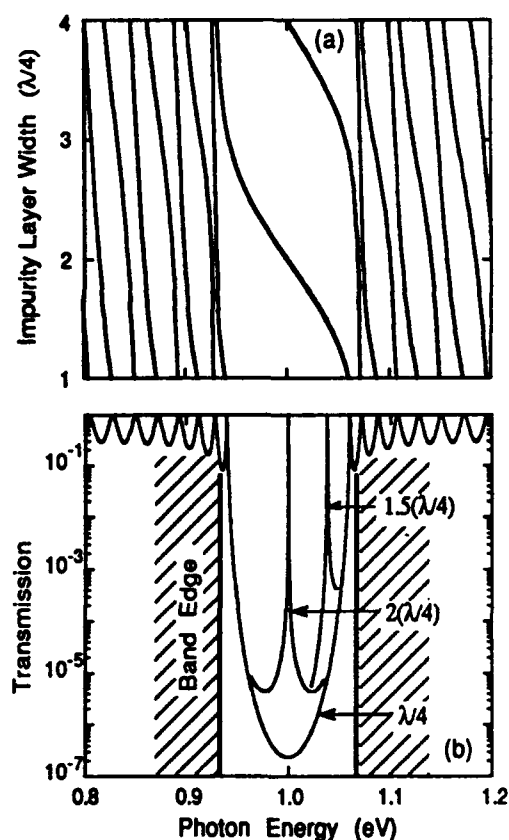

FIG. 1. (a) shows the position of transmission maxima as a function of 'impurity' layer width. (b) Transmission of $\lambda/4$ DBR stack as a function of photon energy. A transmission peak exists in the stop band for 1.5 ($\lambda/4$) and 2 ($\lambda/4$) 'impurity' layer widths. Hatched areas denote the edges of the allowed bands.

occurs in the centre of the stop band (Fig. 1(b) curve $2\lambda/4$). This structure is a $\lambda/2$ cavity between two DBR mirrors. For intermediate 'impurity' layer widths, the structure is neither a perfect DBR nor a perfect FP. The first high energy transmission peak (edge mode) of the perfect mirror moves into the stop band and becomes a "FP-like" minimum. The position of the transmission maxima as a function of layer width and energy is shown in Fig. 1(a). The introduction of a layer of different width creates a defect in the structure. One of the band edge transmission peaks moves into the stop band to become an impurity mode, while other transmission maxima outside of the stop band move a little in energy and display an anti-crossing behaviour. From the analogy with solid state electronics we use the terms: band edge modes, unbound modes and impurity modes to denote the transmission maxima at the stop band, outside the stop band and inside the stop band, respectively. In this terminology the perfect FP corresponds to a deep centre mid-gap impurity state.

Clearly, the allowed photon modes in a one-dimensional band gap structure are very different from the vacuum and this alters spontaneous and stimulated emission
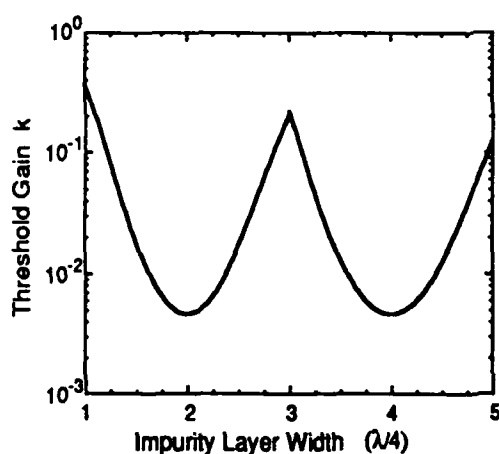
well ($50\mathring{A}$) and place them at the positions of maximum field intensity. The value of g_{th} can be calculated using the matrix method by noting the quantum well gain at which the transmission of the structure diverges to infinity. The variation of g_{th} as a function of 'impurity' layer width is shown in Fig. 2. We have used the imaginary part of the refractive index, k, as a dimensionless gain parameter. (Using $g_{th}=4\pi k/\lambda_0$ where λ_0 is the lasing wavelength, $k=0.1$ corresponds to $g_{th}=10^4$ cm^{-1}). g_{th} decreases as the 'impurity' layer width increases from a $\lambda/4$ DBR to a $\lambda/2$ FP. A further increase in layer width leads to an increase in g_{th} until at $3\lambda/4$ the structure behaves like a DBR again. The change in layer width causes a continuous change in lasing energy. For layers just greater than $3\lambda/4$ the lasing position jumps to higher energies and g_{th} starts to drop once more. There is a drop in g_{th} by two orders of magnitude between edge modes, and mid-gap FP modes. This improvement is due to both the spatial localisation of field intensity and its reduced spectral width. This shows that structures operating on edge modes make unrealistic laser resonators. Only deep impurities i.e. FP microcavities make efficient laser structures.

In conclusion, in this presentation we have brought together the PBG and microcavity approaches to photon mode control. In one dimension, edge modes, impurity modes and FP microcavities are general features of PBGs. The perfect FP is identical to a mid-gap impurity mode, and this mode is the best for localising light, maximising the field intensity and for producing lowest gain threshold in a laser resonator.

FIG. 2. *Variation of dimensionless gain threshold, k, as a function of 'impurity' layer width.*

in such a structure. It can be shown that the FP mode is the best for localization length and field intensity, but the ultimate criterion for evaluating PBG structures and microcavities as laser resonators is threshold gain, g_{th}. To simulate a gain medium we use two layers similar in thickness to a quantum

[1] E. Yablonovitch, Phys. Rev. Lett. **58**, 2059 (1987) and E. Yablonovitch and T. J. Gmitter, Phys. Rev. Lett. **63**, 1950 (1989) and E. Yablonovitch et al. Phys. Rev. Lett. **67**, 2295 (1991).

[2] S. John, Phys. Rev. Lett. **58**, 2486 (1987) and S. John and R. Rangarajan, Phys. Rev. B38, 10101 (1988).

[3] Y. Yamamoto et al. Phys. Rev. A44, 657 (1991) and G. Björk et al. Phys. Rev. A44, 669 (1991).

[4] H. Yokoyama et al. Appl. Phy. Lett. **57**, 2814 (1990) and H. Yokoyama et al. Appl. Phys. Lett. **58**, 2598 (1991).

Measurement of modulation saturation intensity in strain-balanced, undefected InGaAs/GaAsP modulators operating at 1.064 μm

K.W. Goossen, J.E. Cunningham, M.B. Santos and W.Y. Jan

AT&T Bell Laboratories, room 4B-519, Holmdel, NJ 07733   (908) 949-6979

The Nd:YAG laser has been considered as a possible light source for optical computing systems based on p-i(MQW)-n modulators, because of its ability to provide high power with high spectral and spatial quality. However, since this laser operates at 1.064 μm, the GaAs/AlGaAs material system cannot be used. Since the GaAs substrate is a better candidate for large-scale integration than InP, much attention has been focused on InGaAs/GaAs MQW's for this application.[1-4] However, since the MQW must be at least 1 μm thick for useful surface-normal modulation, strain-relief is bound to occur in this system. This relaxation of the lattice results in dislocations which propagate upward resulting in a striated surface,[3] causing diffraction of the light beams. In addition, the defects make the integration of GaAs transistors problematic.

We have shown that the InGaAs/GaAsP material system may be used to grow undefected MQW's on GaAs for modulators at 1.064 μm.[5,6] This is because the addition of phosphorous to the barrier results in negative strain in the barrier balancing the positive strain in the InGaAs well, allowing in principle any number a periods to be grown without having any net strain build up. Our devices are optically smooth and the sharpness of x-ray scattering spectra indicate that no relaxation of the lattice occurs.

In order to strain balance the system at 1.064 μm requires nearly 70 percent mole fraction of phosphorous in the barrier. This results in a direct band gap of nearly 2.4 eV, for a total well-barrier band offset of nearly 1.3 eV. This compares with a total band offset of 0.38 eV in the $GaAs/Al_{0.3}Ga_{0.7}As$ system. Trapping of photogenerated carriers in the wells has been shown to limit the optical power handling capability of $GaAs/Al_{0.3}Ga_{0.7}As$ MQW modulators to low values unless the barriers are made very thin.[7] This is due to exciton broadening and screening of the applied field caused by the carrier build-up. This phenomena of optical intensity saturation is naturally of great concern for the InGaAs/GaAsP system because of the high barriers. However, here we test InGaAs/GaAsP MQW modulators at high intensities with a Nd:YAG laser and find that they actually have higher optical saturation intensities (I_{sat}) than thin barrier $GaAs/Al_{0.3}Ga_{0.7}As$ modulators. We obtain I_{sat} =31 kW/cm^2 for our InGaAs/GaAsP transmission modulator at 1.064 μm, as compared to 16 kW/cm^2 for our thin barrier $GaAs/Al_{0.3}Ga_{0.7}As$ reflection modulator. The value of 31 kW/cm^2 is well above what is required in an optically interconnected processor.

This result is surprising, since the barriers for the $GaAs/Al_{0.3}Ga_{0.7}As$ MQW are four times lower than InGaAs/GaAsP and half as thick (35 Å vs. 65 Å). For completeness we also show in Fig. 4 the saturation performance of a shallow $(GaAs/Al_{0.02}Ga_{0.98}As)$ MQW.[8] This system has been shown to have nearly zero carrier escape time from the well at room temperature due to phonon-mediated escape.[9] However, we find that the InGaAs/GaAs MQW has saturation performance comparable to the shallow MQW, even though its barriers are comparable to the $GaAs/Al_{0.3}Ga_{0.7}As$ MQW. Either the carrier escape mechanism is different and much faster in MQWs with InGaAs as the well or much higher densities of photogenerated carriers can be tolerated in them.

Regardless of the physical ramifications, our main conclusion here is that the InGaAs/GaAsP material system may be used to form undefected MQW's on GaAs whose exciton energy is at wavelengths as long as 1.064 μm, and that such MQW's may form the active region of a high intensity light modulator. We obtain a saturation intensity of 31 kW/cm^2, comparable to that obtained in the thin-barrier GaAs/AlGaAs system. Therefore the wavelength of operation of optical switching systems using modulators may be extended to use the high power Nd:YAG laser without defects and without a penalty in power handling of the modulators.

REFERENCES

[1]   T.E. Van Eck, P. Chu, W.S.C. Chang, and H.H. Wieder, Appl. Phys. Lett. 49, 135 (1986).

[2]   W. Dobbelaere, S. Kalem, D. Huang, M.S. Unlu, and H. Morkoc, Electron. Lett. 24, 295 (1988).

[3]   T.K. Woodward, T. Sizer, D.L. Sivco, and A.Y. Cho, Appl. Phys. Lett. 57, 548 (1990).

[4]   B. Pezeshki, S.M. Lord, and J.S. Harris, Jr., Appl. Phys. Lett. 59, 888 (1991).

[5]   J.E. Cunningham, K.W. Goossen, M. Williams, and W.Y. Jan, Appl. Phys. Lett. 60, 727 (1992).

[6]   K.W. Goossen, J.E. Cunningham, and W.Y. Jan, Electron. Lett. 28, 1833 (1992).

[7]   A.M. Fox, D.A.B. Miller, G. Livescu, J.E. Cunningham, W.Y. Jan, IEEE J. Quantum Electron. 27, 2281 (1991).

[8]   K.W. Goossen, L.M.F. Chirovsky, R.A. Morgan, J.E. Cunningham, W.Y. Jan, IEEE Photon. Tech. Lett. 3, 448 (1991).

[9]   J. Feldman, K.W. Goossen, D.A.B. Miller, A.M. Fox, J.E. Cunningham, W.Y. Jan, Appl. Phys. Lett. 59, 66 (1991).

Fig. 3

Fig. 4

Fig. 1

Fig. 2
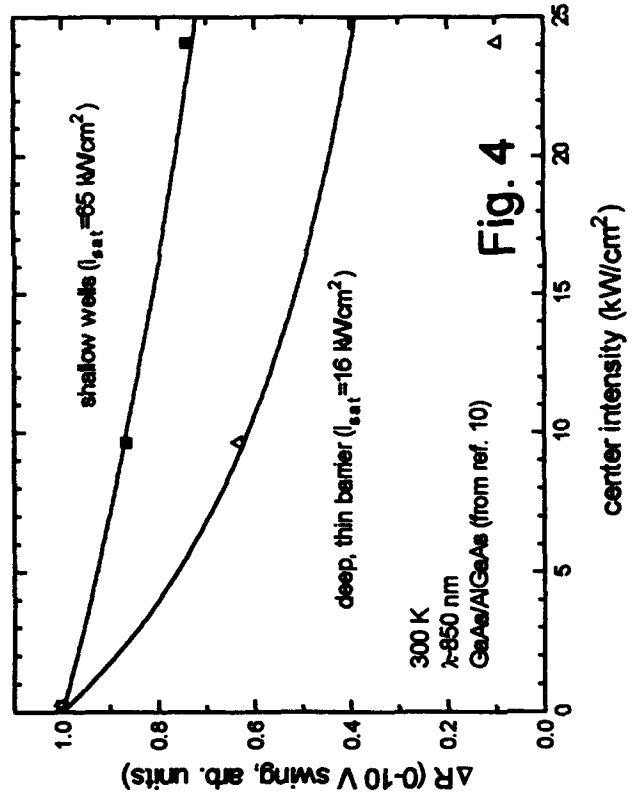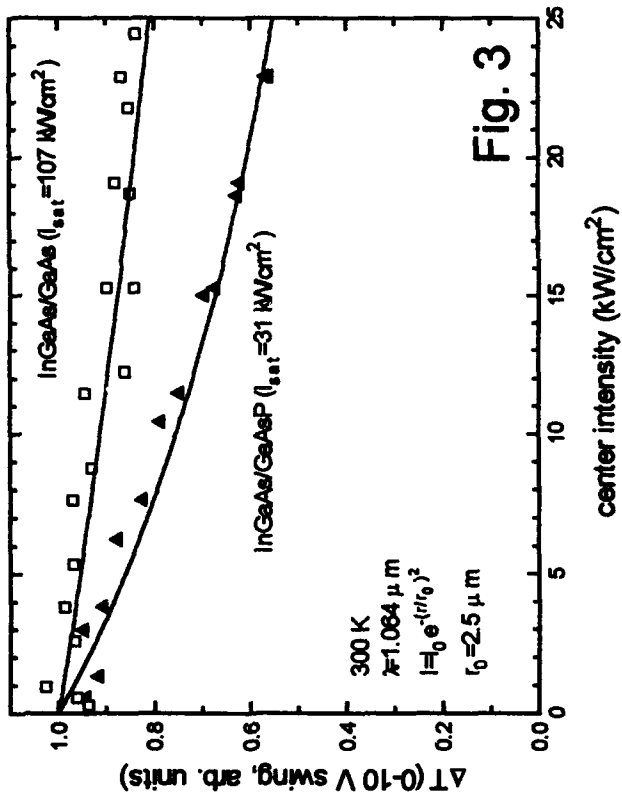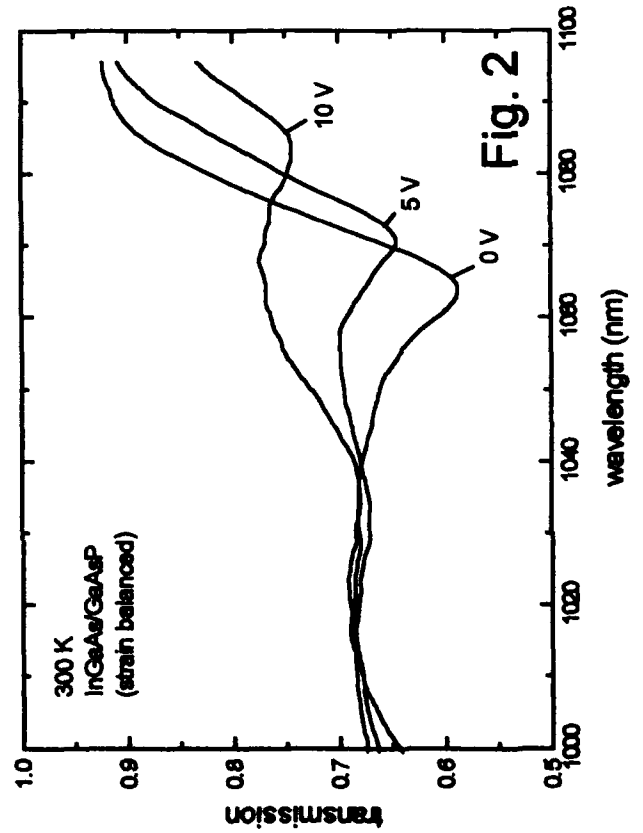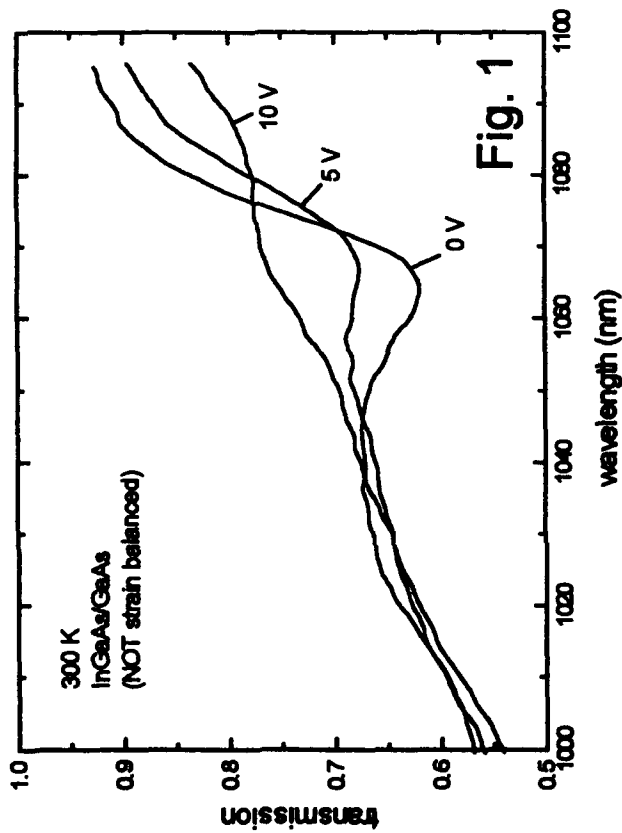
Terahertz Electromagnetic Transients As Probes of a
2-Dimensional Electron Gas

W.J. Walecki, D. Some, V.G. Kozlov, and A.V. Nurmikko
Division of Engineering and Department of Physics
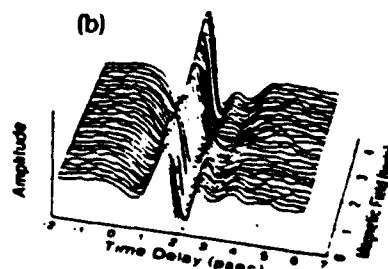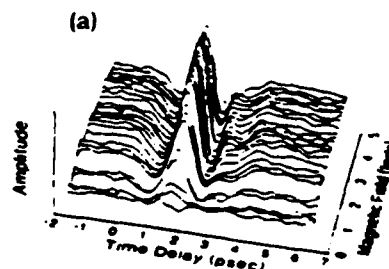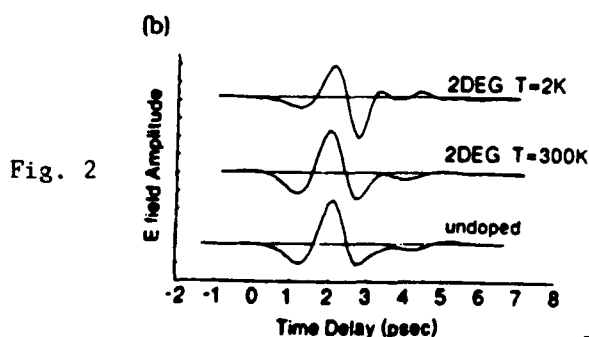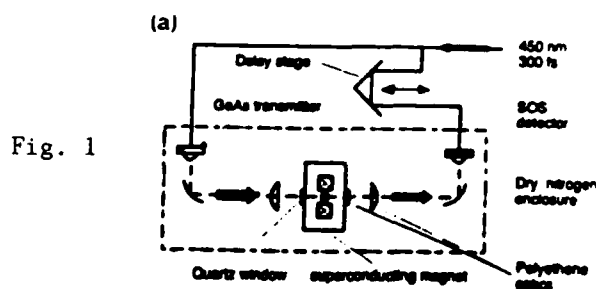Brown University, Providence RI 02912

We demonstrate here that it is experimentally practical to employ the real-time THz probes to access an equilibrium electron gas in a semiconductor heterostructure at a low temperature and magnetic field, and study the response of a 2D electron gas to picosecond transient electric fields in an n-type MQW GaAs/GaAlAs structure. The experimental arrangement is shown in the upper trace of Figure 1. The collimated beam passes a free standing wire grid polarized and is subsequently focused inside a superconducting magnet onto a sample (with a spot size of approximately 6 mm). The crossed polarizer (power) extinction ratio was about $4x10^{-4}$. The average power in the THz beam was measured by a bolometer to be approximately 1 nW, corresponding to an average flux of 10^{4}-10^{5} photons/cm^2 per pulse incident of the samples.

The modulation-doped multiple quantum well (MQW) sample consisted of 84 wells of 100Å individual thickness, with an electron density of $n_s=1.5x10^{11}$ cm^{-2} and a mobility of $5x10^5$ cm^2/Vsec, grown on a semi-insulating GaAs substrate and GaAs/AlAs superlattice buffer layer. The lower trace of Figure 1 shows the comparison of the transmitted THz electric field through the MQW sample at T= 2K and 300 K in comparison with a 'control sample' at T= 2 K. The latter is a 500 μm thick piece of semi-insulating GaAs which mimicks the effects of the substrate of the MQW sample. Apart from a propagation delay, the shape of the THz pulse transmitted through the control sample is identical to that measured through the empty cryostat (window and sample reflection effects occur on a timescale outside that in Fig. 1). Hence the influence of the 2D electron gas is to distort the shape of the transmitted field on the psec timescale in a manner which is directly related to the dynamical conductivity σ(t). The effect is particularly pronounced at T=2 K and, while diminishing with increasing temperature, is readily oberved in our single beam transmission experiment without modulation techniques.

Figure 2(a) shows the transmitted THz electric field as a function of perpendicular magnetic field to $B_z=5$ Tesla at T= 2K for parallel incident and transmitted polarizations. Transport measurements verified the presence of strong quantum Hall plateaus in the transverse Hall resistivity ρ_{xy} and sharp maxima in the longitudinal resistance ρ_{xx}. Note again how the transmitted field at B=0, exhibiting both pronounced 'positive' and 'negative' excursions, is considerably altered in shape from that observed with the undoped control sample, demonstrating the additional response from the currents induced in the 2D electron gas. Fig. 2(a) gives us an indication of the response by the 2D electron gas which is directly connected to the longitudinal "dynamical Hall conductivity" $\sigma_{xx}(t,B)$.

Figure 2(b) displays the contribution by the "transverse dynamical Hall conductivity", $\sigma_{xy}(t,B)$, to the transmitted electric field, measured as a function of the magnetic field in the crossed polarizer configuration. The transmitted zero field amplitude is unresolved from the system noise, but becomes readily observable in small fields (B<< 1 Tesla) and increases strongly with increasing magnetic field. Some variations in the transmitted field shape are seen, but by B=5 Tesla the pulse has again reverted in shape to the incident one. Overall, the behavior is similar to the classical Hall effect. Notably, the pronounced quantum Hall behavior, clearly identified in the dc transport measurements, is not present in the transient data.

[1] Ch. Fattinger and D. Grischkowsky, Appl. Phys. Lett. 56, 506 (1990)
[2] X.-C. Zhang et al, Appl. Phys. Lett. 56, 1011 (1990)

(a)

Fig. 1

(b)

Fig. 2

2DEG T=2K

2DEG T=300K

undoped

PD5-2